

University of **Strathclyde** **Glasgow**

Study and Characterisation of Fasted State Simulated Intestinal
Fluid Reflective of In Vivo Gastrointestinal Variability

Zoe McKinnon

A thesis presented in fulfilment of the requirements for the
degree of Doctor of Philosophy

2024

“I have an original dystopian rock musical that I have spent the last eight years of my life writing”

Jonathan Larson, “tick, tick...BOOM!”

Declaration of Author's Right

This thesis is the result of the author's original research. It has been composed by the author and has not been previously submitted for examination which has led to the award of a degree.

The copyright of this thesis belongs to the author under the terms of the United Kingdom Copyright Acts as qualified by University of Strathclyde Regulation 3.50. Due acknowledgement must always be made of the use of any material contained in, or derived from, this thesis.

Signed: 

Date: 30th November 2024

Acknowledgements

I would first like to thank my supervisor, Professor Hannah Batchelor, for giving me the opportunity to pursue my doctoral studies. Thank you, Hannah, for being a great mentor and for the continuous support over the years. Despite your busy schedule, you consistently responded to emails and provided feedback with an impressive turnaround time, for which I am grateful. Thank you to Martin Ward and the staff at Diamond Light Source for the support with the X-ray scattering instrumentation and analysis and to Panida Punnabhum (Tan!) for the training and support with nanoparticle tracking analysis. I am also grateful to the University of Strathclyde for funding my research.

A special thanks to the other PhD students who I have met along the way, specifically Maria Inês Silva and Dr Jan Goelen, for introducing me to PhD life and for the support you both provided throughout. To everyone in the RW601f office, particularly Tricia Kelly, Callum Davidson, Erin Campbell, Rana Tamimi and Sophie Jolliffe, thank you for providing welcome (and occasionally unwelcome) distractions. Heartfelt thanks to Dr Eleanor Jones for your kindness and for always offering a listening ear in times of stress.

I would like to acknowledge the support provided by Strathclyde University Boat Club (SUBC). Being a part of the club over the duration of my PhD has been a great source of enjoyment and has introduced me to a community of great people. The friendships I have made through SUBC have provided happiness throughout this journey. In particular, I would like to thank Saoirse Keenan, Nicolas Kirsch, Robert Amphlett, Andrew Laird and Matthew Bell. My mum still thinks it is hilarious that I row on the Clyde...

To everyone that I have ran, swam, rowed, cycled and played badminton with, I thank you.

Finally, to my parents and sister, Stuart, Janice and Julie McKinnon. I would like to thank you for the unwavering support, love and endless encouragement over the years, throughout my long academic journey, especially during the most difficult times. Without it I would not have achieved everything that I have. This thesis is dedicated to you.

Abstract

Adequate drug solubility in the gastrointestinal tract is essential for systemic therapy of orally administered medications. In order to measure the solubility of poorly soluble drugs *in vitro*, simulated intestinal fluid (SIF) is often used in place of human intestinal fluid (HIF). A suite of fasted state SIF, based on variability observed in a range of fasted state HIF samples was designed and used to study the relationship between the solubility of eight poorly soluble biopharmaceutics classification system class II drugs and the particle size of the colloidal structures formed by the drugs in the fluid. The drugs of interest included three acidic drugs (naproxen, indomethacin and phenytoin), three neutral drugs (felodipine, fenofibrate, griseofulvin) and two basic drugs (carvedilol and tadalafil). The overall aim of this research is to work towards a better understanding of the colloidal structures formed in SIF.

Solubility was measured using high performance liquid chromatography and results indicated that the solubility was typically greater in the acidic drugs than in the neutrals or bases and that the solubility tended to increase with increasing media point ($\text{pH} \times [\text{TAC}]$). Particle size was determined using both dynamic light scattering and nanoparticle tracking analysis. Dynamic light scattering data confirmed the polydispersity of size distribution within the samples analysed. Typically, as the concentration of amphiphiles (total amphiphile concentration ($[\text{TAC}]$)) is increased, the particle size of the structures measured decreases. A comparison with the solubility data revealed that the general trend indicated that while solubility is to some extent affected by pH and $[\text{TAC}]$ or $(\text{pH} \times [\text{TAC}])$, the relationship between solubility and particle size is linked with $[\text{TAC}]$.

Small angle X-ray scattering (SAXS) analysis was carried out at the Diamond Light Source national facility, using the laboratory SAXS (labSAXS) beamline on drug and drug free SIF samples and the data was processed at the University of Strathclyde. Unfortunately, there was no significant scattering measured in the sample fluids which is thought to be a result of samples that are too weakly scattering to be detected by a labSAXS instrument. The data obtained serves as excellent preliminary data for a future beamtime application using a synchrotron beamline.

The final work explores a model, using simple mathematics, to estimate the number of drug molecules per colloid or mixed micelle structure in a series of SIF. The experimental data, collected in earlier chapters, was applied in both this calculation and a calculation to estimate the solubility enhancement provided in the SIF media. Analysis of the data and results indicates that there is a direct relationship between particle size of the colloidal structures and the number of estimated drug molecules per structure. As expected, as the particle size decreases, as does the estimated number of drug molecules per micelle. The larger structures can accommodate a greater number of drug molecules per micelle.

Solubility enhancement was also calculated, with the acidic drugs, naproxen and indomethacin proving to be most solubility enhanced in the suite of simulated intestinal fluid.

Research Outputs

This thesis contains results that have been published in the following articles.

1. Z. McKinnon, I. Khadra, G. W. Halbert and H. K. Batchelor, Characterisation of colloidal structures and their solubilising potential for BCS class II drugs in fasted state simulated intestinal fluid. *International Journal of Pharmaceutics*. 2024, 665, 124733.
2. Z. McKinnon, H. K. Batchelor, I. Khadra, and G. W. Halbert, Study of in vitro poorly soluble drug solubility into fasted state simulated intestinal fluid reflective of in vivo gastrointestinal variability. *British Journal of Pharmacy*: 2023; 8, 2.
3. Z. McKinnon, H. K. Batchelor, I. Khadra, and G. W. Halbert, Solubility measurement of poorly soluble drugs in fasted state simulated intestinal fluid. *British Journal of Pharmacy* 2022, 7.

Table of Contents

Declaration of Author's Right.....	iii
Acknowledgements.....	iv
Abstract.....	v
Research Outputs.....	vii
Table of Contents.....	viii
List of Figures.....	xii
List of Tables.....	xvii
Abbreviations.....	xix
Chapter 1.....	1
1. Introduction.....	2
1.1. Biopharmaceutics.....	2
1.1.1. Key Concepts.....	2
1.1.1.1. ADME.....	2
1.1.1.2. Bioavailability.....	3
1.1.1.3. Lipinski's Rule of Five.....	4
1.1.2. Biopharmaceutics Classification System.....	4
1.1.2.1. Criteria.....	5
1.2. Solubility.....	6
1.2.1. Factors Affecting Solubility.....	7
1.2.2. Forces Involved in Solubility.....	7
1.2.3. pH, Drug Solubility and Lipophilicity.....	8
1.3. Dissolution.....	9
1.3.1. Dissolution and Solubility.....	9
1.4. Physiology of the Gastrointestinal Tract.....	9
1.4.1. Stomach.....	9
1.4.2. Small Intestine.....	10
1.4.3. Large Intestine.....	10
1.5. Human Intestinal Fluid.....	11
1.5.1. Sample Collection.....	11
1.6. Simulated Intestinal Fluid.....	11
1.6.1. Fasted State Simulated Intestinal Fluid.....	12
1.6.1.1. Compositions of Media.....	12
1.6.1.2. Components in SIF and Colloidal Structures Formed Within SIF.....	14
1.6.2. Fed State Simulated Intestinal Fluid.....	15
1.6.2.1. Limitations of SIFs.....	16
1.7. Critical Micelle Concentration and Micelle Formation.....	16
1.7.1. Micelles and Simulated Intestinal Fluid.....	17

1.8.	Outline of Thesis	19
Chapter 2	21
2.	Solubility Analysis of Fasted State Simulated Intestinal Fluid	22
2.1.	Introduction	22
2.1.1.	Simulated Intestinal Fluid.....	22
2.1.2.	High-Performance Liquid Chromatography (HPLC).....	24
2.1.3.	Objectives.....	25
2.2	Materials	26
2.3.	Methods.....	29
2.3.1.	Creation of Suite of Simulated Intestinal Fluid Media	29
2.3.2.	Simulated Intestinal Fluid Media Preparation.....	29
2.3.3.	Equilibrium Solubility Measurement	30
2.3.4.	HPLC analysis.....	30
2.4.	Results.....	32
2.4.1.	Calibration Information.....	32
2.4.2.	Raw Data	39
2.5.	Discussion.....	39
2.6.	Conclusion.....	46
Chapter 3	47
3.	Dynamic Light Scattering Analysis of Fasted State Simulated Intestinal Fluid	48
3.1.	Introduction and Theory	48
3.1.1.	Instrument Information	49
3.1.2.	Use of DLS in Biopharmaceutics.....	51
3.1.3.	Objectives.....	52
3.2	Materials	52
3.3	Methods.....	52
3.4.	Results and Discussion	53
3.4.1.	Analysis of Size Data Arranged by (pH × [TAC])	59
3.4.2.	Analysis of Size Data Arranged by Drug	63
3.5.	Conclusion.....	69
Chapter 4	70
4.	Nanoparticle Tracking Analysis of Fasted State Simulated Intestinal Fluid	71
4.1.	Introduction and Theory	71
4.1.1.	Instrument Information	72
4.1.2.	Image Optimisation.....	73
4.1.3.	Data Processing.....	74
4.1.4.	Particle Size Definitions and D Values	75
4.1.5.	Use of NTA in Biopharmaceutics	76
4.1.6.	Objectives.....	77

4.2.	Materials and Methods.....	78
4.2.1.	Data Processing.....	79
4.2.2.	Comparison between NS300 and NanoSight Pro.....	79
4.3.	Results and Discussion	80
4.3.1.	Tables of Raw Data	81
4.4.	Summary of NTA Data	100
4.5.	Size and Solubility	101
4.6.	Comparison with DLS Data.....	104
4.7.	Conclusion.....	108
Chapter 5.....		110
5.	Small Angle X-Ray Scattering Analysis of Fasted State Simulated Intestinal Fluid	111
5.1.	Introduction and Theory	111
5.1.1.	Instrument Information	111
5.1.2.	LabSAXS vs. Synchrotron SAXS	114
5.1.3.	Use of SAXS to Image Drug-Containing Colloidal Structures	115
5.2.	Objectives.....	116
5.3.	Materials and Methods.....	116
5.3.1.	Materials	116
5.3.2.	Methods.....	117
5.3.2.1.	Diamond Light Source Application	117
5.3.2.2.	Sample Preparation.....	117
5.3.2.3.	SAXS Data Collection	118
5.3.2.4.	Data Analysis/Processing	119
5.3.2.4.1.	Calibration of Silver Behenate.....	119
5.3.2.4.2.	Creation of Mask File.....	121
5.3.2.4.3.	Processing Pipeline.....	124
5.3.2.4.4.	Background Subtractions	125
5.4.	Results and Discussion	126
5.4.1.	SIF Background and SIF Samples.....	126
5.4.2.	Drug Free Media	128
5.4.3.	Drug Loaded Media.....	130
5.5.	Conclusion.....	132
Chapter 6.....		133
6.	Simulated Intestinal Fluid Mixed Micelle Size and Solubility Relationship	134
6.1.	Introduction and Theory	134
6.2.	Calculation of Drug Incorporation into Micelles Using Mathematical Principles	134
6.3.	Objectives.....	138
6.4.	Methods.....	138
6.4.1.	Theoretical Calculation of Drug Molecules per Mixed Micelle in SIF.....	138

6.4.2.	Solubility Enhancement	141
6.5.	Results and Discussion	142
6.5.1.	Theoretical Calculation of Drug Molecules per Mixed Micelle in SIF.....	142
6.5.2.	Solubility Enhancement	146
6.5.3.	Theoretical Calculation of Drug Molecules per Mixed Micelle in SIF.....	146
6.5.4.	Solubility Enhancement	151
6.5.5.	Relationship with Chemical Structure.....	151
6.5.6.	Use of Biorelevant FaSSIF for Solubility Prediction	153
6.6.	Conclusion.....	154
6.7.	Further Work.....	155
6.7.1.	Molecular Dynamics.....	155
Chapter 7.....		157
7.	Conclusions and Future Outlook.....	158
7.1.	General Conclusions.....	158
7.2.	Further Work.....	159
Appendices.....		162
Appendix 1 – Diamond Light Source Application for Beamtime		163
Appendix 2 – Script Written for SAXS Measurement.....		167
References.....		172

List of Figures

Figure 1.1: The biopharmaceutics classification system, adapted from Reference ¹	5
Figure 2.1: Overview of HPLC system, adapted from Reference ⁵⁵ . Created with Biorender.com	25
Figure 2.2: HPLC calibration data of acidic drugs a) naproxen, b) indomethacin, c) phenytoin, neutral drugs d) felodipine, e) fenofibrate, f) griseofulvin, basic drugs g) carvedilol, h) tadalafil	34
Figure 2.3: Chromatogram of naproxen in the median media showing a retention time of 1.387 minutes and a peak area of 9569593 which correlates to a drug concentration of 6.41 mg/mL or 27.84 mM. Naproxen was detected using a UV wavelength of 254 nm.	35
Figure 2.4: Chromatogram of indomethacin in the median media showing a retention time of 1.860 minutes and a peak area of 9833247 which correlates to a drug concentration of 2.45 mg/mL and 6.85 mM. Indomethacin was detected using a UV wavelength of 254 nm.....	35
Figure 2.5: Chromatogram of phenytoin in the median media showing a retention time of 0.924 minutes and a peak area of 139300 which correlates to a drug concentration of 125.85 µM. Phenytoin was detected using a UV wavelength of 254 nm.....	36
Figure 2.6: Chromatogram of felodipine in the median media showing a retention time of 2.133 minutes and a peak area of 442040 which correlates to a drug concentration of 131.09 µM. Felodipine was detected using a UV wavelength of 254 nm.....	36
Figure 2.7: Chromatogram of fenofibrate in the median media showing a retention time of 2.747 minutes and a peak area of 269500 which correlates to a drug concentration of 38.77 µM. Fenofibrate was detected using a UV wavelength of 291 nm.....	37
Figure 2.8: Chromatogram of griseofulvin in the median media showing a retention time of 1.032 and 1.297 minutes. The peak area is 1688846 and 513738 respectively, which combined gives a total of 2202584. This corresponds to a drug concentration of 161.84 µM. Griseofulvin was detected using a UV wavelength of 291 nm.	37
Figure 2.9: Chromatogram of carvedilol in the median media showing a retention time of 1.369 minutes and a peak area of 3312811 which correlates to a drug concentration of 262.73 µM. Carvedilol was detected using a UV wavelength of 254 nm.....	38
Figure 2.10: Chromatogram of tadalafil in the median media showing a retention time of 1.209 minutes and a peak area of 399630 which correlates to a drug concentration of 25.59 µM. Tadalafil was detected using a UV wavelength of 291 nm.....	38
Figure 2.11: Equilibrium solubility measurements for each drug in FaSSIF media compositions detailed in Table 2.8. Red coloured data points for acidic drugs, green for neutral drugs and blue basic drugs. Reported solubility values for individual drugs in FaSSIF taken from Augustijns <i>et al.</i> and Teleki <i>et al.</i> ^{60, 61}	40

Figure 2.12: Basic Drug Solubility vs Media pH x TAC. a) carvedilol, b) tadalafil. Point labelled indicates media number, see Table 2.3	42
Figure 2.13: Neutral Drug Solubility vs Media pH x TAC. a) felodipine, b) fenofibrate, c) griseofulvin. Point label indicates media number, see Table 2.3.....	43
Figure 2.14: Acidic Drug Solubility vs Media pH and Media pH x TAC. a) naproxen, b) indomethacin, c) phenytoin. Point label indicates media number, see Table 2.3	44
Figure 3.1: Overview of DLS process, adapted from References ^{73, 74, 77} . Created with Biorender.com.....	50
Figure 3.2: Comparative micelle sizes for the fresh blank (drug free) and felodipine structures, measured by DLS in the SIF media: a) minimum, b) Q1, c) median, d) Q3, e) maximum and f) biorelevant.....	54
Figure 3.3: DLS size and intensity distribution for the fresh blank (left) and blank media at 24 hours postproduction (right)	59
Figure 3.4: DLS size and intensity distribution for the a) Minimum b) Q1, c) Median, d) Q3, e) Maximum and f) Biorelevant SIF media.....	61
Figure 3.5: DLS size and intensity distribution for acidic drugs in the SIF media, a) naproxen, b) indomethacin and c) phenytoin	64
Figure 3.6: DLS size and intensity distribution for the neutral drugs in the SIF media, a) felodipine, b) fenofibrate and c) griseofulvin.....	65
Figure 3.7: DLS size and intensity distribution for basic drugs in the SIF media, a) carvedilol and b) tadalafil	65
Figure 3.8: Particle size measured by DLS of the media, with and without drugs	66
Figure 3.9: Plot of solubility and particle size measured by dynamic light scattering of a) naproxen b) indomethacin c) phenytoin d) felodipine e) fenofibrate f) griseofulvin g) carvedilol h) tadalafil in each of the SIF media	68
Figure 4.1: Overview of NTA process, adapted from Reference ⁹³ . Created with Biorender.com	72
Figure 4.2: View of NTA software (NS300) during image processing.....	74
Figure 4.3: NTA size distribution and concentration data for run 1 of phenytoin in the minimum media. Graph has been annotated with reported particle size definitions.....	76
Figure 4.4: Results from the NS300 and NS Pro instruments of small silica nanoparticles provided by Malvern to demonstrate the confidence and comparability of the two instruments used in this study.	80
Figure 4.5: Size distribution and particle concentration of fresh blank media a) Minimum, b) Q1, c) Median, d) Q3, e) Maximum and f) Biorelevant where the black line indicates the first run of the sample, red is the second and purple is the third and final repeat of the sample on the nanoparticle tracking analysis instrument.....	88
Figure 4.6: Size distribution and particle concentration of blank media at the 24 hour timepoint a) Minimum, b) Q1, c) Median, d) Q3, e) Maximum and f) Biorelevant where the black line indicates the	

first run of the sample, red is the second and purple is the third and final repeat of the sample on the nanoparticle tracking analysis instrument.....	89
Figure 4.7: Size distribution and particle concentration of naproxen in the a) Minimum, b) Q1, c) Median, d) Q3, e) Maximum and f) Biorelevant media, where the black line indicates the first run of the sample, red is the second and purple is the third and final repeat of the sample on the nanoparticle tracking analysis instrument.....	91
Figure 4.8: Size distribution and particle concentration of indomethacin in the a) Minimum, b) Q1, c) Median, d) Q3, e) Maximum and f) Biorelevant media, where the black line indicates the first run of the sample, red is the second and purple is the third and final repeat of the sample on the nanoparticle tracking analysis instrument.....	93
Figure 4.9: Size distribution and particle concentration of phenytoin in the a) Minimum, b) Q1, c) Median, d) Q3, e) Maximum and f) Biorelevant media, where the black line indicates the first run of the sample, red is the second and purple is the third and final repeat of the sample on the nanoparticle tracking analysis instrument.....	94
Figure 4.10: Size distribution and particle concentration of felodipine in the a) Minimum, b) Q1, c) Median, d) Q3, e) Maximum and f) Biorelevant media, where the black line indicates the first run of the sample, red is the second and purple is the third and final repeat of the sample on the nanoparticle tracking analysis instrument.....	95
Figure 4.11: Size distribution and particle concentration of fenofibrate in the a) Minimum, b) Q1, c) Median, d) Q3, e) Maximum and f) Biorelevant media, where the black line indicates the first run of the sample, red is the second and purple is the third and final repeat of the sample on the nanoparticle tracking analysis instrument.....	96
Figure 4.12: Size distribution and particle concentration of griseofulvin in the a) Minimum, b) Q1, c) Median, d) Q3, e) Maximum and f) Biorelevant media, where the black line indicates the first run of the sample, red is the second and purple is the third and final repeat of the sample on the nanoparticle tracking analysis instrument.....	98
Figure 4.13: Size distribution and particle concentration of carvedilol in the a) Minimum, b) Q1, c) Median, d) Q3, e) Maximum and f) Biorelevant media, where the black line indicates the first run of the sample, red is the second and purple is the third and final repeat of the sample on the nanoparticle tracking analysis instrument.....	99
Figure 4.14: Size distribution and particle concentration of tadalafil in the a) Minimum, b) Q1, c) Median, d) Q3, e) Maximum and f) Biorelevant media, where the black line indicates the first run of the sample, red is the second and purple is the third and final repeat of the sample on the nanoparticle tracking analysis instrument.....	100
Figure 4.15: Modal size distributions, measured by NTA, of SIF media with and without drugs	101

Figure 4.16: Plot of solubility and particle size measured by nanoparticle tracking analysis of a) naproxen b) indomethacin c) phenytoin d) felodipine e) fenofibrate f) griseofulvin g) carvedilol h) tadalafil in each of the SIF media.....	103
Figure 4.17: NTA and DLS size measurements taken of a) Fresh blank and b) Blank 24 hours in the suite of FaSSIF SIF. Blue points represent NTA data while red points represent DLS data	105
Figure 4.18: NTA and DLS size measurements taken of a) Naproxen, b) Indomethacin and c) Phenytoin in the suite of FaSSIF SIF. Blue points represent NTA data while red points represent DLS data	106
Figure 4.19: NTA and DLS size measurements taken of the neutral drugs, a) Felodipine, b) Fenofibrate and c) Griseofulvin in the suite of FaSSIF SIF. Blue points represent NTA data while red points represent DLS data	107
Figure 4.20: NTA and DLS size measurements taken of the basic drugs, a) Carvedilol and b) Tadalafil in the suite of FaSSIF SIF. Blue points represent NTA data while red points represent DLS data	108
Figure 5.1: Overview of SAXS process, adapted from Reference ¹⁰² . Created with Biorender.com	112
Figure 5.2: Xenocs Xeuss 3.0 LabSAXS instrument at the Diamond Light Source, UK ¹¹³	113
Figure 5.3: Sample holder containing samples for SAXS analysis	118
Figure 5.4: The first step of the powder calibration; identifying the rings of AgBeh.....	119
Figure 5.5: Calibration of AgBeh at 1000 mm. a) AgBeh showing one of the rings clearly, b) AgBeh once the software has identified the rings.....	120
Figure 5.6: Output of the powder calibration check of AgBeh at 4600 mm.....	120
Figure 5.7: Azimuthal integration of a deionised water sample to identify the suitability of the calibration output, the peak at 0 Q indicates that the calibration is satisfactory.....	121
Figure 5.8: Mask used for the data processing step, the bright green areas mask any defective pixels and the regions between detector modules	122
Figure 5.9: 1D output of deionised water, without a mask file applied to enable identification of inflection point. Measured at 1000 mm	123
Figure 5.10: 1D output with calibration, with mask, log scale on both axis (mask hides the dead pixels, takes away the noise)	123
Figure 5.11: Processing pipeline operations for the processing of SAXS data.....	124
Figure 5.12: Comparison between the SIF background (blue) and the drug free Q1 SIF sample (red) measured at 4600 mm.....	126
Figure 5.13: Comparison of biorelevant FaSSIF with a background and a water sample. Biorelevant FaSSIF buffer and water background (red), biorelevant FaSSIF sample (blue) and deionised water (green). Measured at 4600 mm	127
Figure 5.14: Comparison of SIF background samples, both recorded at 4600 mm. Blue – measured on Thursday morning, red – measured on Thursday evening	127

Figure 5.15: Comparison between empty capillary (blue), deionised water background (red) and SIF background (green). Measured at 1000 mm	128
Figure 5.16: Comparison between SIF background (blue), drug free minimum SIF sample (red) and minimum SIF sample with naproxen (green). Measured at 4600 mm	129
Figure 5.17: Comparison of SAXS output between SIF background (blue), and drug free SIF samples; minimum SIF (red), Q1 SIF (green), median SIF (black) and maximum SIF (purple). Measured at 1000 mm.....	130
Figure 5.18: Output of subtracted SAXS data of naproxen SIF samples; minimum SIF (blue), Q1 SIF (red) and median SIF (green). Measured at 4600 mm	130
Figure 5.19: Outputs of subtracted SAXS data; SIF background (blue), drug free minimum SIF (red), naproxen and minimum SIF sample (green). Measured at 1000 mm	131
Figure 5.20: Output of subtracted SAXS data of naproxen SIF samples; minimum SIF (blue), Q1 SIF (red), median SIF (green), biorelevant FaSSIF (black). Measured at 1000 mm	132
Figure 6.1: Number of calculated drug molecules per micelle for each drug in each of the six simulated intestinal fluid media. Red symbols indicate acidic drug data points, green are neutral drug data points and blue are basic drug data points	147
Figure 6.2: Example of a coarse-grained representation of a molecular structure. Based on figures and molecules from Parrow <i>et al.</i> ⁴⁹	155

List of Tables

Table 1.1: Fasted state simulated intestinal fluid compositions and physicochemical characteristics.....	13
Table 1.2: Fed state simulated intestinal fluid composition and physicochemical characteristics	15
Table 2.1: Physicochemical properties and molecular structures of drugs	26
Table 2.2: Molecular weight for each substance used.....	28
Table 2.3: Final concentration of components in the simulated intestinal fluids ²⁶	29
Table 2.4: Preparation of stock components, mass used to create 15 x stock solution	30
Table 2.5: Gradient method used for HPLC analysis	31
Table 2.6: HPLC conditions for each drug material.....	32
Table 2.7: Limit of detection and limit of quantification values calculated for each drug.....	34
Table 2.8: Mean solubility values (μM) of drugs analysed in fasted state simulated media \pm standard deviation, measured by HPLC	39
Table 2.9: Overview of drug solubility in fasted state simulated intestinal fluid, as reported in literature ^{60, 61}	41
Table 2.10: Degree of drug ionisation of acidic and basic drugs analysed, calculated from reported pKa values and pH of SIF media ^{53, 56}	46
Table 3.1: Particle Size Analysis by DLS size \pm standard deviation (intensity dist. d, nm)	53
Table 3.2: PDI values for each of the nine measurements recorded in the minimum SIF.....	56
Table 3.3: PDI values for each of the nine measurements recorded in the Q1 SIF	56
Table 3.4: PDI values for each of the nine measurements recorded in the median SIF	57
Table 3.5: PDI values for each of the nine measurements recorded in the Q3 SIF	57
Table 3.6: PDI values for each of the nine measurements recorded in the maximum SIF	58
Table 3.7: PDI values for each of the nine measurements recorded in the biorelevant SIF.....	58
Table 4.1: Sample dilutions prior to analysis by NTA	78
Table 4.2: Particle size analysis by NTA mean of the modal distribution \pm standard deviation (nm)	80
Table 4.3: Sample information and results of nanoparticle tracking analysis, including modal particle size measured, as well as calculated span and particle concentration (particles/mL) for blank and drug samples in biorelevant FaSSIF media.....	81
Table 4.4: Sample information and results of nanoparticle tracking analysis, including modal particle size measured, as well as calculated span and particle concentration (particles/mL) for blank and drug samples in minimum FaSSIF media.....	82
Table 4.5: Sample information and results of nanoparticle tracking analysis, including modal particle size measured, as well as calculated span and particle concentration (particles/mL) for blank and drug samples in Q1 FaSSIF media	83

Table 4.6: Sample information and results of nanoparticle tracking analysis, including modal particle size measured, as well as calculated span and particle concentration (particles/mL) for blank and drug samples in median FaSSIF media	84
Table 4.7: Sample information and results of nanoparticle tracking analysis, including modal particle size measured, as well as calculated span and particle concentration (particles/mL) for blank and drug samples in Q3 FaSSIF media	85
Table 4.8: Sample information and results of nanoparticle tracking analysis, including modal particle size measured, as well as calculated span and particle concentration (particles/mL) for blank and drug samples in maximum FaSSIF media	86
Table 5.1: Calibration information	121
Table 5.2: Subtracted frame summary.....	125
Table 6.1: Composition of FeSSGF and FeSSIF V2 as reported in Jamil <i>et al.</i> ⁴⁴	136
Table 6.2: Values used in example calculation for the calculation of number of drug molecules per micelle of naproxen in the minimum FaSSIF media.....	141
Table 6.3: Estimated number of drug molecules per mixed micelle	142
Table 6.4: Aqueous drug solubility values, sourced from literature	143
Table 6.5: Drug solubilities in FaSSIF, micelle size and stoichiometric calculations.....	144
Table 6.6: Calculated solubility enhancement values (-fold)	146
Table 6.7: Parameters used in the calculation of number of griseofulvin molecules per micelle of FaSSIF V1 and V2.....	149

Abbreviations

ADME	Absorption, Distribution, Metabolism, Excretion	GI	Gastrointestinal
AgBeh	Silver Behenate	HIF	Human Intestinal Fluid
API(s)	Active Pharmaceutical Ingredient(s)	HPLC	High Performance Liquid Chromatography
BCS	Biopharmaceutics Classification System	MD	Molecular Dynamics
CMC	Critical Micelle Concentration	NTA	Nanoparticle Tracking Analysis
Cryo-EM	Cryo-Electron Microscopy	SAXS	Small Angle X-Ray Scattering
DLS	Dynamic Light Scattering	SIF	Simulated Intestinal Fluid
FaSSIF	Fasted State Simulated Intestinal Fluid	TAC	Total Amphiphile Concentration
FeSSIF	Fed State Simulated Intestinal Fluid		

Chapter 1

Introduction

1. Introduction

1.1. Biopharmaceutics

Biopharmaceutics is the study of the physical and chemical properties of a drug material and the interaction and availability of this within the human body. It encompasses everything from the route of administration to other factors that affect the rate and measure of drug uptake at the site of action¹. The field has evolved from its introduction in the 1960s into a comprehensive discipline that combines knowledge from various scientific and related fields including chemistry, physiology, anatomy and other physical sciences^{1,2}.

Biopharmaceutics is an important area in the field of healthcare as it plays a vital role in development of new drugs. It is integral to the various phases of clinical trials and testing and an understanding of the field is essential for the design of suitable drug candidates, in addition to the optimisation of drug products to ensure they reach and act effectively at their intended target site¹.

1.1.1. Key Concepts

Biopharmaceutics is closely related to pharmacokinetics, which is also essential to the understanding of how drugs interact with the body. This term refers to the fundamental principles that focus on the life cycle of a drug through the body, which is summarised by the absorption, distribution, metabolism and elimination (ADME) processes. Both biopharmaceutics and pharmacokinetics have a strong overlap in the area of drug absorption; biopharmaceutics, due to the drug formulation and how various parameters including solubility and form influence absorption; pharmacokinetics, which uses data from the absorption process to alter the pharmacokinetic profile of a drug which can alter the exposure and hence safety and efficacy¹. This process is critical for achieving systemic drug circulation to underpin an elicited pharmacological response². Both dissolution and solubility play vital roles in the drug delivery and bioavailability of orally administered medications. Dissolution is a kinetic process through which the rate that a drug, or solute, dissolves in a solvent. Solubility is the property of a substance and the ability of a solutes to dissolve into a solvent¹.

1.1.1.1. ADME

The ADME processes describe the movement of a drug within the body, from the site of administration to the elimination or excretion. The first step is the absorption, where a drug must be absorbed across a biological membrane in order to reach the bloodstream for systemic circulation to occur². If the drug

is injected into tissues e.g. intramuscular or taken orally e.g. tablets, this will increase the complexity of the absorption process compared to intravenous administration, as it may have to traverse through multiple membranes prior to diffusing into the bloodstream, compared to that of intravenous drug administration^{1,2}.

Once the drug has reached the bloodstream, it is then able to circulate through the body and can be distributed to body tissues¹. Factors that influence drug distribution include the ability of the drug to diffuse from the blood stream, relative lipophilicity and tissue/plasma protein binding².

Most of the drug that is distributed throughout the body is metabolised in the liver, regardless of the route of administration¹. As the gastrointestinal (GI) tract blood supply is directed via the liver prior to the systemic circulations this first passage through the liver is known as “first pass metabolism” where the most common metabolic pathways are oxidation, reduction and hydrolysis². Structural changes are involved in this process where the a drug is metabolised into various metabolites, which may be physiologically active chemical entities¹. The mechanisms of metabolism are important for detoxifying and eliminating drugs and other foreign materials from the body².

Drugs, both in the unchanged and metabolite forms, are removed from the body via metabolism and excretion, or by a combination of the two mechanisms. This phase of the drugs pharmacokinetic profile are intrinsic to the chemical structure and this is optimised during the drug discovery process².

1.1.1.2. Bioavailability

Bioavailability is a key factor in the effectiveness of medications, as this determines the relative amount of active drug material available in the body in relation to the amount present in the administered dose³.

The bioavailability of a drug is the fraction of administered drug that reaches the systemic circulation in an unchanged form⁴. It also encompasses the rate at which the active substance is absorbed from the administered form and becomes available at the target site in the body³.

The physicochemical properties of a drug material and the route of administration can affect the bioavailability of a drug². The physicochemical and physiological factors that affect the absorption of a drug from the GI following oral administration include: the solubility and dissolution rates within GI luminal fluid; the stability of the drug in the GI milieu, due to parameters such as pH, enzymes and

food interactions; and the ability of the drug to cross the GI absorption barrier, this is further dependent on characteristics including lipophilicity and the partition coefficient¹.

1.1.1.3. Lipinski's Rule of Five

New molecular entities today are typically poorly soluble, lipophilic and larger molecular weight biopharmaceutics classification system (BCS) class II compounds (low solubility, high permeability), which can result in significant issues with achieving adequate exposure/bioavailability⁵. In 1997, Lipinski *et al.* developed a set of guidelines for providing a detailed understanding of the molecular-level characteristics that are present in currently marketed products². According to the rule of 5, an orally active drug is more likely to be successful in the drug discovery setting if there are fewer than 5 hydrogen bond donor groups, fewer than 10 hydrogen bond acceptor groups, the molecular weight of the compound was less than 500 daltons and the calculated logP is less than 5^{1,5}.

A greater quantity of hydrogen bond donors can decrease membrane permeability as a result of the polarity of the compound, likewise, hydrogen bond acceptors also indicate polarity which relates to absorption characteristics. A larger molecular weight of a drug molecule will result in poorer permeability due to the size of the structure. The logP, partition coefficient, is the solubility of a drug in the octanol:aqueous phase, which reflects the relative hydrophilic to lipophilic characteristics of a compound. This value is particularly relevant, as a drug must be soluble in an aqueous system, while an unionised and lipophilic molecule is favoured for membrane permeation. Therefore, a good balance between lipophilicity and hydrophilicity is required¹. The rule of five serves as a useful tool for early drug development, offering an insight into the likelihood of the oral bioavailability of small molecules. It is widely used by pharmaceutical companies to flag compounds with potential solubility and permeability issues^{2,5}.

1.1.2. Biopharmaceutics Classification System

Since its introduction in 1995, the biopharmaceutics classification system (BCS) has been endorsed by regulatory organisations and agencies. It is a tool that aids in pharmaceutical product development and regulatory decisions and is integrated into guidelines for biowaiver granting from organisations such as the European Medicines Agency and the World Health Organisation⁶. Through the understanding of the solubility of a compound in buffered systems and its permeability across biological membranes, the rate limiting factors that regulate the rate and degree of oral drug absorption can be identified. With this information, a prediction can be made of factors that could affect formulation and physiological variables on oral drug bioavailability⁷.

1.1.2.1. Criteria

There are four classes of the BCS which are based on solubility over a pH range and intestinal permeability; each class reflects a distinct expectation of *in vitro-in vivo* correlation. Figure 1.1 shows the four classes of the BCS.

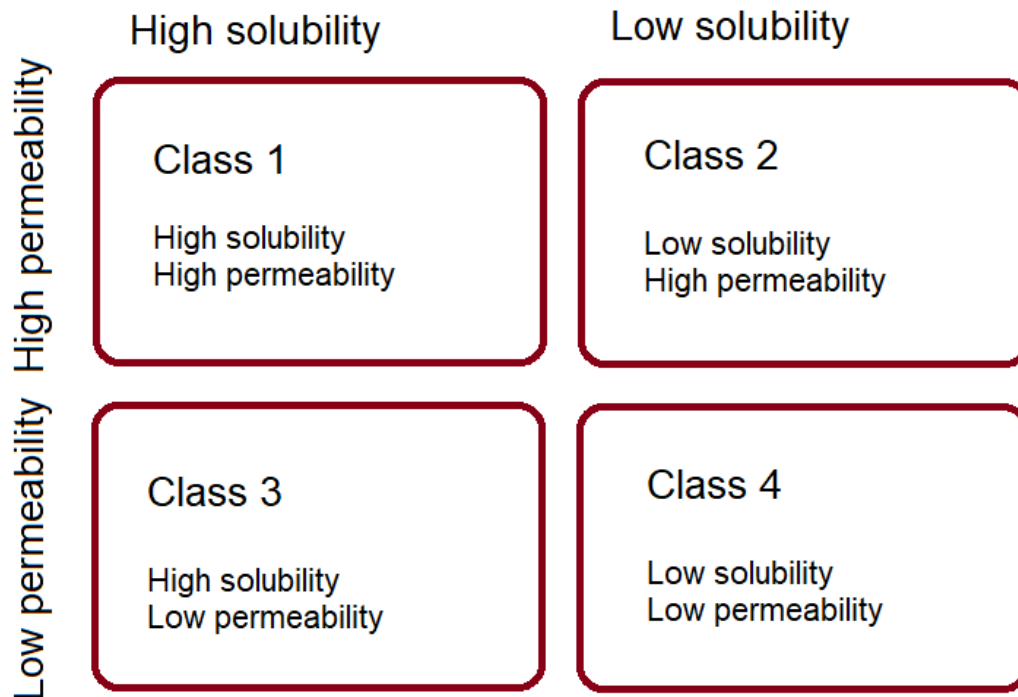


Figure 1.1: The biopharmaceutics classification system, adapted from Reference¹

With the BCS structure of human pharmaceutical materials, drugs can be categorised into one of the four BCS classes:

- Class 1: High solubility, high permeability; these compounds are typically very well absorbed, with gastric emptying generally being the rate-limiting step for absorption
- Class 2: Low solubility, high permeability: these compounds display dissolution rate-limited absorption which may limit the extent of absorption
- Class 3: High solubility, low permeability: these compounds display permeability-limited absorption. Bioavailability can be improved for these drugs by increasing the concentration of drug at the absorptive membrane
- Class 4: Low solubility, low permeability: these compounds are typically not well absorbed and have poor oral bioavailability^{1, 7}

A drug material is classified “highly soluble” if the highest dose strength of the drug can be dissolved in ≤ 250 mL of aqueous media at a pH of between 1.0 and 6.8 and at a temperature of $37\text{ }^{\circ}\text{C} \pm 1\text{ }^{\circ}\text{C}$. The chemical stability of the material must be assured for a time period that includes the last dissolution time point as well as the time needed for the slowest method of analysis⁶. A drug can be considered to have a “high permeability” if the percentage of the drug dose absorbed in humans exceeds 90 % of the dose administered. This is based on work that found a correlation between the human jejunal permeability that was measured using intestinal perfusion and the fraction of the dose absorbed that was collected from pharmacokinetic or mass balance studies⁸.

A drug is “rapidly dissolving” if ≥ 85 % dissolves within 30 minutes (or 15 minutes for “very rapidly dissolving”). For the dissolution testing, standard apparatus is used: apparatus I (basket) at 100 rpm or apparatus II (rotating paddle) at 50 rpm – or 75 rpm if justified – in ≤ 500 mL in each of the following:

- 0.1 M hydrochloric acid or United States Pharmacopeia (USP) specified simulated gastric fluid without enzymes
- pH 4.5 buffer
- pH 6.8 buffer or USP specified simulated intestinal fluid without enzymes

The primary objectives of the classification system is to advance the effectiveness of drug development, enable prediction of *in vivo* pharmacokinetic performance of drug material from measurements of permeability and solubility, and also to aid in formulation design⁶.

1.2. Solubility

Solubility is a measurement for the quantity of substance that can remain in a solvent without precipitation. The solubility of a solute is defined as the analytical measure of its amount in a saturated solution with a designated solvent. Solubility can be represented as concentration, molality and mole fraction, among others^{1, 9}. Typically, in the field of biopharmaceutics, the solute is the drug/active pharmaceutical ingredient (API), while the solvent is variable depending on the target location¹. It is one of the most important and frequently studied characteristics within biopharmaceutics². Equilibrium solubility is the maximum amount of solute that can be dissolved in a solvent when the system reaches equilibrium, while the transient solubility is a temporary solubility that exceeds that of equilibrium solubility but is not stable over time. Transient solubility can occur under certain conditions such as where a solubility enhancing excipient is used¹. Thermodynamic solubility can be defined as the maximum concentration of a compound in solution at equilibrium with its most stable crystalline form

while kinetic solubility can be defined as the concentration at which the substance starts to precipitate when an organic solvent (typically DMSO – dimethyl sulfoxide – is used) is introduced into a buffer solution¹⁰.

1.2.1. Factors Affecting Solubility

A good understanding of the factors affecting solubility is important to address strategies for a drug product formulation which may be required as a result of poor drug solubility². Factors that affect drug solubility include fluid composition, pH and temperature¹. The particle size of the drug also influences the rate of dissolution and transient solubility, as the particle size decreases, the ratio of surface area to volume increases, while greater surface area permits an increased interaction with the solvent, leading to an increased dissolution rate¹¹. The molecular structure of a drug molecule affects solubility as the structure directly determines properties such as the lipophilicity and hydrogen bonding, among others¹.

1.2.2. Forces Involved in Solubility

Solubility involves various intermolecular forces between the solute, the solvent and other solute molecules which will determine how well a solute will dissolve in a solvent. The key forces that are involved in aqueous solubility are hydrogen bonding, Van der Waals and ionic interactions¹.

Hydrogen bonding is a type of dipole-dipole interaction between molecules. This bonding arises from the attractive forces between a hydrogen atom that is covalently bonded to a nitrogen, oxygen or fluorine (i.e. a very electronegative) atom¹². Hydrogen bonding occurs in aqueous media and the ability of a drug to take part in this type of bonding can be determined by the chemical structure of the molecule¹.

Van der Waals forces are another type of interaction that is a result of temporary fluctuations in electron density around atoms and molecules. This leads to the structure having a polarity which results in weak attractions between molecules, where the positive region of one molecule will be positioned near the negative region of another. Although weak, these forces have a considerable effect on solubility as compounds with a similar polarity i.e. both polar or both nonpolar will mix, and those that are mixed i.e. polar/nonpolar combination will not mix. This is the “like dissolves like” rule^{1, 13}.

1.2.3. pH, Drug Solubility and Lipophilicity

A large number of drugs are weak acids or bases, where the solubility of these ionisable compounds is greatly influenced by the pH of the solvent¹. A weak acid can be defined as a neutral molecule that has the ability to reversibly dissociate into a negatively charged ion (anion) and a proton, while a weak base can be defined to be a neutral molecule that can become a positively charged ion (cation) by accepting a proton¹⁴.

The preparation of salt forms is a technique used by the pharmaceutical industry to increase the aqueous solubility of a drug as the salt of an acid or base, typically has a greater solubility than that of the corresponding free drug¹⁵. A salt is an ionic compound, where ionic interactions will arise between ions of opposite charges¹². These forces will increase the solubility of a drug by promoting stronger interactions between the ions of the salt and the polar water molecules¹⁵.

The strength of a weak acid is determined by the pKa value which is equivalent to the pH of the solution where the concentrations of both the protonated and unprotonated forms are equal. The degree of ionisation of a weakly acidic drug is dependent on the pH in relation to the pKa value. The greater the pKa value, the weaker the acid¹². When the pH of the environment is lower than the pKa of the acidic drug, the nonionised/unprotonated form is favoured which will result in the drug being less water soluble but being more lipid soluble^{12, 14}. The unprotonated form of a weak base is the neutral form, this is favoured when the environmental pH is greater than that of the drug's pKa¹⁴.

Acetylsalicylic acid, commonly known as aspirin, is a weak carboxylic acid with a pKa of 3.5. In the acidic environment of the stomach, where the pH is 2, the majority of this drug is in the nonionised, unprotonated form. As it enters the more neutral environment of the small intestine¹², where the pH increases to around pH 6 in the duodenum¹⁶, most of the drug will then be in the ionised form¹². Codeine is a weak base with a pKa value of 7.9. It is nearly fully in the ionised form in the stomach (pH 2)¹⁷.

The ionised form of a drug is more water soluble than the nonionised form as the charged molecules interact more effectively with water through electrostatic and intermolecular interactions. The nonionised, or neutral, form of a drug is a more lipophilic form. This allows the drug to permeate through lipid-rich membranes by passive diffusion².

The lipophilicity of a drug has a considerable role in its solubility characteristics. This is described by the partition coefficient, $\log P$, which is the ratio of the concentration, at equilibrium, of the nonionised compound, between the organic and aqueous phases¹. A higher partition coefficient will indicate high lipophilic properties of a drug, while for hydrophobic and polar drugs, this is the rate-limiting step for drug absorption¹⁸.

1.3. Dissolution

Dissolution is the process in which a drug material dissolves in a solvent to form a solution. It is an important technique in oral biopharmaceutics to predict bioavailability¹. For orally administered solid drugs, dissolution occurs in the stomach and/or small intestine, following gastric emptying and intestinal transit flow. Dissolution will be the rate-limiting step if the process is slow in comparison to the GI transit². Dissolution testing is a crucial step in the formulation of drug products as it supplies information on the rate and extent of drug release under a fixed set of conditions. For poorly soluble drugs, this process can directly impact the pharmacokinetics and is also essential for sustained release formulations in which the controlled rate of drug released from the dosage form determines the amount of drug in solution that is available for absorption¹.

1.3.1. Dissolution and Solubility

Drug compounds that possess high solubility typically have higher dissolution rates. The solubility of weak acids and weak bases depends on the pH of the solvent and the pKa of the drug, so it is essential to measure the aqueous solubility of the drug over the pH range that is found in the body to predict the effect of solubility on dissolution². The process of dissolution starts with a fast increase in the solubilised drug as a result of the concentration gradient that occurs between the solute and solvent. The rate of dissolution will decrease as the solvent nears saturation with the solute and will continue to decrease until it plateaus at the equilibrium solubility, which is the term used for a stable solubility equilibrium^{1, 2}.

1.4. Physiology of the Gastrointestinal Tract

1.4.1. Stomach

The stomach is located between the oesophagus and the small intestine. It is a large hollow organ with the capacity to hold a maximum of 2 to 3 litres of food. The function of the stomach is as a reservoir

for food with the later regions controlling mixing and emptying. The stomach fluid composition in the fasted state contains saliva, gastric secretions such as hydrochloric acid and digestive enzymes, as well as food and refluxed fluids from the duodenum (the first region of the small intestine). The pH of gastric fluid in the fasted state is generally in the acidic region of pH 2-3, although this can fluctuate intra- and inter-individually. Post prandial, the pH typically varies between an increased range of pH 3 to pH 7^{1, 19}.

1.4.2. Small Intestine

The human small intestine is a long, narrow tube, approximately 2-8 m long (in adults) which extends from the stomach to the large intestine. It is divided into three regions, the duodenum, the jejunum and the ileum. The duodenum is the first section of the small intestine and is the smallest at around 25-30 cm and roughly 5 % of the total length of the small intestine. In the fasted state the duodenum has a pH in the range between 5.6 and 7.0, decreasing to around 4.8 to 6.5 in the fed state^{1, 2, 20}. The jejunum is the middle region of the small intestine, which is around 2.5 m in length. The pH of this section is slightly higher than that of the duodenum, with a mean pH value in the fasted state to be 7.5, decreasing to 6.1 in the fed state. The last region of the small intestine is the ileum, which is approximately 3 m long and around 45 % of the total length of the small intestine. In the fasted state, the mean pH of this region is 6.5, while in the fed state, a pH of 7.5 has been reported^{1, 2}. The main function of the small intestine is to facilitate the digestion and absorption processes. The role of the duodenum is to receive the chyme (food and gastric acid) from the stomach, which is then broken down by pancreatic enzymes. The duodenum is also the primary dietary iron absorption location. The role of the jejunum is mainly absorption of carbohydrates, amino acids and fatty acids while the ileum absorbs vitamin B12 and bile acids²⁰.

1.4.3. Large Intestine

The first section of the large intestine, the caecum, is connected to the ileum of the small intestine by the ileo-caecal sphincter. The large intestine is roughly 1.5 m in length and is separated into four regions; caecum, colon, rectum and anal canal. The colon is composed of four sections which are the ascending colon, the transverse colon, the descending colon and the sigmoid colon. In the fasted state, the pH of the large intestine is 7.8 in the ascending colon which decreases to a pH of around 6 in the fed state^{1, 21}. The functions of the large intestine are to absorb water and electrolytes and to produce and store faeces prior to elimination^{1, 21}.

1.5. Human Intestinal Fluid

Human gastrointestinal fluid located within the GI tract governs the intraluminal environment²². Primarily consisting of water, this highlights the importance of oral drug solubility²³. Other components within this fluid, such as bile salts, lipids, enzymes, proteins, cholesterol and electrolytes increase the complexity of the system²⁴. The fluid is essential for food digestion, as well as nutrient and drug absorption²⁵.

1.5.1. Sample Collection

The collection of human intestinal fluid (HIF) samples is an intricate and invasive procedure that requires oral intubation using a nasojejun tube. A double-lumen catheter is inserted into the nose or mouth and is placed near the ligament of treitz²⁶, which is a band of tissue that supports and connect the duodenum to the jejunum, separating the upper and low GI tracts²⁷. The sampling process restricts the volumes available for sampling and clinical studies using this method require ethical approval^{26,28}.

Although HIF is the most appropriate fluid in which to perform *in vitro* studies, there are many limitations associated with this, including practicality and difficulty acquiring samples from patients. It is not realistic to obtain the large sample volumes required for larger scale drug development studies and the variability in composition that is inherent to this type of sample would be unreliable. Therefore, simulated intestinal fluid (SIF) was developed to provide a way to assuage the issues associated with HIF availability and variability^{29,30}.

1.6. Simulated Intestinal Fluid

In order to measure the solubility of poorly soluble drugs *in vitro*, simulated intestinal fluid (SIF) is used in place of human intestinal fluid (HIF)²⁸. Typically, a single fasted state simulated intestinal fluid (FaSSIF) is used^{31,32}, which reflects average compositions of HIF rather than the full extent of variability in composition previously reported²⁶.

There are many factors that affect the dissolution of a drug in the gastrointestinal environment, some are due to the physicochemical properties of the drug and the composition of the dosage form, but some are heavily influenced by the contents of the gastrointestinal tract. Fat levels and the concentration of bile salt are the most significant elements for lipophilic drugs while pH and buffer capacity are more pertinent to ionisable drugs. These parameters are less important for highly soluble

drugs but they can be vital in limiting drug release and bioavailability of formulations containing poorly soluble and/or ionisable drugs. Therefore, when using a media for predicting the *in vivo* dissolution rate based on *in vitro* data, all parameters that could potentially influence drug release from the drug material should be sufficiently simulated³³.

To mirror the human gastrointestinal tract, various media have been designed to simulate the gastric liquid, small intestinal and colonic fluids under pre- and postprandial conditions. These include fasted/fed state simulated gastric fluid (FaSSGF, FeSSGF), fasted/fed state simulated intestinal fluid (FaSSIF, FeSSIF) and fasted/fed state simulated colonic fluid (FaSSCoF and FeSSCoF)³⁴. The first biorelevant media made to simulate intestinal fluid in the fasted and fed state (FaSSIF and FeSSIF, respectively) were introduced in 1998 by Dressman *et al.*³¹ and Galia *et al.*³²

More recently, researchers have created new SIF recipes that are based on the parameter “(pH × [TAC])” where this is the concentration of pH multiplied by the total amphiphile concentration (TAC) present in HIF. This is used in studies which research drug solubility in intestinal fluids as it combines pH with TAC – two important factors that influence drug solubilisation^{24, 35, 36}. As discussed, pH has a critical role on the ionisation state of drug which, therefore, affects their solubility. Weak acids and bases are generally pH dependent². TAC is an indication of the solubilising capacity; this represents the ability of the components e.g. bile salts and phospholipids that are able to form micelles which are then able to solubilise lipophilic drugs. By combining these two factors into one key parameter, this allows the comparison and modelling of drug solubility under conditions that better represent the variable environment of the intestine.

1.6.1. Fasted State Simulated Intestinal Fluid

1.6.1.1. Compositions of Media

Fasted state simulated intestinal fluid (FaSSIF) biorelevant media, which are simulated intestinal fluids, were first created by Galia *et al.* in 1998. These media were designed to closely reflect *in vivo* pH conditions and include biological components e.g. bile salt and phospholipids to simulate the composition and behaviour of actual intestinal fluids in both the fasted and fed state³². Successive work has refined and expanded the initial formulation, with the aim to optimise the composition of the media. The compositions of the various FaSSIF recipes can be found in Table 1.1³⁰.

Table 1.1: Fasted state simulated intestinal fluid compositions and physicochemical characteristics

Component		FaSSIF V1 – Galia 1998 ³²	FaSSIF V2 – Jantratid 2008 ³⁷	FaSSIF V2 plus – Psachoulias 2012 ³⁸	FaSSIF V3 – Fuchs 2015 ³⁴
Bile salt	Na taurocholate (mM)	3	3	3	1.4
	Na glycocholate (mM)	-	-	-	1.4
Phospholipid	Lecithin (mM)	0.75	0.2	0.2	0.035
	Lysolecithin (mM)	-	-	-	0.315
Free fatty acid	Na Oleate (mM)	-	-	0.5	0.315
Cholesterol (mM)		-	-	0.2	0.2
Base	NaOH (mM)	10.5	34.8	34.8	16.56
Salt	NaCl (mM)	105.85	68.62	68.62	93.3
Buffer	KH ₂ PO ₄ (mM)	28.65	-	-	-
	Maleic acid (mM)	-	19.12	19.12	10.26
pH		6.5	6.5	6.5	6.7 ± 0.05
Osmolality (mOsmol kg ⁻¹)		270 ± 10	180 ± 10	180 ± 10	220 ± 10

The first FaSSIF formulation was partially based on available data simulating the conditions in the proximal small intestine from literature and studies that were carried out at the University of Michigan and partially based on the buffer capacities that were measured in a fistulated dog model. Each subsequent version of FaSSIF has improved upon the original by better capturing the variability and complexity of human intestinal fluids. FaSSIF V2, published by Jantratid *et al.* in 2008, modified the bile salt and phospholipid concentrations to more closely align with the values measured in HIF³⁷. The switch from the salt potassium chloride to sodium chloride better represents the ionic composition of HIF, where sodium ions are more prevalent than potassium ions³⁹. The change from the phosphate buffer to maleic acid was to improve the buffering capacity as the maleate buffer can maintain a stable pH range from 5.4 to 6.5, which is suitable for both fasted and fed state fluid, without surpassing the normal physiological osmolarity³⁷. FaSSIF V2 plus, created by Psachoulias *et al.* builds upon version 2

through the incorporation of additional surfactants and lipids, specifically free fatty acid (sodium oleate) and cholesterol. This aids in simulating the lipid diversity observed in intestinal fluid and through the addition of these components, this version of FaSSIF provides a better model in which to study the solubility and absorption of lipophilic compounds that interact with fats³⁸. Finally, the most recent version of FaSSIF, V3, was published in 2015 by Fuchs *et al.* with several adjustments to previous recipes. This fluid includes modified bile salt and phospholipid ratios that reflect updated clinical studies of HIF composition. The addition of sodium glycocholate and lysolecithin are to enhance the physiological relevance of the media by incorporating more components that are naturally present in HIF. Lysolecithin and sodium oleate are hydrolysis products of lecithin and are found a few minutes post biliary secretion in the human duodenum. The increased components have the potential to better reflect HIF composition while simultaneously improving the predictive accuracy for drug solubility and absorption by providing a more realistic micellar environment and increasing lipid diversity reflective of that observed in the small intestine³⁴.

1.6.1.2. Components in SIF and Colloidal Structures Formed Within SIF

Bile salts and lecithin promote the wetting of solid material and the solubilisation of lipophilic drugs into mixed micelles. Sodium taurocholate was selected as a model bile salt as cholic acid, found in human bile and the taurine conjugate has a low pKa value. Therefore, it is unlikely that there will be precipitation or alteration of micelle size due to small variations in pH value. An ideal bile salt concentration for simulating the fasted state is between 3 and 5 mM. Lecithin exists *in vivo* at a ratio between 1:2 and 1:5 with bile salt, so a suitable ratio to simulate this is 1:3 (lecithin: bile salt). A phosphate buffer is used in place of bicarbonate – the physiological buffer – as this would result in a pH fluctuation due to the instability of bicarbonate buffers in standard laboratory conditions³¹.

Bile acids are predominantly found in the bile and are steroidal biological amphiphiles. Derived from cholesterol in the liver, they are then stored in the gallbladder and secreted into the duodenum after food intake. Bile salts are generally hydroxyl derivatives of 5 β -cholanoic acid and have a hydrophobic steroidal skeleton with a hydrophilic face that contains an ionisable carboxyl (unconjugated or glycine-conjugated) or sulfonyl (taurine-conjugated) groups in the molecular structure^{40, 41}. The stereochemistry provide the biological and physicochemical properties of each salt⁴⁰. Typically, sodium taurocholate is used as the bile salt in SIF media, despite the knowledge that there are many different types of bile acids present in HIF e.g. glycocholic acid and taurochenodeoxycholic acid^{26, 30-32}.

Lecithin, a phospholipid surfactant, forms bilayers in water. With the addition of bile salts, the phospholipid bilayers are altered to cylindrical micelles in which the bile salts bind with the lecithin headgroups in a back-to-back formation. The bile salt creates the hemispherical endcaps of the micelles and the hydroxyl groups will hydrogen bond to the phosphates of the lipid therefore providing an increased stability. The hydrophobic face is also protected while the carboxylate or sulfonate groups are exposed to the water⁴⁰. Long *et al.* characterised lecithin and taurodeoxycholate mixed micelles by small-angle neutron scattering and dynamic light scattering and found cylindrical micelles formed. At increased concentrations of the hydrophilic bile salt, the micelles transformed to an ellipsoidal shape as the outer shell of the cylinders were more hydrated. In contrast, as the system was diluted, the lecithin tails were more exposed as the bile salt from the endcaps are removed to counteract the intermicellar concentration of monomers. As an equilibrium is formed between the phospholipid-bile salt and micelle body composition, vesicular structures are formed due to the hydrophobic interactions between the non-polar phospholipid tails and the aqueous environment⁴². The interaction of drugs, particularly poorly aqueous solubility drugs, with these colloidal structures may improve their solubility and the extent of improvement will depend upon the composition present and the strength of the drug-colloid interaction.

1.6.2. Fed State Simulated Intestinal Fluid

Biorelevant media to simulate the postprandial conditions in the small intestine, fed state simulated intestinal fluid (FeSSIF), was also introduced by Galia *et al.* in 1998. FeSSIF has higher concentrations of bile salts and lecithin . The composition of FeSSIF is presented in Table 1.2.

Table 1.2: Fed state simulated intestinal fluid composition and physicochemical characteristics

Composition	FeSSIF V1 – Galia 1998 ³²	FeSSIF V2 – Jantratid 2008 ³⁷
Na taurocholate (mM)	15	10
Lecithin (mM)	3.75	2
Sodium oleate (mM)	-	0.8
Glyceryl mono-oleate (mM)	-	5
Ethanoic acid (mM)	144	-
Sodium chloride (mM)	173	125.5
Sodium hydroxide (mM)	101	81.65
Maleic acid (mM)	-	55.02
pH	5	5.8

Composition	FeSSIF V1 – Galia 1998 ³²	FeSSIF V2 – Jantratid 2008 ³⁷
Osmolarity (mOsmol kg ⁻¹)	635	390 ± 10

The key differences between FaSSIF and FeSSIF lies within the concentration of the surfactants and the buffer system used. The higher bile salt and phospholipid concentrations reflect the postprandial increase in bile production and the increased solubilisation capacity required compared to that of the fasted state^{32, 43, 44}. Ethanoic and maleic acid are used in place of the phosphate buffer system to better replicate the more acidic conditions of the fed state. The pH is lower which requires ethanoic and maleic acid to be used in place of the phosphate buffer system which is optimal closer to the neutral pH of the fasted state fluid³⁷. For poorly soluble drugs, the higher bile salt and lecithin concentrations in FeSSIF compared to FaSSIF can enhance dissolution and increase solubility, which explains why some lipophilic drugs exhibit improved absorption in the fed state¹.

1.6.2.1. Limitations of SIFs

SIF are widely used for assessing drug solubility *in vitro* and predicting the *in vivo* performance of drug materials¹. However, despite this, SIFs have several limitations in fully representing the complex and dynamic environment of the human GI tract. Two major limitations of the fluid include the static nature of the system and the lack of compositional variability. The GI tract is a dynamic system, where *in vivo*, the composition of SIF is constantly changing in response to various factors e.g. pH fluctuations and food intake, moving throughout the tract²⁴. The pH of the small intestine alone steadily increases from pH 6.0 to around pH 7.4 in the terminal ileum¹⁶. While such changes impact the solubility and absorption of drugs, SIFs such as FaSSIF and FeSSIF remain at a fixed composition³². This relates to another limitation of the fluid, the absence of compositional variability. FaSSIF was created composed of mean values from literature and studies conducted in 1998³², but the composition of HIF is known to change considerably between individuals in addition to other day to day fluctuations resulting in intrasubject variability²⁶. Other factors, including age and disease will influence the composition and functionality of gastrointestinal fluids, which directly affect intestinal absorption and immune functions⁴⁵.

1.7. Critical Micelle Concentration and Micelle Formation

Surfactants are amphiphilic molecules that contain both non-polar (hydrophobic) and polar (hydrophilic) regions and will self-assemble into colloidal structures when they are dissolved in aqueous solutions at concentrations above their critical micelle concentration (CMC)¹. Below the CMC,

surfactant molecules will primarily exist as individual molecules and above this concentration, they will agglomerate with other molecules to form micelles. The addition of the surfactant decreases the interfacial energy and removes the contact between the hydrophobic groups and water⁴⁶.

Micelles used in drug delivery are created by water-soluble amphiphilic surfactants which gives them the ability to solubilise hydrophobic drug molecules that are poorly soluble in water. The structure and behaviour of these entities have been extensively studied and large-scale manufacture of drug solutions stabilised by micelles can be achieved. In a dilute environment all normal micelles that are not chemically cross-linked will be broken down into free surfactants. Below the CMC, there will be a loss of micelle structure so the drug loaded into the micelle that was stabilised in the hydrophobic area of the core will become insoluble which in turn can alter the bioavailability and therapeutic efficacy of the drug material⁴⁷.

The solubility of poorly soluble drugs can be improved through the use of surfactants such as bile salts and phospholipids. In biorelevant fluids, these surfactants will form colloidal structures e.g. micelles above the CMC of the surfactant that are structures with a hydrophobic core and a hydrophilic outer shell⁴. The solubilities of hydrophobic drugs in aqueous solutions can be increased considerably which will result in an increased bioavailability⁴⁸.

1.7.1. Micelles and Simulated Intestinal Fluid

A study carried out by Ottaviani *et al.* investigated the importance of CMC for the prediction of solubility enhancement in biorelevant media (FaSSIF V1 and FeSSIF V1). A total of 51 compounds with diverse chemical properties were analysed using HPLC-UV-MS to determine equilibrium solubility and a tensiometer was used to determine surface activity. Physicochemical parameters, including pKa, and lipophilicity were also studied in order to determine their correlations with solubility enhancement. It was found that pure compounds with lower CMC values (those that form micelles more readily) showed a greater ability to be solubilised in FaSSIF colloidal structures while drugs with a high or no CMC presented with negligible solubility enhancements in FaSSIF. This indicates that the integration of the compound into the biorelevant micellar structure is essential for solubilisation and hydrophobicity alone cannot fully predict the solubility enhancement.

The work presented in this thesis differs from this study by Ottaviani *et al.*, which focused on using CMC as a predictive tool for solubility enhancement in FaSSIF media. This thesis explores how the composition and physical properties of colloidal structures affect the solubility of poorly water soluble

BCS class II drugs. A key advancement lies in the development and use of a suite of SIFs that more accurately reflects the variability observed in human intestinal fluids, rather than relying on a single standard formulation. This study is the first in reported literature that applies nanoparticle tracking analysis (NTA) to characterise colloidal structures in these fluids which offer a new insight beyond conventional dynamic light scattering (DLS). By using both DLS and NTA it is revealed that solubility does not simply correlate with particle size, but rather with a combination of factors including total amphiphile concentration ([TAC]), colloidal density and drug/media interactions.

Structural analysis using small angle X-ray scattering (SAXS) analysis of sodium taurodeoxycholate bile salt micelles and bile salt/phospholipid mixed micelle solutions revealed consistent oblate ellipsoidal structures⁴¹. The data generated from the SAXS for these micelles was able to be modelled as monodisperse units which indicates a high degree of regularity between the structures. As the concentration of the bile salt was altered, the size of the micelles formed did not significantly change which was thought to be due to the deuterated water used which would result in weaker intermolecular interactions and different micellar aggregation properties. Sodium taurocholate and lecithin SIF displayed polydisperse structures that were determined to be vesicles rather than dense micelles. In particular, the scattering profile of FaSSIF revealed large vesicular structures with thick bilayer membranes of ~ 40 Å. Analysis at higher lipid concentrations, such as those of FeSSIF, revealed “rod/worm-like” micelles which evolved to vesicles at the lower lipid concentrations, as those recognised in FaSSIF media⁴¹.

The solubility of different compounds in HIF is associated with the colloidal structures that form by the various components in the intestinal fluid, e.g. micelles and vesicles of diverse morphologies⁴⁹. Due to the complex nature of HIF and SIF and the various structures that form based on fluid composition, it is currently not possible to simply predict the degree of solubility change with changing media.

A study analysing the biorelevant FaSSIF versions 1, 2 and 3 used cryogenic transmission electron microscopy to identify the colloidal structures present in each media. In FaSSIF V1 various vesicles and micelles were found as well as agglomerates of micelles. In FaSSIF V2, vesicles and micelles were detected with the most frequent form found was the thread-like micelle. The most common structure identified in the FaSSIF V3 media was the disc shaped micelle, with other globular micelles and vesicles also present in the sample. The data showed that as the composition of the media were altered, the particle size and shapes of the colloidal structures formed were also altered⁵⁰. The colloidal structures of FaSSIF V3 are different to those of versions 1 and 2 as a result of the different composition of FaSSIF

V3 as it includes addition components, such as glycocholate, lysophosphatidylcholine and sodium oleate³⁴. Both unilamellar and multilamellar vesicles were observed in samples of all three fasted state media⁵⁰.

Although some progress has been made in the area, there is still a need to understand the composition-structure-solubility relationship for SIF to better understand solubility enhancement that will occur for some drugs within HIF, compared to that of a simple buffer system.

1.8. Outline of Thesis

The overall aim of this research is to work towards a better understanding of the colloidal structures formed in simulated intestinal fluid. In the intestinal environment, colloidal structures form such as micelles and vesicles between a drug and other components present in the intestinal fluid. These structures formed can encapsulate drugs and increase their solubility in the intestinal fluid, leading to improved bioavailability. Limited work in this field has characterised bile salt micelles and some drugs colloids in biorelevant simulated intestinal fluid^{41, 51}. This work will focus on providing a deeper understanding of the relationships between the solubility, amphiphile concentration and the size of colloidal structures formed in simulated intestinal fluid through the design of a new suite of simulated intestinal fluids and the characterisation of drug and drug free samples by solubility and particle size analysis techniques. The main aim can be divided into four experimental chapters and one theoretical chapter which are laid out as follows:

- i. Chapter 2 creates a new suite of simulated intestinal fluid that is reflective of *in vivo* gastrointestinal variability. The solubility of eight biopharmaceutical classification system class II drugs is measured by high performance liquid chromatography and the relationship between solubility and $(\text{pH} \times [\text{TAC}])$ is investigated
- ii. Chapter 3 analyses the size of colloidal structures formed in drug and drug free samples of simulated intestinal fluid by dynamic light scattering to investigate trends relating to solubility and particle size of the colloidal structures formed in the fluids and how this is linked to pH and [TAC] or $(\text{pH} \times [\text{TAC}])$
- iii. Chapter 4 analyses the size of colloidal structures formed in drug and drug free samples of simulated intestinal fluid by nanoparticle tracking analysis to further investigate trends between increasing $(\text{pH} \times [\text{TAC}])$ and drug type (acid/neutral/base). A comparison is included here with the particle size data measured by dynamic light scattering in chapter 3

- iv. Chapter 5 analyses the size of colloidal structures formed in drug and drug free samples of simulated intestinal fluid by small angle X-ray scattering, using the labSAXS beamline at the Diamond Light Source national facility. The data obtained here serves as preliminary data for future synchrotron beamtime applications
- v. Chapter 6 uses a theoretical model to predict the number of drug molecules per micelle. This model uses data experimentally obtained in earlier chapters with the aim of determining the relationship between the particle size of the colloidal structures and the estimated number of drug molecules per micelle
- vi. Chapter 7 provides the outcomes for the thesis and future work directions

Chapter 2

Solubility Analysis of Fasted State Simulated
Intestinal Fluid

2. Solubility Analysis of Fasted State Simulated Intestinal Fluid

2.1. Introduction

Adequate drug solubility in the gastrointestinal (GI) tract is essential for systemic therapy of orally administered medications. In order to measure the solubility of poorly soluble drugs *in vitro*, simulated intestinal fluid (SIF) is used in place of human intestinal fluid (HIF). However, typically fasted state simulated intestinal fluid (FaSSIF) is used^{31, 32} which reflects average compositions of HIF rather than the full extent of variability in composition previously reported²⁶.

2.1.1. Simulated Intestinal Fluid

In order to use a series of SIF that better represents the variability observed in HIF previous work reported by Khadra *et al.* (2015) found that six factors (pH, sodium taurocholate, lecithin, sodium phosphate, sodium chloride and sodium oleate) individually exert a statistically significant influence on drug solubility³⁰. The most significant factor affecting acidic drugs was pH. The combination of pH and the concentration of solubilising amphiphile components in SIF (bile salt, lecithin and fatty acid (sodium oleate)) was significant for neutral and basic drugs⁵². Further statistical analysis of a published data set of HIF by Pyper *et al.* used a five dimensional approach, treating each SIF component (pH, bile salt, lecithin, fatty acid and cholesterol) as a separate dimension, in order to examine the limitations of design of experiments (DoE) and SIF²⁴. Cholesterol was initially not studied as a factor in 2015 by Khadra *et al.* as the influence of cholesterol on drug solubility was not well established in literature, with the main contributors to micelle formation and drug solubilisation were considered to be bile salts and phospholipids. The advances in the understanding of the composition of HIF in more recent years had led to the knowledge that the presence of cholesterol has a more significant role in drug solubilisation in HIF. An 8 point and a centre point was identified and used by Abuhassan *et al.* to explore the equilibrium solubility of poorly soluble drugs in fasted state SIF compared with that of the DoE studies²⁸. This work builds on this by using the components that have been discovered to significantly affect drug solubility in intestinal fluid and at concentrations that are biologically relevant to the human intestinal environment. This study used five simulated intestinal fluid recipes; the minimum, Q1, median, Q3 and maximum [pH × total amphiphile concentration (TAC)] points from the work previously reported by Riethorst *et al.*²⁶ FaSSIF V1, from biorelevant.com was used as a comparator within this study.

Biorelevant FaSSIF version 1 was chosen, rather than the more recent version 3 for multiple practical and scientific reasons. Firstly, FaSSIF V1 is the most widely used version in both academic and industry settings, which make it a widely recognised medium for solubility studies. Using this version allows for the comparison of findings directly with the existing literature. Secondly, FaSSIF V1 is known to be relatively monodisperse and is consistent when made in multiple batches. This is vital for analytical techniques such as dynamic light scattering (DLS) and nanoparticle tracking analysis (NTA), which was used for the first time on simulated intestinal fluid (SIF) samples in this study. In contrast to this, the more recent FaSSIF version 3 contains additional components, including glycocholate and lysophosphatidylcholine, which make it more compositionally complex and subject to greater polydispersity in the resulting colloidal structures, which in turn may complicate data analysis and interpretation. Finally, the role of FaSSIF in this thesis is to act as a fixed comparator to the recently created suite of SIFs which were designed to capture the natural variability observed in human intestinal fluids. As both FaSSIF V1 and V3 represent fixed formulations, substituting V3 in place of V1 would not have contributed any additional value to the primary aim of this thesis – to examine how variability in intestinal fluid composition influences drug solubility and colloidal structure. Therefore, FaSSIF V1 was chosen as a reliable, well-established control that aligned with the experimental aims and kept consistency with existing solubility data in the published literature.

A recent study carried out by Abuhassan *et al.* investigated the solubility behaviour of twenty-one drugs in nine biorelevant fasted intestinal media to identify if there were any consistencies between the drugs and drug classes⁵³. The nine-point media used in this study was created by a multidimensional analysis to cover 90 % of the variability found fasted state HIF samples and covered a pH range from 5.72 to 8.04 and a [pH x total amphiphile concentration (TAC)] range of 15.07 to 122.4^{24, 28}. The acidic drugs analysed here were found to show a general increase in solubility and similar behaviour with deviations that are primarily associated with pKa and smaller fluctuations that are due to other amphiphiles in the media. The lowest and highest solubility measurements of the neutral and basic drugs was typically found in the lowest and highest (pH × [TAC]) media points, although there is less consistency than that detected with the acids⁵³.

There were a few drugs that were found to not follow the general trends including phenytoin and zafirlukast. Phenytoin has a pKa value greater than the highest pH therefore this drug is in the nonionised form and for both drugs, their solubility is greatest in the media with the highest (pH × [TAC]) which suggests that solubilisation by the amphiphilic components is the most likely explanation. Four categories were suggested to classify the behaviours, two based on the physicochemical

properties and two categories dependant on solubility behaviour. The acidic drugs, where $pK_a < 6.3$, are found in category 1. The equilibrium solubility is directly linked with the pH of the media and the drugs share solubility behaviour. Category 2 contains weakly acidic drugs ($pK_a > 8$), as well as basic and neutral drugs where the equilibrium solubility tends to increase with increasing ($pH \times [TAC]$) although there is no consistency between behaviour. Category 3 lies within that of category 2 where the drugs are either neutral or nonionised within the pH range of the media and analysis of these drugs shows a lack of sensitivity to the composition of media. Category 4 is less defined and drugs that do not show a solubility relationship between the pH and TAC would fit here as well as drugs that would show a reduced solubility with an increase of pH or TAC. Examples of this category include probucol and atazanavir⁵³. This work highlighted that there are general trends of solubility behaviour found according to the properties of a drug and the composition of SIF media, however it is not predictable or a direct consequence of pH or TAC or ($pH \times [TAC]$).

2.1.2. High-Performance Liquid Chromatography (HPLC)

High-performance liquid chromatography (HPLC) is an analytical technique that is used for the separation of compounds. The fundamental principle of this technique is based on the differences in the analyte polarity and affinity for the stationary and mobile phase. There are many parts to a HPLC system but the main components typically include: the pump, this provides the continuous high pressure flow of the mobile phase through the instrument; injector, introduces the sample into the system and mixes it with the mobile phase; column, this is where the separation occurs as the mobile phase will interact with the stationary phase; detector, the device used to register the appearance of analytes. Typically, UV (ultraviolet) detectors are used in pharmaceutical analysis as they enable monitoring of the UV absorbance. The stronger the interaction between the mobile phase and the stationary phase, the longer the retention of the analyte on the column. Compounds with a lower affinity for the stationary phase will elute sooner, thus resulting in separation and varying retention times⁵⁴. Figure 2.1 shows an overview of the HPLC system⁵⁵.

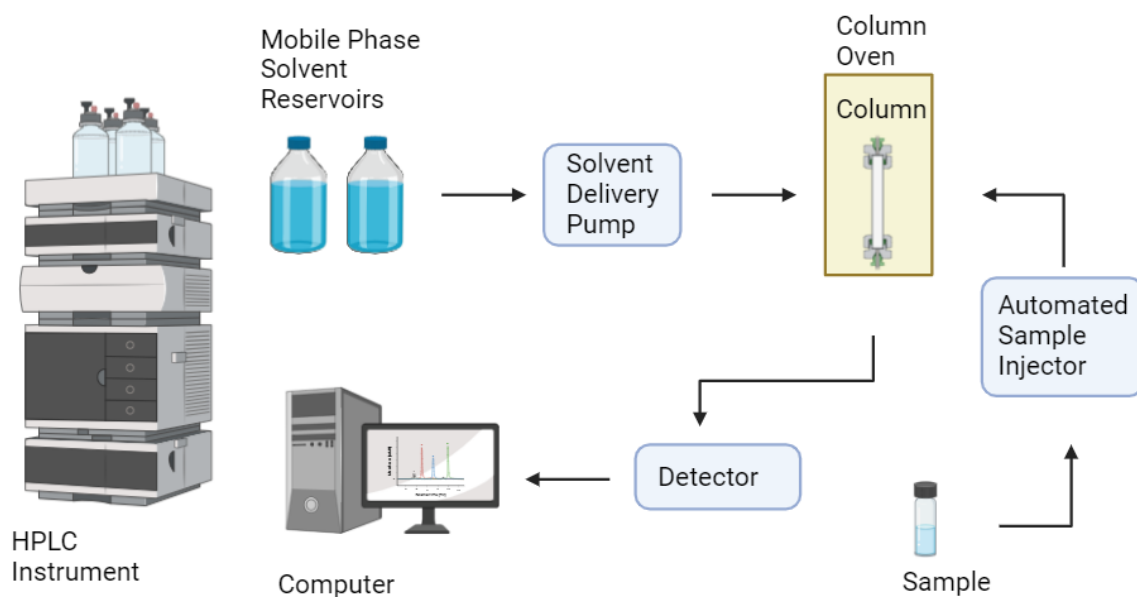


Figure 2.1: Overview of HPLC system, adapted from Reference⁵⁵. Created with Biorender.com

There are different types of HPLC such as normal phase, reverse phase, ion exchange and size exclusion chromatography. The dominant molecular interaction employed in normal phase HPLC are polar forces, while dispersive forces i.e. hydrophobic and Van der Waals interactions are used in reverse phase HPLC. Normal phase HPLC uses nonpolar solvents as the mobile phase with a polar modifier (such as methanol) in small volumes which enables control of analyte retention in the column. The stationary phase is typically a column packed with porous oxides such as silica which is populated with hydroxyl groups on its surface, resulting in a highly polar surface region of the material. Reverse phase HPLC uses a hydrophobic surface of the stationary phase, such as a C₈ or C₁₈ column and a polar mobile phase such as a water/acetonitrile mixture⁵⁴.

Reverse phase HPLC is used in this study to quantify the BCS class II drug that is solubilised in the SIF media. In order to quantify the solubility of each drug in each simulated intestinal fluid sample, a calibration curve was first carried out. This utilises a series of known concentrations of drug in solvent (in this case, mobile phase b was used) and the response/area under the peak detected is assigned to the concentration.

2.1.3. Objectives

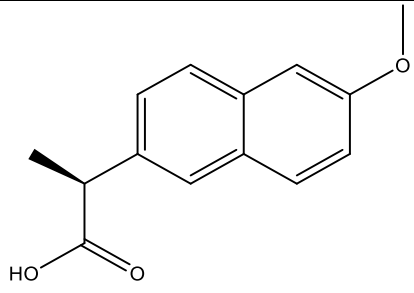
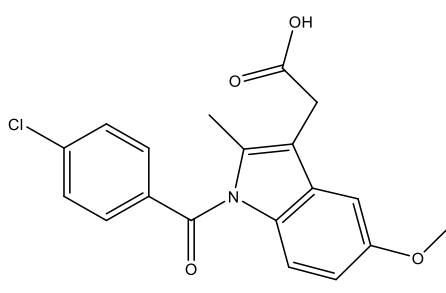
The objectives of this study were to investigate eight poorly soluble drugs (BCS class II) at equilibrium solubility in fluid that represent human intestinal fluid from individual data sets. Trends relating to

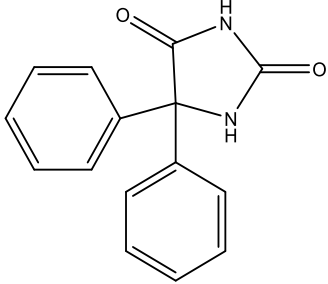
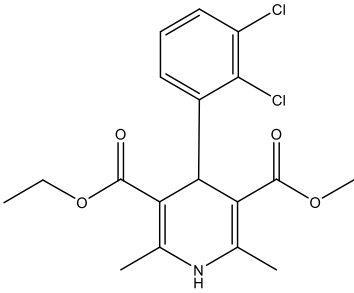
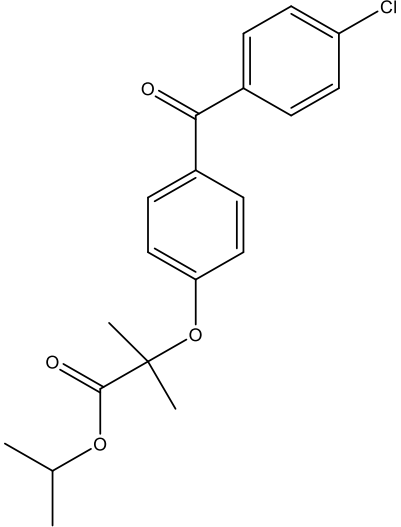
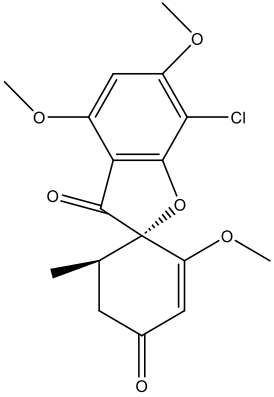
solubility and drug type/class were identified and discussed, with the primary objective to determine whether solubility is linked to pH or ($\text{pH} \times [\text{TAC}]$).

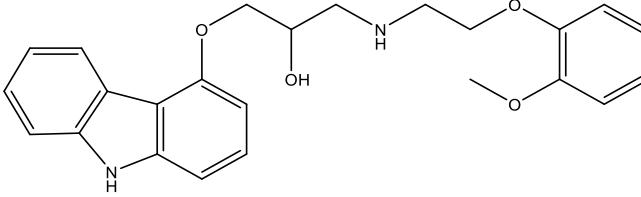
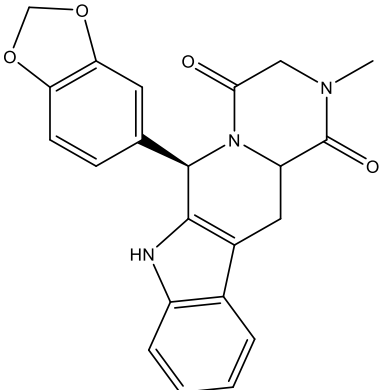
2.2 Materials

Sodium taurocholate (bile salt), sodium oleate (free fatty acid) cholesterol, ammonium formate, sodium chloride, hydrochloric acid, potassium hydroxide, naproxen, indomethacin, phenytoin, fenofibrate, griseofulvin, carvedilol and tadalafil were purchased from Merck Chemicals Ltd. Lecithin, (phosphatidylcholine from Soybean "98%"), was purchased from Lipoid company, Germany. Felodipine was purchased from Stratech. Chloroform was purchased from Rathburn Chemical Company. Formic acid and sodium phosphate monobasic monohydrate were bought from Fisher Scientific. The physicochemical properties of the drugs analysed in this study are displayed in Table 2.1. The water was ultrapure Milli-Q water and the acetonitrile was HPLC grade from VWR.

Table 2.1: Physicochemical properties and molecular structures of drugs

Compound	Acidic/basic/neutral	pKa	logP	Structure
Naproxen	Acidic	4.15	3.18	
Indomethacin	Acidic	4.5	4.27	

Compound	Acidic/basic/neutral	pKa	logP	Structure
Phenytoin	Acidic	8.33	2.47	
Felodipine	Neutral	-	3.86	
Fenofibrate	Neutral	-	5.2	
Griseofulvin	Neutral	-	2.18	

Compound	Acidic/basic/neutral	pKa	logP	Structure
Carvedilol	Basic	7.8	4.2	
Tadalafil	Basic	3.5	2.89	

Data sourced from Abuhassan *et al.* and DrugBank, with structures created using ChemDraw^{53, 56}

The molecular weights for each substance used in this study can be found in Table 2.2.

Table 2.2: Molecular weight for each substance used

Component	Molecular Weight (g/mol)
Sodium taurocholate	537.7
Phosphatidylcholine	786.1
Sodium oleate	304.4
Cholesterol	386.7
Naproxen	230.3
Indomethacin	357.8
Phenytoin	252.3
Felodipine	384.3
Fenofibrate	360.8
Griseofulvin	352.8
Carvedilol	406.5
Tadalafil	389.4

2.3. Methods

2.3.1. Creation of Suite of Simulated Intestinal Fluid Media

Based on a study by the Augustijns group, fasted human intestinal fluid (HIF) samples were collected and analysed, with each component being quantified²⁶. Using this data, five simulated intestinal fluid (SIF) recipes were created, which encompassed the full range of HIF samples, corresponding to the minimum, Q1, median, Q3, and maximum values of pH × [total amphiphile concentration (TAC)]. FaSSIF V1, supplied by Biorelevant (Biorelevant.com, London, UK), was used as a control. The composition of the media used is shown in Table 2.3.

Table 2.3: Final concentration of components in the simulated intestinal fluids²⁶

Media	Bile Salt (mM)	Phospholipid (mM)	Free Fatty Acid (mM)	Cholesterol (mM)	pH	pH x [TAC] (mM)
Minimum (1)	1.60	0.17	0.07	0.04	2.41	4.54
Q1 (2)	2.34	0.16	1.18	0.06	7.23	27.04
Median (3)	3.10	0.39	1.69	0.08	7.92	41.63
Q3 (4)	5.43	0.57	2.59	0.12	7.75	67.58
Maximum (5)	36.18	5.78	15.03	0.20	8.01	458.05
Biorelevant (6)	3	0.75	-	-	6.50	24.38

2.3.2. Simulated Intestinal Fluid Media Preparation

Solubility studies were conducted in triplicate. To create each of the five simulated intestinal media, a concentrated stock solution 15 times the mass of bile salt (sodium taurocholate), phospholipid (soybean lecithin) and fatty acid (sodium oleate) in chloroform was prepared. The mass of each component for the concentrated stock solution can be found in Table 2.4. For each of the media recipes, a solution 1500 times greater the mass of cholesterol in chloroform was prepared and an aliquot was transferred to the stock solution as it was not possible to weigh the low amounts of cholesterol required. The chloroform was then evaporated off with a nitrogen gas to produce a dry film which was resuspended in 3 mL of water and stirred to create a homogenous mixture. This was transferred to a 5 mL volumetric flask and made to volume with water. Table 2.4 shows the composition of each media point and target pH.

Table 2.4: Preparation of stock components, mass used to create 15 x stock solution

Media	Bile salt (mg)	Phospholipid (mg)	Free Fatty Acid (mg)	Cholesterol (mg)	pH	[pH x TAC] (mM)
Minimum	64.5	10.0	1.6	116.0	2.41	4.54
Q1	94.4	9.4	26.9	174.0	7.23	27.04
Median	122.6	23.0	38.6	348.0	7.92	41.63
Q3	219.0	33.6	59.1	232.0	7.75	67.58
Maximum	1459.0	340.7	343.2	580.0	8.01	458.05

2.3.3. Equilibrium Solubility Measurement

This protocol has been previously validated to ensure equilibrium solubility is achieved post 24 hours with no methodological interference^{30, 52, 57}. An excess of drug, which was above its solubility limit was added to 15 mL centrifuge tubes (Corning® tubes). The specific mass of excess drug used (approximately 14 mg) serves as an approximation of the quantity added, but it is important to note that the key factor is ensuring the drug concentration was above the solubility limit, regardless of the pH conditions. Equal aliquots (each of 267 µL) of simulated intestinal media (as described in Table 2.4), buffer (sodium phosphate monobasic monohydrate, 28.4 mM), salt (sodium chloride, 105.9 mM) were then added to the tubes and water (3.199 mL) was added to complete the final aqueous system to a total volume of 4 mL. The pH was adjusted to target value ± 0.02 using KOH and/or HCl as required (no more than 10 % of the final volume was added during pH adjustment). The tubes were placed on an orbital shaker for 1 hour after which the pH was adjusted if required according to the target values in Table 2.4. Tubes were secured in a rotary shaker at 37 °C for 24 hours. After 24 hours, excess drug was still visibly present in the tubes, indicating that the amount added exceeded the solubility limit. Post-incubation, 1 mL from each tube was centrifuged in a 1.5 mL centrifuge tube (Eppendorf® tube) for 15 minutes at 10,000 rpm then the supernatant was analysed by HPLC. The sample was not filtered prior to analysis.

2.3.4. HPLC analysis

Reverse phase HPLC analysis was performed on a Shimadzu LC-2040C 3D HPLC instrument using a gradient method. The column used was Xbridge® C₁₈ 5 µm (2.1 × 50 mm) at 30 °C. Mobile phase A was made by adding 1576.5 mg (10 mM) of ammonium formate to 2.5 L of deionised water. This was adjusted to pH 3.0 (± 0.1) with formic acid. Mobile phase B was made by adding 1576.5 mg (10 mM)

of ammonium formate to HPLC grade acetonitrile:water (9:1), total volume of 2.5 L. Flow rate used was 1 mL/min (with the exception of carvedilol where 0.7 mL/min was used). The gradient used for analysis can be found in Table 2.5.

Table 2.5: Gradient method used for HPLC analysis

Time (minutes)	Mobile Phase A (%)	Mobile Phase B (%)
0.0	70	30
3.0	0	100
4.5	70	30
8.0	0	0

The full run for each sample was a total of 8 minutes. The retention time, analysis wavelength, injection volume and flow rate for each active pharmaceutical ingredient is found in Table 2.6. The flow rate of carvedilol is lower than the other drugs in order to increase the retention time to prevent it from eluting in the void volume. This is defined as the total volume of mobile phase that is held within the HPLC column⁵⁸. If the flow rate was greater, the drug will elute earlier which will yield inaccurate data.

Other HPLC method conditions that vary depending on the drug that is analysed are the detection wavelength and the injection volume. Typically, drugs that contain aromatic rings or a high degree of conjugation are detected at 254 nm due to their absorbance characteristics exhibited. Aromatic rings absorb UV light at this wavelength due to the $\pi \rightarrow \pi^*$ electronic transitions while transitions such as $n \rightarrow \pi^*$ occur at the higher 291 nm wavelength for other conjugated systems such as those containing ketones and aldehydes⁵⁹.

The injection volume for the majority of the drugs analysed was 10 μ L. However, a volume of 20 μ L was required for phenytoin and a volume of 50 μ L was required for tadalafil. This was due to the poor signals that resulted from the lower injection volume that did not make drug quantification possible. Other issues that may arise from low injection volumes include a reduced sensitivity and poor signal to noise ratio. A low sample concentration relative to the baseline noise may result in poor peak detection and unreliable analyte quantification⁵⁵. During the method development and validation stage (performed by previous group members), these conditions have been optimised to ensure there is optimal sensitivity and specificity in the detection and quantification of each drug in SIF samples.

Table 2.6: HPLC conditions for each drug material

Drug	Retention time (min)	Detection (nm)	Injection volume (μ L)	Flow rate (mL/min)
Naproxen	1.3	254	10	1.0
Indomethacin	1.8	254	10	1.0
Phenytoin	1.1	254	20	1.0
Felodipine	2.4	254	10	1.0
Fenofibrate	2.7	291	10	1.0
Griseofulvin	1.2	291	10	1.0
Carvedilol	1.3	254	10	0.7
Tadalafil	1.4	291	50	1.0

Drug solubility in fasted state simulated intestinal fluid was sourced from literature and compared to the results measured from this study^{60, 61}.

The previously validated HPLC methodology was used for this analysis to maintain consistency and ensure reliable measurements of drug concentrations. The same drugs were analysed in simulated intestinal fluid (SIF), which contains the same components as used in previous studies but at different concentrations^{28, 36, 52, 57}. Since the analytical method has already been proven to accurately quantify the drugs in similar conditions, further optimisation of the HPLC conditions were not necessary. The method is considered robust and suitable for the current study, as it provides accurate measurements of drug concentrations even in the newly created suite of SIF.

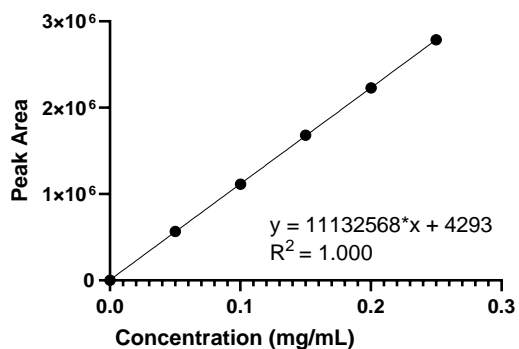
2.4. Results

2.4.1. Calibration Information

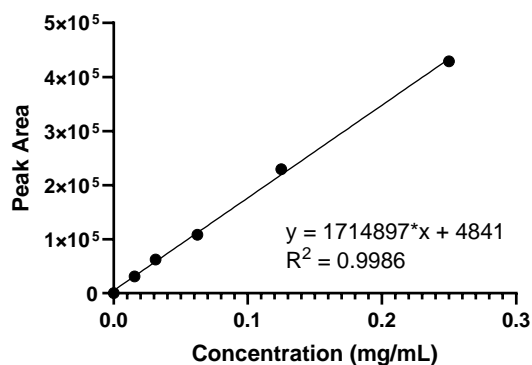
To be able to quantify the concentration of drug solubilised in each simulated intestinal fluid sample, calibration curves were required of each drug. The calibration curves for each drug were generated by preparing dilutions of known drug concentrations in mobile phase B (starting with either 1.0 mg/mL or 0.25 mg/mL). The HPLC method used for analysis can be found in Section 2.3.4. The area under the curve was noted for each concentration of drug which was then plotted as calibration curves for further analysis. The calibration curves, Figure 2.2, fit the data well with the R^2 values (linear regression coefficient of calibration curve, $N = 6$ points) for all drugs are above 0.993 which enables them to be

used for the quantification of the drug that is solubilised in each SIF. The R^2 values and equations can be found within each graph in Figure 2.2.

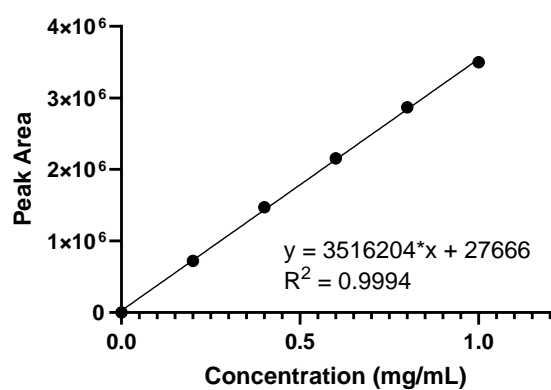
a)



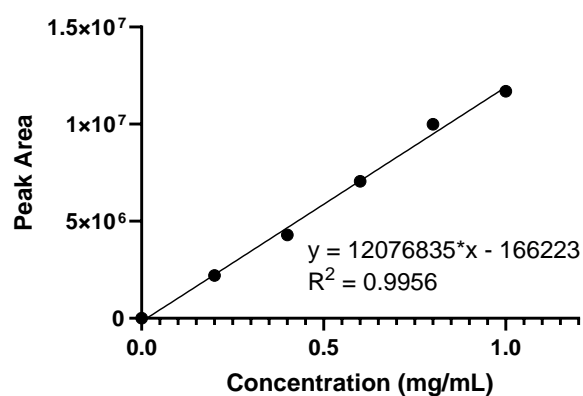
b)



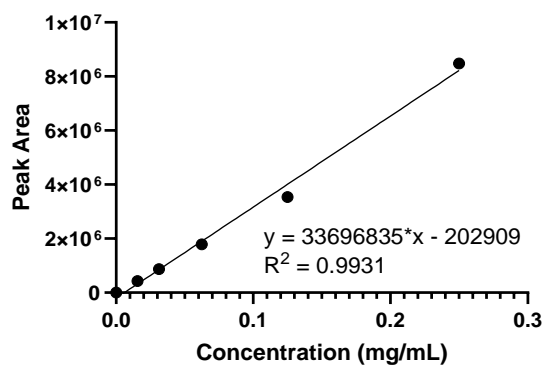
c)



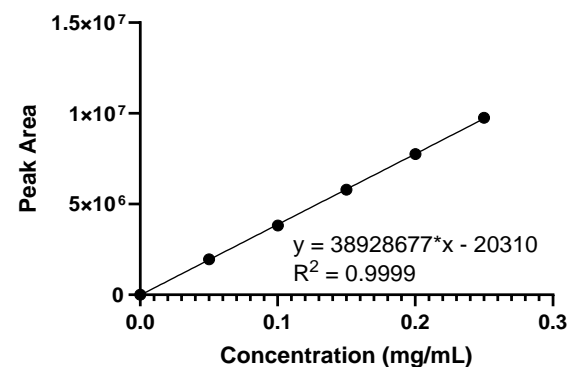
d)



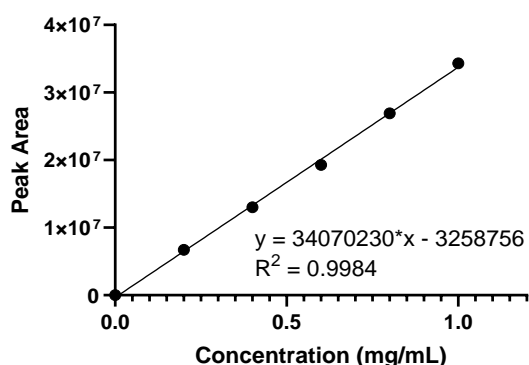
e)



f)



g)



h)

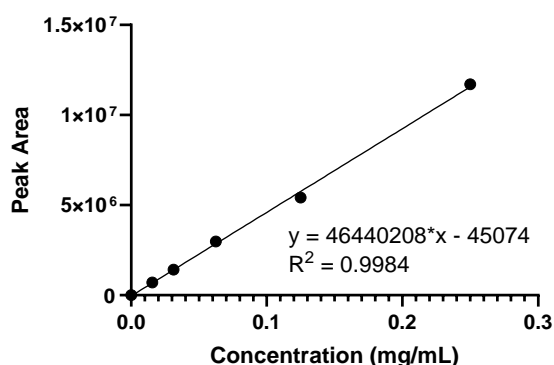


Figure 2.2: HPLC calibration data of acidic drugs a) naproxen, b) indomethacin, c) phenytoin, neutral drugs d) felodipine, e) fenofibrate, f) griseofulvin, basic drugs g) carvedilol, h) tadalafil

The limit of detection and limit of quantification calculated, which are the lowest concentration of analyte that can be reliably detected and quantified, respectively, with acceptable precision and accuracy can be found in Table 2.7¹².

Table 2.7: Limit of detection and limit of quantification values calculated for each drug

Drug	Limit of detection (μM)	Limit of quantification (μM)
Naproxen	6.4	21.6
Indomethacin	142.6	432.2
Phenytoin	138.1	418.6
Felodipine	316.1	957.9
Fenofibrate	80.4	243.5
Griseofulvin	18.4	48.5
Carvedilol	133.9	406.1
Tadalafil	35.9	108.9

An example chromatogram of each drug is presented in Figure 2.3-Figure 2.10. The acidic drugs naproxen, indomethacin and phenytoin can be found in Figure 2.3, Figure 2.4 and Figure 2.5. A chromatogram of each of the neutral drugs felodipine, fenofibrate and griseofulvin can be found in Figure 2.6, Figure 2.7, Figure 2.8, respectively, while the same for the basic drugs carvedilol and tadalafil is presented in Figure 2.9 and Figure 2.10.

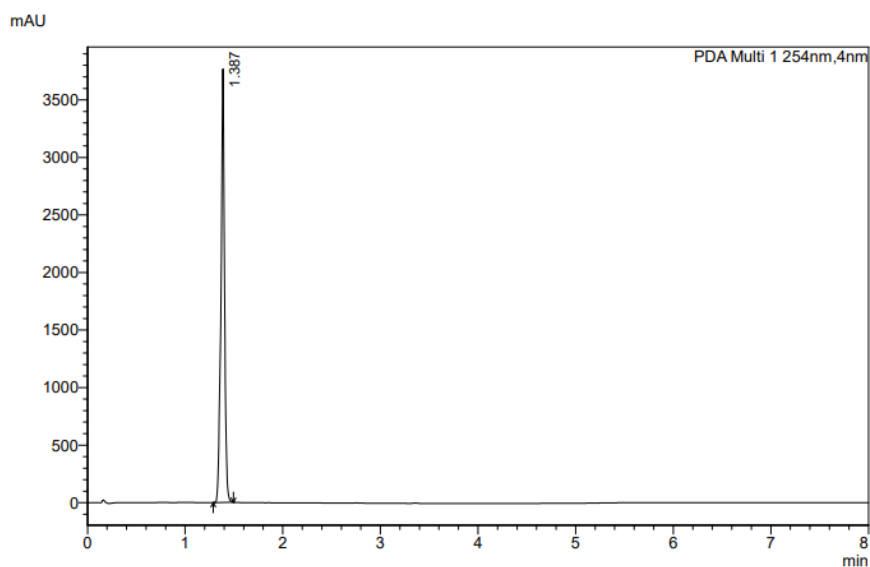


Figure 2.3: Chromatogram of naproxen in the median media showing a retention time of 1.387 minutes and a peak area of 956953 which correlates to a drug concentration of 6.41 mg/mL or 27.84 mM. Naproxen was detected using a UV wavelength of 254 nm.

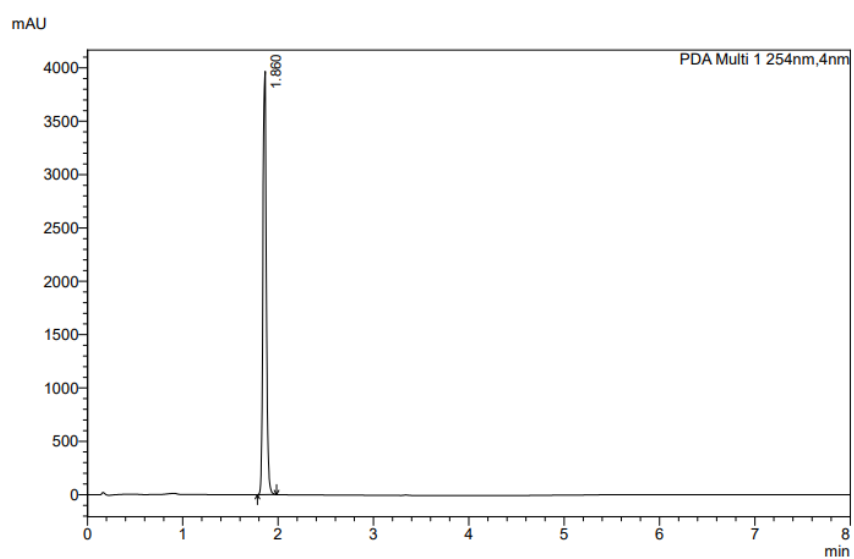


Figure 2.4: Chromatogram of indomethacin in the median media showing a retention time of 1.860 minutes and a peak area of 9833247 which correlates to a drug concentration of 2.45 mg/mL and 6.85 mM. Indomethacin was detected using a UV wavelength of 254 nm.

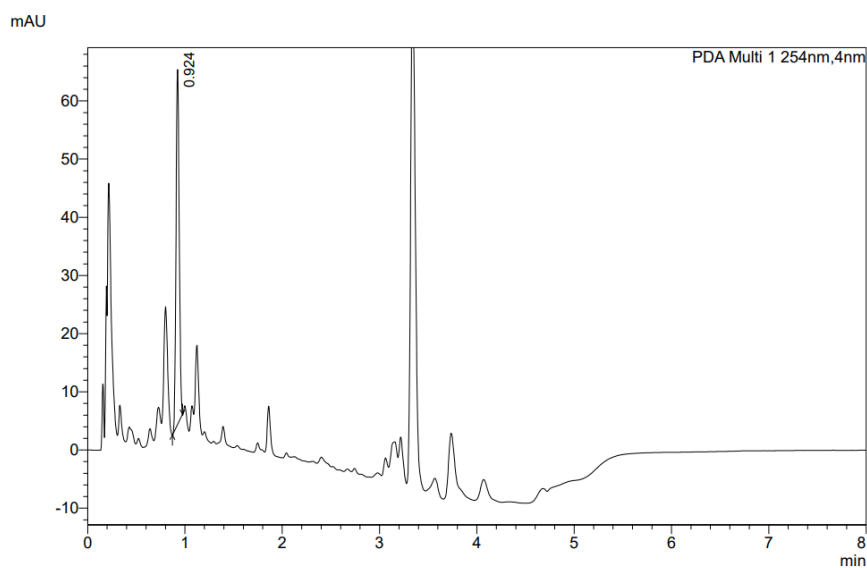


Figure 2.5: Chromatogram of phenytoin in the median media showing a retention time of 0.924 minutes and a peak area of 139300 which correlates to a drug concentration of 125.85 μM . Phenytoin was detected using a UV wavelength of 254 nm.

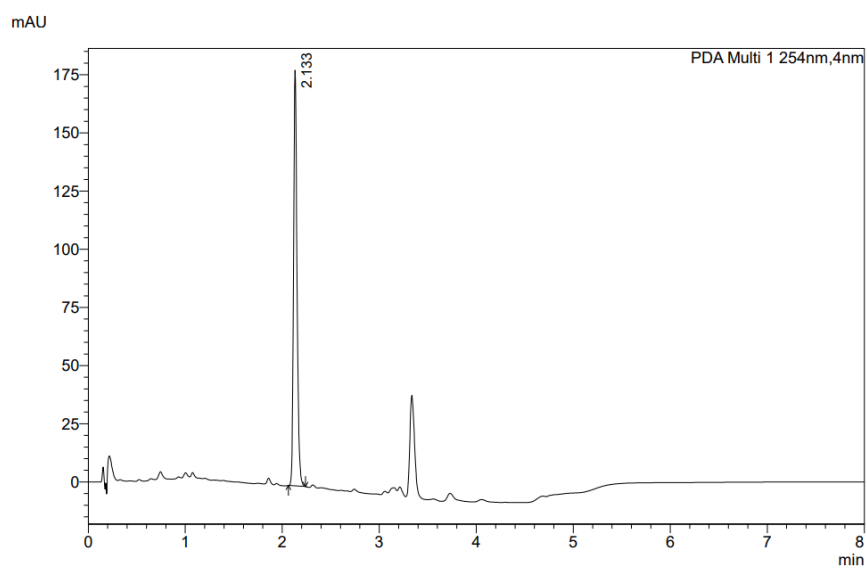


Figure 2.6: Chromatogram of felodipine in the median media showing a retention time of 2.133 minutes and a peak area of 442040 which correlates to a drug concentration of 131.09 μM . Felodipine was detected using a UV wavelength of 254 nm.

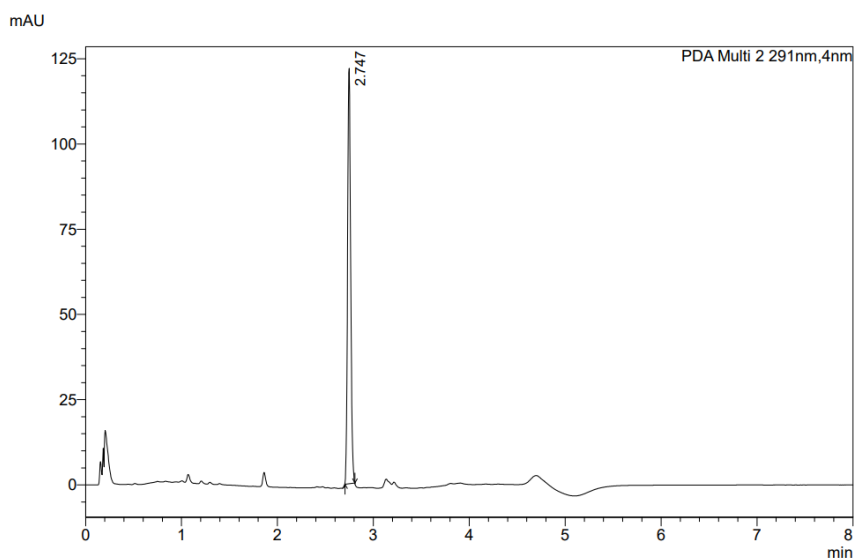


Figure 2.7: Chromatogram of fenofibrate in the median media showing a retention time of 2.747 minutes and a peak area of 269500 which correlates to a drug concentration of 38.77 μM . Fenofibrate was detected using a UV wavelength of 291 nm.

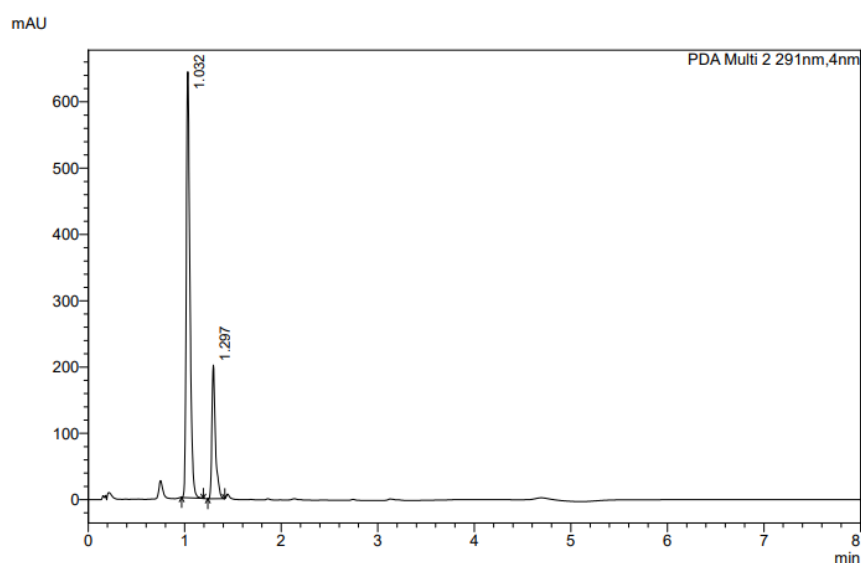


Figure 2.8: Chromatogram of griseofulvin in the median media showing a retention time of 1.032 and 1.297 minutes. The peak area is 1688846 and 513738 respectively, which combined gives a total of 2202584. This corresponds to a drug concentration of 161.84 μM . Griseofulvin was detected using a UV wavelength of 291 nm.

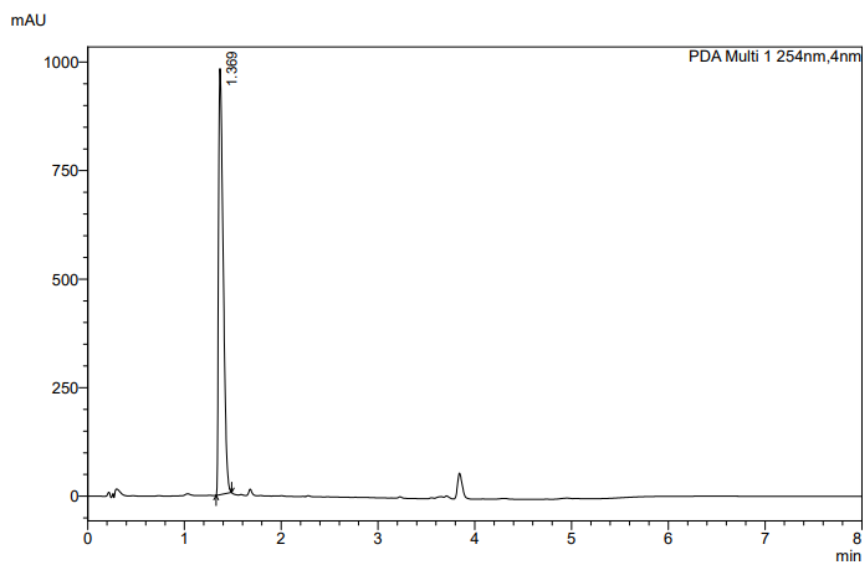


Figure 2.9: Chromatogram of carvedilol in the median media showing a retention time of 1.369 minutes and a peak area of 3312811 which correlates to a drug concentration of 262.73 μM . Carvedilol was detected using a UV wavelength of 254 nm.

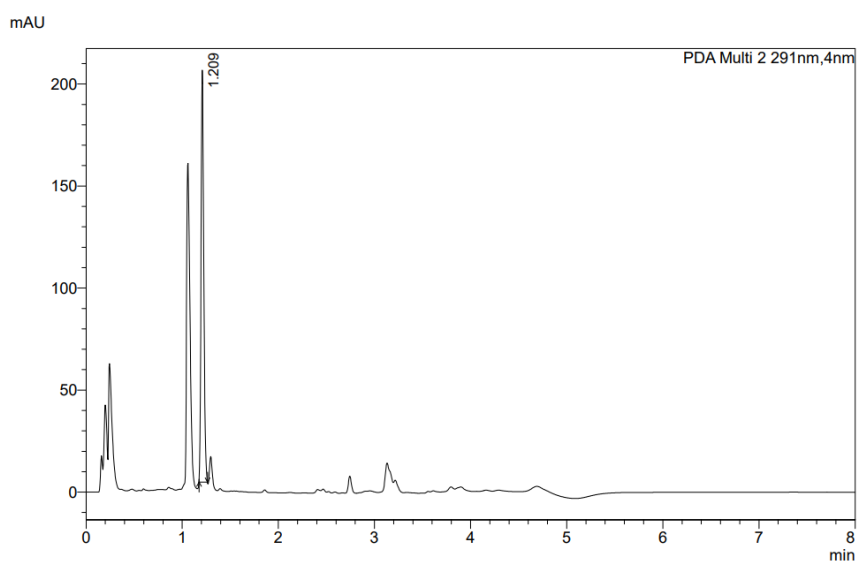


Figure 2.10: Chromatogram of tadalafil in the median media showing a retention time of 1.209 minutes and a peak area of 399630 which correlates to a drug concentration of 25.59 μM . Tadalafil was detected using a UV wavelength of 291 nm.

The other peaks present in the chromatograms, which are not that of the drug of interest, are thought to be other components within the simulated intestinal fluid. Taurocholic acid, which is the bile salt used in the formulation has a known retention time of 3.1 minutes⁶².

2.4.2. Raw Data

The mean equilibrium drug solubility results, where n=3, of the eight drugs analysed in the six fasted state media points are presented in Table 2.8.

Table 2.8: Mean solubility values (μM) of drugs analysed in fasted state simulated media \pm standard deviation, measured by HPLC

Drug	Media					
	Minimum	Q1	Median	Q3	Maximum	Biorelevant
Naproxen		25633.5 \pm	28609.5 \pm	25736.2 \pm	25009.5 \pm	2391.5 \pm
	105.4 \pm 0.4	225.1	996.2	523.2	361.2	32.2
Indomethacin		3433.5 \pm	6842.8 \pm	7045.1 \pm	13310.6 \pm	
	51.9 \pm 0.1	19.5	20.7	1.5	131.9	355.0 \pm 4.9
Phenytoin	60.3 \pm 1.7	55.3 \pm 0.5	125.9 \pm 0.9	112.2 \pm 1.9	330.1 \pm 7.4	83.8 \pm 2.2
Felodipine	57.5 \pm 0.2	73.2 \pm 0.3	132.8 \pm 1.5	212.6 \pm 2.0	926.6 \pm 8.8	140.8 \pm 2.7
Fenofibrate	21.5 \pm 0.3	27.5 \pm 0.2	38.8 \pm 0.1	40.9 \pm 0.4	170.5 \pm 1.3	48.8 \pm 0.9
Griseofulvin		165.0 \pm		186.6 \pm		
	106.5 \pm 1.8	4.5	163.7 \pm 2.2	11.7	306.7 \pm 6.8	159.4 \pm 6.2
Carvedilol	1406.2 \pm	205.9 \pm			1235.5 \pm	
	33.9	0.5	261.8 \pm 1.4	313.7 \pm 2.6	27.1	234.1 \pm 3.9
Tadalafil	14.4 \pm 0.5	14.5 \pm 0.1	24.0 \pm 0.6	28.9 \pm 0.5	127.3 \pm 2.1	25.2 \pm 0.3

2.5. Discussion

As the pH \times [TAC] increased, the solubility of most drugs showed an increasing trend. The acidic drugs showed the strongest effect, with naproxen and indomethacin displaying a considerably increase in solubility as the pH \times [TAC] increased. The pKa values of these drugs are 4.15 and 4.5, respectively, meaning they are almost completely ionised in most of the SIF media, which leads to enhanced solubility as a result of increased interactions with the amphiphilic components of the media^{28, 56}. The neutral drugs (felodipine, fenofibrate and griseofulvin) displayed an increased solubility at higher pH \times [TAC] values, specifically moving from the Q3 to the maximum media point. This suggests that there is an increased interaction between the higher concentration of bile salt, phospholipid, fatty acid and cholesterol which will in turn aid micelle formation and therefore, drug solubilisation. Felodipine, with a logP of 3.86, displayed the greatest increase in solubility between these two points, surpassing that of fenofibrate (logP value of 5.2)^{28, 56}. While fenofibrate is more lipophilic, the strong hydrophobicity of this drug may limit the interactions with the more polar regions of the micelles. The basic drug,

tadalafil, with a lower pKa value of 3.5 showed limited solubility in the minimum media point²⁸. The solubility of this drug considerably increased in the maximum media, when pH × [TAC] was greatest. This indicates that there is strong solubilisation by the amphiphilic components of the SIF.

The solubility of weakly basic biopharmaceutical classification systems (BCS) class II drugs such as carvedilol and tadalafil are pH dependent. This group of drugs have a complex solubility pattern in gastrointestinal (GI) fluid as a result of the pH gradient found during the progression along the GI tract from stomach to the later parts of the intestine⁶³. The solubility of these two drugs in the suite of media studied ranged from 1406 ± 34 to $1235 \pm 27 \mu\text{M}$ (carvedilol) and 14.4 ± 0.5 increasing to $127.3 \pm 2.1 \mu\text{M}$ (tadalafil). The high value observed for carvedilol in the minimum media point is due to the affinity this drug shows at the low pH value. Carvedilol will ionise and solubilise in the acidic pH of the stomach, progressing to the environment of the small intestine and lower solubility, drug precipitation may occur at this site⁶³.

Figure 2.11 shows the equilibrium solubility values for each drug in each of the simulated intestinal fluid. Drug solubility values for the drugs of interest, as reported in literature, are presented in Table 2.9. The drug solubility values are measured in biorelevant and non-biorelevant FaSSIF.

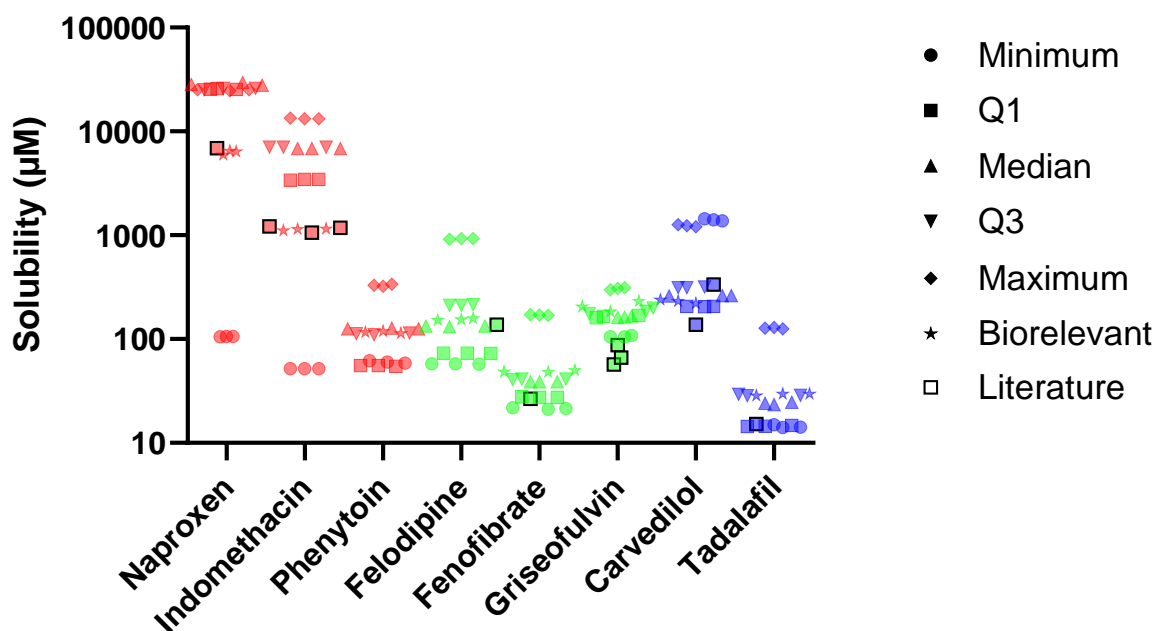


Figure 2.11: Equilibrium solubility measurements for each drug in FaSSIF media compositions detailed in Table 2.8. Red coloured data points for acidic drugs, green for neutral drugs and blue basic drugs. Reported solubility values for individual drugs in FaSSIF taken from Augustijns *et al.* and Teleki *et al.*^{60, 61}

Table 2.9: Overview of drug solubility in fasted state simulated intestinal fluid, as reported in literature^{60, 61}

Drug	Solubility (μM)	Reference
Naproxen	6882.65 ± 438.63	Telekei <i>et al.</i>
Indomethacin	1178.59 ± 49.19	Telekei <i>et al.</i>
	1060.60 ± 16.0	Augustijns <i>et al.</i>
	1218.0 ± 94.0	Augustijns <i>et al.</i>
Felodipine	137.9 ± 4.3	Augustijns <i>et al.</i>
Fenofibrate	26.6 ± 3.8	Augustijns <i>et al.</i>
Griseofulvin	66.33 ± 5.10	Telekei <i>et al.</i>
	87.7 ± 1.4	Augustijns <i>et al.</i>
	56.7 ± 2.5	Augustijns <i>et al.</i>
Carvedilol	137.52 ± 2.46	Telekei <i>et al.</i>
	334.6 ± 8.7	Augustijns <i>et al.</i>
Tadalafil	15.15 ± 1.79	Telekei <i>et al.</i>

Figure 2.12 presents the solubility plots for the basic drugs. A large increase in solubility is observed between the Q3 and maximum media point for carvedilol. This increase is interesting as the pH of the maximum media point is now greater than the pKa value of the drug (7.8^{64}) which is contrary to the expected behaviour where the solubility of the weakly basic drug should decrease when $\text{pH} > \text{pKa}$. This is also observed in tadalafil between these two SIF points, but is unrelated to pKa as the pH of the media does not exceed the pKa of tadalafil ($\text{pKa} = 10^{52}$). The data show that the solubility is linked to the [TAC] to a greater extent than the pH for these weak bases. The equilibrium solubility of carvedilol in the minimum media is measured to be $1406 \pm 34 \mu\text{M}$ while the pH of the media is 2.41. Carvedilol will be in the fully ionised form and displays the standard pH-dependent solubility profile at low pH of a weakly basic drug where a high solubility is observed. This data is in agreement with work carried out by Hamed *et al.* that investigated the solubility and dissolution behaviour of carvedilol in various simulated gastric and intestinal fluids. The researchers recorded a saturation solubility of carvedilol in blank simulated fasted state gastric fluid at a low pH of 1.6 to be $2399 \pm 41 \mu\text{g/mL}$ ($5900 \pm 100 \mu\text{M}$)⁶³.

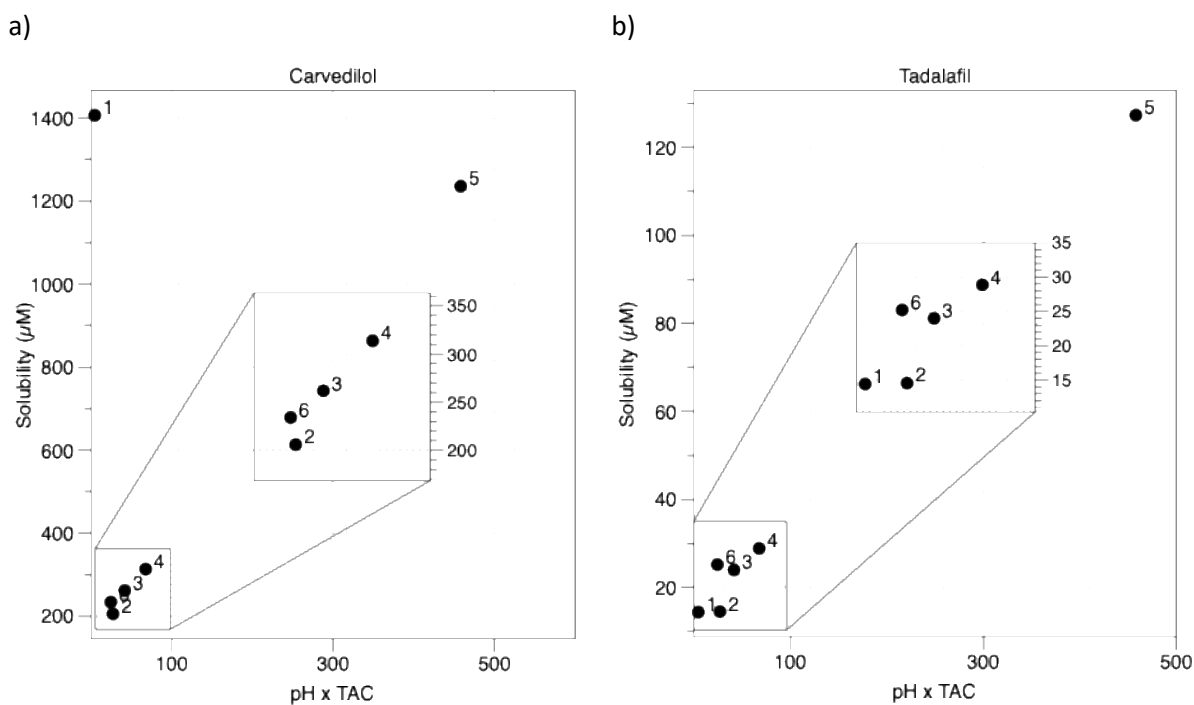


Figure 2.12: Basic Drug Solubility vs Media pH x TAC. a) carvedilol, b) tadalafil. Point labelled indicates media number, see Table 2.3

Figure 2.13 presents the solubility plots for the neutral drugs. A visual analysis of the plots indicates that the neutral drugs analysed (felodipine, fenofibrate and griseofulvin) have solubility values which similarly steadily increase with increasing media point. There is a considerable increase in all three drug solubilities between media Q3 and the maximum media point (points 4 and 5 on the graphs, respectively). This is caused by an increased interaction between the greater concentration of media components and the neutral drugs. There is a considerable increase in all three drug solubilities between media Q3 and the maximum media point. This is related to the non-linear increase in [TAC] in these media.

The formation of a higher concentration of colloidal structures is a result of the increase in concentration of the various media components i.e. bile salt, phospholipid, fatty acid and cholesterol. Bhat *et al.* investigated the solubilisation capabilities of surfactants on erythromycin and concluded cationic surfactants, such as cetyltrimethylammonium bromide, showed the highest molar solubilisation for the drug due to electrostatic interactions. Also observed was enhanced solubility in nonionic micellar solution e.g. Brij 58 (polymer of ethylene glycol and cetyl alcohol)⁶⁵. Boyd *et al.* carried out a review on the solubilisation of drugs by surfactant micelles in aqueous solutions and found a significant increase in drug solubilisation capacity with increasing surfactant chain length. They also noted that colloidal instability of drug loaded micelles are a major challenge when they are added

to a medium containing bile salt⁶⁶. De Smidt *et al.* showed that above the apparent sodium taurocholate CMC, the solubility of griseofulvin increases linearly with the concentration of bile salt⁶⁷. Here, they measured the CMC of to be 5.2 mM⁶⁷ which is considerably greater than the ~3 mM reported in other literature^{41, 68}. As the bile salt concentration increases from 5.43 mM (Q3) to 36.18 mM (maximum), this could explain the large solubility increase.

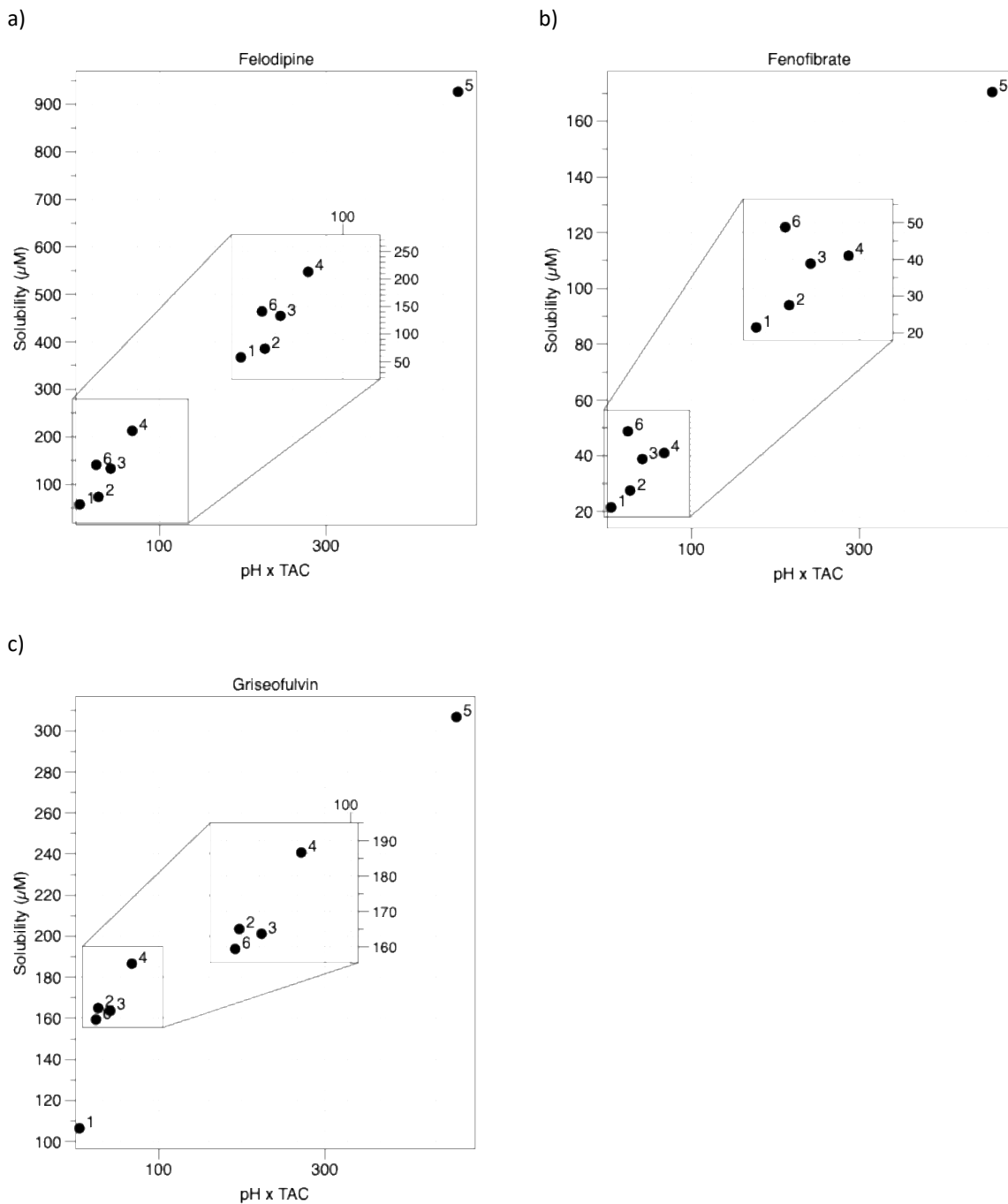


Figure 2.13: Neutral Drug Solubility vs Media pH x TAC. a) felodipine, b) fenofibrate, c) griseofulvin. Point label indicates media number, see Table 2.3

The solubility plot for the acidic drugs is presented in Figure 2.14. ($\text{pH} \times [\text{TAC}]$) has been used for phenytoin due to work carried out by Inês Silva *et al.* suggests for this drug, both the concentration and amphiphile content influence the drug solubility more so than pH alone for other acidic drugs (including naproxen and indomethacin). This is due to a lower mono-exponential pH correlation coefficient for phenytoin than other weakly acidic drugs, including naproxen and indomethacin⁶⁹.

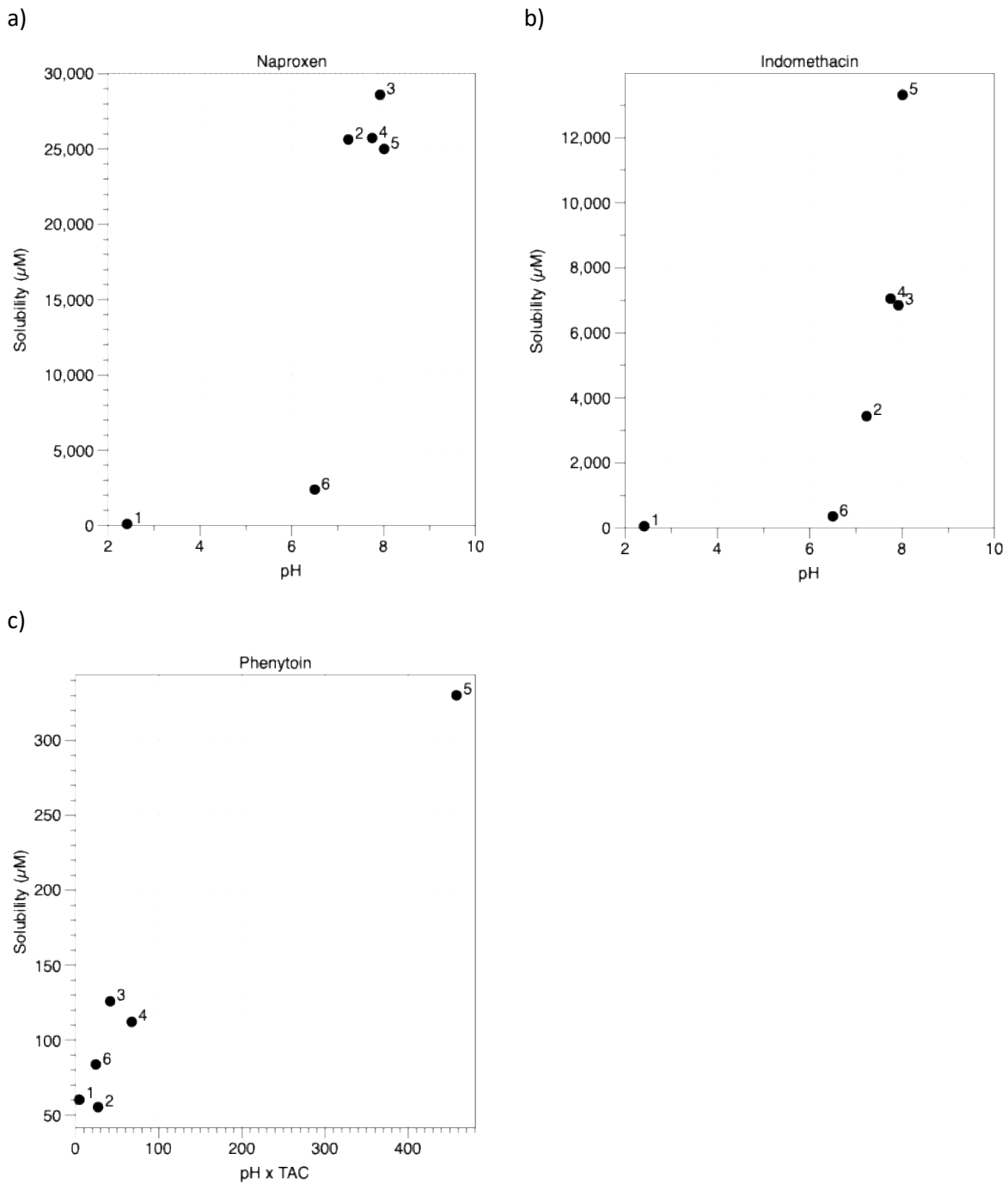


Figure 2.14: Acidic Drug Solubility vs Media pH and Media pH x TAC. a) naproxen, b) indomethacin, c) phenytoin. Point label indicates media number, see Table 2.3

As expected, the acidic drugs analysed (naproxen, indomethacin and phenytoin) have a higher solubility value in the intestinal fluid, compared to the neutral and basic drugs. As the drugs are weakly acidic, they have a considerably lower solubility in the minimum media point where the pKa values are greater than that of the pH (2.41 ± 0.02) at 4.15, 4.5 and 8.33 respectively⁵⁶. As the pH of the media increases to the Q1 media point to a value of 7.23 ± 0.02 there is a substantial increase in solubility of the naproxen and indomethacin which is a result of the pH being greater than that of the pKa values. There is a slight increase at the median media point due to a higher pH value than the Q3 point (7.92 ± 0.02 and 7.75 ± 0.02 , respectively). A large increase in solubility should be observed for phenytoin if it were added to a media with a pH greater than 8.33, although that is beyond the scope of this work as the pH of our sample data does not reach this.

There is a considerable spread of lipophilicity of the drugs analysed in this study, ranging from the antifungal drug griseofulvin with a logP value of 2.18, to the antilipemic drug fenofibrate with a logP of 5.2⁵³. All drugs analysed possess a positive logP value, indicating that the drugs are more lipophilic than hydrophilic. Naproxen and indomethacin have pKa values of 4.15 and 4.5 therefore they will be nearly fully ionised in all media with the exception of the minimum media. When in the ionised form, it is anticipated that they will associate with the hydrophilic outer colloidal layer which may influence the size of the resulting colloidal structure. Carvedilol has a pKa of 7.8, therefore the majority of the drug will be in an ionised form in all media other than the median and maximum which have pH values of 7.92 and 8.01. It is expected that it will be nearly fully ionised in the minimum media where the pH is 2.41 and less ionised in the other media in which the pH is greater at around 7 pH units. The weakly basic drug tadalafil has a low pKa value at 3.5 which indicates that this drug will be in the nonionised (unprotonated) form in the acidic pH of the minimum media, while it will be in the ionised form in the other SIF media where the pH is greater than the pKa. The calculated degree of ionisation for the acidic and basic drugs analysed can be found in Table 2.10. The pKa values have been sourced from literature^{53, 56}.

Table 2.10: Degree of drug ionisation of acidic and basic drugs analysed, calculated from reported pKa values and pH of SIF media^{53, 56}

pKa	Drug	Media	Minimum	Q1	Median	Q3	Maximum	Biorelevant
		pH	2.41	7.23	7.92	7.75	8.01	6.50
4.15	Naproxen		2.2 %	99.9 %	99.9 %	99.9 %	99.9 %	99.6 %
4.5	Indomethacin		0.9 %	99.8 %	99.9 %	99.9 %	99.9 %	99.0 %
8.33	Phenytoin		99.9 %	92.7 %	72.1 %	78.9 %	67.2 %	98.5 %
7.8	Carvedilol		99.9 %	78.8 %	43.1 %	52.9 %	38.1 %	95.2 %
3.5	Tadalafil		92.5 %	0 %	0 %	0 %	0 %	0 %

2.6. Conclusion

To conclude, the work carried out in this chapter designed and created a new suite of simulated intestinal fluid that is reflective of *in vivo* gastrointestinal variability. The composition encompassed that which was revealed from a range of human intestinal fluid samples from a clinical study. The solubility of eight poorly soluble BCS class II drugs were measured and the findings showed that the solubility was typically greater in the acidic drugs than in the neutrals or bases and that the solubility tended to increase with increasing media point (pH × [TAC]).

Chapter 3

Dynamic Light Scattering Analysis of Fasted State
Simulated Intestinal Fluid

3. Dynamic Light Scattering Analysis of Fasted State Simulated Intestinal Fluid

3.1. Introduction and Theory

Dynamic light scattering (DLS), is a technique that measures fluctuations in light intensity. It is sometimes referred to as photon correlation spectroscopy and quasi-elastic scattering and is used for the analysis of disperse systems^{70, 71}. It is based on the principle of Brownian motion and the elastic electromagnetic scattering of dispersed particles. Particles that are dispersed within a liquid move randomly in all directions and continually collide with solvent molecules^{72, 73}. Energy is transferred from the bombardment which results in movement of macromolecular particles. The magnitude of the motion is dependent on the size, temperature and viscosity of the solvent and from this, the hydrodynamic diameter can be determined through the measurement of the particles speed^{70, 73}. The Stokes-Einstein equation, Equation 1, is used to calculate the translational diffusion coefficient D_T and from this, the particle size/hydrodynamic radius can be determined^{71, 73}.

Equation 1: Stokes-Einstein equation^{71, 73}

$$D_T = \frac{k_B T}{6\pi\eta R_h}$$

Where:

D_T = Translational diffusion coefficient [m^2/s]

k_B = Boltzmann constant [m^2kg/Ks^2]

T = Temperature [K]

η = Viscosity [Pa.s]

R_h = Hydrodynamic radius [m]

The translational diffusion coefficient is a property that provides the velocity of the Brownian motion and is dependent on many things. There are many factors that affect the diffusion rate of the particles which include: the ionic strength of the medium, the ions and overall ionic concentration may alter the thickness of the Debye length; surface structure of the particle, the surface and orientation can increase or decrease the rate of diffusion e.g. if the structure is flat vs upright/uneven; and the presence of non-spherical particles. The Debye length is the electric double layer of the particle. If the medium has a low conductivity, the particles will have an extended Debye length, resulting in a lower

rate of diffusion and a greater hydrodynamic diameter, while a medium with a higher conductivity will lessen the layer, giving a lower apparent diameter⁷⁴.

One of the key theories used in dynamic light scattering is the Lorenz-Mie solution, more commonly referred to as the Mie theory. It is used to describe the elastic scattering of electromagnetic waves of light from atomic and molecular particles that have diameters greater than the wavelength of incident light⁷⁵. If the size of the particles that are analysed become approximately equal to the wavelength of the incident light from the beam source, this will result in the observation of a complex function of maxima and minima with respect to angle. The software used to interpret and convert the DLS data collected using a Zetasizer Nano instrument (Malvern, UK.) uses this theory to convert the intensity distribution into the volume distribution⁷⁴. The intensity distribution provides the quantity of light scattered by the sample particles, while the Mie theory scattering formula gives the information on the scattering of particles with a known dimension.

The size measurement of the particles can be collected by monitoring the movement of particles over a particular time frame due to the variance of diffusion rate of the different sized particles. Larger particles will diffuse at a slower rate compared to that of smaller particles and will adopt similar positions across multiple time points. This is unlike the smaller particles e.g. solvent molecules which move faster and will not remain in analogous positions⁷⁰.

3.1.1. Instrument Information

DLS instruments record measurements using different angles of detection. The three common angles of detection are at 90 °, 173 ° (also known as backscatter) and 158 °. A high scattering angle can neglect the effect of any rotational diffusion that is contributed and observed in the autocorrelation output therefore the translational diffusion coefficient (D_T) can be calculated. The laser source does not completely penetrate the full sample and cuvette, so the backscattering system enables the recording of D_T for samples that are more concentrated as the multiple scattering phenomenon can be prevented⁷⁰. The multiple scattering phenomenon occurs when photons that are scattered from a sample are then scattered again by neighbouring particles before reaching the instrument detector. This phenomenon will increase the randomness of the scattering signal while decreasing the correlation, resulting in the output presenting particles that are moving at an increased rate to their true speed. The result of this, is the measurement will be biased towards smaller sized particles⁷⁶. Larger sized contaminants and dust can scatter more light in the forward direction as the scattering becomes wavelength independent in contrast to particles of smaller sizes that scatter almost evenly in

the two directions⁷⁰. This is due to Rayleigh scattering, which is defined as the scattering of light caused by particles that are smaller than 10 % of the wavelength of the light^{70, 75}. This is elastic scattering and occurs without the loss of energy or change of wavelength⁷⁵. Using a backscattering detection system can aid in the avoidance of scattering contributions caused by Rayleigh scattering for larger particles⁷⁰.

A simplified diagram of a DLS system can be found in Figure 3.1. A single frequency laser (in this study a 632.8 nm laser) is used to provide a light source to illuminate the particles that are contained within the sample cuvette. The majority of the source will pass through the sample without being scattered, however, some will be scattered by the incident light in all directions. The refracted light will be identified by the detector at a certain angle (this work uses backscattering at 173°), then this signal is used to calculate the diffusion coefficient by the Stokes-Einstein equation, Equation 1. An attenuator is used to reduce the intensity of the light from the laser beam, as too much light may overload the detector. The correlator is the digital signal processing board which takes the intensity signal from the detector then compares this at multiple time intervals in order to derive the varying intensity rate^{73, 77}.

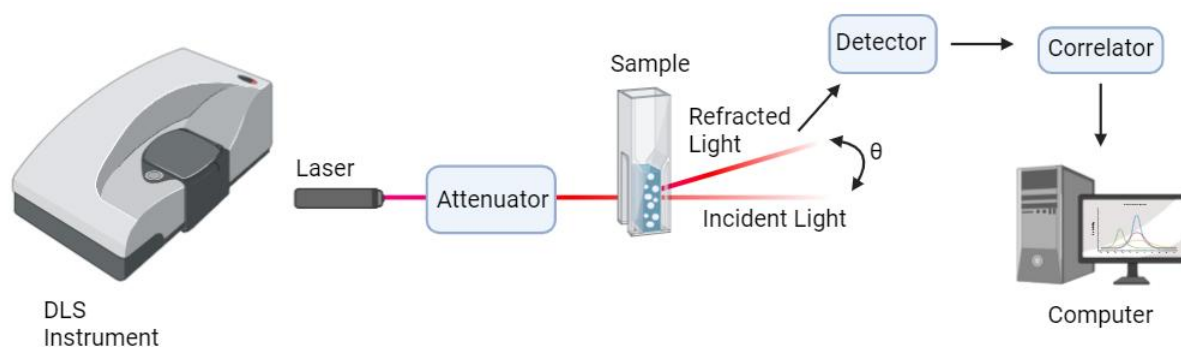


Figure 3.1: Overview of DLS process, adapted from References^{73, 74, 77}. Created with Biorender.com

Techniques used for the measurement of particle size all have a fundamental flaw when measuring the size of particles that are non-spherical in geometry. Spherical particles are the only geometric shape that can be accurately measured by a single value. The hydrodynamic diameter that is measured by the DLS instrument of a non-spherical particle is the diameter of a sphere that possesses the same translational diffusion rate as the particle⁷⁴. The initial distribution generated by DLS is the intensity distribution which can be converted, using the Mie theory to a volume distribution which characterises the relative sample components by their mass/volume in place of their scattering⁷⁸. The assumptions required for this include: the molecules are monodisperse and spherical in geometry and there is no error in the intensity distribution. The optical properties, such as the refractive index and the viscosity of the particles must also be known^{70, 78}.

Upon the addition of a drug, above the critical micelle concentration (CMC) of the surfactants, an amphiphilic drug can interact with the bile salt by means of synergistic interactions to form spherical or ellipsoidal micelles. The bile salt can undergo micellisation to form bile salt micelles, then subjected to inclusion of amphiphilic drug material this can then form drug loaded-bile salt mixed micelles⁴⁰.

3.1.2. Use of DLS in Biopharmaceutics

This technique has been used in the field of bioscience to determine the particle size and provide aggregation information on various proteins, nucleic acids and viruses⁷⁰.

An interesting use of DLS for the analysis of SIF was carried out by Khoshakhlagh *et al.* to investigate the nanostructure of fasted state SIF with cholesterol. The structures formed were more accurately identified using small-angle neutron scattering. Four BCS class II hydrophobic drugs (fenofibrate, danazol, griseofulvin and carbamazepine) were selected and a drug solubility study was carried out in order to examine how the increasing addition of cholesterol, at the same concentrations found in human bile, to the biorelevant *in vitro* media affects the drug solubility and associated lipid nanostructures. After centrifugation to remove the excess drug in the samples, the particle size distribution was determined by DLS using a Zetasizer Nano-ZS (Malvern, UK). First measured was a drug-free reference (blank) of various intestinal model media and cholesterol. The main particles in all media were vesicles with an average size of between 25 and 70 nm before and after centrifugation, respectively.

The nanoparticles that formed from the bile acid, lecithin, cholesterol, and drugs were analysed by DLS. The mean size of the primary particles in the intestinal model media containing drug and cholesterol were found to be between the following: fenofibrate, 25 and 44 nm; carbamazepine, 32 and 46 nm; danazol, 26 and 59 nm, and griseofulvin had an average particle size between 30 and 58 nm. In all samples, a decrease in particle size was observed with increasing cholesterol concentration. However, at high concentrations of cholesterol, the major particle size of carbamazepine increased to 44 nm and the major particle size in the griseofulvin sample increased to 49 nm. This was thought to be cholesterol-rich discotic particles⁷⁹.

Dynamic light scattering measurements recorded by Clulow *et al.* provided particle size analysis data of fasted state SIF bile salt micelles, mixed micelles of bile salt/phospholipid/buffer and biorelevant media. 5 mM sodium taurodeoxycholate in a 50 mM tris buffer formed micelles that were found to be 4.9 ± 0.9 nm (intensity distribution); mixed micelles of 5 mM sodium taurodeoxycholate/5 mM 1,2-

dioleoyl-*sn*-glycero-3-phosphatidylcholine/50 mM tris buffer gave a size intensity distribution 5.4 ± 0.9 nm, while the biorelevant FaSSIF media had a distribution of 48.0 ± 6.6 nm⁴¹. Dynamic light scattering carried out by Doak *et al.* of poorly soluble drugs found colloid formation in fed state simulated intestinal fluid. The BCS class II drug, itraconazole, was measured to have a solubilised micellar diameter of 129 ± 9.6 nm while the antiretroviral drug, delavirdine was determined to have a solubilised micellar diameter of 125.6 ± 66.0 nm⁵¹. This information regarding the change in size of colloidal structures in the presence and absence of a drug could provide key insights into how the drug-colloid complexes form. The full extent of the relationship between the size of the mixed micelles formed once a drug has been solubilised into the colloidal structure is yet to be understood.

3.1.3. Objectives

The objectives of this chapter are to analyse the samples, by dynamic light scattering, of blank and drug loaded SIF media at equilibrium solubility in SIF fluids that represent human intestinal fluid based on individual data sets. Trends related to the particle size measured and the solubility of a series of drugs measured by HPLC from Chapter 2, were identified and discussed, with the primary objective to determine whether the particle size of the colloidal structures formed is linked to solubility and/or to pH or (pH \times [TAC]).

3.2 Materials

Materials used to create SIF can be found in Section 2.2. In addition, 1 mL syringes, 2 mL syringes and 13 mm membrane with a 0.45 μ m pore size PTFE syringe-filters were purchased from Fisher Scientific. Disposable semi-micro cuvettes were from VWR.

3.3 Methods

The simulated fluid/drug samples were created using the method described in Section 2.3.2. Particle size of the samples was measured via dynamic light scattering (DLS) using a Zetasizer Nano-ZS (Malvern Instruments, Malvern, UK), which uses a helium neon (HeNe) laser and an avalanche photo diode detector⁸⁰. The instrument was switched on and allowed to warm up for around 20 minutes to enable stabilisation of the laser and for the sample holder to equilibrate at the desired temperature. Back-scattered light from a 632.8 nm laser (4 mW output) at an angle of 173 ° at 37 °C was used to determine the particle size distributions and hydrodynamic diameters. Each sample was prepared in the same way as for the solubility measurement then filtered with a 0.45 μ m membrane and the initial 0.5 mL

of filtrate was discarded prior to analysis to remove any particulate matter from the filter; sample was then transferred into a semi-micro disposable cuvette. The instrument was equilibrated for 2 minutes before each measurement and the auto attenuator function was used to identify the optimum position for analysis. Three batches were prepared and three measurements were taken for each sample and the mean \pm standard deviation for the most prominent peak in the size distribution by intensity from each individual run of 12-16 measurements was reported (n=9). The intensity distribution was chosen as it is the first order result generated by the instrument and does not involve any assumptions regarding the Mie scattering theory, unlike the volume distribution which assumes that the particles are spherical, homogenous and that the optical properties are known. Also assumed is that the intensity distribution is correct⁷⁸. The number of measurements taken was due to the knowledge that polydisperse samples affect DLS results.

3.4. Results and Discussion

The results of the particle size analysis by DLS can be found in Table 3.1. Solubility data recorded in Chapter 2 was used for the analysis in this section. Hydrodynamic diameters determined by DLS for the solutions of drug in simulated intestinal fluid. The peak diameter and standard deviation for the most prominent peak in the size distribution by intensity from each individual run of 12-16 measurements are given. The samples designated “fresh blank” and “blank 24 hours” are both drug-free media that is analysed fresh (approximately 2 hours postproduction) and 24 hours postproduction, respectively. DLS measurements of blank buffer (no bile/phospholipids etc.) were attempted although it was not found to be possible to determine any size data. This indicates, as anticipated, that there are no particles present. The data showed that particle sizes were generally measured to decrease with increasing pH \times [TAC]. The smallest sizes measured were found to be in the maximum media point where the pH \times [TAC] is greatest. The sizes of particles in this fluid were all found to be around 5 nm, regardless of the drug that has been added.

Table 3.1: Particle Size Analysis by DLS size \pm standard deviation (intensity dist. d, nm)

Drug	Media					
	Minimum	Q1	Median	Q3	Maximum	Biorelevant
Fresh blank	8.5 \pm 0.2	100.0 \pm 1.6	150.8 \pm 5.3	205.2 \pm 4.9	1.7 \pm 0.1	80.6 \pm 1.7
Blank 24 hours	12.5 \pm 0.5	132.9 \pm 2.3	155.2 \pm 6.8	1.4 \pm 0.1	1.7 \pm 0.1	70.3 \pm 2.9

Drug	Media					
	Minimum	Q1	Median	Q3	Maximum	Biorelevant
Indomethacin	126.2 ± 2.5	19.1 ± 0.3	29.2 ± 1.6	6.0 ± 0.1	5.7 ± 0.7	131.0 ± 5.8
Phenytoin	117.1 ± 1.5	16.6 ± 0.4	23.5 ± 0.8	6.5 ± 0.1	5.2 ± 0.2	122.9 ± 3.0
Felodipine	170.3 ± 5.4	17.9 ± 0.6	19.3 ± 1.2	6.1 ± 0.1	5.1 ± 0.2	85.6 ± 1.2
Fenofibrate	123.5 ± 3.9	16.9 ± 0.3	20.6 ± 2.5	6.5 ± 0.2	5.5 ± 0.1	101.9 ± 1.9
Griseofulvin	128.9 ± 2.4	18.4 ± 0.2	22.8 ± 1.3	6.8 ± 0.2	5.1 ± 0.3	17.9 ± 1.6
Carvedilol	162.6 ± 2.3	121.8 ± 1.8	199.4 ± 2.2	179.0 ± 3.6	5.3 ± 0.2	623.8 ± 12.9
Tadalafil	132.1 ± 2.3	19.7 ± 0.7	23.0 ± 0.7	6.4 ± 0.1	5.3 ± 0.1	92.2 ± 1.8

^aIntensity distribution of main peak, average of three runs, three measurements per run on each sample (n=9)

The different concentrations of the media points may result in the presence of various bile salt/phospholipid/surfactant structures, this may explain some of the polydispersity observed in the data. A comparison of the structure sizes of the fresh blank and felodipine samples in the SIF media, measured by DLS can be found in Figure 3.2. The shapes in this image are used to visually reflect the size difference between the particles measured in each of the fluids.

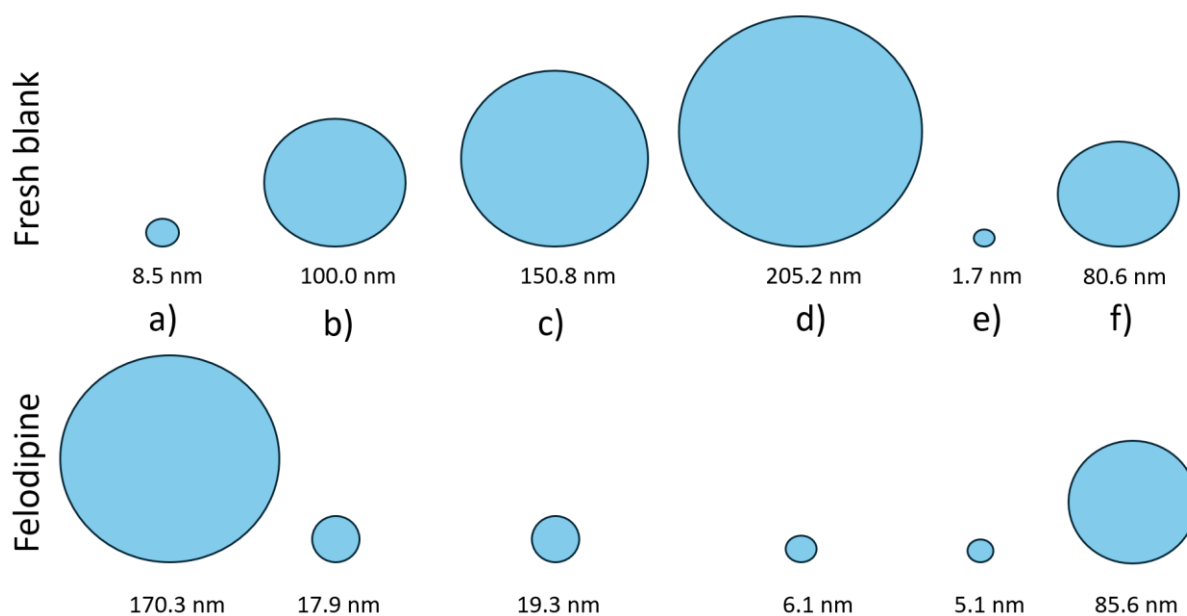


Figure 3.2: Comparative micelle sizes for the fresh blank (drug free) and felodipine structures, measured by DLS in the SIF media: a) minimum, b) Q1, c) median, d) Q3, e) maximum and f) biorelevant

Kloefer *et al.* analysed blank/drug free FaSSIF media using DLS (Zetasizer ZS, Malvern Instruments) and measured the colloidal particle size to be 49.2 ± 0.4 nm. However, Kloefer *et al.* used the z-average and

polydispersity index to collect their results which uses a cumulant method⁸¹ while the data in this study was collected using the mean value of the primary peak of the intensity distribution. The z-average recorded for fresh blank biorelevant FaSSIF was 77 ± 1.4 nm while the polydispersity index (PDI) was found to be 0.03 ± 0.01 (unitless). As the z-average is very similar to the primary peak intensity recorded for the fresh blank media (80.6 ± 1.7 nm), this indicates that the fresh blank biorelevant FaSSIF media is monodisperse. After 24 hours, the blank biorelevant FaSSIF media had a z-average of 67 ± 2 nm and a PDI of 0.03 ± 0.02 , compared to the primary peak intensity measured of 70 ± 3 nm. Guidance states that samples with a PDI smaller than 0.05 are infrequently observed other than with highly monodisperse standards while samples with a PDI greater than 0.7 indicate a very broad size distribution⁷⁸. The z-average recorded for the fresh blank minimum media was 7.5 ± 0.3 nm and the PDI was 0.25 ± 0.01 which increased after 24 hours to 16.4 ± 5.3 nm and 0.44 ± 0.09 , respectively. This emphasises that this suite of SIF media is fairly polydisperse therefore the intensity data was used for data analysis. The PDI values for each of the measurements recorded in each of the simulated intestinal media can be found in Table 3.2-Table 3.7.

Table 3.2: PDI values for each of the nine measurements recorded in the minimum SIF

Drug	Measurement								
	1	2	3	4	5	6	7	8	9
Fresh blank	0.239	0.233	0.235	0.263	0.271	0.266	0.254	0.251	0.243
Blank 24 hours	0.348	0.333	0.340	0.436	0.610	0.577	0.453	0.451	0.446
Naproxen	0.183	0.191	0.191	0.175	0.173	0.175	0.163	0.153	0.175
Indomethacin	0.178	0.206	0.206	0.165	0.169	0.178	0.184	0.192	0.191
Phenytoin	0.287	0.293	0.284	0.286	0.277	0.278	0.406	0.410	0.396
Felodipine	0.499	0.494	0.488	0.243	0.244	0.254	0.557	0.560	0.545
Fenofibrate	0.461	0.473	0.471	0.398	0.318	0.322	0.443	0.439	0.441
Griseofulvin	0.236	0.240	0.241	0.218	0.228	0.220	0.199	0.196	0.186
Carvedilol	0.154	0.165	0.171	0.127	0.142	0.161	0.169	0.151	0.161
Tadalafil	0.444	0.438	0.444	0.429	0.427	0.334	0.462	0.456	0.462

Table 3.3: PDI values for each of the nine measurements recorded in the Q1 SIF

Drug	Measurement								
	1	2	3	4	5	6	7	8	9
Fresh blank	0.474	0.346	0.464	0.550	0.550	0.547	0.581	0.555	0.560
Blank 24 hours	1.000	1.000	1.000	0.898	0.894	0.899	0.589	0.597	0.600
Naproxen	0.197	0.202	0.206	0.270	0.272	0.276	0.304	0.303	0.304
Indomethacin	0.274	0.236	0.240	0.260	0.237	0.232	0.279	0.283	0.289
Phenytoin	0.225	0.226	0.217	0.267	0.261	0.237	0.349	0.343	0.359
Felodipine	0.271	0.265	0.266	0.373	0.385	0.387	0.308	0.302	0.297
Fenofibrate	0.442	0.493	0.475	0.296	0.289	0.282	0.312	0.316	0.311
Griseofulvin	0.310	0.312	0.316	0.342	0.338	0.341	0.231	0.232	0.235
Carvedilol	0.194	0.194	0.198	0.118	0.107	0.120	0.093	0.108	0.115
Tadalafil	0.587	0.601	0.618	0.356	0.365	0.363	0.487	0.472	0.465

Table 3.4: PDI values for each of the nine measurements recorded in the median SIF

Drug	Measurement								
	1	2	3	4	5	6	7	8	9
Fresh blank	0.308	0.311	0.304	0.303	0.303	0.310	0.260	0.265	0.280
Blank 24 hours	0.327	0.324	0.322	0.349	0.498	0.360	0.504	0.495	0.471
Naproxen	0.156	0.146	0.167	0.131	0.122	0.127	0.179	0.172	0.163
Indomethacin	0.413	0.408	0.400	0.443	0.437	0.434	0.371	0.372	0.372
Phenytoin	0.217	0.213	0.220	0.299	0.266	0.300	0.425	0.485	0.511
Felodipine	0.423	0.421	0.424	0.296	0.411	0.392	0.288	0.294	0.288
Fenofibrate	0.212	0.197	0.196	0.511	0.553	0.582	0.234	0.227	0.273
Griseofulvin	0.255	0.302	0.291	0.430	0.376	0.404	0.251	0.253	0.252
Carvedilol	0.215	0.230	0.225	0.198	0.200	0.213	0.100	0.127	0.128
Tadalafil	0.170	0.164	0.163	0.237	0.224	0.224	0.404	0.384	0.413

Table 3.5: PDI values for each of the nine measurements recorded in the Q3 SIF

Drug	Measurement								
	1	2	3	4	5	6	7	8	9
Fresh blank	1.000	1.000	1.000	0.682	0.676	0.678	0.561	0.549	0.566
Blank 24 hours	0.391	0.257	0.259	0.265	0.262	0.399	0.117	0.256	0.278
Naproxen	0.162	0.175	0.168	0.156	0.158	0.166	0.131	0.126	0.124
Indomethacin	0.412	0.397	0.391	0.456	0.452	0.431	0.307	0.306	0.297
Phenytoin	0.134	0.444	0.432	0.197	0.393	0.502	0.395	0.396	0.390
Felodipine	0.235	0.146	0.140	0.333	0.339	0.280	0.178	0.196	0.161
Fenofibrate	0.126	0.106	0.367	0.229	0.123	0.108	0.416	0.420	0.415
Griseofulvin	0.493	0.470	0.467	0.100	0.432	0.180	0.149	0.333	0.301
Carvedilol	0.050	0.090	0.075	0.072	0.063	0.099	0.045	0.060	0.082
Tadalafil	0.161	0.441	0.442	0.235	0.339	0.425	0.169	0.109	0.374

Table 3.6: PDI values for each of the nine measurements recorded in the maximum SIF

Drug	Measurement								
	1	2	3	4	5	6	7	8	9
Fresh blank	0.264	0.247	0.378	0.188	0.184	0.186	0.300	0.300	0.346
Blank 24 hours	0.274	0.296	0.328	0.348	0.340	0.335	0.521	0.205	0.296
Naproxen	0.096	0.119	0.117	0.104	0.120	0.104	0.135	0.124	0.127
Indomethacin	0.125	0.124	0.136	0.246	0.243	0.244	0.110	0.103	0.105
Phenytoin	0.248	0.242	0.246	0.267	0.264	0.274	0.183	0.185	0.182
Felodipine	0.217	0.222	0.221	0.232	0.238	0.237	0.198	0.198	0.204
Fenofibrate	0.209	0.204	0.199	0.249	0.254	0.260	0.197	0.208	0.204
Griseofulvin	0.257	0.233	0.208	0.212	0.211	0.215	0.270	0.261	0.246
Carvedilol	0.158	0.150	0.153	0.167	0.183	0.160	0.117	0.119	0.119
Tadalafil	0.181	0.183	0.185	0.234	0.246	0.246	0.187	0.168	0.154

Table 3.7: PDI values for each of the nine measurements recorded in the biorelevant SIF

Drug	Measurement								
	1	2	3	4	5	6	7	8	9
Fresh blank	0.050	0.026	0.014	0.035	0.024	0.032	0.035	0.058	0.022
Blank 24 hours	0.034	0.012	0.002	0.026	0.018	0.010	0.064	0.039	0.028
Naproxen	0.244	0.239	0.244	0.188	0.184	0.189	0.474	0.329	0.311
Indomethacin	0.592	0.571	0.585	0.532	0.544	0.558	0.564	0.546	0.556
Phenytoin	0.312	0.293	0.275	0.450	0.326	0.296	0.463	0.435	0.450
Felodipine	0.072	0.080	0.064	0.075	0.059	0.066	0.093	0.058	0.052
Fenofibrate	0.092	0.073	0.078	0.116	0.102	0.101	0.116	0.098	0.086
Griseofulvin	0.246	0.169	0.363	0.366	0.207	0.132	0.299	0.366	0.227
Carvedilol	0.478	0.551	0.534	0.575	0.597	0.592	0.890	0.643	0.742
Tadalafil	0.138	0.141	0.122	0.176	0.168	0.172	0.205	0.191	0.163

3.4.1. Analysis of Size Data Arranged by (pH × [TAC])

As (pH × [TAC]) influenced the overall solubility of drugs this trend was used to present the size data. Figure 3.3 shows the size and intensity distribution measured for the fresh blank media and the blank media, 24 hours postproduction. There does not appear to be variation when time is increased for the minimum, median, maximum and biorelevant media points, however, a notable difference can be seen for the Q1 and Q3 media points. The distribution measured in the blank Q1 media point has become multimodal at 24 hours, with small peaks appearing around 5 and 10 nm. The z-average recorded for fresh blank Q1 media was 58.7 ± 6.7 nm (compared to the primary peak intensity distribution of 100.0 ± 1.6 nm) and the PDI was 0.51 ± 0.07 , after 24 hours the z-average decreased to 43.7 ± 18.7 nm while the PDI increased to 0.83 ± 0.18 .

Essentially, the average size across the distribution decreases while the polydispersity of the blank media increases to broad size distribution as time is increased. The Q3 distribution has stayed constant with the number of peaks but the primary peak is now around 1 nm when in the fresh media it was around 205 nm. The z-average of the fresh Q3 media was recorded to be 82 ± 31 nm while the PDI was 0.75 ± 0.19 which both decreased to 13 ± 10 nm and 0.28 ± 0.08 , respectively. This data shows that the distribution is widely spread with multiple peaks recorded. Interestingly, the PDI decreases considerably between samples, over time, which would suggest that the sample distribution becomes less broad and more monodisperse. However, from the distribution graph, this is not the case. This highlights that while the primary peak is used for polydisperse samples, the entire distribution should be considered during data analysis.

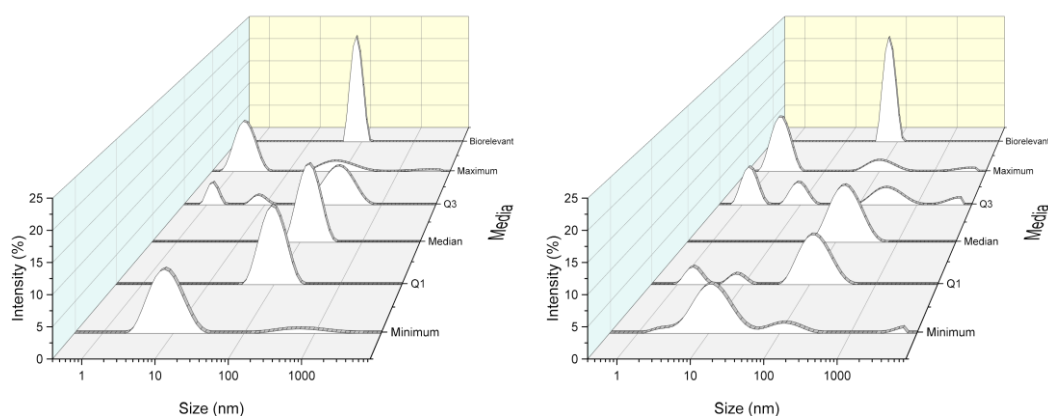


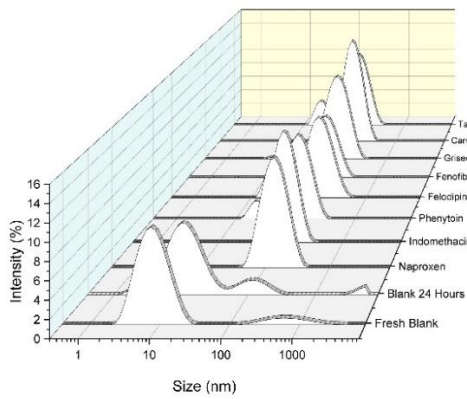
Figure 3.3: DLS size and intensity distribution for the fresh blank (left) and blank media at 24 hours postproduction (right)

It is clear from the size distribution for the fresh blank/drug free Q1, median and biorelevant media that particles of a similar size and dispersity are measured. This could indicate that similar colloidal units are formed within the media which may determine the solubility. The Q3 and maximum media also show a primary peak around the same size region which could suggest the same. As the [TAC] of the minimum media is below that of the CMC, the presence of colloidal structures within this media are not expected and the structures measured here are simple amphiphilic molecules. As the (pH x [TAC]) is increased, there is an increased proportion of smaller sized units, although this is absent from the median media point. These could be self-assembled aggregates of the components as they approach and exceed their respective CMCs, however this would not explain the lack of polydispersity measured in the median media point.

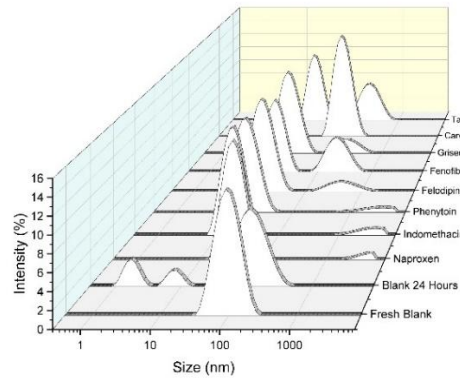
The lipophilic drug molecules have been suggested to be located at the hydrophobic core of the micelle structure while the hydrophilic outer layer provides protection from steric hinderance and prevents the structure from detection by the reticuloendothelial system⁸². There is a considerable spread of lipophilicity of the drugs analysed in this study, ranging from the antifungal drug griseofulvin with a logP value of 2.18, to the antilipemic drug fenofibrate with a logP of 5.2⁵³. All drugs analysed possess a positive logP value, indicating that the drugs are more lipophilic than hydrophilic.

Figure 3.4 shows the size and intensity distribution measured for the SIF media. The size of the structures in the minimum fluid are small yet they increase by at least 10-fold from the blank media at the 24 hour timepoint and greater still compared to the fresh media ($p < 0.05$), in the presence of drug which may indicate that the drug is interacting with the colloidal structures perhaps stabilising the colloids into some larger aggregate or form. In the Q1 media the size of the blank and drug containing colloidal structures exhibit the opposite behaviour where the larger colloidal structures are measured in the blank media which decrease in size by around 6-fold, from a particle size of >100 nm to around 15-30 nm (with the exception of carvedilol).

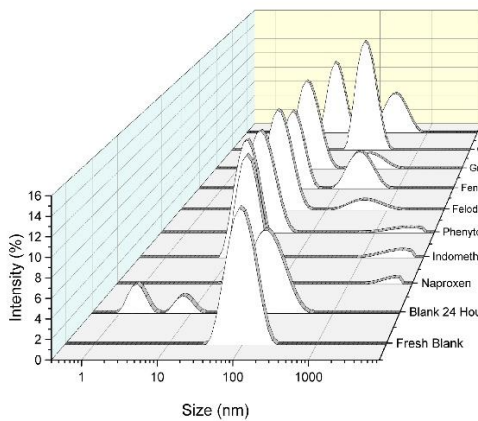
a)



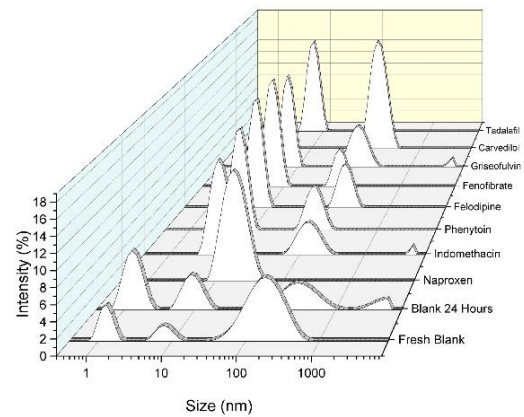
b)



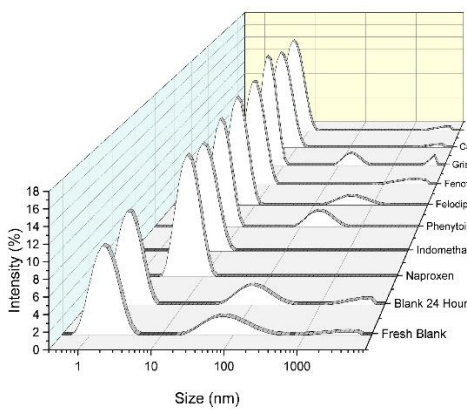
c)



d)



e)



f)

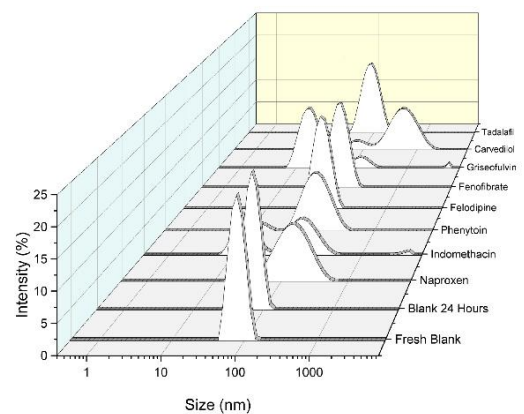


Figure 3.4: DLS size and intensity distribution for the a) Minimum b) Q1, c) Median, d) Q3, e) Maximum and f) Biorelevant SIF media

The particle size of the fresh blank media, presented in Figure 3.4, ranged from 8.5 ± 0.2 nm in the minimum media point decreasing to 1.7 ± 0.1 nm in the maximum media point while the size for fresh blank biorelevant FaSSIF v1 (Biorelevant.com) was measured to be 80.6 ± 1.7 nm. The concentration

of sodium taurocholate is 1.60 and 2.34 mM in the minimum and Q1 media points, which is lower than the ~3 mM CMC typically reported for this bile salt^{40, 41, 68}. However, as this data shows colloidal structures are detected in both media. It is also possible for the other components to associate with the bile salt to form colloidal structures. A comparable theory is the formation of mixed micelle structures from both bile salts and phospholipids. It has previously been shown that this could create a mixed bilayer disk structure with bile salt molecules surrounding the boundary of the disk which would result in a diverse range of structure sizes i.e. polydispersity of the sample⁸³.

Polydispersity was observed for the blank Q1 media after 24 hours where some of the smaller particles only present at 24 hours are the same size as those present in the blank minimum media (both fresh and at 24 hours). The drug containing colloids seem to be smaller for each drug in the Q1 media compared to the minimum which is interesting as this opposes the trend seen for the blank media.

The pattern of peaks for the median fluid is similar to that observed for Q1 where there was a change from fresh to 24 hour blank media of an increase in the proportion of smaller particles. Polydispersity was observed for the same drugs in the median media as for those with Q1 media: felodipine; griseofulvin and tadalafil.

The Q3 media shows much more polydispersity compared to that observed for the minimum; Q1 and median fluids. As with all previous media after 24 hours there was a significant proportion of colloidal structures <10 nm in diameter in the blank media. With the exception of naproxen, all drug containing media show a multi-modal distribution of colloidal particles. In many cases there are two distinct populations; those with a size of around 100 nm and those about 10 nm. It would be very interesting to know more about the composition of these structures. The change in Q3 compared to the previous media discussed (minimum; Q1 and median) is the appearance of a colloidal structure at 100 nm. It may be that the increased [TAC] enables these structures to be formed whereas the previously lower concentrations meant that these structures were not present.

A large decrease in particle size measured in the maximum media point to around 5-6 nm. The structures that were present for the median and Q3 media at 100 nm are no longer present at the same intensity for all drugs.

The biorelevant media shows a more consistent size of ~100 nm with no change from fresh to the 24 hour sample. This is similar to the profiles observed for the median and Q3 media, however, it is a

quite different profile to the other fluids which may have implications of the structures likely to be formed *in vivo* and how this may affect the overall solubility.

Prior to DLS analysis, the samples were filtered through a 0.45 μm filter. However, from the intensity distribution of some of the drugs it can be seen that the instrument has detected particles greater than this size. It may be possible that the colloidal units formed are flexible and are able to navigate through the membrane. A different theory is that the structures split apart, then once through the membrane they then coalesce into the larger arrangements, or as there are also some larger particles in the blank media, they may simply be foreign particles.

Although this study is focused on the fasted state with the media points created from real data from a clinical study analysing fasted state human intestinal fluid, the composition of the maximum media point is closer to that of the fed state. Biorelevant FeSSIF is created with a bile salt concentration of 15 mM and a phospholipid concentration of 3.75 mM³², generating a bile/lecithin ratio of 4:1. Comparing this to the composition of the maximum media point which has a concentration of 36.18 mM and 5.78 mM for bile salt and phospholipid, respectively giving a ratio of approximately 6.26:1. Xie *et al.* analysed the micelles formed in biorelevant FaSSIF V1 and FeSSIF by DLS and the results of this study characterised micelles of a mean size of 7 nm in the fed state and 78 nm in the fasted state which is in agreement with the data measured by DLS in this study⁸⁴, as the fresh biorelevant FaSSIF media was recorded to have a hydrodynamic diameter of 81 ± 2 nm. Xie *et al.* did not report details on the method used to report size and it has been assumed that the z-average was used. In parallel to this difference in size distribution there is also typically an increase in solubility in the fed state which may be related to the density of colloidal structures or possibly the increase in surface area whereby the smaller size increases the overall potential for drugs to interact with these colloidal structures from within the media.

3.4.2. Analysis of Size Data Arranged by Drug

The intensity size distributions for the acidic drugs; naproxen, indomethacin and phenytoin, can be found in Figure 3.5. Naproxen in the different fluids primarily shows a monomodal distribution while indomethacin and phenytoin also show bimodal distributions and peaks with shoulders. There is a small peak that is observed at >1000 nm in the Q1 media for all three acids which may be attributed to a micellar structure but at this size range, this may also be caused by dust/foreign particulates in the sample.

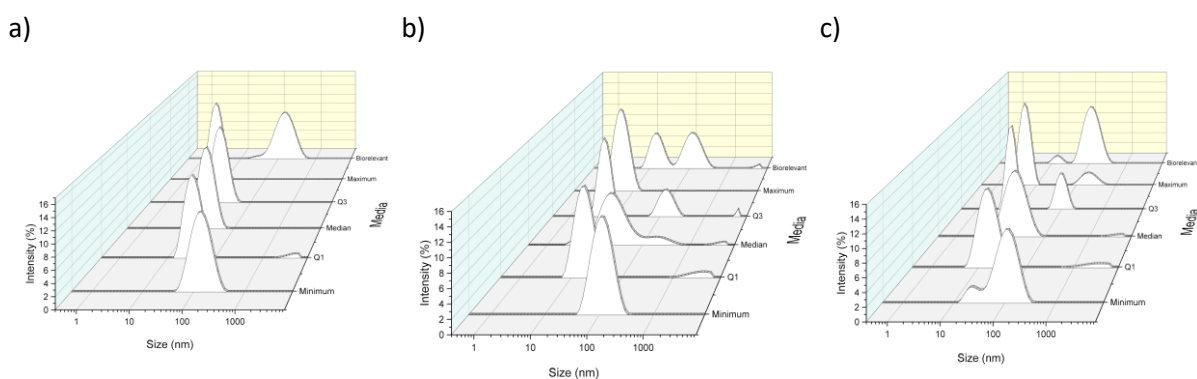


Figure 3.5: DLS size and intensity distribution for acidic drugs in the SIF media, a) naproxen, b) indomethacin and c) phenytoin

Compared to the blank media, the intensity distribution for naproxen shows an almost completely monodisperse dispersion of structures in each of the media points. This may be a result of the drug being fully solubilised into the core of the colloidal units or aggregates creating a uniformity of sized structures. There is a large increase in solubility of naproxen from the minimum media of $105.4 \pm 0.4 \mu\text{M}$ to the Q1 media point of $25633.5 \pm 225.1 \mu\text{M}$ which is accompanied by the considerable hydrodynamic diameter measurement decrease from $145.7 \pm 2.5 \text{ nm}$ to $34.1 \pm 1.4 \text{ nm}$ in the Q1 media. This could indicate that above the CMC of the SIF components, the drug is better solubilised into the core of the micelle which then results in a decreased size of the drug loaded colloidal structures that are formed. This is also observed for indomethacin where the mean solubility drastically increases from $51.9 \pm 0.1 \mu\text{M}$ to $3433.5 \pm 19.5 \mu\text{M}$ while the particle size of the structures decreases from $126.2 \pm 2.5 \text{ nm}$ to $19.1 \pm 0.3 \text{ nm}$ moving from the minimum to the Q1 media.

Figure 3.6 shows the size and intensity for the neutral drugs analysed, felodipine, fenofibrate and griseofulvin. The trends in the size graphs for the three drugs are very similar with the exception of the minimum media where the shape of the size peak is slightly different. The minimum media for felodipine and fenofibrate shows a bimodal peak, with felodipine being more defined. The minimum peak for griseofulvin is monomodal with some smaller particles detected. As this media is below the CMC of the components, the bimodality observed may be due to monomers of bile salts/phospholipid molecules. Another difference that can be seen between graphs is the bimodal peak measured in the biorelevant media for griseofulvin while the other two drugs show strong single peaks at 85.6 nm and 101.9 nm for felodipine and fenofibrate, respectively while the primary peak measured for griseofulvin is considerably lower at 17.9 nm .

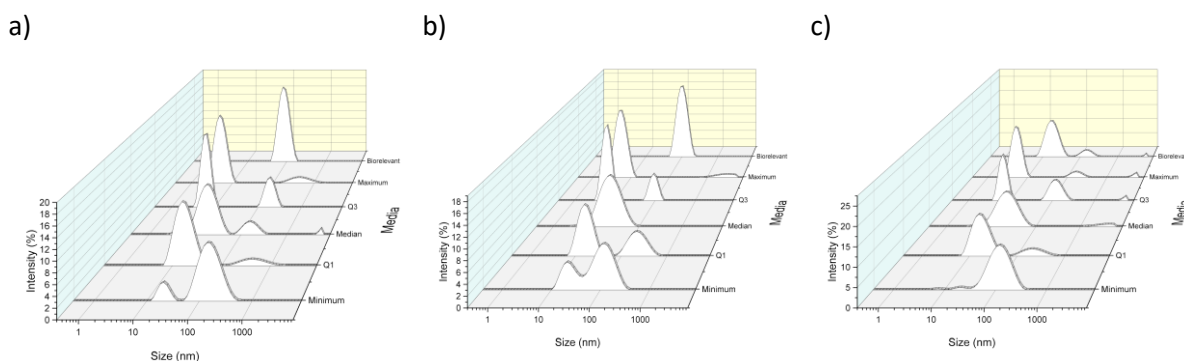


Figure 3.6: DLS size and intensity distribution for the neutral drugs in the SIF media, a) felodipine, b) fenofibrate and c) griseofulvin

The size and intensity distributions measured by DLS for the basic drugs, carvedilol and tadalafil can be found in Figure 3.7. Interestingly, the size distribution outputs for carvedilol show strong monomodal peaks in the new suite of SIF recipes and a bimodal distribution in the biorelevant FaSSIF media. This suggests that the carvedilol is interacting with the components of the simulated fluid and the resulting mixed micelle structures formed consist solely of one size which conflict with the theory that the resulting structures are polydisperse. The distribution trends for tadalafil are unlike those of carvedilol. Both bimodal and monomodal peaks are observed by DLS and the size measured of the primary peak tends to decrease with increasing media point, originating at a modal size of 132.1 nm in the minimum point decreasing to 5.3 nm in the maximum media and 92.2 nm in biorelevant media.

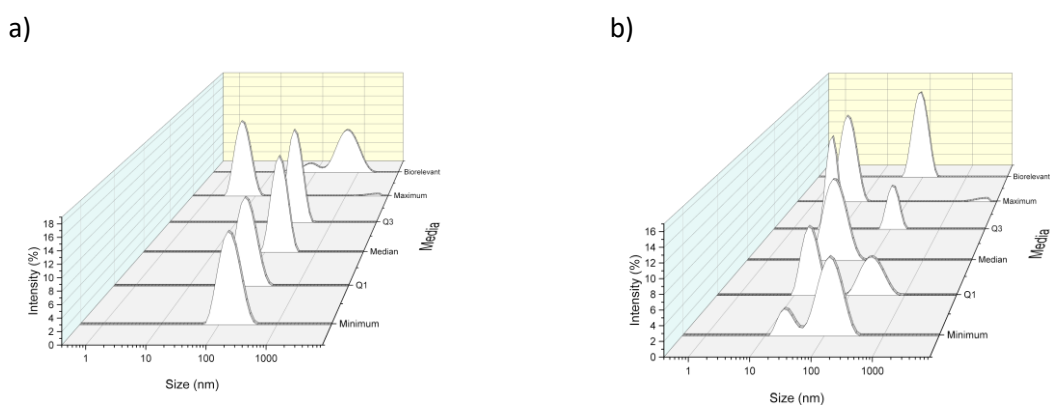


Figure 3.7: DLS size and intensity distribution for basic drugs in the SIF media, a) carvedilol and b) tadalafil

There does not appear to be an obvious link between the solubility of tadalafil and the particle size of the structures measured. Generally, the solubility increases with increasing (pH x [TAC]), while the

particle size tends to decrease. However, the changes are not to the same magnitude to which a relationship between the two can be confirmed.

The particle size of the structures measured by DLS can be found in Figure 3.8. For all drugs and media, with the exception of the blank 24 hours data point in the Q3 media, the lowest size measured was in the biorelevant media point. Typically, the largest size of drug in the media was measured in the minimum media point.

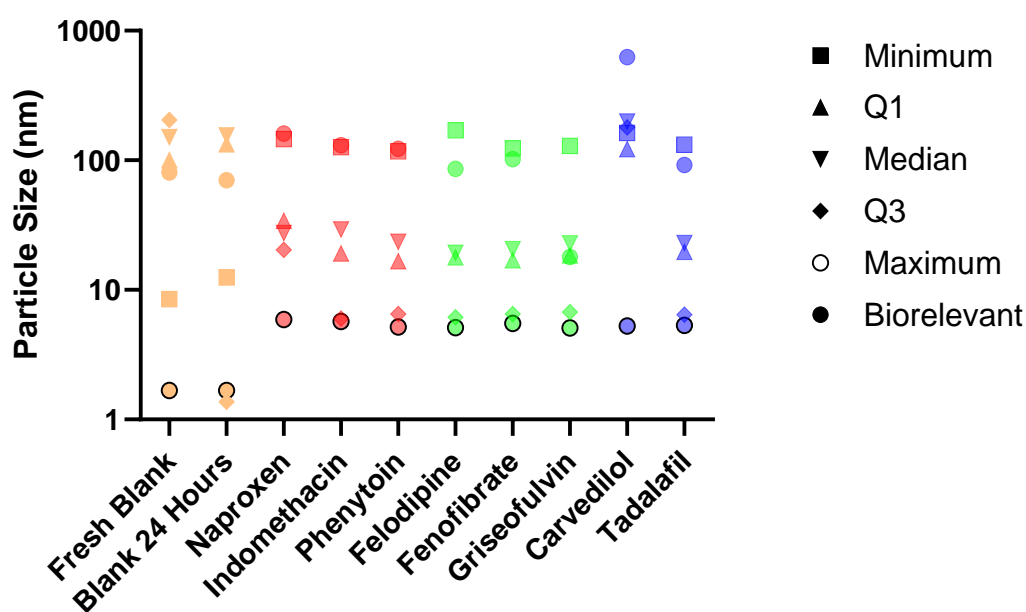
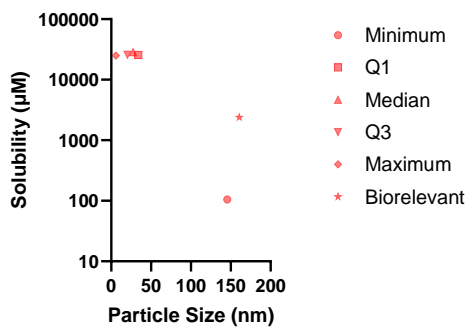


Figure 3.8: Particle size measured by DLS of the media, with and without drugs

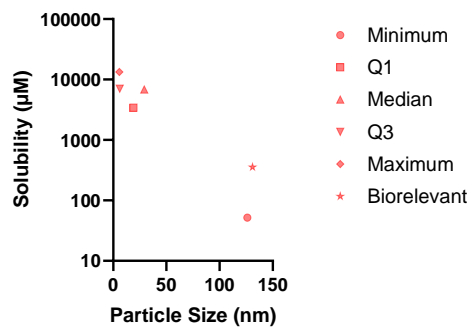
The correlation between solubility and particle size data measured by DLS for each of the drugs in the SIF media can be found in Figure 3.9. A similar trend is observed for all three acidic drugs, the drug in the minimum and biorelevant media points have a lower solubility and greater particle size (between 100-200 nm) than the other four fluids which measure a much greater solubility but lower particle size (<50 nm). It is interesting that the plots of indomethacin and phenytoin show the markers for the different media in the same location relative to the other markers e.g. the maximum media point has the greatest solubility and lowest particle size which is of a slightly higher solubility than that of the drug in the Q3 and median fluid points, which are of a similar solubility but the particle size is measured to be slightly larger in the median SIF than the Q3 media. As the concentration of amphiphiles increases with increasing media point, the solubility of drug also increases and with that there is a decrease in particle size of the colloidal structures formed. This may be due to lipophilic drugs being solubilised

into the hydrophobic core of the micelle structure and increased interactions between drug and micelle. As previously discussed, micelles are not expected within the minimum media due to the low [TAC] which is below the CMC of the components. Therefore, this in part explains the low solubility of the drugs measured here, while the greater particle size is thought to be simply free molecules of the components as the particle size is dissimilar to the greater media points where micellar aggregates are expected.

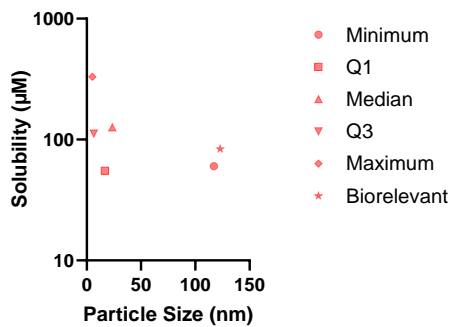
a)



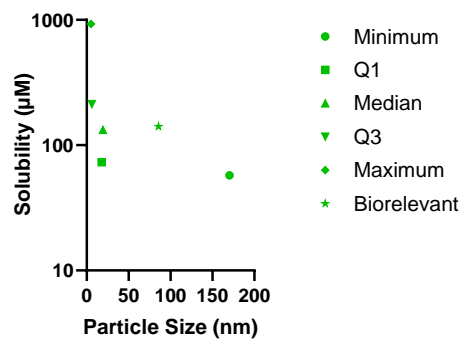
b)



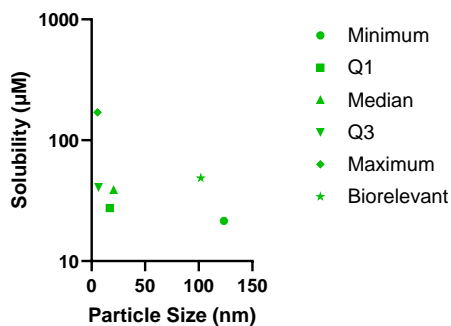
c)



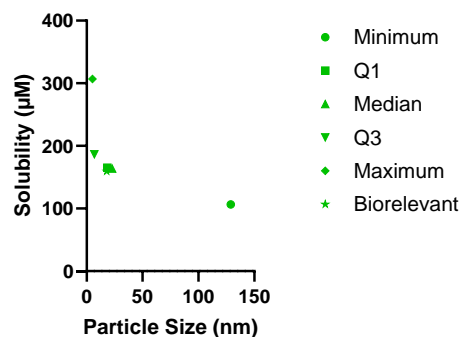
d)



e)



f)



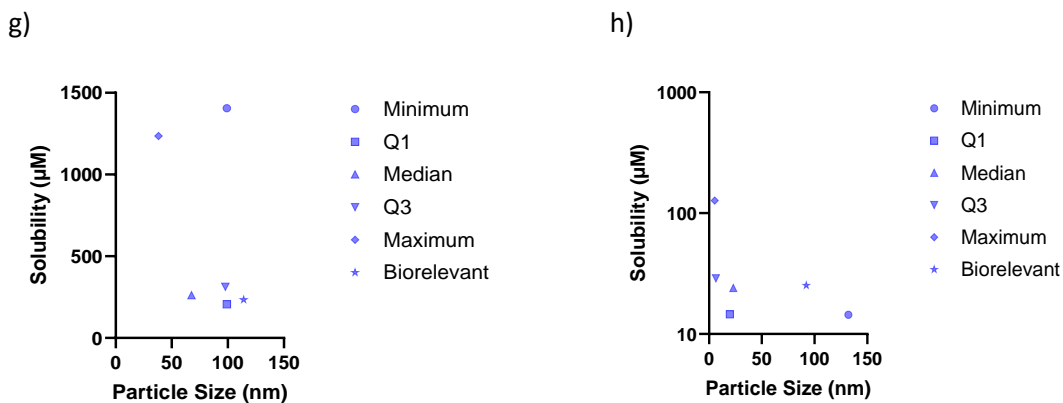


Figure 3.9: Plot of solubility and particle size measured by dynamic light scattering of a) naproxen b) indomethacin c) phenytoin d) felodipine e) fenofibrate f) griseofulvin g) carvedilol h) tadalafil in each of the SIF media

A similar trend is found in the neutral drugs in the SIF media as observed in the acidic drugs. As expected, the minimum point shows the lowest solubility values with the greatest particle size recorded and the highest solubility and smallest particle sizes were measured in the maximum SIF media points. The solubility of the drugs in the biorelevant media is similar to that of the Q1, median and Q3 fluids, however, for felodipine and fenofibrate the particle size in the biorelevant media is closer to that of the minimum media. This suggests that the drug is solubilising to the same extent as within the SIF media but there are potentially interactions between felodipine/fenofibrate and the composition of the biorelevant media that results in a larger particle size measurement. This is not observed in griseofulvin so it is not strictly a phenomenon associated with neutral drugs.

A visual analysis of the basic drug carvedilol indicates that the relationship between solubility and particle size here is unlike the other drugs. A few points to note from the carvedilol plot include: the minimum particle size is as expected when compared to the other drugs however a very high solubility is recorded in this point; the Q1, median and Q3 points all have much greater sizes of colloidal structures formed while the solubility of the three points are similar as per the other drugs; the maximum media point is the only point that behaves in a comparable nature to all of the drugs analysed, where both a high solubility and small particle size is measured. Tadalafil follows the same trends as the other drugs although the solubility is much lower while the particle size is similar to the acids and neutrals. The general trend recorded in nearly all of the drugs indicates that while solubility is to some extent affected by pH and [TAC] or (pH × [TAC]) the relationship between solubility and particle size is linked with the total concentration of amphiphiles ([TAC]).

3.5. Conclusion

In conclusion, the work carried out in this chapter analysed drug and drug free samples of simulated intestinal fluid that is reflective of *in vivo* gastrointestinal variability by dynamic light scattering. The intensity distribution was used, in place of the z-average or volume distribution, from the data output due to the polydispersity present in the samples. Trends relating to solubility and particle size were identified and it was found that in nearly all of the drugs analysed, the general trend indicates that while solubility is to some extent affected by pH and [TAC] or (pH × [TAC]), the relationship between solubility and particle size is linked with the total concentration of amphiphiles ([TAC]). As the (pH × [TAC]) increased, the solubility of the acidic drugs (naproxen, indomethacin and phenytoin) also increased and with that a decrease in particle size of the colloidal structures was observed. A similar trend was found in the neutral drugs (felodipine, fenofibrate and griseofulvin) in the SIF media. The basic drug carvedilol measured much greater sizes of colloidal structures formed in the Q1, median and Q3 media, while the drug solubility in this media was comparable to the other drugs analysed. It was found that the other basic drug analysed, tadalafil, followed the same general trends as the other drugs, with the particle size of the structures being comparable, the solubility was measured to be much lower.

Chapter 4

Nanoparticle Tracking Analysis of Fasted State
Simulated Intestinal Fluid

4. Nanoparticle Tracking Analysis of Fasted State Simulated Intestinal Fluid

4.1. Introduction and Theory

Nanoparticle tracking analysis (NTA) uses laser light scattering microscopy in combination with a camera to record the movement of the nanoparticles in solution. The NTA software is then able to use the recording to identify individual nanoparticles and track the movement of these under Brownian motion. The particle size of the identified particles is then determined from the Stokes-Einstein equation⁸⁵. The primary advantage of using NTA compared to DLS, is that NTA has the ability to detect small and weakly scattering particles that are amongst larger, stronger scattering particles⁸⁶. The method by which DLS calculates particle size makes it very sensitive to the existence of larger particles which in turn means that the presence of dust particles or large particle aggregates can prevent accurate calculation of particle size⁸⁵. NTA has been used for many different types of samples in a variety of fields including evaluating environmental samples and aggregates of nanoparticles and proteins⁸⁶, however, it has yet to be used to study simulated intestinal media.

Both the NanoSight NS300 and the NanoSight Pro (this instrument is also referred to as NS Pro and NTA Pro) are laser-based, light scattering instruments that enable nanoparticle characterisation by simultaneously tracking the Brownian motion of detected particles. With suitable instrument configurations, information can be collected regarding the size distribution, concentration, polydispersity and fluorescence of the sample. The NS300 can detect nanoparticle of the range 10 to 2000 nm, while the NS Pro can measure particles in a liquid suspension between 10 to 1000 nm^{87, 88}. The NTA instrument is useful for polydisperse samples as it can generate multimodal data sets by measuring the Brownian motion to calculate the diffusion coefficient of each particle. The hydrodynamic diameters of each particle are then determined via the Stokes-Einstein equation⁸⁹, Equation 2 (a detailed description of this equation can be found in Section 3.1). The captures taken by the instrument can detect the displacement of particles which are converted into particle tracks. If the threshold distance is met, the instrument confirms the tracked particle⁹⁰.

Equation 2: Stokes-Einstein equation^{71, 73}

$$D_T = \frac{k_B T}{6\pi\eta R_h}$$

Where:

D_T = Translational diffusion coefficient [m^2/s]

k_B = Boltzmann constant [$\text{m}^2\text{kg}/\text{Ks}^2$]

T = Temperature [K]

η = Viscosity [Pa.s]

R_h = Hydrodynamic radius [m]

4.1.1. Instrument Information

Particles suspended in a liquid are loaded into the laser module sample chamber/flow cell via syringe⁹¹. NTA uses a laser beam to irradiate the sample which causes the scattering of light by particles that possess a different refractive index to that of the surrounding medium i.e. the diluent⁹². Available laser wavelengths for the NTA instruments are 405 nm (violet), 488 nm (blue), 532 nm (green) and 642 nm (red)^{87, 91}. The intensity and wavelength of the source is chosen to ensure appropriate scattering occurs from the particles that does not destroy, bleach or modify them in any way. Photobleaching occurs when the fluorophores are exposed to light that causes irreversible damage and results in the loss of fluorescence ability. For fluorescently labelled particles in a non-fluorescent scattering medium, a monochromatic source should be selected that has a wavelength analogous to the excitation wavelength of the fluorophore and the optical filters that are used in the collection of the signal^{91, 92}.

Magnifying optics are used, including lenses, filters and mirrors, to collect the scattered light and are visualised by a detector. Typically, a charge coupled device or a complementary metal oxide semiconductor camera is used that are sensitive enough to the image the light scattered by particles within the sample. The data is recorded and the software is then able to analyse and track the positions of particles as a function of time which enables the analysis of the particles' movement⁹². A basic overview of an NTA system is presented in Figure 4.1.

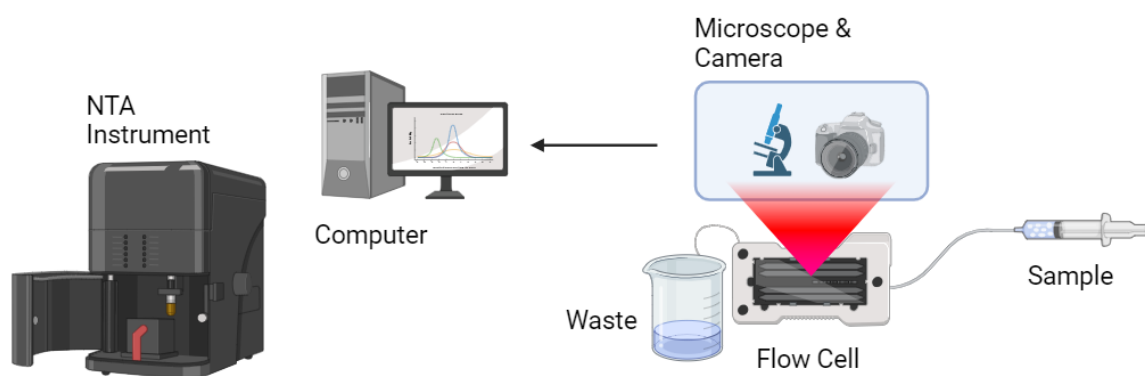


Figure 4.1: Overview of NTA process, adapted from Reference⁹³. Created with Biorender.com

As is the case with any instrument, there are assumptions that must be made and limitations associated with this technique. The range that is able to be practically measured generally ranges from 10 nm to 1000 nm, although this is sample and instrument/system dependent. The measurements are made through the tracking of particle under Brownian motion, therefore as the size of the particles increase, this will result in a decrease in Brownian motion which will ultimately cease once the sample particles exceed the maximum size range. When this occurs, NTA will not be appropriate for particle size analysis. On the other end of the size range, if a particle is too small then due to the refractive index of the particles in relation to the medium and the camera sensitivity of the instrument, this will not be correctly detected⁹⁴. Similarly to DLS, there are assumptions linked to the technique and also to the Stokes-Einstein equation (Equation 2). The particles are assumed to be moving freely and uncorrelated in the three directions under the influence of Brownian motion and for the duration of the instrument measurement time, the particles must be colloidally stable⁹⁵.

4.1.2. Image Optimisation

The image optimisation process is more involved for the NanoSight NS300 instrument as the NTA Pro is more automated in comparison. The NS300 optimisation process involves iterative adjustments to find the optimal beam position, camera level, camera focus and sample concentration. The beam position of the instrument is put into position and calibrated by the manufacturer and should not really be required to move, although small adjustments may be required if the beam is not in the middle of the field of view. The camera level must be adjusted so that the particles in the sample are seen clearly but no more than around 20 % are saturated. If the camera level is too great, the particles will become saturated which will show as coloured pixels, depending on which laser is being used.

The focus of the instrument should be adjusted to ensure clear and sharp images of the particles that are to be analysed are obtained. It may be difficult to obtain perfect spherical focus as the particles are constantly moving but if they are not satisfactory and are indistinct, this will produce inaccurate data. The particle concentration must be optimised as if this is too great, this could prevent accurate particle tracking and if it is too low, this will need longer capture and analysis times to yield statistically significant results. The NS instruments work with particle concentrations in the range of around 10^7 - 10^9 particles/mL⁸⁷. The NanoSight Pro instrument uses an automated camera and focus system, which is the default setting, in which the software automatically determines the optimal camera and focus settings for each sample. The brightness and contrast will change, as well as the focus to determine the optimum settings for analysis, although this can also be done manually. The NS Pro software also

provides an assessment on the camera image quality, giving feedback on whether the sample is suitable for NTA measurements⁹¹.

4.1.3. Data Processing

Data processing was carried out using the instrument software, NS Explorer version 1.0 (NS Pro) and NanoSight NTA software version 3.4 (NS300). The NS Explorer software automatically processes the data collected in the background, producing the record information and data graphs of size (nm) vs. concentration (particles/mL)⁸⁸. The detection threshold, which sets the minimum brightness of pixels considered for tracking, is manually set when using the NS300 instrument. If this is set too low, more pixels that may be particles are detected while at the same time background noise can be tracked. On the other hand, if this is set too high, pixels that are particles will be excluded from the data collection⁸⁷.

The red crosses that appear are considered to be particles that the software recognises as being more reliable, while blue crosses are particles that have been detected with less confidence. The detection threshold should be selected so there are as few blue crosses as possible. Blue particles could be a result of excluded particles or detection errors. As the NS300 software process the captured data, the red particle “tracks” are observed on the display which present the Brownian motion of the particles measured⁸⁷, this can be seen in Figure 4.2.

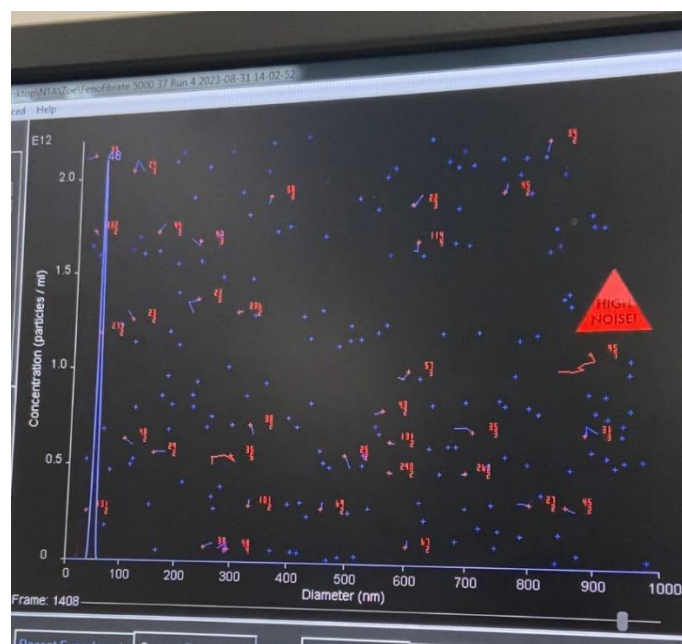


Figure 4.2: View of NTA software (NS300) during image processing

This figure demonstrates the processing of the data collected by NTA. There is a high level of noise detected and a very low concentration of sample that has been measured, which may be a result of an air bubble trapped in the system. When this occurs, this will significantly affect the particle tracking and data quality as there is a decreased sample volume that is able to flow through the system to be measured. This measurement would not be suitable for analysis. Section 4.1.2 details the requirements for the minimum quality of a measurement.

4.1.4. Particle Size Definitions and D Values

Once the raw data is processed, the measured data can be exported for further analysis. The modal particle size is the most frequently measured particle size, which is the strongest peak in the range, while the mean particle size is the average particle size across the distribution recorded. The modal particle size is generally used to describe the particle size rather than the mean, due to the non-parametric/skewed nature of the data sets, especially those of polydisperse nature⁹⁶.

Other useful data collected is the standard deviation which measures the spread of the distribution of size and the D10, D50 and D90, which signify the percentage of particles that are measured to be of equal size or under the diameter recorded. For example, D10 = 41 indicates that 10 % of the total particles measured are equal to or less than 41 nm⁹⁶.

The span of the volume-based size distribution can be calculated using Equation 3⁹⁶.

Equation 3:

$$Span = \frac{(D90 - D10)}{(D50)}$$

The span is a common metric used for evaluating the width of a size distribution. The calculated, unitless, value numerically represents the range of the distribution which provides an insight into the total spread of particle sizes recorded. This can be used to gauge the polydispersity of a sample. Samples with a span of 0-0.5 are typically monodisperse, such as size standards beads. Increasing to samples with a span of 0.5-1.0 are fairly monodisperse, such as liposomes and lipid nanoparticles. Samples with a span greater than 1.0 are labelled to be polydisperse. Typical polydisperse samples include exosomes and aggregated proteins⁹⁶.

Figure 4.3 graphically presents the difference between the D values (D10, D50 and D90), along with the mean, mode and median particle size that is given on the standard NTA size distribution of a polydisperse sample. The results of this graph are from a measurement of the polydisperse sample of phenytoin in the minimum media.

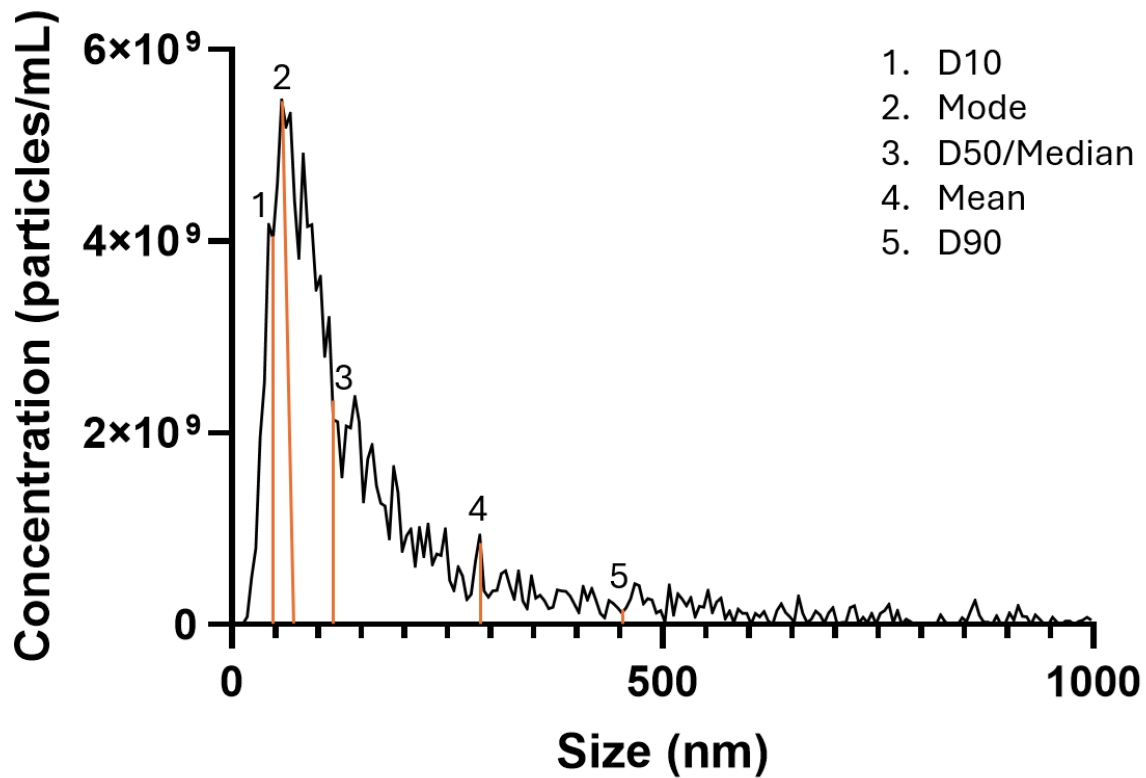


Figure 4.3: NTA size distribution and concentration data for run 1 of phenytoin in the minimum media. Graph has been annotated with reported particle size definitions

4.1.5. Use of NTA in Biopharmaceutics

This technique has been used in the field of bioscience to detect and characterise particle size distribution and concentration of various polymers, protein samples and vaccines^{90, 97, 98}. It has yet to be used for the analysis of simulated intestinal fluid.

An interesting use of NTA for the analysis of a rabies vaccine was carried out by Sanchez *et al.* to detect and determine the size and concentration of particles in suspension through the vaccine production process. It is necessary to monitor vaccines during the manufacture process to guarantee the potency and consistency between batches of the final vaccine is of required standard. Aggregation may occur during the production of the vaccine which will jeopardise the safety and therapeutic efficacy. Using a

NanoSight NS300 instrument (Malvern, UK), each sample of purified rabies vaccine (with/without antibodies, at different stages of manufacture and different formulations) was added to 0.5 mL NaCl then diluted in PBS at a 1:200 dilution prior to analysis. Results from this study indicate that the particle size distribution were similar, showing a monomodal distribution, between the drug substance during the manufacture and the final vaccine product. The diameters recorded ranged from around 100 nm to 250 nm with a mean particle size of around 150 nm⁹⁸. It is interesting that this study reports the mean size measured rather than the modal size. This may be due to the absence of polydispersity recorded of the samples analysed as the figures present are near total monodispersity in the form of a sole peak.

Bannon *et al.* used NTA in order to analyse particle size and aggregation of nanoparticles in blood plasma. This is important as a successful drug delivery vehicle must be able to be stable in blood for it to circulate around the body and the behaviour must be fully understood. Again, a NanoSight NS300 (Malvern, UK) was used, this time to detect and measure particle size and aggregation of fluorescently labelled polystyrene nanoparticle in goat blood plasma. Fluorescence is used here to lessen the scattering effect caused by the various parts of the blood plasma. Unmodified and modified (with various PEGylations) of polystyrene samples were measured in saline and in goat blood plasma and the calculated protein corona thickness in goat blood plasma was recorded. It was found that the calculated thickness did not vary considerably between the unmodified and PEGylated particles which was unexpected. This was thought to be due to the incorporation of the soft protein corona in the NTA measurements, as the altering of the flow rate on the instrument will result in a change in the shear force applied to the particles which will in turn lead to a change in the adherence of the proteins to the polystyrene particles.

4.1.6. Objectives

The objectives of this chapter are to measure the samples of both the new suite of SIF and biorelevant media, with and without the addition of drugs, by nanoparticle tracking analysis. Trends relating to size with regards to increasing (pH × [TAC]) (media point) and/or drug type were identified. A discussion on particle size and solubility is also included as well as a comparison between the particle size data presented in this chapter, that is measured by nanoparticle tracking analysis and the data presented in Chapter 3, that is recorded by dynamic light scattering.

4.2. Materials and Methods

Using the materials and method for creating the simulated intestinal fluid described in Chapter 2, the eight drugs of interest were solubilised in the SIF for 24 hours at 37 °C. NTA measurements were performed with a NanoSight instrument (Malvern, UK), both the NanoSight NS300 and NanoSight Pro systems were used, due to instrument availability, with a 488 nm blue laser. Samples were diluted, using Gilson pipettes (P10, P200, P1000, P5000) to a suitable dilution to enable analysis to occur as recommended in the manufacturer protocols. A suitable dilution is one which meets the optimum measurement requirements as given by manufacturers. Optimum measurement for this instrument is 20-80 particles per frame with the measured concentration range is 10^6 to 10^9 particles per mL. The NS Pro instrument was used for the majority of samples, while the NS300 instrument was used to measure all samples of the maximum media point. The NS300 was also used to record data on the fresh blank Q3 sample, as well as the drugs griseofulvin, carvedilol and tadalafil in the Q3 media SIF.

The dilution factors can be found in Table 4.1, these were of a range of 10-5000 which varied depending on drug and media. A 1 mL disposable syringe was used to inject the samples into the instrument chamber. Triplicate measurements on each sample were taken consecutively, each consisting of 5 captures with 750 frames per capture (each capture was 1 minute in duration), using the NTA instrument script capability. The syringe pump speed for analysis was 1.5 mL/minute and the distribution type used was “raw” which is recommended for polydisperse samples. The instrument was flushed with deionised water between samples. After video capture, the next stage of analysis was data processing of the raw data.

Table 4.1: Sample dilutions prior to analysis by NTA

Drug	Media	Dilution Factors					Biorelevant
		Minimum	Q1	Median	Q3	Maximum	
Fresh blank		1000	1000	1000	50	500	5000
Blank	24 hours	1000	1000	1000	1000	1000	5000
Naproxen		1000	1000	1000	1000	100	2000
Indomethacin		1000	10	1000	100	10	1000
Phenytoin		500	1000	1000	1000	10	1000
Felodipine		1000	100	1000	1000	100	5000
Fenofibrate		500	100	500	1000	100	5000
Griseofulvin		500	1000	500	100	50	1000
Carvedilol		1000	1000	1000	100	50	500
Tadalafil		1000	1000	1000	100	50	1000

4.2.1. Data Processing

Data processing was carried out using the instrument software, NS Xplorer version 1.0 (NS Pro) and NanoSight NTA software version 3.4 (NS300). The span of the volume-based size distribution is calculated using Equation 3. The modal data collected is used in this equation. This shows the spread of the data which has been normalised with the midpoint. The mean of the modal size distributions, standard deviations and other data can be found in Table 4.2.

4.2.2. Comparison between NS300 and NanoSight Pro

As both the NS300 and NanoSight Pro instruments were used, due to instrument availability, it was necessary to ensure confidence and comparability of the two instruments. Personal correspondence, via email to the Applications Team at Malvern stated the following:

“Firstly, both instruments undergo the same verification process, with the same standards. Once a known standard has been measured and successfully passed in both instruments, the results from each are considered reliable.

Regarding comparability, it varies depending on the samples. The NanoSight Pro has improved sensitivity attributed to enhanced image resolution, enabling better tracking of smaller particles. Additionally, results may exhibit reduced noise due to the utilization of a trained neural network algorithm. Also, the implementation of automation significantly reduces user bias.

In practical terms, results for monodisperse samples should be comparable. However, differences may be observed in polydisperse samples, particularly towards the smaller size range.

An attached measurement [Figure 4.4] of small silica particles (resembling biological particles in terms of optical properties) demonstrates this difference, with the NS Pro notably more sensitive in measuring the smaller population than the NS300. Hence, when comparing samples, it is crucial to consider that NS Pro results may better detect and size the smaller range, while the underlying method remains consistent.”

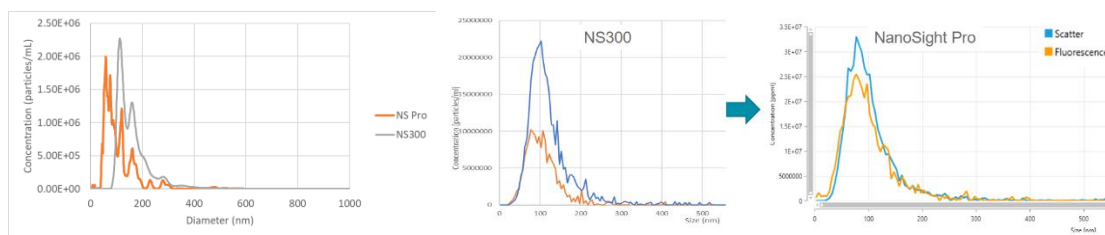


Figure 4.4: Results from the NS300 and NS Pro instruments of small silica nanoparticles provided by Malvern to demonstrate the confidence and comparability of the two instruments used in this study

4.3. Results and Discussion

NTA was used to measure the concentrations and modal size distributions of the samples which could be compared to the measurements recorded by DLS. The mean and standard deviation of the modal distributions measured by NTA for each of the blank and drugs samples in each of the suite of SIF media can be found in Table 4.2. It is important to note that the particle concentration measured for a high percentage of the samples exceeds the optimal concentration for measurement as per the instrument guidelines^{87, 88}. This is due to the high dilution factor required in order to achieve the required number of particles detected per frame that would enable size measurements to occur.

Table 4.2: Particle size analysis by NTA mean of the modal distribution \pm standard deviation (nm)

Drug	Media	Minimum	Q1	Median	Q3	Maximum	Biorelevant
Fresh blank		55.8 \pm 2.9	75.8 \pm 11.5	90.8 \pm 2.9	168.6 \pm 16.8	175.4 \pm 18.3	60.8 \pm 2.9
Blank 24 hours		87.5 \pm 18.0	89.2 \pm 12.6	69.2 \pm 7.6	85.8 \pm 10.4	106.5 \pm 42.8	58.1 \pm 1.9
Naproxen		69.2 \pm 2.9	79.2 \pm 2.9	77.5 \pm 5.0	65.8 \pm 5.8	107.4 \pm 3.5	59.2 \pm 2.9
Indomethacin		67.5 \pm 0.0	75.8 \pm 2.9	62.5 \pm 0.0	64.2 \pm 2.9	100.4 \pm 31.3	59.2 \pm 2.9
Phenytoin		64.2 \pm 5.8	59.2 \pm 2.9	70.8 \pm 7.6	59.2 \pm 2.9	75.2 \pm 2.9	72.5 \pm 0.0
Felodipine		75.8 \pm 2.9	55.8 \pm 2.9	79.2 \pm 2.9	74.2 \pm 2.9	135.5 \pm 6.4	64.2 \pm 2.9
Fenofibrate		55.8 \pm 2.9	215.8 \pm 23.6	80.8 \pm 2.9	95.8 \pm 5.8	142.3 \pm 78.9	69.2 \pm 2.9
Griseofulvin		80.8 \pm 2.9	127.5 \pm 5.0	64.2 \pm 5.8	115.6 \pm 7.8	124.6 \pm 19.4	75.8 \pm 2.9
Carvedilol		99.2 \pm 2.9	99.2 \pm 12.6	67.5 \pm 0.0	97.8 \pm 2.3	38.1 \pm 5.1	114.2 \pm 5.8
Tadalafil		75.8 \pm 2.9	79.2 \pm 5.8	64.2 \pm 2.9	90.3 \pm 2.2	248.3 \pm 49.0	72.5 \pm 5.0

Raw data from the nanoparticle tracking analysis can be found in Tables 4.3-4.8 for each of the blank and drug samples in the various FaSSIF media.

4.3.1. Tables of Raw Data

Table 4.3: Sample information and results of nanoparticle tracking analysis, including modal particle size measured, as well as calculated span and particle concentration (particles/mL) for blank and drug samples in biorelevant FaSSIF media

Media	Sample	Mode (nm)	D10 (nm)	D50 (nm)	D90 (nm)	Span	Concentration (particles/mL)	Dilution
Biorelevant	Fresh	60.8 ± 2.9	45.2 ± 0.6	65.5 ± 0.3	99.9 ± 4.8	0.8 ± 0.1	430.0 x10 ¹⁰ ± 19.0 x10 ¹⁰	5000
	Blank 24 hours	58.1 ± 1.9	31.5 ± 2.5	56.6 ± 0.8	81.2 ± 0.8	0.9 ± 0.1	450.0 x10 ¹⁰ ± 54.0 x10 ¹⁰	5000
	Naproxen	59.2 ± 2.9	47.1 ± 2.5	91.2 ± 4.3	221.5 ± 14.2	1.9 ± 0.1	49.0 x10 ¹⁰ ± 12.0 x10 ¹⁰	2000
	Indomethacin	59.2 ± 2.9	46.3 ± 1.1	84.1 ± 2.4	214.0 ± 21.5	1.9 ± 0.2	180.0 x10 ¹⁰ ± 79.0 x10 ¹⁰	1000
	Phenytoin	72.5 ± 0.0	51.2 ± 0.5	83.4 ± 3.8	217.0 ± 59.9	1.9 ± 0.6	83.0 x10 ¹⁰ ± 22.0 x10 ¹⁰	1000
	Felodipine	64.2 ± 2.9	47.6 ± 0.8	78.3 ± 1.2	181.3 ± 5.9	1.7 ± 0.1	630.0 x10 ¹⁰ ± 130.0 x10 ¹⁰	5000
	Fenofibrate	69.2 ± 2.9	51.9 ± 3.4	88.6 ± 2.3	173.9 ± 9.3	1.4 ± 0.1	250.0 x10 ¹⁰ ± 50.0 x10 ¹⁰	5000
	Griseofulvin	75.8 ± 2.9	68.5 ± 2.3	161.9 ± 10.2	508.7 ± 35.7	2.7 ± 0.1	43.0 x10 ¹⁰ ± 3.9 x10 ¹⁰	1000
	Carvedilol	114.2 ± 5.8	89.8 ± 1.7	227.3 ± 3.5	795.4 ± 55.6	3.1 ± 0.2	8.6 x10 ¹⁰ ± 1.2 x10 ¹⁰	500
	Tadalafil	72.5 ± 5.0	52.9 ± 4.3	97.3 ± 9.9	238.8 ± 43.9	1.9 ± 0.2	53.0 x10 ¹⁰ ± 1.9 x10 ¹⁰	1000

Table 4.4: Sample information and results of nanoparticle tracking analysis, including modal particle size measured, as well as calculated span and particle concentration (particles/mL) for blank and drug samples in minimum FaSSIF media

Media	Sample	Mode (nm)	D10 (nm)	D50 (nm)	D90 (nm)	Span	Concentration	Dilution
Minimum	Fresh	55.8 ± 2.9	41.6 ± 0.3	71.6 ± 2.9	164.1 ± 27.7	1.7 ± 0.3	42.0 x10 ¹⁰ ± 19.0 x10 ¹⁰	1000
	Blank 24 hours	87.5 ± 18.0	54.1 ± 2.5	97.4 ± 3.3	207.4 ± 3.5	1.6 ± 0.1	34.0 x10 ¹⁰ ± 2.6 x10 ¹⁰	1000
	Naproxen	69.2 ± 2.9	51.5 ± 3.4	95.3 ± 5.8	219.2 ± 2.3	1.8 ± 0.1	45.0 x10 ¹⁰ ± 2.9 x10 ¹⁰	1000
	Indomethacin	67.5 ± 0.0	48.8 ± 1.8	89.7 ± 3.4	223.7 ± 5.9	1.9 ± 0.1	45.0 x10 ¹⁰ ± 4.4 x10 ¹⁰	1000
	Phenytoin	64.2 ± 5.8	51.4 ± 2.3	114.7 ± 4.9	439.9 ± 15.6	3.4 ± 0.3	13.0 x10 ¹⁰ ± 1.0 x10 ¹⁰	500
	Felodipine	75.8 ± 2.9	59.6 ± 3.5	108.9 ± 8.1	217.6 ± 24.1	1.5 ± 0.1	16.0 x10 ¹⁰ ± 2.1 x10 ¹⁰	1000
	Fenofibrate	55.8 ± 2.9	43.7 ± 0.4	77.3 ± 0.6	160.9 ± 5.4	1.5 ± 0.1	14.0 x10 ¹⁰ ± 0.6 x10 ¹⁰	500
	Griseofulvin	80.8 ± 2.9	53.6 ± 1.6	95.7 ± 4.3	206.8 ± 17.1	1.6 ± 0.1	9.9 x10 ¹⁰ ± 1.9 x10 ¹⁰	500
	Carvedilol	99.2 ± 2.9	64.6 ± 1.1	125.9 ± 5.2	359.8 ± 36.1	2.3 ± 0.2	29.0 x10 ¹⁰ ± 2.4 x10 ¹⁰	1000
	Tadalafil	75.8 ± 2.9	56.0 ± 1.6	96.9 ± 0.9	186.1 ± 5.8	1.3 ± 0.1	44.0 x10 ¹⁰ ± 2.1 x10 ¹⁰	1000

Table 4.5: Sample information and results of nanoparticle tracking analysis, including modal particle size measured, as well as calculated span and particle concentration (particles/mL) for blank and drug samples in Q1 FaSSIF media

Media	Sample	Mode (nm)	D10 (nm)	D50 (nm)	D90 (nm)	Span	Concentration	Dilution
Q1	Fresh	75.8 ± 11.5	53.1 ± 3.9	91.9 ± 7.7	182.9 ± 4.3	1.4 ± 0.2	350.0 x10 ⁹ ± 39.0 x10 ⁹	1000
	Blank 24 hours	89.2 ± 12.6	64.8 ± 3.7	132.7 ± 11.3	345.7 ± 43.1	2.1 ± 0.1	230.0 x10 ⁹ ± 12.0 x10 ⁹	1000
	Naproxen	79.2 ± 2.9	48.8 ± 0.3	92.3 ± 1.9	190.8 ± 12.0	1.5 ± 0.1	250.0 x10 ⁹ ± 32.0 x10 ⁹	1000
	Indomethacin	75.8 ± 2.9	59.5 ± 1.5	110.6 ± 2.8	285.9 ± 24.3	2.1 ± 0.3	5.0 x10 ⁹ ± 0.6 x10 ⁹	10
	Phenytoin	59.2 ± 2.9	46.9 ± 1.7	95.8 ± 7.9	231.7 ± 29.1	1.9 ± 0.1	130.0 x10 ⁹ ± 11.0 x10 ⁹	1000
	Felodipine	55.8 ± 2.9	43.2 ± 0.7	78.5 ± 3.4	174.9 ± 12.8	1.7 ± 0.1	75.0 x10 ⁹ ± 17.0 x10 ⁹	100
	Fenofibrate	215.8 ± 23.6	143.9 ± 6.8	254.8 ± 9.1	434.2 ± 15.3	1.1 ± 0.1	9.5 x10 ⁹ ± 0.6 x10 ⁹	100
	Griseofulvin	127.5 ± 5.0	85.6 ± 3.7	148.7 ± 2.8	251.9 ± 1.6	1.1 ± 0.1	97.0 x10 ⁹ ± 14.0 x10 ⁹	1000
	Carvedilol	99.2 ± 12.6	76.5 ± 6.7	146.5 ± 16.9	294.9 ± 33.1	1.5 ± 0.1	240.0 x10 ⁹ ± 95.0 x10 ⁹	1000
	Tadalafil	79.2 ± 5.8	59.4 ± 2.9	106.8 ± 4.9	203.8 ± 18.9	1.4 ± 0.2	190.0 x10 ⁹ ± 20.0 x10 ⁹	1000

Table 4.6: Sample information and results of nanoparticle tracking analysis, including modal particle size measured, as well as calculated span and particle concentration (particles/mL) for blank and drug samples in median FaSSIF media

Media	Sample	Mode (nm)	D10 (nm)	D50 (nm)	D90 (nm)	Span	Concentration	Dilution
Median	Fresh	90.8 ± 2.9	61.9 ± 0.6	104.4 ± 0.9	196.8 ± 2.5	1.3 ± 0.1	63.0 x10 ¹⁰ ± 7.4 x10 ¹⁰	1000
	Blank 24 hours	69.2 ± 7.6	47.7 ± 1.5	87.3 ± 2.9	186.1 ± 5.6	1.6 ± 0.1	69.0 x10 ¹⁰ ± 12.0 x10 ¹⁰	1000
	Naproxen	77.5 ± 5.0	50.7 ± 1.2	91.9 ± 2.5	200.1 ± 8.8	1.6 ± 0.1	24.0 x10 ¹⁰ ± 1.3 x10 ¹⁰	1000
	Indomethacin	62.5 ± 0.0	49.2 ± 1.1	90.5 ± 10.7	201.6 ± 19.5	1.7 ± 0.1	25.0 x10 ¹⁰ ± 3.5 x10 ¹⁰	1000
	Phenytoin	70.8 ± 7.6	50.9 ± 0.9	92.2 ± 3.1	209.1 ± 10.9	1.7 ± 0.1	22.0 x10 ¹⁰ ± 4.9 x10 ¹⁰	1000
	Felodipine	79.2 ± 2.9	60.3 ± 1.9	116.4 ± 1.7	257.4 ± 12.5	1.7 ± 0.1	15.0 x10 ¹⁰ ± 1.6 x10 ¹⁰	1000
	Fenofibrate	80.8 ± 2.9	55.3 ± 1.2	104.9 ± 5.9	224.9 ± 8.6	1.6 ± 0.1	8.9 x10 ¹⁰ ± 0.4 x10 ¹⁰	500
	Griseofulvin	64.2 ± 5.8	44.1 ± 1.7	80.7 ± 4.9	206.1 ± 18.5	2.0 ± 0.3	11.0 x10 ¹⁰ ± 0.9 x10 ¹⁰	500
	Carvedilol	67.5 ± 0.0	48.9 ± 0.6	87.9 ± 3.8	210.8 ± 13.3	1.8 ± 0.1	24.0 x10 ¹⁰ ± 3.9 x10 ¹⁰	1000
	Tadalafil	64.2 ± 2.9	49.0 ± 5.9	82.2 ± 6.8	173.9 ± 10.3	1.5 ± 0.3	27.0 x10 ¹⁰ ± 1.1 x10 ¹⁰	1000

Table 4.7: Sample information and results of nanoparticle tracking analysis, including modal particle size measured, as well as calculated span and particle concentration (particles/mL) for blank and drug samples in Q3 FaSSIF media

Media	Sample	Mode (nm)	D10 (nm)	D50 (nm)	D90 (nm)	Span	Concentration	Dilution
Q3	Fresh	168.6 ± 16.8	130.3 ± 6.7	257.9 ± 39.7	474.4 ± 60.2	1.3 ± 0.1	3.7 x10 ¹⁰ ± 0.1 x10 ¹⁰	50
	Blank 24 hours	85.8 ± 10.4	55.0 ± 2.5	110.5 ± 8.8	262.2 ± 15.8	1.9 ± 0.1	38.0 x10 ¹⁰ ± 10.0 x10 ¹⁰	1000
	Naproxen	65.8 ± 5.8	43.9 ± 0.9	86.9 ± 4.7	225.2 ± 16.7	2.1 ± 0.1	22.0 x10 ¹⁰ ± 7.9 x10 ¹⁰	1000
	Indomethacin	64.2 ± 2.9	48.8 ± 2.5	102.5 ± 12.1	362.8 ± 42.4	3.1 ± 0.1	2.7 x10 ¹⁰ ± 0.4 x10 ¹⁰	100
	Phenytoin	59.2 ± 2.9	47.2 ± 1.7	91.8 ± 4.7	259.9 ± 36.8	2.3 ± 0.3	28.0 x10 ¹⁰ ± 2.3 x10 ¹⁰	1000
	Felodipine	74.2 ± 2.9	54.9 ± 2.7	106.4 ± 2.6	237.5 ± 15.8	1.7 ± 0.1	23.0 x10 ¹⁰ ± 7.1 x10 ¹⁰	1000
	Fenofibrate	95.8 ± 5.8	70.3 ± 1.4	128.4 ± 0.5	262.7 ± 4.2	1.5 ± 0.1	12.0 x10 ¹⁰ ± 1.5 x10 ¹⁰	1000
	Griseofulvin	115.6 ± 7.8	82.8 ± 3.4	139.1 ± 25.0	254.0 ± 12.6	1.3 ± 0.2	2.2 x10 ¹⁰ ± 0.1 x10 ¹⁰	100
	Carvedilol	97.8 ± 2.3	88.3 ± 1.4	118.1 ± 5.8	235.7 ± 10.3	1.3 ± 0.1	2.1 x10 ¹⁰ ± 0.2 x10 ¹⁰	100
	Tadalafil	90.3 ± 2.2	80.1 ± 2.9	112.7 ± 8.9	205.9 ± 24.3	1.1 ± 0.1	2.6 x10 ¹⁰ ± 0.6 10 ¹⁰	100

Table 4.8: Sample information and results of nanoparticle tracking analysis, including modal particle size measured, as well as calculated span and particle concentration (particles/mL) for blank and drug samples in maximum FaSSIF media

Media	Sample	Mode (nm)	D10 (nm)	D50 (nm)	D90 (nm)	Span	Concentration	Dilution
Maximum	Fresh	175.4 ± 18.3	118.2 ± 28.7	196.5 ± 24.9	331.6 ± 36.1	1.1 ± 0.1	110.0 x10 ⁹ ± 59.0 x10 ⁹	500
	Blank 24 hours	106.5 ± 42.8	75.0 ± 33.9	147.4 ± 35.7	268.5 ± 35.1	1.4 ± 0.4	260.0 x10 ⁹ ± 68.0 x10 ⁹	1000
	Naproxen	107.4 ± 3.5	87.2 ± 4.8	120.3 ± 4.1	188.3 ± 17.2	0.8 ± 0.1	30.0 x10 ⁹ ± 12.0 x10 ⁹	100
	Indomethacin	100.4 ± 31.3	70.3 ± 31.2	225.1 ± 67.8	421.0 ± 115.8	1.6 ± 0.1	1.9 x10 ⁹ ± 0.6 x10 ⁹	10
	Phenytoin	75.2 ± 2.9	65.9 ± 4.2	169.9 ± 7.5	426.2 ± 15.8	2.1 ± 0.2	5.1 x10 ⁹ ± 1.9 x10 ⁹	10
	Felodipine	135.5 ± 6.4	111.6 ± 13.9	186.7 ± 10.2	420.1 ± 10.6	1.7 ± 0.2	48.0 x10 ⁹ ± 8.5 x10 ⁹	100
	Fenofibrate	142.3 ± 78.9	106.3 ± 44.9	182.4 ± 90.4	359.6 ± 92.8	1.5 ± 0.5	22.0 x10 ⁹ ± 11.0 x10 ⁹	100
	Griseofulvin	124.6 ± 19.4	83.1 ± 4.9	146.3 ± 49.3	311.3 ± 146.1	1.4 ± 0.5	7.7 x10 ⁹ ± 6.7 x10 ⁹	50
	Carvedilol	38.1 ± 5.1	39.6 ± 4.9	106.6 ± 5.6	296.9 ± 21.1	2.4 ± 0.3	13.0 x10 ⁹ ± 4.3 x10 ⁹	50
	Tadalafil	248.3 ± 49.0	164.2 ± 29.4	304.9 ± 50.9	534.8 ± 24.7	1.3 ± 0.3	19.0 x10 ⁹ ± 7.9 x10 ⁹	50

A video captured by the NanoSight Pro instrument showing light scatter from polydisperse phenytoin mixed micelle structures in the minimum simulated intestinal fluid media can be found with the DOI: [10.15129/069fff16-cdd0-42f2-85a7-ae97f04fba75](https://doi.org/10.15129/069fff16-cdd0-42f2-85a7-ae97f04fba75)

It is necessary to dilute samples before analysis by NTA to ensure that the sample is not too concentrated, as this will generate inaccurate results⁸⁹. To identify optimum sample concentration for analysis, sequential dilutions were made and the final dilutions of each sample prior to analysis can be found in Table 4.1. All samples were diluted with ultrapure Milli-Q water. The drug loaded samples in the new suite of media are buffered with sodium phosphate monobasic monohydrate while the biorelevant samples contain monobasic sodium phosphate dihydrate buffer. The fresh blank and blank 24 hours samples in the new suite of media do not contain buffer.

It is worth noting that the span calculated for nearly all of the samples analysed is greater than or equal to 1. This indicates that the samples are polydisperse in nature.

Figure 4.5 to Figure 4.14 show the modal size distribution for each of the sample replicates measured by NTA. Each figure shows either the blank media or a drug in the suite of different FaSSIF media.

The modal size and particle concentration of the fresh blank media of our suite of FaSSIF and biorelevant media, measured by NTA can be found in Figure 4.5. There is a distinct difference in concentration between the three runs of the fresh blank minimum media (Figure 4.5.a) which may be caused by an increased number of particles detected during the third run. It is important to note, that while the concentration of particles varies for the three repeats of the sample, the modal size distribution does not fluctuate significantly and is measured to be 55.8 ± 2.9 nm.

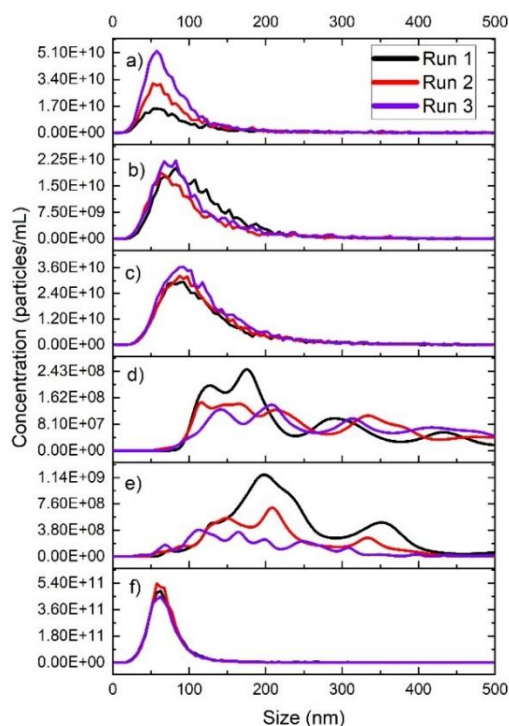


Figure 4.5: Size distribution and particle concentration of fresh blank media a) Minimum, b) Q1, c) Median, d) Q3, e) Maximum and f) Biorelevant where the black line indicates the first run of the sample, red is the second and purple is the third and final repeat of the sample on the nanoparticle tracking analysis instrument

The fresh blank Q1 and median media (Figure 4.5 b and c) present broad singular peaks. The modal size recorded here is 75.8 ± 11.5 nm and 90.8 ± 2.9 nm, respectively. The particle sizes recorded here are all below 200 nm with no larger particles detected for these samples.

The fresh blank samples of the Q3 and maximum media can be found in Figure 4.5.d and Figure 4.5.e. These distributions show particle greater particle sizes with smaller particles (<100 nm) absent. The size distributions of these samples appear significantly different to the other samples within this figure and there are a few theories for that. The first is that there is increased polydispersity within the media that the instrument is detecting. Due to the nature of the sample (increased polydispersity with increasing (pH × [TAC])) and measurement technique (the sample is syringe-loaded through the system), there will not be a uniform polydispersity that is able to be detected by the instrument. This may cause larger particles to sediment within the syringe and go through the instrument in spurts which may explain the reason for the lack of overlap for the individual runs. The other theory is that the samples here have exceeded the measurement capabilities of the instrument. The samples are within the optimum measurement parameters, both particle concentration and particles per frame,

therefore the data produced should be reliable. It should be noted that the fresh blank Q3 and maximum samples were taken on the NS300 instrument which, was found to have a learning curve for the user and without the processing automation of the NTA Pro, had an increased user bias.

The fresh blank biorelevant media (Figure 4.5.f) shows a very clear, clean monodisperse peak at 60.8 ± 2.9 nm, with neatly overlapping repeats, which is in the expected size range of this sample⁵⁰. There is no polydispersity or large particles recorded in this sample.

The modal size and particle concentration of the blank media of our suite of FaSSIF and biorelevant media, measured by NTA at the 24 hour timepoint, can be found in Figure 4.6. The graphs of the size distribution for the minimum, Q1, median and Q3 appear to be of a similar shape – a broad single peak. The shape of the graphs do not vary between the four different medias and the modal particle size remains relatively consistent ranging from 69.2 ± 7.6 nm in the median media, increasing in particle size to 89.2 ± 12.6 nm in the Q1 media.

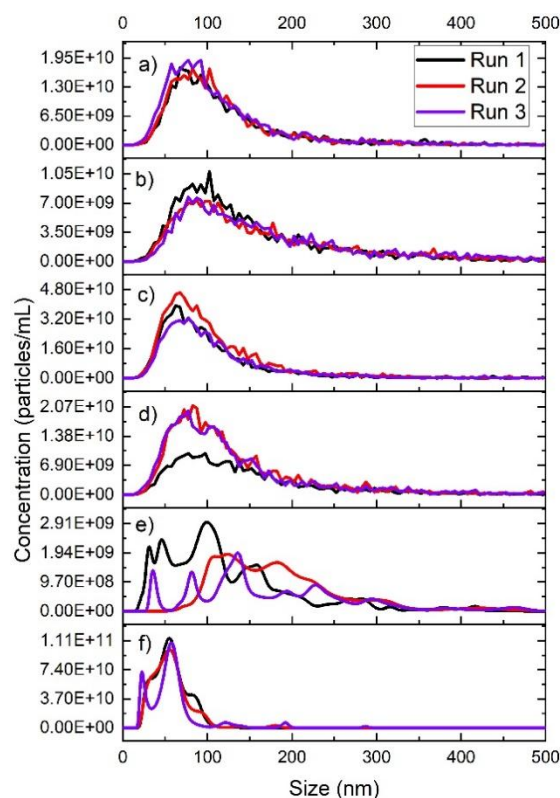


Figure 4.6: Size distribution and particle concentration of blank media at the 24 hour timepoint a) Minimum, b) Q1, c) Median, d) Q3, e) Maximum and f) Biorelevant where the black line indicates the first run of the sample, red is the second and purple is the third and final repeat of the sample on the nanoparticle tracking analysis instrument

As already discussed, it would seem that the instrument is unable to provide a replicable size distribution for the maximum media point that is reliable (Figure 4.6.e.). The biorelevant media at the 24 hour time point (Figure 4.6.f.) measures a modal particle size of 58.1 ± 1.9 nm, which is almost unchanged from the size measurement of this sample at the “Fresh”/2 hour time point (60.8 ± 2.9 nm). This sample has become more polydisperse as time is increased. As can be seen in Table 4.3, the span of the data is approximately the same, however, the spread of data has moved towards smaller particle sizes measured as the D10 is decreased from 45.2 ± 0.6 nm in the fresh sample to 31.5 ± 2.5 nm at the 24 hour timepoint, while the D90 has decreased from 99.9 ± 4.8 nm to 81.2 ± 0.8 nm.

The size distribution and particle concentration of the acidic drug naproxen in the suite of SIF media can be found in Figure 4.7. The modal particle size of naproxen measured in the minimum media (Figure 4.7.a.) is 69.2 ± 2.9 nm which increases to 79.2 ± 2.9 nm in the Q1 media point (Figure 4.7.b.). The size remains relatively unchanged as the ($\text{pH} \times [\text{TAC}]$) is increased in the median media at 77.5 ± 5.0 nm (Figure 4.7.c.). The sample of naproxen in the Q3 media appears to be less reproducible than the samples of lower amphiphile concentration, with less overlap of the size distribution runs. Although, the modal particle size measured in this media point is not significantly different to the other samples, as it is recorded to be 65.8 ± 5.8 nm. Naproxen in the maximum media point measures a particle size of 107.4 ± 3.5 nm and the size distribution output shows a lack of smaller particles detected, when compared to this drug in the other media points. The D10 of this sample is 87.2 ± 4.8 nm, compared to that of the minimum media which is recorded to be 51.5 ± 3.4 nm. The size distribution output for naproxen in the biorelevant media can be found in Figure 4.7.f. The modal particle size measured for this sample is 59.2 ± 2.9 nm and a dilution of 2000 was required for analysis to occur. The size distribution graph of this sample appears to be of a similar shape and span to this drug in our suite of FaSSIF (with the exception of the maximum media point) which suggests that the drug is behaving in a similar fashion in both of the different types of media.

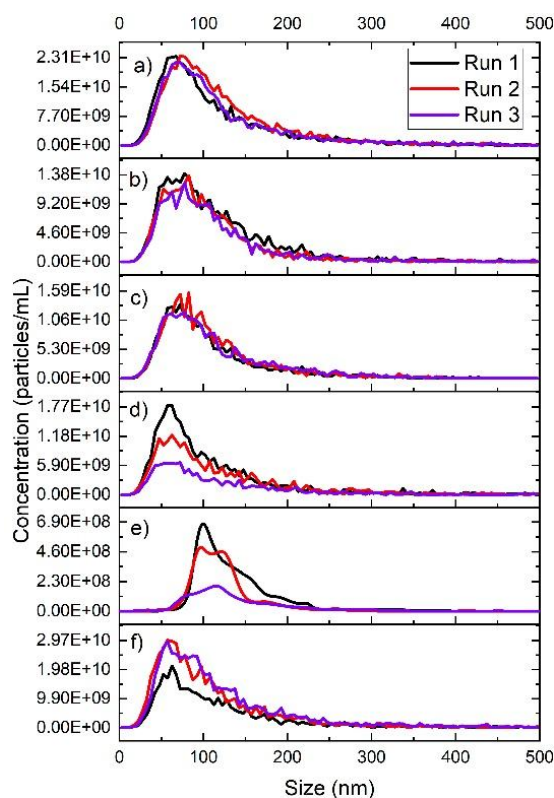


Figure 4.7: Size distribution and particle concentration of naproxen in the a) Minimum, b) Q1, c) Median, d) Q3, e) Maximum and f) Biorelevant media, where the black line indicates the first run of the sample, red is the second and purple is the third and final repeat of the sample on the nanoparticle tracking analysis instrument

The concentration of particles detected of naproxen in the suite of simulated media varies and can be found within the raw data tables. This is plotted along with particle size data in Figure 4.7. There does not appear to be any definitive trends with relation to the concentration of particles detected (particles/mL) and the size of particles measured. From the raw data, moving from the Q1 to the median to the Q3 media points, a decrease in particle size is present alongside a decrease in particle concentration measured. This concentration data is not fully comparable of the drug in the whole suite of SIF fluid as different dilution factors are used prior to analysis which will affect the concentration of particles. As the minimum, Q1, median and Q3 media points with naproxen solubilised are diluted to a factor of 1000 with deionised water, it is assumed that the particle concentrations can be compared. As the dilution factor is increased to a factor of 5000 for the drug solubilised in the biorelevant media, with the deionised water, the particle concentration ($4.27 \times 10^{11} \pm 1.92 \times 10^{11}$ particles/mL) is on the higher size of the concentrations measured, while the modal particle size of the structures is measured to be 59.2 ± 2.9 nm. When comparing the modal particle size/concentration/dilution of naproxen in the maximum media, the dilution factor decreases to 100 with deionised water while the particle

concentration also decreases to $3.04 \times 10^{10} \pm 1.23 \times 10^{10}$ particles/mL. The modal particle size of naproxen in the maximum media is greatest of this drug in any of the SIF media at 107.4 ± 3.5 nm.

As the samples are diluted with deionised water, this could affect the micelles by decreasing the (pH x [TAC]) which may result in this being less than the CMC of the amphiphiles. If this were the case, the drug loaded mixed micelles would disintegrate and drug precipitation would occur. A study analysing the influence of dilution on the morphology and stability of blank and drug-loaded polymeric micelles found that the micelles disintegrated to various extents in all samples analysed. The samples were diluted systematically to a factor of 1000 and the results indicated that the micelles above the CMC are reduced to their fundamental constituent molecules once the dilution is below the concentration at which molecular aggregation occurs⁹⁹.

The particle size distributions and particle concentration of indomethacin in the suite of SIF is displayed in Figure 4.8. The modal particle size measured of this drug in the minimum media to the Q3 media remains fairly constant, reaching a minimum of 62.5 ± 0.0 nm in the median media, to a maximum of 75.8 ± 2.9 nm in the Q1 media. The NTA instrument provides high resolution and sensitivity but is not sufficiently accurate to detect differences as small as 0.01 nm between two modal measurements. This highlights that it is essential to consider modal data alongside D-values (i.e. D10, D50 and D90) and span information to allow for a more robust analysis of the range and distribution characteristics of the particle size of the structures measured. The span of the distributions are also fairly wide with indomethacin in the minimum media having a span of 1.9 ± 0.1 with the D90 to be 223.7 ± 5.9 nm and the sample in the Q3 media has a greater span of 3.1 ± 0.1 with the D90 calculated to be 362.8 ± 42.4 nm. The size distribution of indomethacin in the maximum media point can be found in Figure 4.8.e. This sample appears to be too polydisperse for the instrument to be able to take reproducible measurements. A dilution of 10 with deionised water was required in order to reach an optimal particle per frame concentration for measurement. The modal particle size measured for the sample of indomethacin in the biorelevant media was 59.2 ± 2.9 nm and the mean particle concentration recorded was $17.7 \times 10^{11} \pm 7.9 \times 10^{11}$ particles/mL.

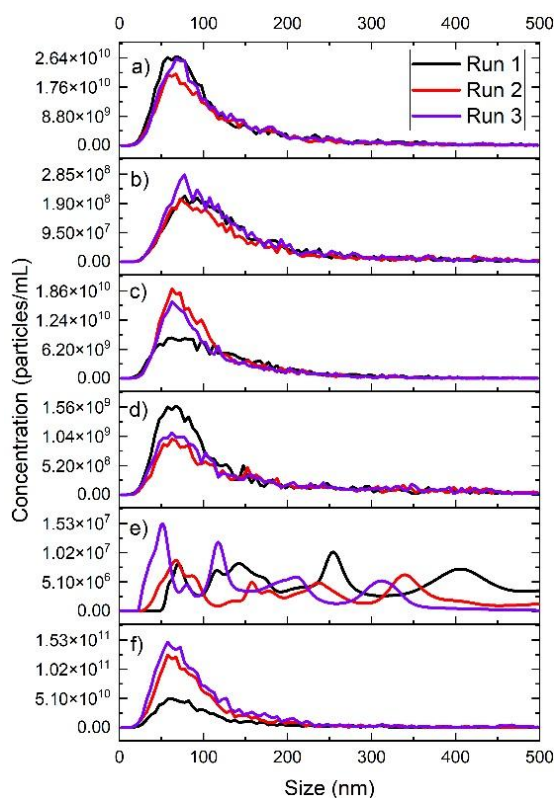


Figure 4.8: Size distribution and particle concentration of indomethacin in the a) Minimum, b) Q1, c) Median, d) Q3, e) Maximum and f) Biorelevant media, where the black line indicates the first run of the sample, red is the second and purple is the third and final repeat of the sample on the nanoparticle tracking analysis instrument

The concentration of particles measured in the minimum media point was $44.8 \times 10^{10} \pm 4.4 \times 10^{10}$ particles/mL at a dilution factor of 1000 which decreased to $24.9 \times 10^{10} \pm 3.5 \times 10^{10}$ particles/mL in the median media at the same dilution factor with deionised water. This also suggests that smaller particles are detected as [TAC] increases at a lower concentration of particles. However, as the particle size increases from the Q1 media to the maximum media (the dilution factor of both samples is 10), the modal particle size increases, while the particle concentration decreases from $5.0 \times 10^9 \pm 0.6 \times 10^9$ to $1.9 \times 10^9 \pm 0.63 \times 10^9$ particles/mL. This data suggests that as the size increases, the particle number decreases; the colloids are forming fewer larger particles.

The particle size distributions and concentrations for phenytoin in the suite of SIF is presented in Figure 4.9. As observed for the other acidic drugs, the outputs for the media of lower ($\text{pH} \times [\text{TAC}]$) i.e. minimum to Q3 media display a size distribution of a similar shape – one large broad peak. The modal particle size is measured to be 64.2 ± 5.8 nm in the minimum media, which is then recorded to be 59.2 ± 2.9 nm in the Q3 media then increasing to 75.2 ± 2.9 nm in the maximum media point. This drug

differs to the other two in the class in the maximum media point (Figure 4.9.e.), where a single large peak dominates the distribution graph. It would appear here that this point, where before there was more uncertainty as to whether the instrument has the ability to measure particles in this media, it seems more possible for this drug as the multiple runs are more overlapping in comparison. This sample required a dilution of 10, with deionised water, while the minimum sample required a dilution of 500 and the biorelevant sample required a dilution of 1000.

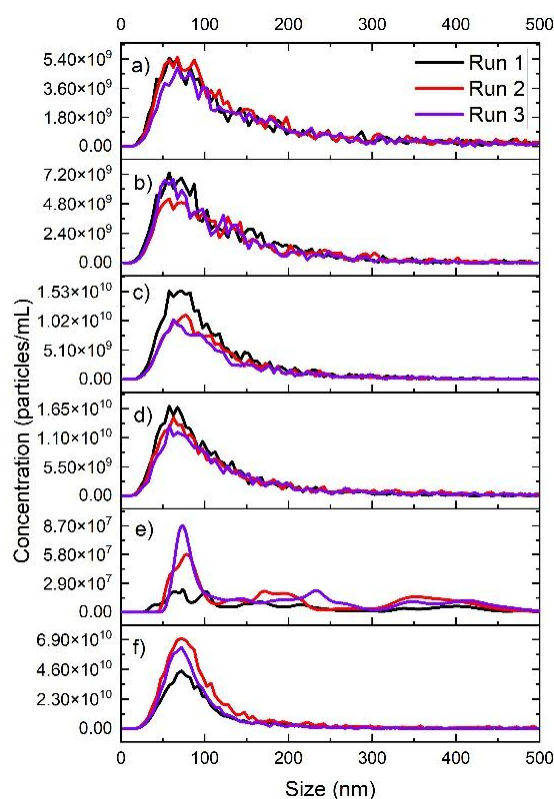


Figure 4.9: Size distribution and particle concentration of phenytoin in the a) Minimum, b) Q1, c) Median, d) Q3, e) Maximum and f) Biorelevant media, where the black line indicates the first run of the sample, red is the second and purple is the third and final repeat of the sample on the nanoparticle tracking analysis instrument

As the $(\text{pH} \times [\text{TAC}])$ is increased from the Q1 media point to the median, the particle concentration is increased from $12.9 \times 10^{10} \pm 1.1 \times 10^{10}$ to $22.1 \times 10^{10} \pm 4.9 \times 10^{10}$ particles/mL, while the modal particle size also increases. Moving to the drug sample solubilised in the Q3 media point, the concentration further increases, although the modal particle size measured decreases. This suggests that there is not a clearly defined relationship between the particle size and concentration.

The particle concentration and modal particle size distribution for felodipine in the FaSSIF media points can be found in Figure 4.10. Felodipine was diluted by a factor of 1000 in the minimum media and by a factor of 100 in the Q1 media in order to obtain a good level of particles detected by the instrument. The modal size measured by in the minimum media was 75.8 ± 2.9 nm which then decreased to 55.8 ± 2.9 nm in the Q1 media.

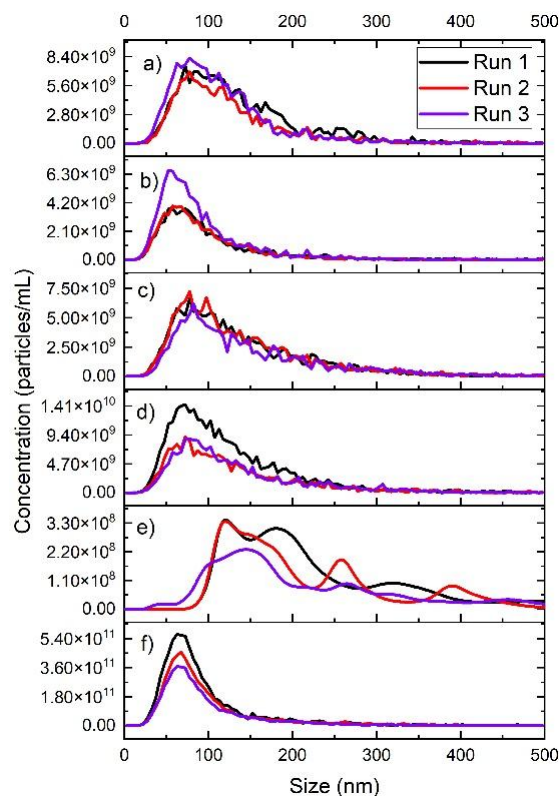


Figure 4.10: Size distribution and particle concentration of felodipine in the a) Minimum, b) Q1, c) Median, d) Q3, e) Maximum and f) Biorelevant media, where the black line indicates the first run of the sample, red is the second and purple is the third and final repeat of the sample on the nanoparticle tracking analysis instrument

In the median and Q3 media, felodipine was diluted by a factor of 1000 and the modal sizes determined were 79.2 ± 2.9 nm and 74.2 ± 2.9 nm, respectively. Only a dilution of a dilution of 100 was required for felodipine in the maximum media point while a factor of 5000 was required in the biorelevant media. The modal sizes determined were 135.5 ± 6.4 nm and 64.2 ± 2.9 nm, respectively.

The increase in particle size to 135.5 nm in the maximum media is linked to the increase in solubility measured in this media at 926.6 μ M. As the solubility substantially increases, the particle size also considerably increases for this data point. A greater quantity of drug is solubilised into the core of the micelle which may result in the larger size of colloidal structure observed. The maximum media point

for felodipine also shows a distinctive multimodality that is not observed to the same extent as the other media points. Although, the dilution factors are not the same in all media so that must also be taken into account.

It is apparent that felodipine in the biorelevant media shows a monomodal distribution, which is expected of the drugs in this media. This further gives evidence that a poorly soluble drug in biorelevant FaSSIF results in monodisperse structures.

The particle size distributions and particle concentration of the neutral drug, fenofibrate in the suite of SIF media is presented in Figure 4.11. The distribution of the drug in the neutral media is displayed in Figure 4.11.a., which measures a modal particle size of 55.8 ± 2.9 nm, at a dilution of 500 with deionised water. The D90 of this distribution (160.9 ± 5.4 nm) is smaller than the drug in the median (224.9 ± 8.3 nm) and Q3 (262.7 ± 4.2 nm) media which show size distributions of the same shape. The span of the data remains fairly consistent which suggests that the particle size of this drug is increasing as $(\text{pH} \times [\text{TAC}])$ increases.

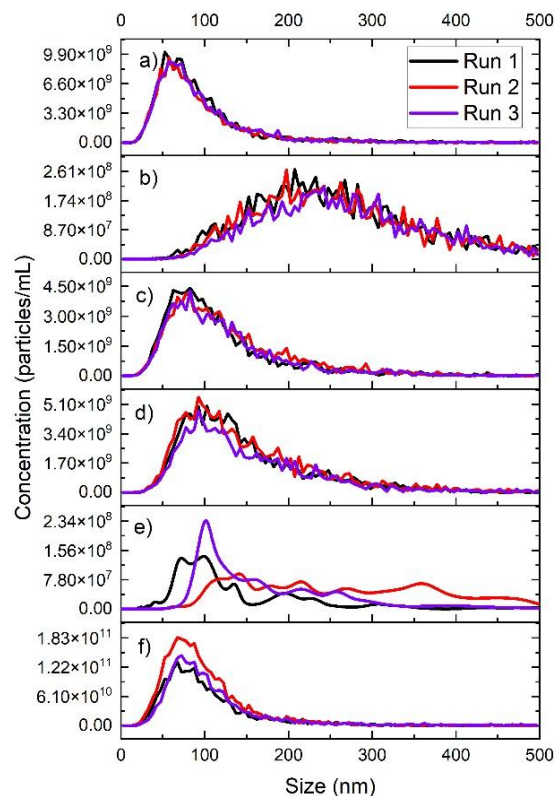


Figure 4.11: Size distribution and particle concentration of fenofibrate in the a) Minimum, b) Q1, c) Median, d) Q3, e) Maximum and f) Biorelevant media, where the black line indicates the first run of the sample, red is the second and purple is the third and final repeat of the sample on the nanoparticle tracking analysis instrument

The particle size distribution of fenofibrate in the Q1 SIF media point is displayed in Figure 4.11.b. This output is unusual and is almost unlike any other distribution graph of the samples in this study. The modal particle size of this sample is 215.8 ± 23.6 nm with the D10 recorded to be 143.9 ± 6.8 nm and the D90 calculated to be 434.2 ± 15.3 nm. The dilution required was a factor of 100 with deionised water to enable a satisfactory number of particles per frame for analysis to occur. The cause of this is unclear and it may be useful to repeat this measurement at a dilution factor of 100 or even at 1000 in order to explicitly rule out the effect of the dilution. There does not appear to be a relationship between this distribution and solubility. The DLS measurement for this sample shows a bimodal distribution, where the primary peak occurs at around 17 nm and the secondary peak at approximately 240 nm.

The size distribution for fenofibrate in the maximum media fluid can be found in Figure 4.11.e. This sample appears to be polydisperse, measuring a modal particle size of 142.3 ± 78.9 nm. As with other drug samples in this media, it does not seem show reproducibility over multiple measurements, which is not surprising due to the polydisperse nature of these samples. Larger particles are found in this sample compared to other samples as the D10 is 106.3 ± 44.9 nm and the D90 is 359.6 ± 92.8 nm. The graph showing the distribution of fenofibrate in the biorelevant media (Figure 4.11.f.) displays a similar shape and modality to the other distributions of this drug in the minimum, median and Q3 SIF media.

The particle size distribution for the griseofulvin drug samples in the suite of SIF and biorelevant media can be found in Figure 4.12. The modal particle size of the drug measured in the minimum media is 80.8 ± 2.9 nm which is increased to 127.5 ± 5.0 nm in the Q1 media point. This distribution is interesting, as it is wider than most found in this study. It is similar to that of fenofibrate in the same media which indicates that something is affecting the particles and micelles which result in a myriad of different sizes of particles and structures. Although for griseofulvin in the Q1 media, it does not visually seem to affect the structures to quite the same extent as can be seen in the distribution of fenofibrate (Figure 4.11.b.).

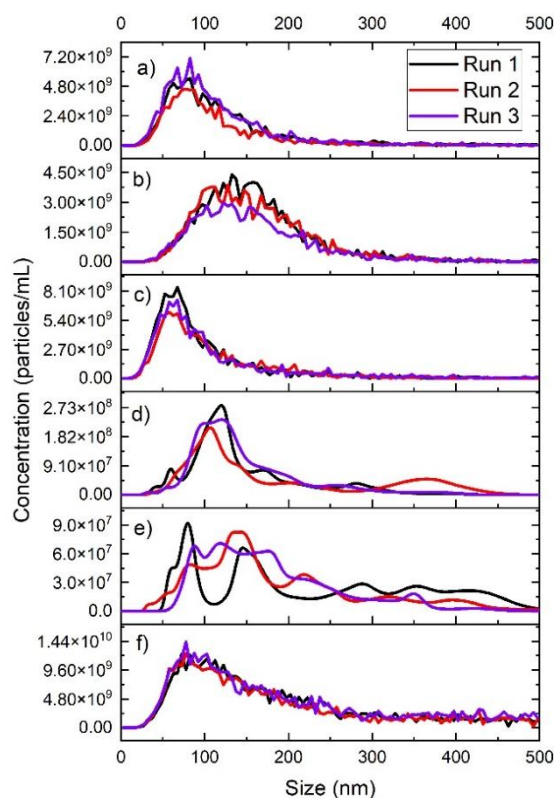


Figure 4.12: Size distribution and particle concentration of griseofulvin in the a) Minimum, b) Q1, c) Median, d) Q3, e) Maximum and f) Biorelevant media, where the black line indicates the first run of the sample, red is the second and purple is the third and final repeat of the sample on the nanoparticle tracking analysis instrument

The modal particle size of the drug in the median media was recorded to be 64.2 ± 5.8 nm which increases significantly to 115.6 ± 7.8 nm in the Q3 media (Figure 4.12.d.). There appears to be increased polydispersity in this sample, with larger particles detected around 300-400 nm, although this may be due to user error and bias that is associated with switching instruments for this sample to the NS300. The distribution of griseofulvin in the maximum media shows a polydispersity that does not seem to be reliably reproducible. The modal size measured here is 124.6 ± 19.4 nm with a large distribution spread. The D10 of this sample is 83.1 ± 4.9 nm and the D90 is measured to be 311.3 ± 146.1 nm. The size distribution of the drug in the biorelevant media can be found in Figure 4.12.f. The modal particle size measured of this sample was 75.8 ± 2.9 nm. The peak for this sample is particularly broad with a span calculated to be 2.7 ± 0.1 . The D10 of this sample is 68.5 ± 2.3 nm and the D90 is measured to be 508.7 ± 35.7 nm.

The particle size distribution of the drug carvedilol in the suite of SIF and biorelevant media can be found in Figure 4.13. The modal particle size measured for the drug in the minimum media was $99.2 \pm$

2.9 nm which remained fairly constant in the Q1 media at a size of 99.2 ± 12.6 nm. As with the neutral drugs fenofibrate and griseofulvin, there seems to be something affecting the particles and colloidal structures in this media, as the distribution is fairly intense and broad.

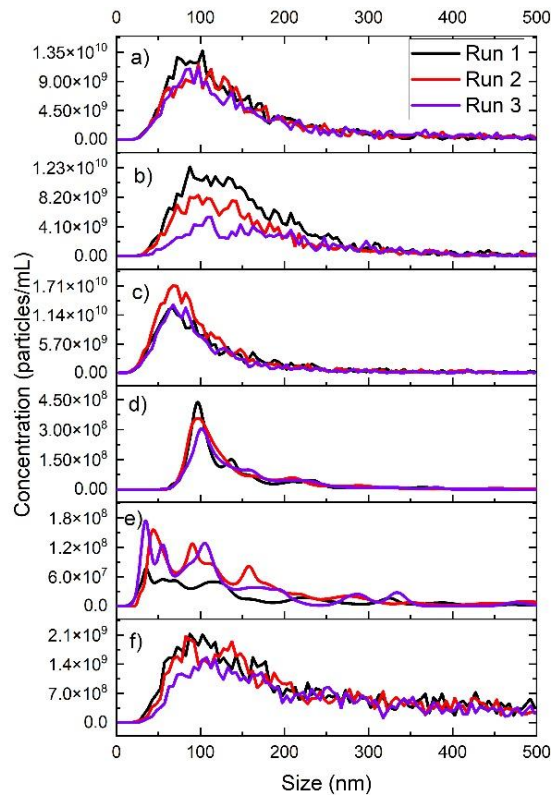


Figure 4.13: Size distribution and particle concentration of carvedilol in the a) Minimum, b) Q1, c) Median, d) Q3, e) Maximum and f) Biorelevant media, where the black line indicates the first run of the sample, red is the second and purple is the third and final repeat of the sample on the nanoparticle tracking analysis instrument

The particle concentration measured of carvedilol in the minimum, Q1 and median media points does not change significantly, decreasing from $28.8 \times 10^{10} \pm 2.41 \times 10^{10}$ particles/mL in the minimum media to $24.1 \times 10^{10} \pm 3.90 \times 10^{10}$ in the median media point while the modal particle size measured decreases from 99.2 ± 2.9 to 67.5 ± 0.0 nm, respectively.

The particle size distribution of the basic drug tadalafil in the suite of SIF and biorelevant media, measured by nanoparticle tracking analysis, is presented in Figure 4.14. The size distribution does not appear to visually change significantly in the fluids (with the exception of the maximum media Figure 4.14.e.) and the data looks to be reproducible with the overlapping distributions from the multiple measurements. The modal size of tadalafil measured in the minimum media is 75.8 ± 2.9 nm which

slightly increases to 79.2 ± 5.8 nm in the Q1 media point. This decreases to 64.2 ± 2.9 in the median media, as does the D90 value from 203.8 ± 18.9 nm in the Q1 media to 173.9 ± 10.3 nm. The modal size measured of the drug in the Q3 media (Figure 4.14.d.) is 90.3 ± 2.2 nm which increases to 248.3 ± 49.0 nm. Again, this sample is potentially too polydisperse for the instrument to reliably measure reproducible results.

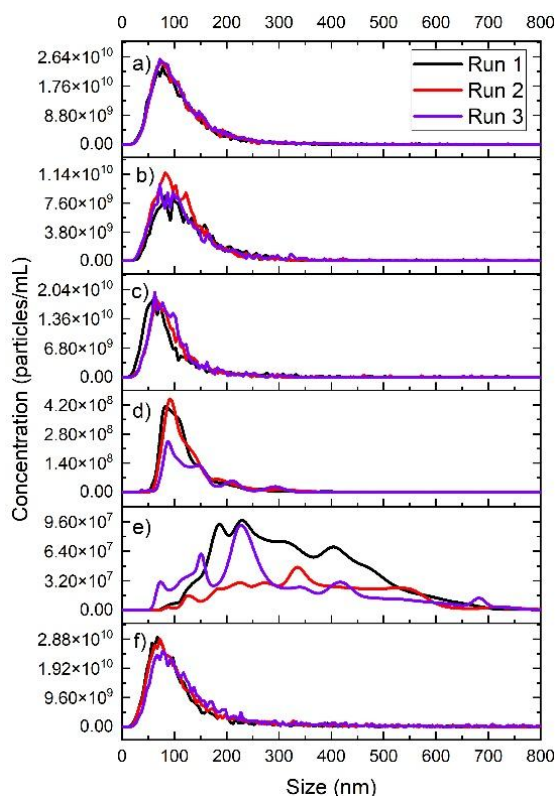


Figure 4.14: Size distribution and particle concentration of tadalafil in the a) Minimum, b) Q1, c) Median, d) Q3, e) Maximum and f) Biorelevant media, where the black line indicates the first run of the sample, red is the second and purple is the third and final repeat of the sample on the nanoparticle tracking analysis instrument

The drug sample of tadalafil in the biorelevant media is reported to measure a modal size of 72.5 ± 5.0 nm with a dilution of 1000 with deionised water required for data capture.

4.4. Summary of NTA Data

The modal size distributions of the SIF media measured by NTA, with and without drugs can be found in Figure 4.15. It can be seen from this figure that most of the sizes determined lie between 50 to 100 nm with a few outliers. Typically, the drug solubilised in the maximum media point results in the

greatest modal size measured with a few exceptions. The first occurs in fenofibrate, where the largest size measured is in the Q1 media, although there is a large standard deviation recorded for the maximum media point which may be caused by a large inhomogeneity of sized particles. The largest particle size for griseofulvin was also measured to be in the Q1 media point. Lastly, this occurs in carvedilol, where the largest sized particles were found to be in the biorelevant media, although taking standard deviations of the samples into account, the particles are not considerably greater than the drug in the minimum or Q1 media. This does not agree with the data recorded by DLS, where the greatest mean particle size measured with either in the minimum media point, or in the biorelevant media point. It is possible that the dilution of the samples alters the colloidal structures, especially in the higher (pH x [TAC]) media points. As discussed previously, where the (pH x [TAC]) is greatest in the maximum media point, this SIF sample is closer to that of the fed state and the addition of the diluent at such high volumes may alter the colloidal structure of the drug loaded micelles resulting in structures that are a ten-fold increased in size than those detected by DLS.

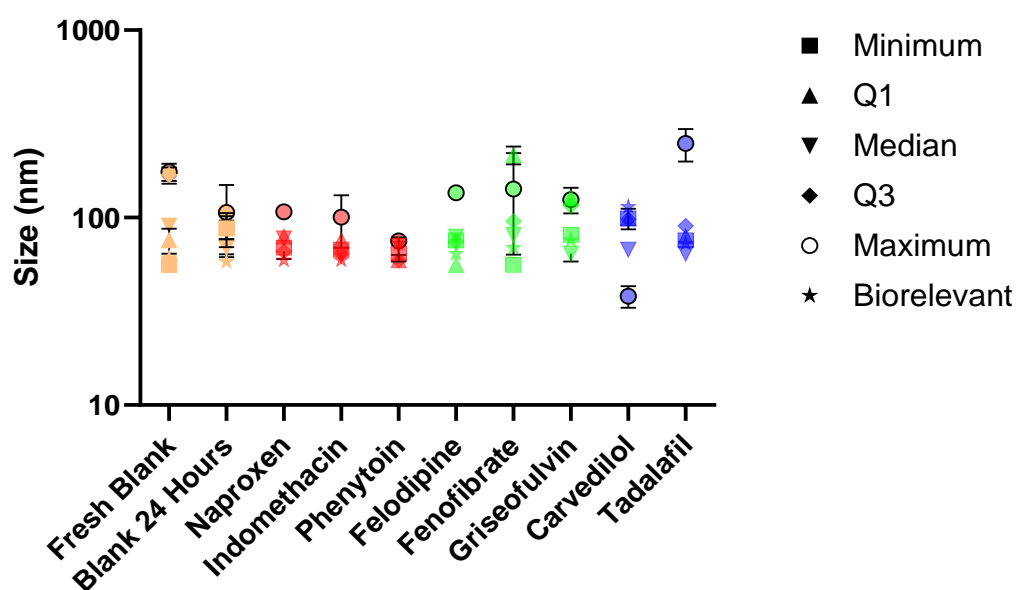


Figure 4.15: Modal size distributions, measured by NTA, of SIF media with and without drugs

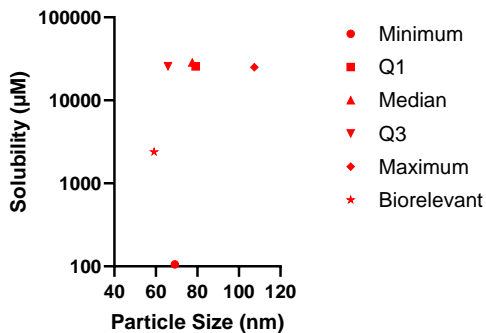
4.5. Size and Solubility

The solubility and particle size data measured by NTA for each of the drugs in the SIF media can be found in Figure 4.16. A similar trend is seen in the acidic drugs naproxen and indomethacin, the particle size recorded of the structures in biorelevant media are the smallest while the solubility of the drug in the minimum media is lower, larger structures are measured. For both drugs the particle size and

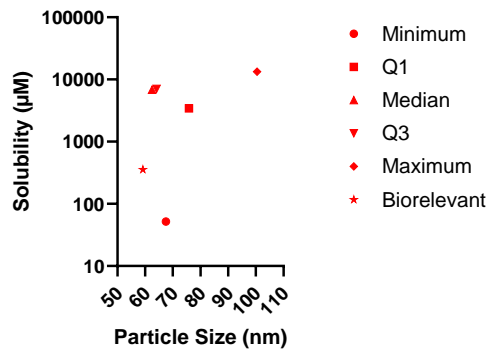
solubility are both greatest in the maximum SIF media. A similar pattern can be observed in both graphs, although the solubility of naproxen is around a ten-fold greater than that of indomethacin.

Another similarity between the two drugs is the particle size and solubility of the samples in the Q1, median and Q3 media; they can be found in the same region of the graph. The trends observed between the two drugs indicate that the drugs solubilise into the different media in a similar way and they interact with the amphiphiles of each media in a similar manner to produce colloidal units that are comparable in size. Like with naproxen and indomethacin, the solubility and particle size of phenytoin measured in the maximum media is found to be the largest. The particle size of the structures in the minimum media are of a similar diameter to the other acids, although the solubility is much greater in comparison to the other solubility measurements in the other media of this drug. Unlike the other acids, the solubility and particle size of phenytoin varies between the Q1/median/Q3 media, with the lowest solubility recorded in the Q1 media and the largest particle size measured in the median media, although it is worth noting that the standard deviation of this measurement is bigger – around 7 nm. Phenytoin in the biorelevant FaSSIF media shows a larger particle diameter than that of the other acidic drugs, this is interesting as the solubility is considerably lower however the particle size is around 10 nm bigger than naproxen/indomethacin in the biorelevant media.

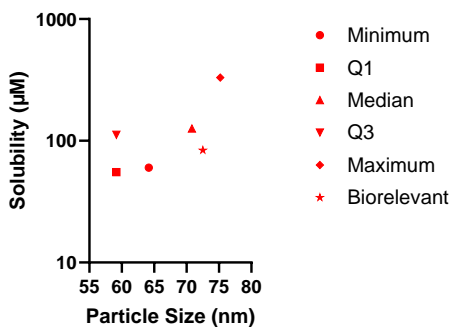
a)



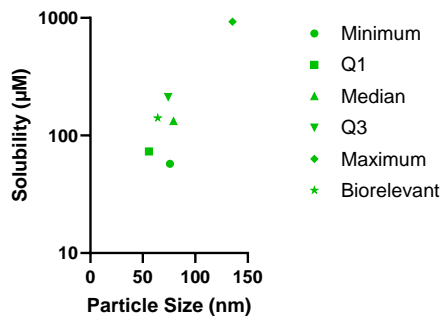
b)



c)



d)



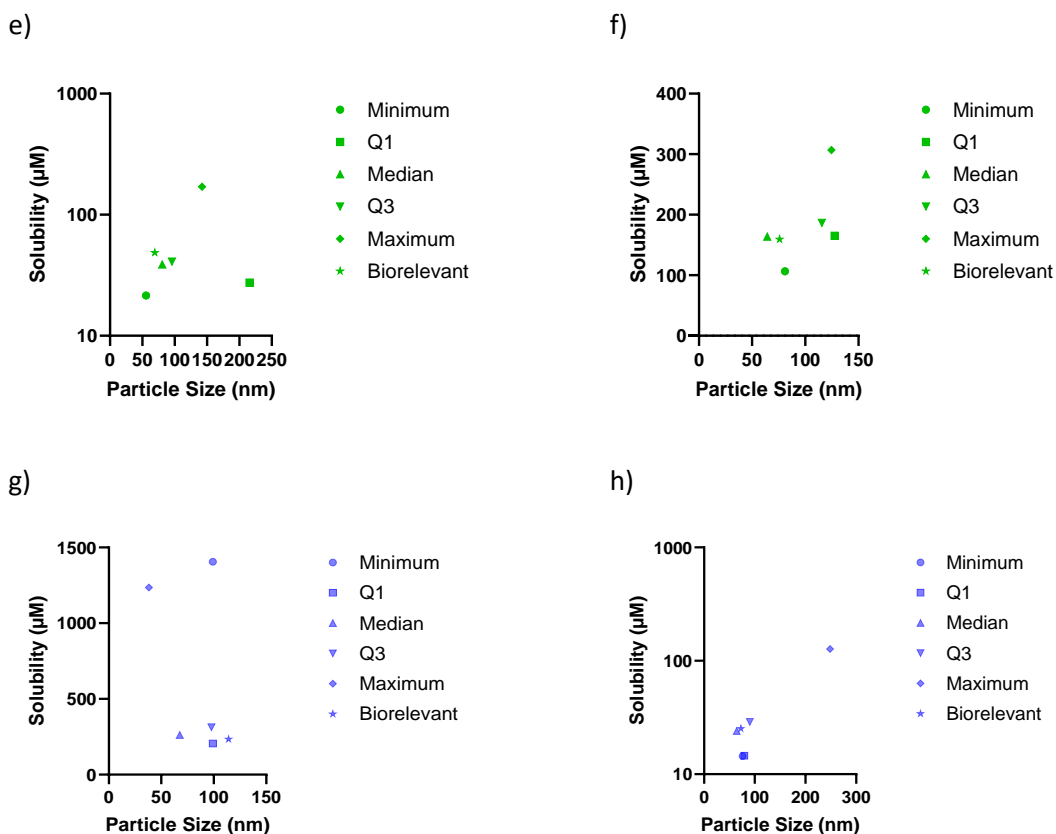


Figure 4.16: Plot of solubility and particle size measured by nanoparticle tracking analysis of a) naproxen b) indomethacin c) phenytoin d) felodipine e) fenofibrate f) griseofulvin g) carvedilol h) tadalafil in each of the SIF media

There are fewer similarities between the solubility and particle size data of the neutral drugs. The highest and lowest drug solubility for the three neutral drugs was measured in the maximum and minimum media, respectively. The particle size and solubility measurements in the median, Q3 and biorelevant media are found close to each other, possibly suggesting link here between the neutral drugs and particle size/solubility.

There does not seem to be obvious trends between the basic drugs and solubility/particle size. The highest solubility value of carvedilol was recorded in the minimum media point which is dissimilar to the other drugs measured as this typically point typically showed the lowest drug solubility. Although the solubility recorded in the maximum point was considerably greater than the other media, this point showed the smallest particle diameter of all carvedilol structures at a size of 38.1 ± 5.1 nm. This data point is interesting, as carvedilol is a basic, hydrophobic drug it is less influenced by pH. This suggests that the drug is interacting with the higher concentration of amphiphiles, resulting in a

smaller colloidal structure. Tadalafil does not show much variability in solubility and particle size. With the exception of the maximum media point, the drug has a solubility between 14 and 28 μM and a particle size between 64 and 90 nm. This indicates that this drug is not heavily affected by changes in pH and amphiphile concentration, especially in comparison to the other drugs studied. The data measured of tadalafil in the maximum media shows a much larger solubility and particle size which may suggest that, at much higher amphiphile concentrations (such as in the fed state) the drug may solubilise at a higher concentration and form larger colloidal structures.

4.6. Comparison with DLS Data

A visual comparison of the size data measured by NTA and DLS of the blank media can be found in Figure 4.17. The modal size data recorded by NTA, of three replicates of the same sample ($N = 3$), is compared to the mean size data measure by DLS, of three replicates of three different samples ($N = 9$). Figure 4.17.a. shows the spread of size data of the fresh blank media where a trend of increasing particle size with increasing ($\text{pH} \times [\text{TAC}]$) can be observed for both the DLS and NTA data. The biggest difference in size is found in the maximum media point, where the DLS data measures the sample to be 1.7 ± 0.1 nm while the NTA measures the sample to be 175.4 ± 18.3 nm. The biorelevant sample is measured to be 80.6 ± 1.7 nm by DLS and 60.8 ± 2.9 nm at a dilution factor of 5000 with deionised water by NTA. The samples measured at the 24 hour timepoint is presented in Figure 4.17.b. It can be seen here that the NTA data becomes more consistent in size, regardless of the increasing concentration of amphiphiles. A large decrease in particle size can be seen for both types of measurements in the Q3 media but to different magnitudes. The NTA detects a size decrease of around 80 nm while the DLS measures a particle size decrease of around 200 nm. Interestingly, the biorelevant sample does not considerably change by measure of either instrument as time is increased, as a change can be observed for the other media samples.

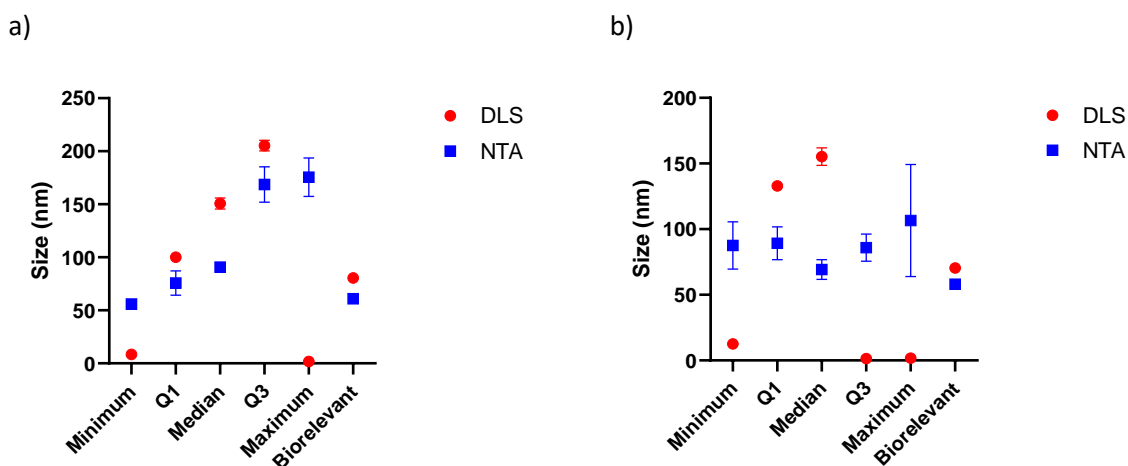
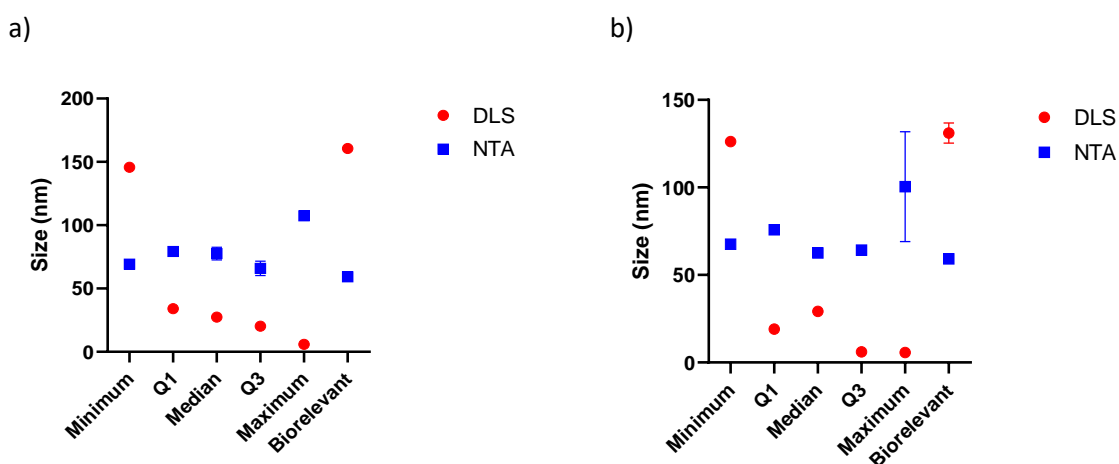


Figure 4.17: NTA and DLS size measurements taken of a) Fresh blank and b) Blank 24 hours in the suite of FaSSiF SIF. Blue points represent NTA data while red points represent DLS data

The size comparison for the acidic drugs, naproxen, indomethacin and phenytoin, measured by NTA and DLS can be found in Figure 4.18. There is a distinct pattern that is found within these figures and the behaviour of the micelles is almost identical between the three drugs. Initially, the particle size is measured to be greater in the minimum media, in the undiluted samples, measured by DLS. This has been explained previously, as it is thought that there are no micelles in this sample as the components are below the critical micelle concentrations. Therefore, it is expected that this sample consists of free molecules and monomer of the substituent components. The three acidic drug samples in the minimum media have been diluted by a factor of 1000 for naproxen/indomethacin and by a factor of 500 for the phenytoin sample, with deionised water. This has caused a reduction in particle size, by around 100 nm (compared to the DLS undiluted sample), which may be a result of dilution affecting the interactions between the colloidal particles and, consequently, the structures they form.



c)

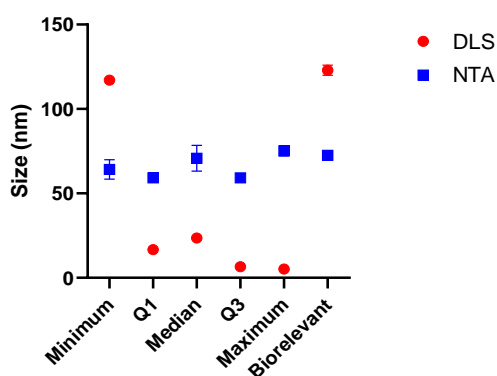


Figure 4.18: NTA and DLS size measurements taken of a) Naproxen, b) Indomethacin and c) Phenytoin in the suite of FaSSiF SIF. Blue points represent NTA data while red points represent DLS data

The low particle size measured by DLS of the acidic drugs in the Q1 media which continues to decrease is a result of the solubilisation of the drug into the micelles. As the total amphiphile concentration is increased, the acidic drugs are better solubilised which may be linked to a decrease in particle size. The particle size of the acidic drugs measured by NTA does not vary between the media points with the exception of the maximum media. The data measured in this study by DLS seems to envelope this with the minimum and biorelevant point are both at the larger end of the size scale and the other media points are measured to be at the smaller size of the figure. A study carried out by Anton Paar (a company that manufacture instruments such as those to measure light scattering and viscosity) characterised micelles of the amphiphilic surfactant disodium cocoamphoacetate using DLS in order to identify the effects of dilution on particle size. Their data showed a ten-fold increase in the 1:100 dilution (in deionised water) from 10 nm in the stock solution to over 100 nm which was thought to be either due to the enlargement of individual micelles as a result of increasing hydration, or due to micelle aggregation¹⁰⁰.

The size comparison for the neutral drugs, felodipine, fenofibrate and griseofulvin, is presented in Figure 4.19. The modal size data is used from the NTA measurements while the mean size data is used from the results of the DLS experiments. Similarly to the acidic drugs, the neutral drugs display a similar pattern. The DLS mean size data is greater in the minimum media by around 100 nm compared to the modal data measured by NTA. As the size measured by DLS decreased as the concentration of amphiphiles is increased, the size measured by NTA increases considerably in the Q1 media for the neutral drugs fenofibrate and griseofulvin, where a wide particle size distribution is recorded and the data measured is in agreement with a study on micelle characterisation carried out by Anton Paar. This

is thought to be a result of dilution in combination with the variance in size and behaviour of the particles depending on their concentration due to interactions that occur between the particles themselves and/or the solvent¹⁰⁰. The particle size distribution for these points can be found in Figure 4.11.b. and Figure 4.12.b.

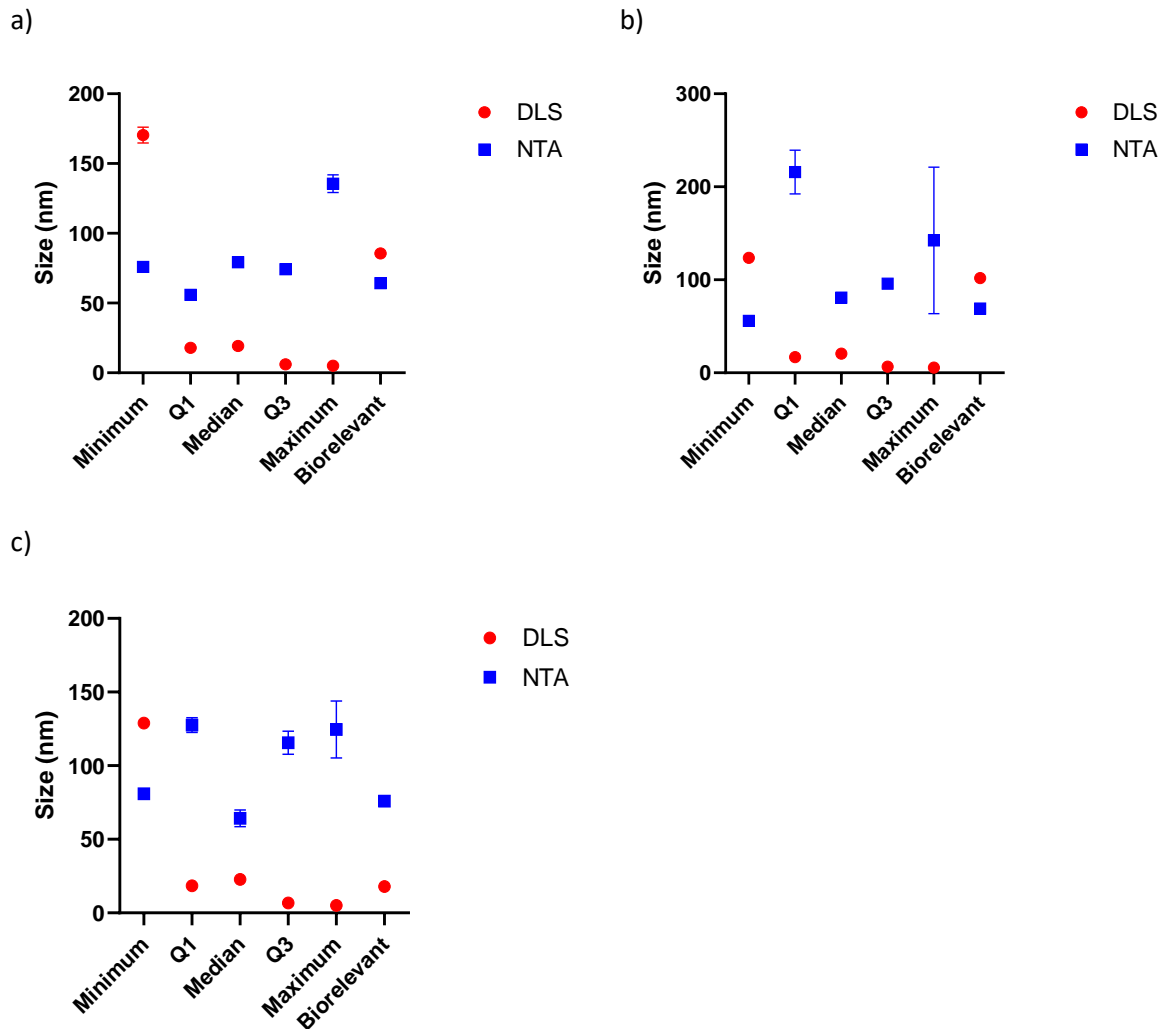


Figure 4.19: NTA and DLS size measurements taken of the neutral drugs, a) Felodipine, b) Fenofibrate and c) Griseofulvin in the suite of FaSSiF SIF. Blue points represent NTA data while red points represent DLS data

The particle size measured in the median media by DLS for the neutral drugs is around 20 nm while the NTA measurement records a particle size of 60-80 nm. The size measured does not change considerably by either method on moving to the Q3 media for felodipine or fenofibrate. However, a large increase in size measured by the NTA for the drug griseofulvin is recorded while the DLS measurement decreases to around 6 nm, in line with the other neutral drugs. There is increased polydispersity found within this sample, compared to the others and the large size increase was

thought to be associated with switching from the NS Pro instrument to the NS300 and the bias associated with this. The distribution for this sample can be found in Figure 4.12.d.

The size comparison between the modal data measured by NTA and the mean data recorded by DLS for the basic drugs, carvedilol and tadalafil, can be found in Figure 4.20. Note, the graphs here use the logarithmic scale for the y-axis rather than the linear scale, as seen for the other figures displaying this data. In contrast to the other drugs, the DLS size measurements for carvedilol are greater than those taken by NTA for the first four media points, which then decrease upon dilution. The DLS size measurement taken in the maximum media, 5.3 ± 0.2 nm, is significantly lower than the other measurements which is a result of the high concentration of drug solubilised into this media point. This sample required a dilution of 50 with deionised water which has increased the modal size distribution recorded by NTA to 38.1 ± 5.1 nm.

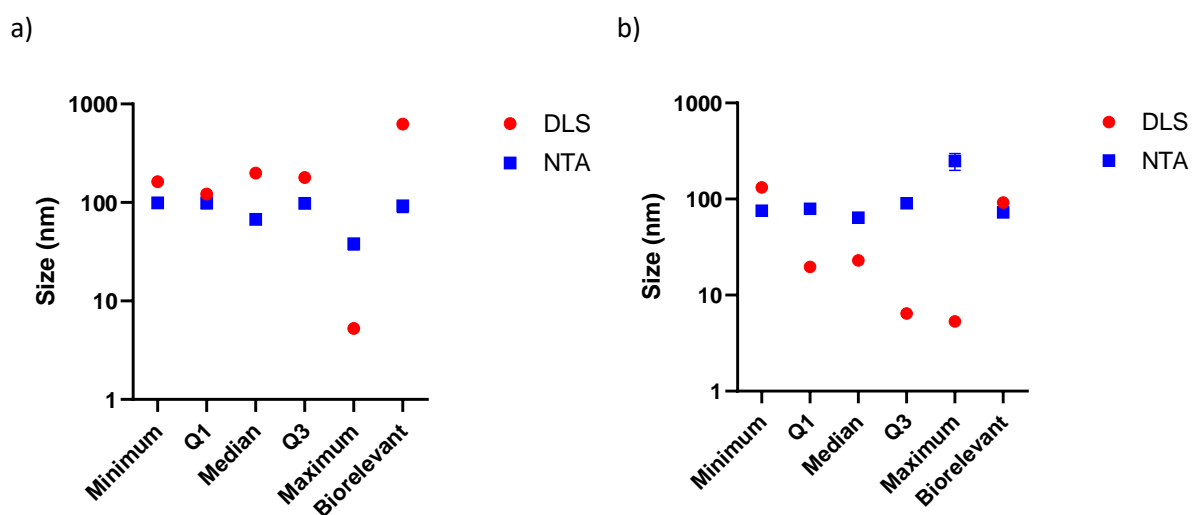


Figure 4.20: NTA and DLS size measurements taken of the basic drugs, a) Carvedilol and b) Tadalafil in the suite of FaSSiF SIF. Blue points represent NTA data while red points represent DLS data

4.7. Conclusion

In conclusion, the work carried out in this chapter analysed drug and drug free samples of simulated intestinal fluid that is reflective of *in vivo* gastrointestinal variability by nanoparticle tracking analysis. The span was used to confirm the polydisperse nature of the samples. Different dilution factors, ranging between 10-5000 were required for each sample, to allow optimised measurements to occur. This varied depending on the drug and media of each sample. Processing of the raw data captured was

carried out using the instrument software. This was automated using the NTA Pro instrument and performed manually when using the NS300 instrument.

Trends relating to size with regards to increasing ($\text{pH} \times [\text{TAC}]$) (media point) and/or drug type were identified and it was found that typically, the drug solubilised in the maximum media point (the greatest ($\text{pH} \times [\text{TAC}]$) value) resulted in the greatest modal size measured. A discussion on particle size and solubility was included. The key findings for the acidic drugs indicate that the smallest particle sizes are typically observed in biorelevant media, while the drug solubility is lower, in the minimum media, larger structures are measured. Both particle size and solubility reach their highest levels in the maximum SIF media. Additionally, the Q1, median, and Q3 media samples of these drugs appear in the same region of the graph, suggesting that they interact similarly with the amphiphiles in each medium.

There were less similarities observed between the solubility and particle size of the neutral drugs. The highest and lowest drug solubilities for the neutral drugs was measured in the maximum and minimum media, respectively. This was found to coincide with the maximum drug loaded structures having a high particle size and the minimum drug loaded structures possessing a smaller particle size. There were not any obvious trends or similarities found for the basic drugs analysed.

A comparison of the NTA data measured in this chapter was provided with the data of the samples measured by dynamic light scattering. A key difference in sample preparation prior to analysis is that DLS uses undiluted samples. A distinct pattern was found in the size comparison of the acidic drugs between the two different measurement techniques. As the total amphiphile concentration is increased, the acidic drugs are better solubilised which may be linked to a decrease in particle size, measured by dynamic light scattering. The particle size of the acidic drug samples measured by NTA did not vary considerably, which may be a result of dilution. The neutral drugs presented a similar pattern to the acidic drugs. The basic drug loaded samples of carvedilol exhibited a greater particle size measurement by DLS than for NTA (with the exception of the maximum SIF sample). This was thought to be a result of the high concentration of drug solubilised into the media point.

Chapter 5

Small Angle X-Ray Scattering (SAXS) Analysis of Fasted State Simulated Intestinal Fluid

5. Small Angle X-Ray Scattering Analysis of Fasted State Simulated Intestinal Fluid

5.1. Introduction and Theory

Small angle X-ray scattering (SAXS) is a powerful technique used for investigating the nanostructures formed by colloidal dispersions¹⁰¹. As electromagnetic radiation penetrates matter, some of the radiation will be scattered due to the electron density inhomogeneities of colloidal size existing within the sample^{102, 103}. The scattered radiation intensity profiles obtained hold information that can provide structure size and other morphological characteristics of the sample material. The scattered intensity pattern, $I(q)$, is expressed as a function of the scattering angle or magnitude of the momentum transfer vector, q , which is related to the scattering angle and the wavelength of the incident X-ray^{102, 104}. This is given by Equation 4.

Equation 4

$$q = \frac{4\pi}{\lambda} \sin\theta$$

Where:

q = momentum transfer, magnitude of the scattering vector [nm^{-1}]

λ = wavelength of the incident X-rays in vacuum [nm]

θ = half of the total scattering angle (between the incident and scattered beam) [deg or rad]

SAXS is currently widely used to research the dynamics and structure of assemblies in various environments. It is used to study a variety of samples in the fields of pharmaceuticals, biology and material science and includes studies of drug microgel self-assemblies as well as biomolecular structures of nucleic acids and organic-inorganic composites¹⁰⁵⁻¹⁰⁸.

5.1.1. Instrument Information

The key components of a SAXS instrument include; an X-ray source, which generates the X-rays for the experiment; optics, used to generate a monochromatic X-ray beam; collimation system, restricts the beam to a well-defined area; sample holder, which holds the sample in the path of the X-ray beam;

beam stop, ; and a detector, which measures the X-rays scattered by the sample¹⁰². A simplified diagram of the SAXS process is presented in Figure 5.1.

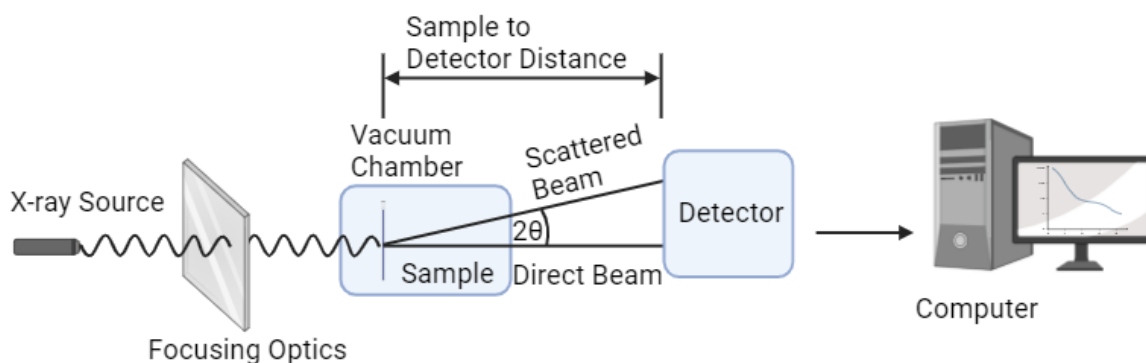


Figure 5.1: Overview of SAXS process, adapted from Reference¹⁰². Created with Biorender.com

The X-ray source generates the X-rays that interact with the sample, enabling the scattering data to be collected. The intensity and wavelength of the X-rays directly affect the resolution and range of the data measured^{103, 109}. The X-ray source of a typical laboratory-based SAXS (labSAXS) instrument creates X-rays from an X-ray tube, where electrons are generated at a cathode and are then accelerated towards the anode. There are various types of anode material used in SAXS that each have their own advantages and limitations. The most commonly used anode material is copper, with a λ (wavelength) of 1.54 Å and energy of 8.04 keV¹⁰³. Molybdenum and gallium sources are also frequently used, with a λ of 0.71 Å and 1.34 Å and energy of 17.4 keV and 9.25 keV, respectively^{103, 110}. Copper anodes are well-suited for general SAXS experiments, while molybdenum and gallium sources are used when higher energy X-rays are required e.g. for samples that are denser. The gallium metaljet source uses a liquid-metal jet anode which is in the molten phase and continuously regenerates, while the standard solid-metal anode is damaged by the beam of electrons¹¹¹.

The role of the optical system in a SAXS instrument is to shape, focus and monochromatise the X-ray beam prior to its interaction with the sample. A monochromator crystal is placed in front of the collimation system so that the sample is hit with monochromatic X-ray radiation. Single crystal monochromators are commonly made from silicon¹⁰³ and are cut along specific planes e.g. 111. The beam will then be reflected off the crystal at a single wavelength, in line with Bragg's law for the angle and cut of the monochromator crystal. Other types of monochromators are used such as double crystal systems and wider bandpass monochromators, depending on the setup of the SAXS instrument¹¹². Mirrors and lenses are also used to focus and shape the beam¹⁰³.

A collimation system is required in a SAXS instrument for the purpose of adjusting the beam. This part of the instrument ensures that the beam is correctly directed, parallel and well-defined prior to reaching the sample. The two types of collimation systems are point and line. Point collimation systems use several pinholes or crossed slits which create a highly focused beam with a small diameter (<0.8 mm). This configuration is generally used for isotropic samples (uniform properties in all directions), as the scattering pattern will appear symmetrically around the beam axis but is also suitable for anisotropic samples. Line collimation systems restrict the beam so that it is narrow and elongated, with a typical dimension of 20×0.3 mm. This type of collimation illuminates a larger sample volume, compared to point collimation and the scattered intensity is greater at the same flux density, which is useful for systems where the scattered intensity needs to be higher. For isotropic systems, line collimation can result in smearing (which is the term used to describe blurring or loss of resolution in the data) which can be corrected by a deconvolution process (removing the effects of smearing to recover the higher-resolution scattering data), but this process will increase uncertainties. Point collimation is more precise for isotropic and anisotropic samples, although line collimation offers the higher intensity at the expense of potential smearing¹⁰². An image of the labSAXS instrument (Xenocs, Xeuss 3.0) at the Diamond Light Source facility can be found in Figure 5.2.



Figure 5.2: Xenocs Xeuss 3.0 LabSAXS instrument at the Diamond Light Source, UK¹¹³

The primary function of the beamstop is to block the direct beam that has not been scattered by the sample. This is to prevent damage occurring to the sensitive detector and also improve the signal-to-noise ratio. Beamstops are typically made of a high Z (atomic number) metal such as tungsten or lead, which can effectively absorb X-rays¹⁰⁹.

The last key component of the SAXS instrument is the detector, which measures the X-rays scattered by the sample. They are designed to capture detailed scattering profiles with high sensitivity and spatial resolution¹⁰³. Photon counting detectors such as the Pilatus and Eiger detectors (Dectris Ltd., Switzerland) are widely used in SAXS experiments and are 2D silicon detectors. They are single photon counting detectors which measure individual photons as they strike the detector with high precision and limited noise. They are commonly used in both labSAXS and synchrotron instruments due to the high precision and excellent signal-to-noise ratios^{107, 110, 114, 115}.

5.1.2. LabSAXS vs. Synchrotron SAXS

SAXS instruments can be roughly categorised into two groups; laboratory-based SAXS (labSAXS) and synchrotron SAXS with each having their own advantages and limitations. LabSAXS instruments are generally easier to access (some universities own a labSAXS instrument) while synchrotron SAXS instruments are located in large-scale facilities such as the Diamond Light Source in Oxfordshire (UK national facility), the European Synchrotron Radiation Facility in Grenoble, France and the Australian Synchrotron in Melbourne, Australia. Synchrotron SAXS instruments such as the I22 beamline at the Diamond Light Source require research proposals, typically 6 months to 1 year in advance of beamtime allocation. This will require planning in advance of the experiment and beam time access is limited during allocated slots, which will also require careful planning and preparation¹¹⁶.

One of the key differences between a labSAXS instrument (such as the Xeuss 3.0, Xenocs, France) and a synchrotron SAXS beamline such as I22 is the X-ray source. Typically, labSAXS will have an X-ray source such as a gallium metaljet liquid (Excillum, Sweden) which is a conventional microfocus tube with the standard solid metal anode that is replaced by a liquid-metal jet. The gallium alloy has an emission of 9.2 keV¹¹¹. The X-ray source on the I22 beamline uses synchrotron radiation, which is far more intense than the labSAXS source. Synchrotron X-ray beams are generated by accelerating electrons through large circular storage ring that produces X-rays that are orders of magnitude brighter than any laboratory source. The energy range of I22 is 3.7-22 keV¹⁰⁷. The higher energy and higher flux (which is a measure of the photons passing through a unit area per second) capabilities of the synchrotron source mean that the quality of the data and efficiency of the measurements are also superior. The higher flux of the synchrotron means that more photons are interacting with the sample which will increase the intensity of the scattered X-rays, resulting in stronger signals detected and an improved signal to noise ratio, enabling the measurements of more precise data¹⁰⁶. The higher flux of the synchrotron X-rays also significantly reduces the time required to acquire high-quality signals. This allows for faster data collection, enabling capture of reliable data on timescales as short as

milliseconds. The rapid acquisition is essential for studying dynamic processes such as phase transitions^{106, 107}.

In addition, synchrotron sources allow for a wider range of q values (scattering vector) to be measured, including lower q values¹¹⁷. The I22 beamline has the ability to detect scattering at a sample to detector distance from 1.9 to 9.9 m, at 0.25 m increments¹⁰⁷, while the detector of the XeuSS 3.0 can extend to approximately 5 m from the sample. At longer distances, the detectors will capture smaller scattering angles, which correspond to lower q values. At these lower values, larger-scale features can be determined such as particle size and overall shape. At higher q values, structural information of smaller scale features such as bilayer's arrangement and structure can be identified¹¹⁸.

5.1.3. Use of SAXS to Image Drug-Containing Colloidal Structures

A recent study by Al-Tikriti *et al.* used SAXS (XeuSS 3.0, Xenocs, France) in order to study the self-assembly of amphiphilic drugs in polyacrylate microgels. The size, shape and structure was characterised of drug micelles formed from hydrochloride salts of three basic drugs; amitriptyline, chlorpromazine and doxepin. The drug micelles that were formed when incorporated into polyacrylate microgels were analysed under varying drug concentrations and ionic strengths. The findings from this study presented indicate that amitriptyline formed oblate-shaped micelles at low drug concentrations which changed into spherical micelles as the drug concentration increased. Both chlorpromazine and doxepin primarily formed oblate-shaped micelles which did not undergo considerable shape transformations. The study provided insights into the behaviour of amphiphilic drug molecules within polyacrylate microgels and the use of SAXS enabled measurements of drug loaded micelle shapes, as well as aggregation numbers and micelle packing within the microgel matrix¹⁰⁵.

Clulow *et al.* used SAXS (SAXS/WAXS beamline, Australian Synchrotron) to study the structural properties of solubilising nanoaggregates in various types of simulated intestinal fluids. Measurements were recorded on both in-house prepared mixed micelles and bile salt micelle solutions, as well as on commercially available sodium taurocholate/lecithin based media (FaSSIF V1 and FeSSIF V1 and V2, biorelevant.com). The in-house micelles were manufactured using sodium taurodeoxycholate (NaTDC) and 1,2-dioleoyl-*sn*-glycero-3-phosphatidylcholine (DOPC). The SAXS beamline was used to record the scattering profiles of the fasted and fed samples composed of different lipid concentrations and created using different methods of preparation. Their findings show that the in-house manufactured NaTDC/DOPC consistently formed oblate ellipsoidal micelles regardless of the lipid concentration or preparation conditions which were also highly homogeneous in size and shape. The biorelevant fasted

state fluids formed vesicles and over time a small increase in vesicle size was recorded which may be a result of slow vesicle aggregation. The fresh samples were measured to have a diameter of 35.1 ± 2.5 nm, while the two day old samples were measured to have a diameter of 36.9 ± 2.7 nm. The fed state biorelevant samples formed prolate ellipsoidal micelles which had a recorded diameter of 5.5 ± 0.2 nm which remained stable at 5.4 ± 0.2 nm in the fresh sample and two day old sample, respectively. The FeSSIF V2 contains an increased number of digestion materials, including glyceryl monooleate and sodium oleate which resulted in larger micellar structures recorded by SAXS with a diameter of 6.5 ± 0.3 nm in both the fresh and two day old samples. This study revealed the detailed structures of SIFs and highlighted the need for consideration of SIF composition in pharmaceutical research as the structural differences present within the various SIF colloidal structures will lead to considerable variations in drug absorption predictions⁴¹.

5.2. Objectives

The aim of this chapter is to measure the samples of both the new suite of SIF and biorelevant media, with and without the addition of drugs, by SAXS. As SIFs have not yet been analysed by a labSAXS instrument, we are not sure if it is possible to obtain any useable data from this experiment, therefore this work is very much exploratory and focuses on discovery, rather than confirmation. The aim is to determine the particle size (and shape, if possible) of the colloidal structures formed in the SIF samples and compare this data to the data recorded by dynamic light scattering and nanoparticle tracking analysis.

5.3. Materials and Methods

5.3.1. Materials

In addition to the materials used to create the samples (described in Chapter 2), 1 mL syringes and PTFE (polytetrafluoroethylene) syringe-filters (13 mm membrane with a $0.45 \mu\text{m}$ pore size) were purchased from Fisher Scientific, UK. The materials supplied by Diamond Light Source used for sample preparation include capillary tubes (one end closed, $1.56 \times 5.00 \times 50$ mm, Vitrex Medical, Denmark), Makrolon[®] single lumen solid (Spectrum Plastics Group, New York, US), Loctite[®] double bubble two part epoxy (Henkel AG & Co., Germany) and Sterican[®] hypodermic needles with luer lock, 0.80×120 mm, 21 G (Braun, Germany). The vacuum oven used is a Heraeus Vacutherm[™] model Vt6025 (Thermo Electron Corporation, now Thermo Fisher Scientific, US).

5.3.2. Methods

5.3.2.1. Diamond Light Source Application

A rapid access proposal was submitted to the Diamond Light Source facility to apply for beamtime on the labSAXS instrument (P38 beamline). This was peer-reviewed by the team at Diamond and was promptly accepted. A copy of the proposal can be found in Appendix 1.

5.3.2.2. Sample Preparation

Samples of each of the five media were prepared at the University of Strathclyde (as described in Chapter 2) to the point where the chloroform was evaporated with nitrogen. The beakers containing the dry film of SIF were sealed securely with parafilm then placed into the freezer for around 24 hours when they could be shipped in dry ice to the Diamond Light Source facility. The samples of SIF were placed into the freezer on arrival at Diamond.

Samples were taken out of the freezer and left to thaw at room temperature for approximately one hour. Samples of the SIF and drug loaded samples were prepared as described in Section 2.3.2. Briefly, they were then reconstituted with ~3 mL ultrapure deionised water, transferred to a 5 mL volumetric flask and made to volume with deionised water. An excess of drug above its solubility limit was added to a 15 mL centrifuge tube (Corning® tubes). Equal aliquots (each of 267 μ L) of simulated intestinal media, buffer and salt were added to the tubes with 3199 μ L of deionised water was added to complete the final volume to a total of 4 mL. The pH was adjusted to target value \pm 0.02 using KOH and/or HCl as required. The target pH values can be found in Table 2.4. The tubes were then secured on a rotary shaker (shipped from Strathclyde, same as used in previous experimental chapters) for 24 hours at room temperature. Note that 25 °C was used rather than 37 °C in Chapter 2, as no suitable heating facilities were available at the Diamond Light Source site.

Each sample was filtered and transferred to a capillary tube. The tube was then plugged with polycarbonate which was then sealed with epoxy sealant. The samples were added to the capillary rack which was then placed into the vacuum oven for 30 minutes, which can be seen in Figure 5.3. This was to ensure the samples were completely sealed prior to SAXS analysis.

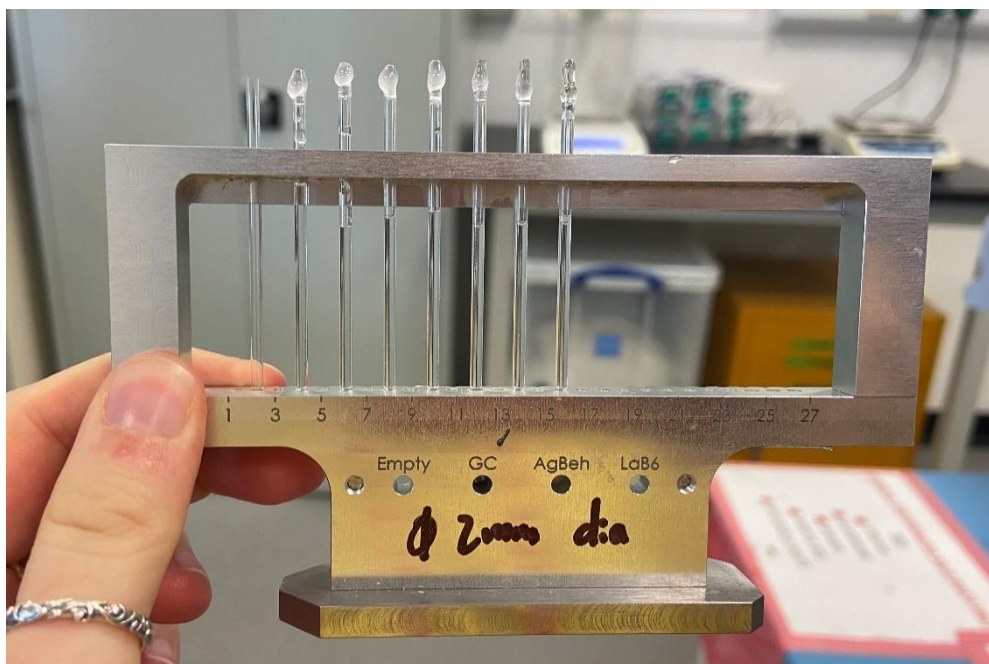


Figure 5.3: Sample holder containing samples for SAXS analysis

5.3.2.3. SAXS Data Collection

The sample holder was added to the sample chamber of the labSAXS instrument (Xeuss 3.0, Xenocs, France) then the air was removed from the chamber so the chamber was under vacuum (this is to minimise the scattering by air). A gallium metaljet X-ray source (Excillum, Sweden) was used for the duration of this experiment with a silicon Eiger R 1M detector (Dectris Ltd., Switzerland). The code written in order for SAXS measurements to be performed can be found in Appendix 2. The scan time for each sample was 3600 seconds (1 hour) with 1 exposure taken per sample. Each sample was measured at a distance of 1000 mm and 4600 mm (1 m and 4.6 m). In this chapter, measurements are reported in millimetres (mm), as this is the unit used by the instrument's software during data collection. Prior to sample measurement, measurements were taken of the standard silver behenate (AgBeh) to allow for powder calibrations to occur. AgBeh is used as it has a well-defined structure that produces sharp and reproducible peaks, providing a reliable reference for scattering. A calibration is required in order to accurately determine the sample to detector distance. At the 4600 mm distance, a virtual detector calibration measurement was recorded of AgBeh, which extends the q -range to wider angles while producing a composite image of 3 different exposures. The scan time for AgBeh calibrations was 900 seconds (15 minutes). Due to analysis time constraints and instrument issues (the X-ray source switched off overnight during the first run of data collection), it was not possible to take measurements of all the samples planned. The data recorded was saved in the nexus file format which is compatible with SAXS processing software.

5.3.2.4. Data Analysis/Processing

5.3.2.4.1. Calibration of Silver Behenate

The first step to process SAXS data is to perform a calibration. Calibration data was recorded of silver behenate (AgBeh) in order to measure and identify the beam centre position, the sample to detector distance and to also calibrate the q-value (scattering vector). AgBeh is used as the standard due to the well-defined diffraction peaks that are evenly distributed in the $1.5\text{-}20.0^\circ$ 2θ range. This results in a scattering pattern composed of distinct rings that are characterised by d-spacing of 58.38 \AA . D-spacing is the distance between adjacent planes of atoms or molecules in a crystalline material^{106, 119}. A virtual detector image is taken at the 4.6 m distance which allows enhanced resolution at low q-values which corresponds to small scattering angles. The virtual detector can give information on the long-range structure. Figure 5.4 shows the first step of the calibration process, which is identifying the rings of AgBeh in the powder calibration perspective of Dawn. Dawn version 2.35.0, is the data analysis software used to process and visualise SAXS data.

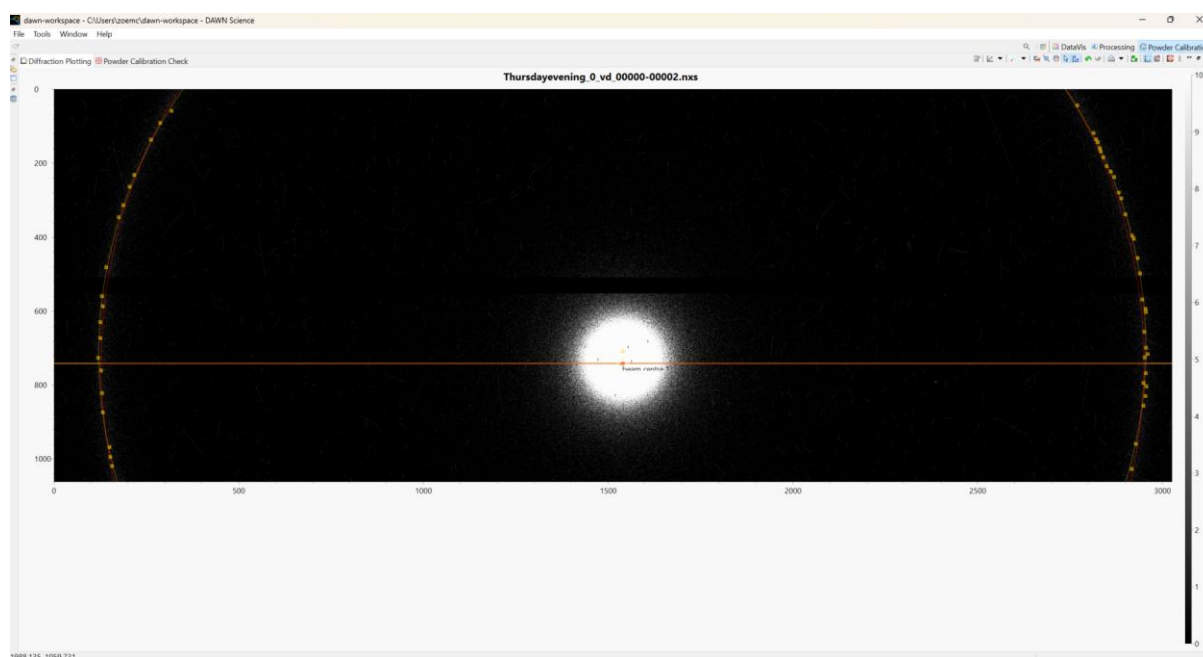


Figure 5.4: The first step of the powder calibration; identifying the rings of AgBeh

Figure 5.5 shows the calibration of AgBeh at the 1000 mm (1 m) detector distance, before and after the rings have been identified by the software. A new calibration must be carried out every time the detector is moved. The d-spacing is labelled on the calibrations towards the left of the inner ring (58.38 \AA).

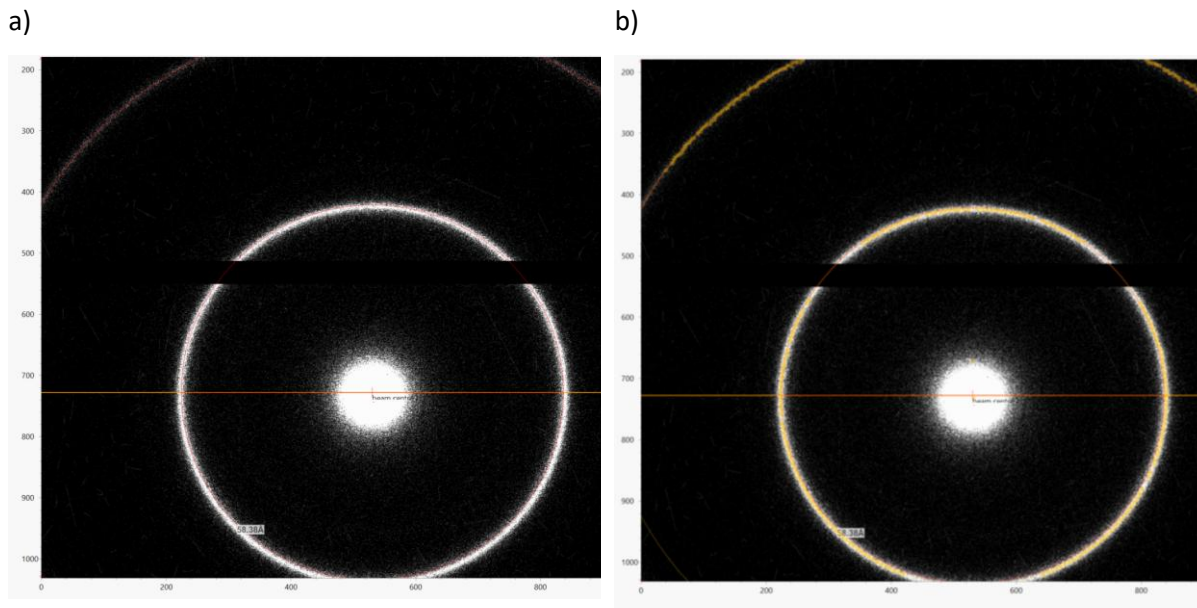


Figure 5.5: Calibration of AgBeh at 1000 mm. a) AgBeh showing one of the rings clearly, b) AgBeh once the software has identified the rings

The powder calibration check output of the silver behenate, measured at 4600 mm can be found in Figure 5.6. The peaks of the scattering vector (Q) align with the assigned positions for this calibrant, which indicates that the calibration have been calibrated suitably to be used for the next processing step.

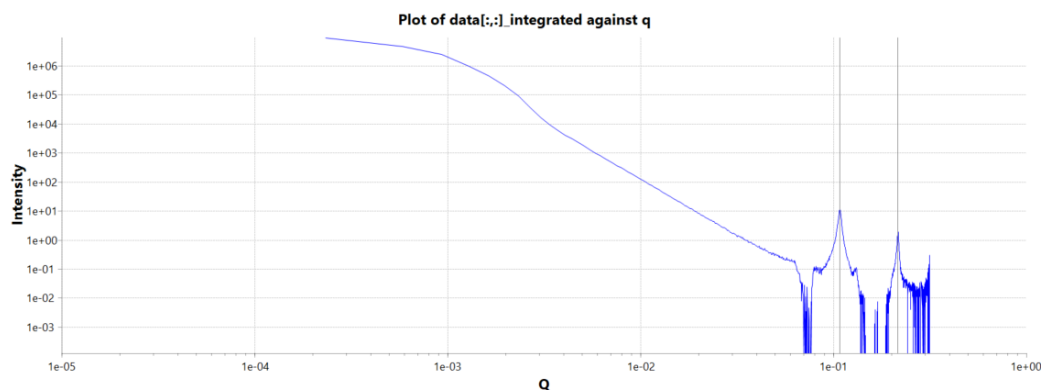


Figure 5.6: Output of the powder calibration check of AgBeh at 4600 mm

Figure 5.7 shows the 1D reduced output (the azimuthal integration) of a deionised water sample to gauge the accuracy of the calibration data (without a mask file applied). The peak at 0 q indicates that the calibration is satisfactory and the calibration process has successfully identified the centre of the X-ray beam spot. Note, the x-axis here is in linear scale which is simply to check the location of the peak.

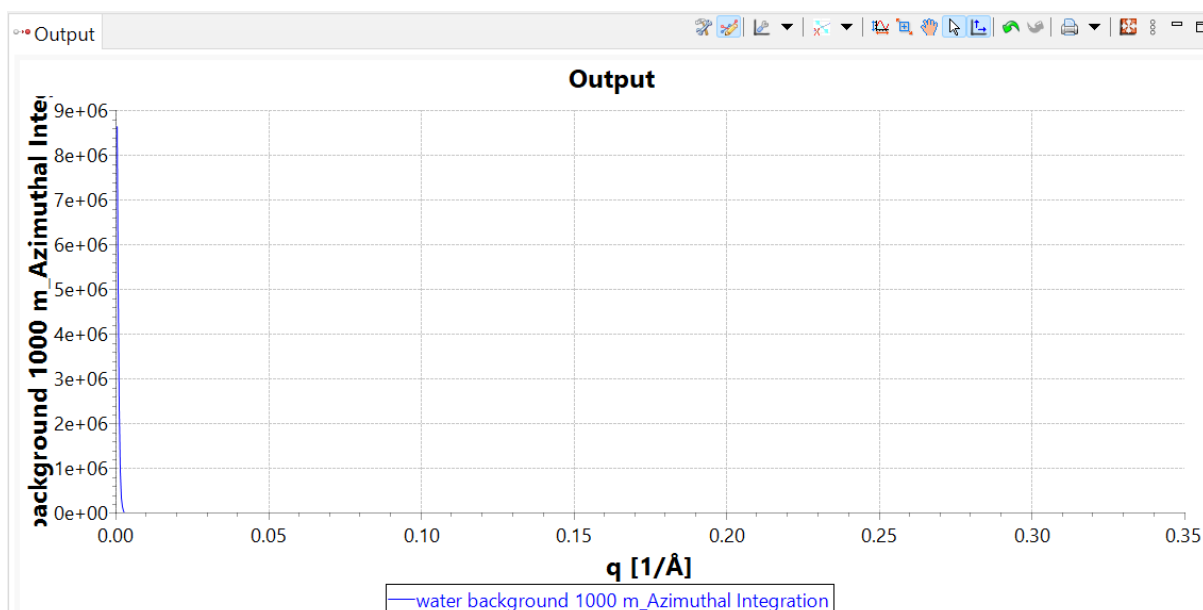


Figure 5.7: Azimuthal integration of a deionised water sample to identify the suitability of the calibration output, the peak at 0 Q indicates that the calibration is satisfactory

The calibration data identified from the different calibrations performed is presented in Table 5.1. This information is then used in the processing pipeline to process the raw data collected by the labSAXS instrument.

Table 5.1: Calibration information

Parameter	Run 1(4600 mm)	Run 2 (4600 mm)	Run 2 (1000 mm)
Sample to detector distance (mm)	4609.2	4607.6	1007.2
λ (keV)	9.25	9.25	9.25
Beam centre x (pixel)	531.9	532.6	531.6
Beam centre y (pixel)	732.0	730.0	731.8
Pixel size (mm)	0.075	0.075	0.075
Pitch (degree)	0	0	0
Roll (degree)	0	0	0
Yax (degree)	0	0	0

5.3.2.4.2. Creation of Mask File

The mask file was created in the “Data Vis” perspective of Dawn. A background file was loaded into the software (either the empty capillary or a deionised water sample, any file can be used here), and

the lower pixel threshold was set to “0”, which will cover the region between the detector modules and any dead pixels which are speckled around the detector modules. A circle was selected from the “Draw Regions” tab which was manually drawn over the beam spot. This output of this process can be seen clearly in Figure 5.8. The bright green regions are the mask which will be applied to the processing stage in order to process the raw files without these regions distorting any data. A different mask file is generated for each processing event, specifically each time the detector is repositioned (a total of three times over the duration of the experiment).

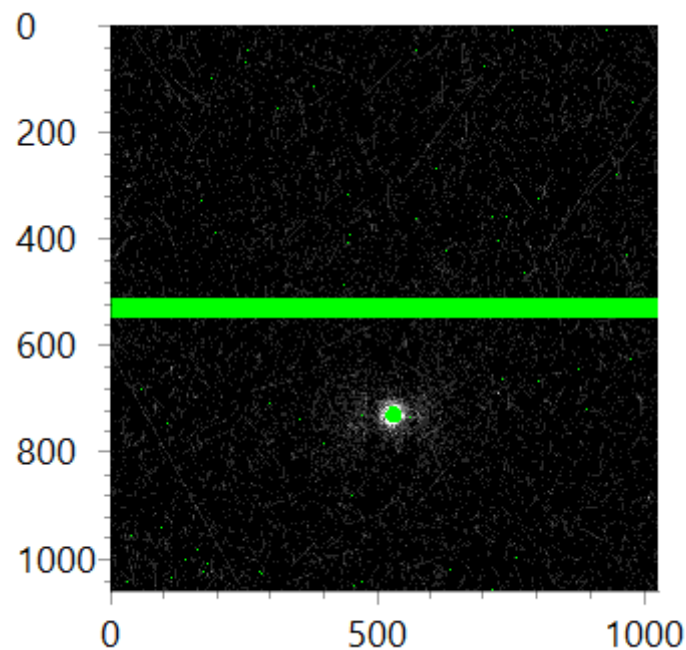


Figure 5.8: Mask used for the data processing step, the bright green areas mask any defective pixels and the regions between detector modules

There is still some brightness observed around the green (circle) region that covers the beam. This is not concerning, as once the beam is masked, the software rescales the data, highlighting the next brightest region which is that nearest to the beam. However, this area should not be masked, as it contains the sample data that is being measured. Typically, SAXS instruments will have a “beam stop” which physically block the most central, intense parts of the X-ray beam, protecting the detector. This region also requires masking. However, the Xeuss 3.0 labSAXS instrument at the Diamond Light Source does not use a physical beam stop.

The 1D reduced data (azimuthal integration) of deionised water, measured at 1000 mm, is presented in Figure 5.9. The calibration information has been applied to the data processing, but a mask file has

not yet been used. This enables the identification of the inflection point, where a sample signal begins to be detected. The inflection point in this figure occurs at an intensity of $\sim 1E01$. The mask, once applied, should cover the signal up to this point, as the detected signal before then corresponds to the beam source rather than that of the sample.

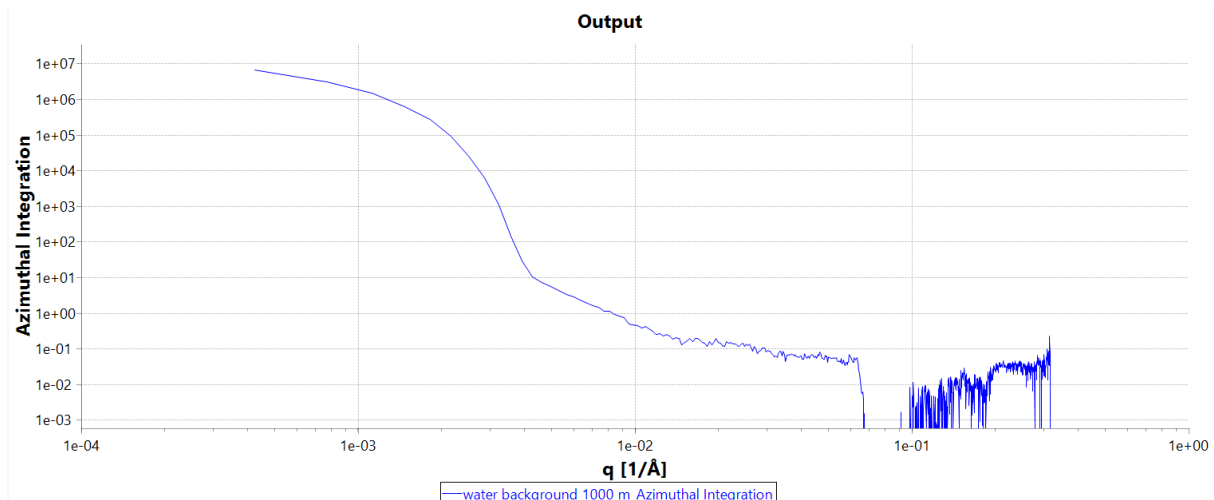


Figure 5.9: 1D output of deionised water, without a mask file applied to enable identification of inflection point. Measured at 1000 mm

The 1D reduced data of deionised water, measured at 1000 mm, is presented in Figure 5.10. Both the calibration information and mask file have been applied to process this file. As the inflection point was identified to be at an intensity of $\sim 1E01$ (y-axis), the mask file created must have a mask that is large enough to cover the beam signal up to this intensity. Since the signal peaks around this value, this confirms that the mask file adequately covers the beam, ensuring any signal detected beyond this point originates from the sample of interest.

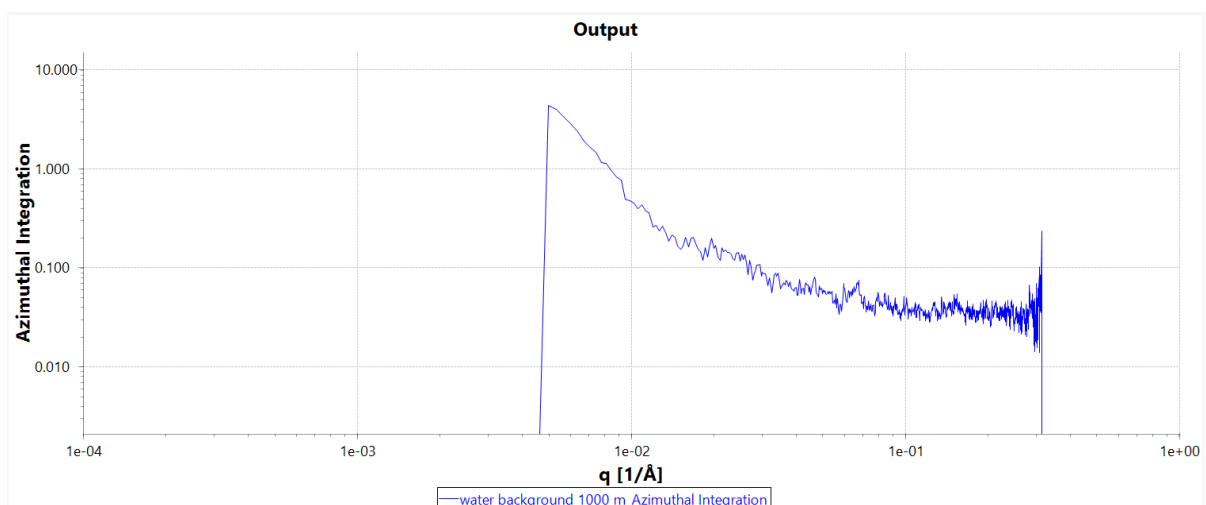


Figure 5.10: 1D output with calibration, with mask, log scale on both axis (mask hides the dead pixels, takes away the noise)

5.3.2.4.3. Processing Pipeline

An overview of the processing pipeline operations for the process of SAXS data to obtain reduced SAXS data can be found in Figure 5.11. A powder calibration is carried out on AgBeh to calibrate the sample to detector distance and the scattering angle. It is also required to ensure the accuracy of the scattering vector/ q -value. This calibration file is attached to the “Import Detector Calibration” operation of the pipeline. The mask file is created using a raw SAXS data file to exclude regions of the detector from data analysis. The detector will collect scattered X-rays, however, not every area of the detector will yield useful information. Unwanted regions of the detector include defective pixels, including dead pixels which do not record any data, and hot pixels which show exceptionally high signals. The mask file is attached to the “Import Mask From File” operation of the pipeline¹²⁰.

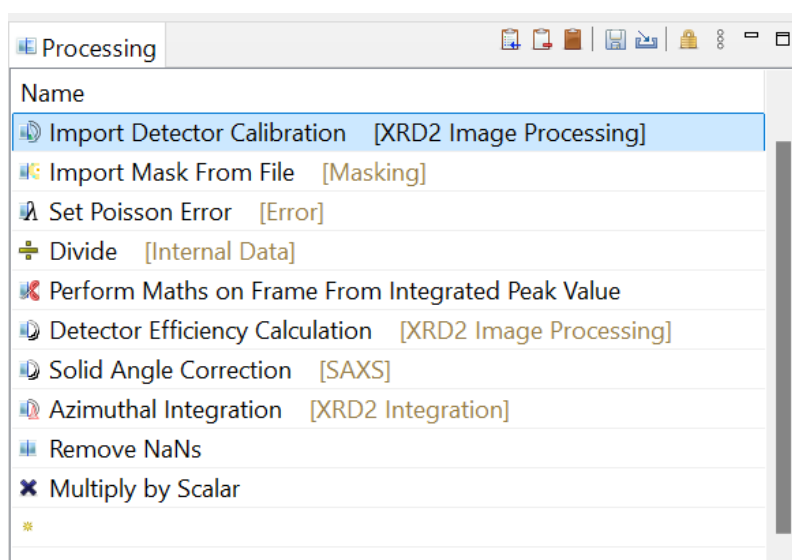


Figure 5.11: Processing pipeline operations for the processing of SAXS data

The Poisson error is calculated to incorporate the variation in intensity for pixels within an area. This operation has no options available and when added to the pipeline, calculates the required error values. The “Divide [Internal Data]” operation divides every pixel by some number that is derived from a 10 x 10 box around the hottest pixel. The data is normalised in case the beam fluctuates and this step also allows comparison of data¹²⁰.

The “Solid Angle Correction” for a SAXS beamline is generally minimal, this considers the different angles that the photons are hitting the detector surface. Moving from the centre of the detector and beam centre outwards to the edge of the detector, the angle at which the photons strike the detector increases, which is taken into account by this operation. The “Azimuthal Integration” is the final data

reduction step to reduce the data from a two dimensional image to a line plot. The output from this operation is intensity (unitless) vs. q (scattering vector, \AA^{-1}), I vs. q data¹²⁰.

5.3.2.4.4. Background Subtractions

Once the files have been processed, using the processing pipeline in Section 5.3.2.4.3., to produce the reduced data, the final step to produce subtracted datafiles for further analysis is to carry out background subtractions. This allows for the isolation of the scattering intensity of the pure sample¹⁰⁹.

Using the “Subtract Frame [External Data]” operation, the data to be processed is loaded into the “Data Slice View” and the dataset “/processed/result/data [902]” is selected which is 1D line data. The data that is to be subtracted is loaded into the file value in the “Model ‘Subtract Frame’” and the dataset value for this is “/processed/results/data”. The files can then be processed to produce the final subtracted datasets for further analysis. A summary of the files used for background subtractions can be found in Table 5.2.

Table 5.2: Subtracted frame summary

Sample	Subtracted frame/data (processed file)
Empty capillary	N/A
Water background	Empty capillary
Biorelevant buffer background	Water background
Biorelevant FaSSIF	Biorelevant buffer background
SIF background ^a	Water background
Minimum blank sample	SIF background ^a
Q1 blank sample	SIF background ^a
Median blank sample	SIF background ^a
Maximum blank sample	SIF background ^a
Minimum and naproxen	Minimum blank sample
Minimum and tadalafil	Minimum blank sample
Q1 and naproxen	Q1 blank sample
Median and naproxen	Median blank sample
Median and tadalafil	Median blank sample
Biorelevant and naproxen	Biorelevant FaSSIF

^aSIF background sample contains phosphate buffer, salt and water

5.4. Results and Discussion

The following figures are the outputs of the subtracted frame processing operation. Unfortunately, the samples are too weakly scattering to be detected by the labSAXS instrument. Correspondence with Dr Andrew Clulow, Senior Beamline Scientist at the Australian Synchrotron facility, confirmed the lack of scattering in the SIF and drug samples compared to that of the background samples. It is thought that the lipids are scattering too weakly to be observed above the baseline, which is a known issue, particularly with fasted state media, even on the synchrotron beam. Dr Clulow also confirmed the lack of any noticeable diffraction of the crystalline drugs at the wider angles.

5.4.1. SIF Background and SIF Samples

A comparison between the SIF background sample (phosphate buffer, salt and water) and a blank/drug free SIF media (Q1) can be found in Figure 5.12. Both measurements were taken at 4600 mm.

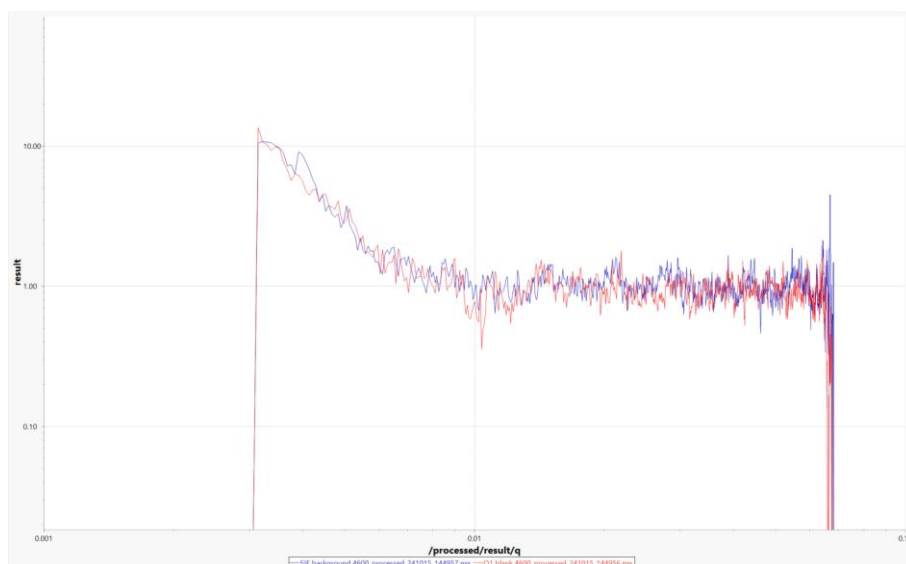


Figure 5.12: Comparison between the SIF background (blue) and the drug free Q1 SIF sample (red) measured at 4600 mm

A comparison of the biorelevant FaSSIF with the corresponding background sample and deionised water, measured at 4600 mm, is presented in Figure 5.13.

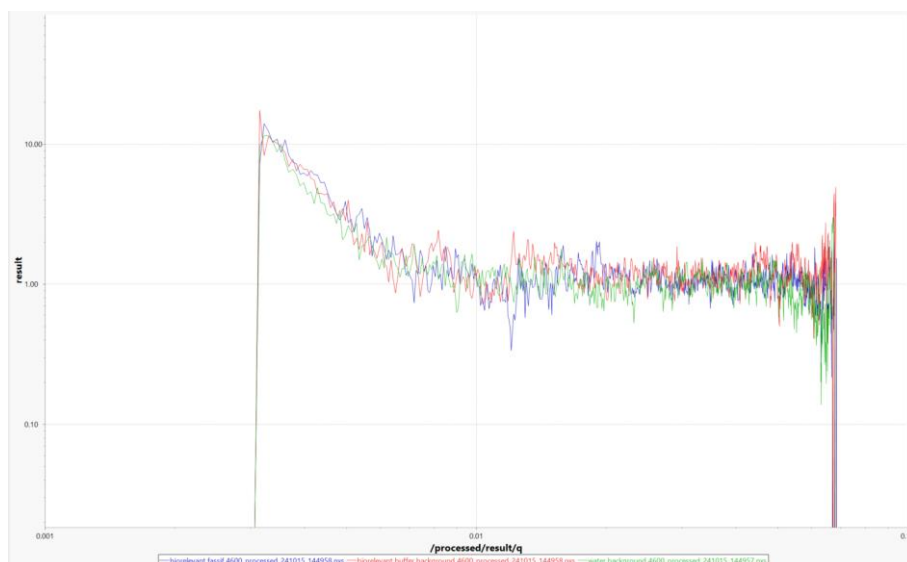


Figure 5.13: Comparison of biorelevant FaSSIF with a background and a water sample. Biorelevant FaSSIF buffer and water background (red), biorelevant FaSSIF sample (blue) and deionised water (green). Measured at 4600 mm

Samples of SIF background i.e. phosphate/buffer/water were taken during two separate runs of the instrument (15/08/2024, morning and evening) which led to the subtracted data outputs provided in Figure 5.14. Although both measurements have been recorded at 4600 mm, the data in red is recorded over a slightly longer q-range. This is due to small difference in the sample to detector distance, which highlights the requirement for new calibration measurements to be recorded each time the detector moves position. The relationship between q-value and detector distance can be explained by Equation 4. A shorter sample to detector distance enables the capture of larger scattering angles (θ) which correspond to higher q-values.

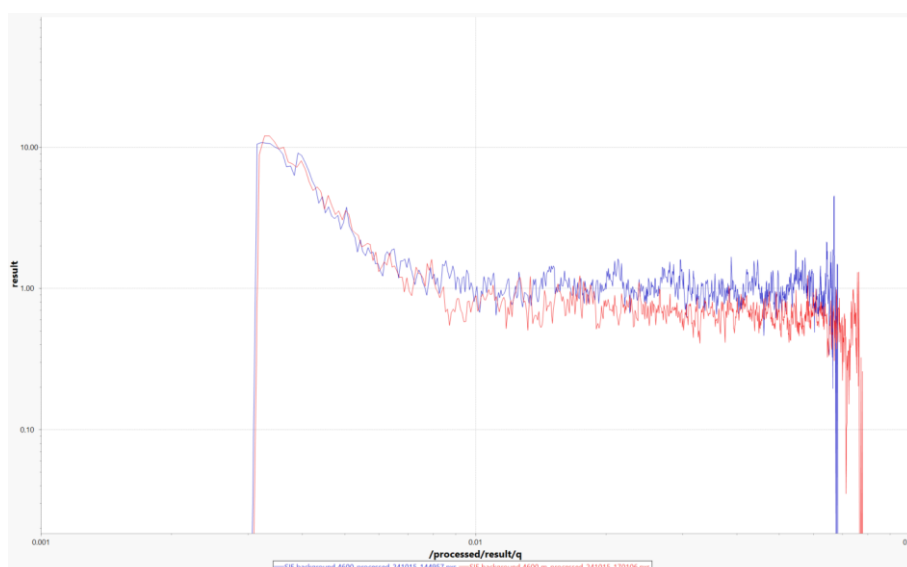


Figure 5.14: Comparison of SIF background samples, both recorded at 4600 mm. Blue – measured on Thursday morning, red – measured on Thursday evening

A comparison between the empty capillary, deionised water and SIF background (phosphate buffer/salt/water), measured at 1000 mm can be found in Figure 5.15. While the scattering profiles of the samples exhibit the same overall shape, there appears to be a noticeable difference between the intensities of the scattering. However, if error bars were to be added to this figure, they would likely overlap, indicating that the scattering intensities are not significantly different and that the variations observed are within the margin of error.

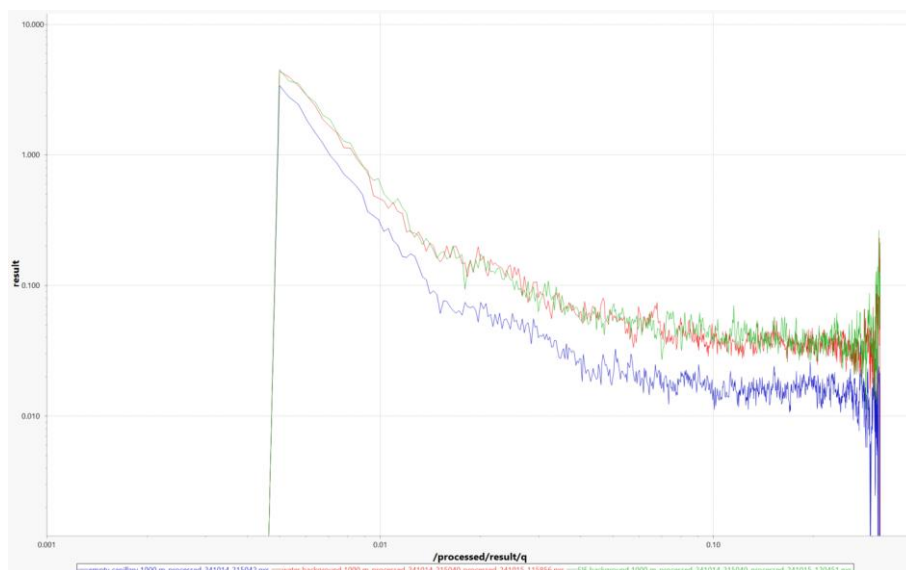


Figure 5.15: Comparison between empty capillary (blue), deionised water background (red) and SIF background (green). Measured at 1000 mm

5.4.2. Drug Free Media

A comparison between the subtracted data of the SIF background (phosphate buffer/salt/water), the drug free minimum SIF and the minimum SIF with naproxen is presented in Figure 5.16. The samples here were measured at 4600 mm.

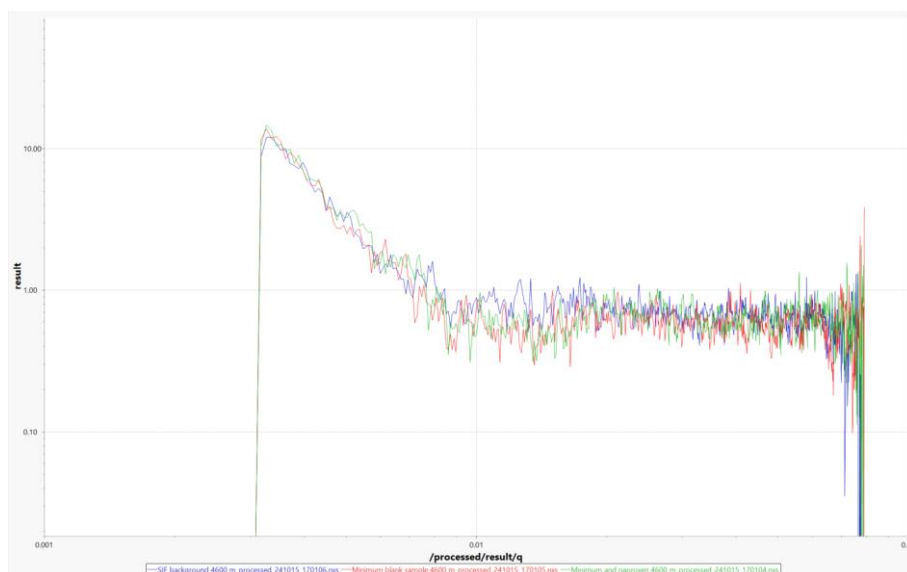


Figure 5.16: Comparison between SIF background (blue), drug free minimum SIF sample (red) and minimum SIF sample with naproxen (green). Measured at 4600 mm

Figure 5.17 shows the comparison of the subtracted data of the SIF background (phosphate buffer/salt/water) and drug free SIF sample of the minimum, Q1, median and maximum fluids, measured at 1000 mm. It was not possible to record a measurement of the Q3 sample as the polycarbonate capillary tube plug was not fully sealed with epoxy and due to time constraints, it was not possible to prepare the sample again. If a capillary tube is not correctly sealed prior to SAXS analysis, this could leave to a few issues including sample leakage, external contaminants entering the tube and evaporation of a volatile sample which could lead to unreliable and inaccurate measurements. In extreme cases, an insufficiently sealed capillary tube may cause damage to the SAXS instrument, specifically the sensitive detectors or electronics which emphasises the requirement of a properly sealed sample.

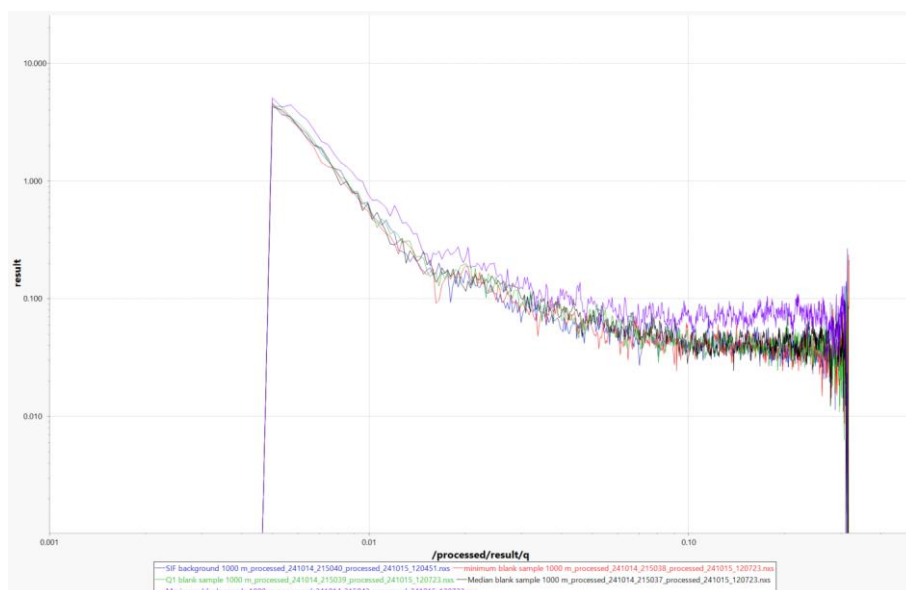


Figure 5.17: Comparison of SAXS output between SIF background (blue), and drug free SIF samples; minimum SIF (red), Q1 SIF (green), median SIF (black) and maximum SIF (purple). Measured at 1000 mm

5.4.3. Drug Loaded Media

The subtracted data outputs of the naproxen SIF samples can be found in Figure 5.18. The samples of SIF measured with naproxen are that of the minimum, Q1 and median fluids. The measurements in this figure were recorded at 4600 mm.

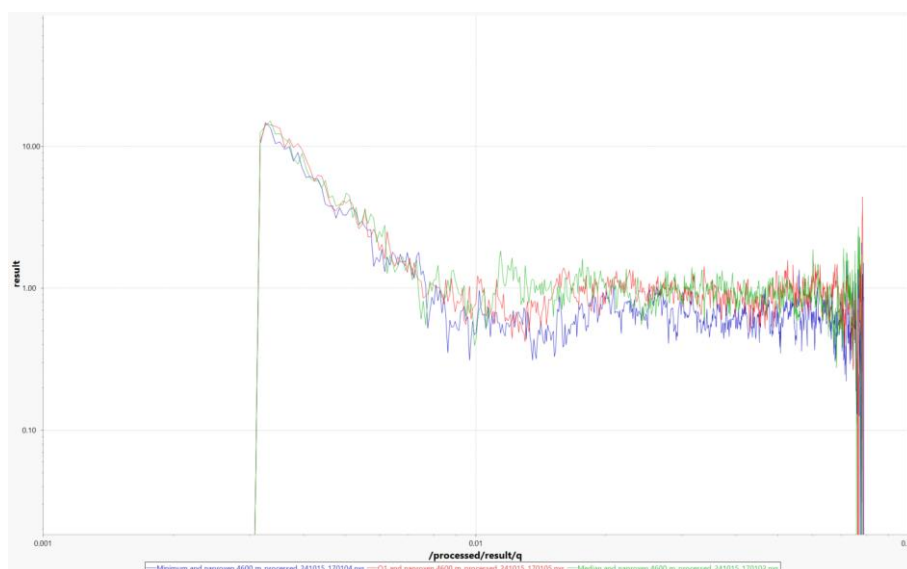


Figure 5.18: Output of subtracted SAXS data of naproxen SIF samples; minimum SIF (blue), Q1 SIF (red) and median SIF (green). Measured at 4600 mm

The SAXS outputs of the SIF background (phosphate buffer/salt/water), the drug free minimum SIF and the minimum SIF with naproxen is presented in Figure 5.19. The measurements in this figure were recorded at 1000 mm.

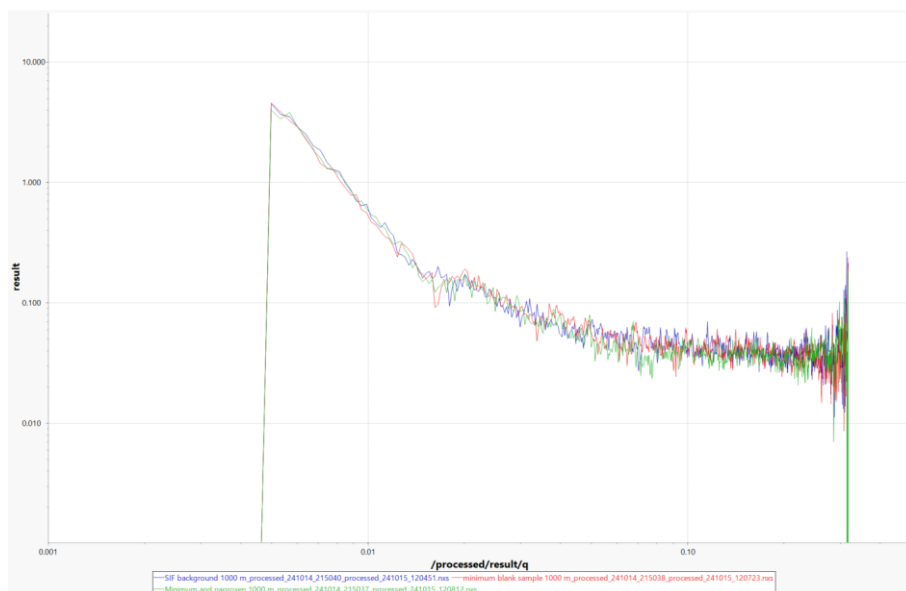


Figure 5.19: Outputs of subtracted SAXS data; SIF background (blue), drug free minimum SIF (red), naproxen and minimum SIF sample (green). Measured at 1000 mm

The outputs of the subtracted SAXS data of naproxen loaded SIF samples can be found in Figure 5.20. Measurements have been recorded of naproxen in the minimum, Q1, median and biorelevant FaSSIF samples at 1000 mm. If the labSAXS instrument was able to scatter the samples, it is expected that there would be a difference in intensities (of at least by a power of 10) recorded on the scattering profiles with multiple bumps or oscillations measured around the 0.02 Q value⁴¹, which are features that are characteristic of structural arrangements such as particles, micelles or aggregates with the FaSSIF media.

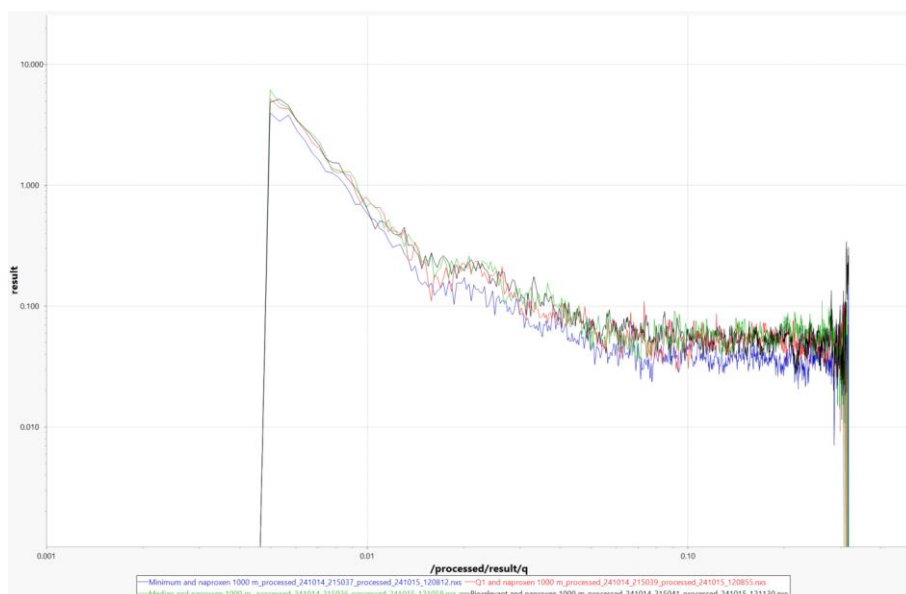


Figure 5.20: Output of subtracted SAXS data of naproxen SIF samples; minimum SIF (blue), Q1 SIF (red), median SIF (green), biorelevant FaSSIF (black). Measured at 1000 mm

5.5. Conclusion

Samples of SIF (both biorelevant media and the suite of SIF, designed in earlier chapters of this work) with and without drugs were analysed on the labSAXS beam. The data obtained was processed using the Dawn software, which required calibrations and the creation of mask files. Unfortunately, there was no significant scattering measured in the sample fluids e.g. drug free media or media with drug dissolved, above the background samples e.g. water or buffer/salt/water. This is thought to be a result of samples that are too weakly scattering to be detected by a labSAXS instrument. Similar samples of FaSSIF, run by Dr Clulow and his team at the Australian synchrotron did show scattering when measured by the beamlines, however, the data from this work also showed nothing visible in the same Q^{-1} region as was measured by the labSAXS instrument at the Diamond Light Source.

The data recorded in this chapter demonstrates the need for analysis by synchrotron SAXS in order to properly visualise the colloidal structures. The data collected here also serves as excellent preliminary data for a future synchrotron beamtime application, which is the next steps of the work presented in this chapter.

Chapter 6

Simulated Intestinal Fluid Mixed Micelle Size and Solubility Relationship

6. Simulated Intestinal Fluid Mixed Micelle Size and Solubility Relationship

6.1. Introduction and Theory

Mathematical modelling is used within biopharmaceutics as a predictive tool to provide insights into various processes. Although it is primarily theoretical, the results and data generated lead to practical outcomes after the comparison and verification stages¹²¹. It has been used widely in the field of pharmaceuticals and biopharmaceutics for many purposes including optimising the design of novel dosage forms to aid in drug development, as well as predicting drug behaviour in simulated biorelevant media^{122, 123}. While the relationship between micelle size and solubility has been studied extensively, gaps remain in understanding the role of total amphiphile concentration. In particular, how varying surfactant types and concentrations influence micelle formation and drug loading capacity. Factors such as critical micelle concentration (CMC) and the dynamic behaviour of mixed micelles in biorelevant media can significantly impact drug solubilisation and absorption capacities. Further exploration of these aspects may provide valuable insights into improving solubility and bioavailability of poorly soluble drugs *in vivo*.

6.2. Calculation of Drug Incorporation into Micelles Using Mathematical Principles

The initial calculation, derived from solubility and micelle diffusivity measurements, by Balakrishnan *et al.* was used to predict the degree to which surfactants enhance griseofulvin dissolution in various anionic (sodium dodecyl sulfate – SDS), cationic (cetyl trimethyl ammonium bromide - CTAB) and neutral (Tween 80 and Cremophor EL) pharmaceutical surfactants. The solubility analysis, determined by HPLC, found that at high surfactant concentrations, the drug solubility increased considerably in all surfactants, also known as solubility enhancement. This was more so for the ionic surfactants at enhancements of 107-fold for the SDS and 31-fold for the CTAB. The neutral surfactants Tween 80 and Cremophor EL had a much lower solubility enhancement at 4-fold and 3-fold, respectively. It is known that surfactants increase the solubility of the drug through the formation of micelles, although the low diffusivity of drug-loaded micelles can limit the rate of dissolution. Results of the diffusivities for the griseofulvin micelles were measured to be 10- and 20-fold lower than the diffusivities recorded for the

drug free molecules which emphasize that the diffusivity of the micelles is an essential factor that affects the dissolution enhancement¹²⁴.

Equation 5: Model to predict surfactant enhanced dissolution

$$\Phi = 1 + \frac{f_m}{f_f} \cdot \frac{D_{D-M}^{2/3}}{D_D^{2/3}}$$

Where:

f_f is the free drug fraction

f_m is the micelle drug fraction

D_D is the diffusivity of the free drug

D_{D-M} is the diffusivity of the drug-loaded micelle

The model created was used to predict the dissolution enhancement of SDS and CTAB and demonstrated values that were in agreement with the measured values, with the prediction error calculated to be only 12 %. The model slightly underpredicted the dissolution enhancement of the neutral surfactants¹²⁴.

The limitations of this original work include the limited scope of the surfactants (two ionic and two non-ionic) and one model drug (the neutral drug, griseofulvin), the static diffusivity measurements and *in vitro* nature of the study which will not accurately represent the dynamic environment of the human gastrointestinal tract and finally, the assumption of uniform micelle behaviour for all micelles. Drug loaded or surfactant concentration is not taken into account which will affect the dissolution rates of the different molecules that are being measured¹²⁴.

The second study uses a model that had been developed by Balakrishnan *et al.* in 2004 in order to predict dissolution of drugs into various surfactant solutions. The aims of this study were to quantitatively evaluate how the solubility and diffusivity of drugs, mediated by biorelevant media, contribute to improved drug dissolution in fed state simulated gastric fluid (FeSSGF) and fed state simulated intestinal fluid, V2 (FeSSIF V2), which were chosen due to their high surfactant and colloid content, respectively. The composition of the two fluids can be found in Table 6.1. Three BCS class II model drugs, one weak acid (ibuprofen), one weak base (ketoconazole) and one neutral drug (griseofulvin) were used for the analysis⁴⁴.

Table 6.1: Composition of FeSSGF and FeSSIF V2 as reported in Jamil *et al.*⁴⁴

Component	FeSSGF	Component	FeSSIF V2
NaCl	237.02 mM	Sodium taurocholate	10 mM
Acetic acid	17.12 mM	Lecithin	2 mM
Sodium Acetate	29.75 mM	Glyceryl Monooleate	5 mM
Milk/acetate buffer	1:1	Sodium Oleate	0.8 mM
HCl /NaOH conc. <i>qs ad</i> ^a	pH 5	Maleic Acid	55.02 mM
NaCl	237.02 mM	NaOH	81.65 mM
		NaCl	125.5 mM
		HCl /NaOH conc. <i>qs ad</i> ^a	pH 5.8

^aas much as is sufficient

Experimental data of intrinsic drug dissolution was collected using the Wood apparatus while the solubility data was collected by HPLC and diffusivity of drug-loaded colloids in the fluids were obtained from laser diffraction and dynamic light scattering. This data then enabled the prediction and assessment of the contribution of surfactant-mediated dissolution which then allowed for the evaluation of the number of drug molecules per individual colloid structure⁴⁴. A detailed explanation and example of this calculation can be found in Section 6.4.1.

It was found that griseofulvin presented the highest biorelevant media solubility enhancement and dissolution with a 652-fold increase in FeSSGF and a 190-fold increase in FeSSIF V2. The FeSSIF V2 mixed micelles and FeSSGF fat globules are both larger in size and slower diffusing compared to micelles formed in pharmaceutical surfactant systems (as described in the study by Balakrishnan *et al.*)¹²⁴. The number of drug molecules per colloid varied across the drugs, with the highest calculated to be 4.57×10^{11} molecules of ibuprofen incorporated into individual fat globules of FeSSGF and the lowest calculated to be 4,000 molecules of ketoconazole incorporated into individual FeSSIF V2 mixed micelles. The number of drug molecules per colloid/mixed micelle was estimated to be significantly greater in the FeSSGF than in the FeSSIF V2⁴⁴.

The diffusivity of the FeSSIF V2 mixed micelles were significantly lower than that of the free drug, resulting in limited dissolution enhancement regardless of the increase in solubility. The mixed micelles

were recorded to be around 120-fold slower than free griseofulvin and 100-fold slower than free ketoconazole. Ibuprofen dissolution was essentially not enhanced in this fluid as the solubility was minimally enhanced and the mixed micelles were measured to be around 80-fold slower than the free drug. The fat globules of FeSSGF were also recorded to be diffuse considerably slower in comparison to the free drugs therefore contributing to a significant attenuation in the solubility benefits. The fat globules of FeSSGF were recorded to be 4,000-fold, 7,000-fold and 21,000-fold slower than free drug of griseofulvin, ketoconazole and ibuprofen, respectively. This is not surprising due to larger size of the globules compared to the free drug. The biorelevant media exhibited a sizeable enhancement in solubility but a minimal enhancement in dissolution due to the large size and slow diffusion rates of the drug-loaded colloids and globules which may limit the overall drug absorption potential *in vivo*⁴⁴.

The final study uses the same model created by Balakrishnan *et al.* to predict dissolution of drugs into fasted state biorelevant media. The aims of this study were to quantitatively evaluate how the solubility and diffusivity of drugs, mediated by biorelevant media, contribute to improved drug dissolution in fasted state simulated gastric fluid (FaSSGF) and fasted state simulated intestinal fluid, V2 (FaSSIF V2). Again, three BCS class II model drugs, one weak acid (ibuprofen), one weak base (ketoconazole) and one neutral drug (griseofulvin) were used for the analysis. The Wood apparatus was used to measure the dissolution of the drugs into the biorelevant media, as well as into their analogous “surfactant-free” media. The results suggest minimal to no improvement in solubility or dissolution due to the fairly large size and slow diffusion of the FaSSGF and FaSSIF V2 mixed micelles. The experimental data was carried out in this study as per the fed state study¹²². The data measured enabled an estimate of the number of drug molecules per individual colloid and a detailed explanation and example of this calculation can be found in Section 6.4.1.

It was found that the three drugs analysed presented similar biorelevant gastric fluid media (FaSSGF) enhancement, compared to the control of the media without surfactant components (i.e. sodium taurocholate and lecithin), at 1.06-, 1.03- and 1.16-fold for griseofulvin, ketoconazole and ibuprofen, respectively. A 1-fold enhancement indicates that no solubility enhancement has occurred which is not surprising due to the low surfactant levels present within the stomach. Similar fold enhancements were measured in FaSSIF V2 which is again, due to the low surfactant levels present within the intestine. FaSSGF and FaSSIF V2 mixed micelles are substantially larger in size than those formed by pharmaceutical surfactants (i.e. the study carried out by Balakrishnan *et al.*)¹²⁴ which allow them to accommodate more drug molecules per micelle. The estimated number of drug molecules per micelle of FaSSGF was calculated to be 938,000, 4,790,000 and 45,400,000 for griseofulvin, ketoconazole and

ibuprofen in FaSSGF, respectively. The number of drug molecules per micelle in FaSSIF V2 was estimated to be 48, 49 and 4,160 for griseofulvin, ketoconazole and ibuprofen, respectively. The polydispersity index measured by dynamic light scattering for the samples were below 0.3 for the drug loaded samples of both FaSSGF and FaSSIF V2, which indicates a monodisperse distribution¹²².

The diffusivity results of the FaSSGF and FaSSIF V2 mixed micelles showed that the micelles were large and slow-diffusing compared to the free drug molecules. However, they were smaller and faster-diffusing than drug-bound fat globules and mixed micelles from FeSSGF and FeSSIF V2. Both the dissolution and solubility enhancement of FaSSGF and FaSSIF V2 were found to be minimal.

The limitations of the two studies include: the limited drug selection, which may not represent every BCS class II drug; the simplified assumptions in modelling, assumptions including constant diffusivity values and uniform size distributions are made; the limited variation in biorelevant media, it is known that human gastric and intestinal fluids have varying compositions and concentrations of bile salts, phospholipids etc.

6.3. Objectives

The objectives of this chapter are to review relevant studies that have quantified the drug loaded micelle using simple maths and volume ratios. The studies were reviewed in order to understand the theory, assumptions and key concepts for integrating the “Polli method” into the solubility and particle size data collected in previous chapters of this thesis (Chapter 2 and Chapter 3, respectively). The “Polli method”, previously applied to surfactants and drug loaded biorelevant simulated gastric and intestinal fluid, will then be applied to our data, in combination with values sourced from literature, in order to predict the number of drug molecules per micelle of our systems of simulated intestinal fluid. Finally, trends will be identified and analysed relating to the predicted number of drug molecules per micelle and their relationship with drug solubility and particle size will be investigated.

6.4. Methods

6.4.1. Theoretical Calculation of Drug Molecules per Mixed Micelle in SIF

The solubility and DLS data were used to estimate the mean number of drug molecules per mixed micelle. The method used here has been previously published^{44, 122, 124}. For each SIF media, the solubility data was used to first calculate the number of mixed micelle entrapped drug molecules in

1 L of drug loaded media by finding the difference between the total $[D_t]$ and free drug (the aqueous solubility, where no amphiphiles are present) $[D]$ solubilities, dividing this by the molecular weight of the drug then multiplying this by Avogadro's constant:

$$n \cdot [D - M] = [D_t] - [D]$$

Where $n \cdot [D - M]$ is the concentration of drug that is simulated intestinal fluid bound to the mixed micelle. Using the hydrodynamic diameter data of the drug loaded mixed micelles measured by DLS, the weight of each drug loaded mixed micelle was calculated for each litre of media by multiplying the volume of the mean primary peak intensity distribution by the assumed density of the colloidal material (1 g/mL).

Following this, the number of mixed micelles per 1 L of media was calculated by finding the total mass of the amphiphiles in the simulated media then dividing this value by the mass of one drug loaded micelle and incorporating a factor to scale up to 1L.

Finally, the number of drug molecules per mixed micelle was determined by dividing the number of micelle entrapped drug molecules in 1 L of drug loaded media by the number of micelles calculated in 1 L of media. The assumptions made that enabled this calculation are (i) a monodisperse spherical particle geometry and density of 1000 g/L, (ii) each mixed micelle is made of bound drug and surfactant and (iii) all components contribute proportionally to each micelle.

An example of this calculation for the number of drug molecules per micelle of naproxen in the minimum FaSSIF media is shown here. The values used for this calculation can be found in Table 6.2.

Concentration of drug that is FaSSIF mixed micelle bound (measured by the difference between the total (measured by HPLC, Chapter 2) and free drug (aqueous, literature value) solubilities $[D_t]$ and $[D]$, respectively) is:

$$n \cdot [D - M] = 0.0243 - 0.0159 = 0.0084 \text{ g/L}$$

Note, the solubility values recorded by HPLC in Chapter 2 are reported in mM and μM . Here, they have been converted to g/L for use in this calculation.

The number of micelle entrapped drug molecules in 1 L of drug-loaded FaSSIF is calculated by dividing the concentration of drug that is FaSSIF mixed micelle bound by the molecular weight of naproxen (230.26 g/mol) then multiplying this by Avogadro's constant:

$$\left(\frac{n[D - M]}{MW}\right) \times 6.022 \times 10^{23} =$$

$$\left(\frac{0.0084}{230.26}\right) \times 6.022 \times 10^{23} = 2.19 \times 10^{19} \text{ (no units)}$$

The volume of the sphere is calculated using the radius of the size intensity distribution (72.9 nm; note that this value is half of the diameter which is the value measured using DLS) using the equation to find the volume of a "sphere":

$$\frac{4}{3}\pi r^3 =$$

$$\frac{4}{3}\pi \times 72.9^3 = 1.62 \times 10^6 \text{ nm}^3$$

The mass of 1 "sphere" of a naproxen loaded micelle is calculated by multiplying the volume of a single micelle by the assumed density of a micelle (1000 g/L or 1×10^{-21} g/nm³):

$$1.62 \times 10^6 \times 1 \times 10^{-21} = 1.62 \times 10^{-15} \text{ g}$$

The number of micelles per 1 L of FaSSIF is then calculated by adding the concentration of the amphiphiles in the minimum media (i.e. the bile salt, phospholipid, free fatty acid and cholesterol = 1.031 g/L) with the concentration of naproxen that is FaSSIF mixed micelle bound in the minimum media (measured by HPLC, 0.0084 g/L). This is divided by the mass of 1 naproxen loaded drug "sphere" i.e. micelle (1.62×10^{-15} g):

$$\frac{(1.031 + 0.0084)}{1.62 \times 10^{-15}} = 6.41 \times 10^{14} \text{ (no units)}$$

The number of drug molecules per micelle is then calculated as the number of micelle entrapped drug molecules in 1 L of drug-loaded FaSSIF (2.19×10^{19}), divided by the number of micelles per 1 L of FaSSIF (6.41×10^{14}):

$$\frac{2.19 \times 10^{19}}{6.41 \times 10^{14}} = 34,123$$

Giving a total number of drug molecules per micelle of naproxen in the minimum FaSSIF media to be approximately 34,100.

Table 6.2: Values used in example calculation for the calculation of number of drug molecules per micelle of naproxen in the minimum FaSSIF media

Parameter	Value
[Dt] concentration in simulated media (g/L)	0.0243 (\pm 0.0001)
[D] concentration in aqueous media (blank) (g/L)	0.0159
[Dt]-[D] = n[D-M] Concentration of drug that is mixed micelle bound (g/L)	0.0084
Total concentration of amphiphiles in minimum media (g/L). Calculated as the concentration of bile; lecithin and cholesterol in each media	1.031
Number of micelle entrapped drug molecules in 1 L of drug-loaded FaSSIF	2.19×10^{19}
Volume of intensity distribution (nm^3)	1.62×10^6
Assumed density of "sphere" i.e. micelle (g/nm^3)	1×10^{-21}
Molecular weight of naproxen (g/mol)	230.26
Avogadro's constant (mol^{-1})	6.022×10^{23}
Mass of 1 naproxen loaded drug micelle (g)	1.62×10^{-15}
Number of micelles per 1 L of FaSSIF	6.41×10^{14}
DLS size data, radius of intensity distribution (nm)	72.9

The details of values used in this calculation for the full series of drugs can be found in Table 6.5 in Section 6.5.1.

6.4.2. Solubility Enhancement

A calculation, using Equation 6 was performed for each of the drug samples in each of the simulated intestinal fluid samples in order to identify the -fold solubility enhancement in each of the fluids compared to that of the drug in blank samples (aqueous solubility).

Equation 6: Solubility enhancement calculation

$$\text{Solubility enhancement} = \frac{\text{Solubility in biorelevant media}}{\text{Aqueous solubility}}$$

The aqueous drug solubility values were taken from literature (presented in Table 6.4) and used as the “solubility in control” data, while the solubility in biorelevant media values were measured by HPLC in Chapter 2.

6.5. Results and Discussion

6.5.1. Theoretical Calculation of Drug Molecules per Mixed Micelle in SIF

The estimated number of drug molecules per mixed micelle for each of the drugs in each of the six SIF is presented in Table 6.3.

Table 6.3: Estimated number of drug molecules per mixed micelle

Drug	Media					Biorelevant
	Minimum	Q1	Median	Q3	Maximum	
Naproxen	34,100	41,900	20,400	6,710	47	1,090,000
Indomethacin	1,760,000	6,120	21,900	192	164	1,980,000
Phenytoin	2,000,000	5,760	16,200	348	174	2,320,000
Felodipine	4,060,000	4,670	5,910	189	110	515,000
Fenofibrate	1,650,000	4,270	7,660	241	146	924,000
Griseofulvin	1,910,000	5,600	10,600	275	118	5,190
Carvedilol	3,340,000	1,400,000	6,150,000	4,450,000	116	188,000,000
Tadalafil	1,870,000	6,150	9,880	216	123	634,000

The drug solubilities, micelle sizes and stoichiometric calculations can be found in Table 6.5. Micelle diameters were measured via dynamic light scattering and used to estimate micelle size, assuming a spherical geometry and density of 1 g/cm³. A monodisperse distribution of micelle structures is also assumed. Drug solubilities in the simulated media are the same as in Table 2.8, recorded by HPLC. Aqueous drug solubility values have been obtained from literature and can be found in Table 6.4.

Table 6.4: Aqueous drug solubility values, sourced from literature

Drug	Aqueous solubility (g/L)	Source
Naproxen	0.0159	Wishart <i>et al.</i> ⁵⁶
Indomethacin	0.0088	Comer <i>et al.</i> ¹²⁵
Phenytoin	0.014	Schwartz <i>et al.</i> ¹²⁶
Felodipine	0.0197	Wishart <i>et al.</i> ⁵⁶
Fenofibrate	0.000291	Granero <i>et al.</i> ¹²⁷
Griseofulvin	0.00864	Wishart <i>et al.</i> ⁵⁶
Carvedilol	0.0279	Hamed <i>et al.</i> ⁶³
Tadalafil	0.00073	Choi <i>et al.</i> ¹²⁸

Table 6.5: Drug solubilities in FaSSIF, micelle size and stoichiometric calculations

Drug	Media	[Dt] concentration in simulated media (g/L)	[D] concentration in aqueous media (blank) (g/L)	n[D-M] ^a (g/L)	DLS size ^a (intensity dist. d, nm) (drug loaded micelle diameter)	Mass 1 sphere (g) (drug loaded micelle weight)	Number of micelle entrapped drug molecules in 1 L of drug-loaded FaSSIF	Number of micelles per 1 L of FaSSIF	Number of drug molecules per micelle
Naproxen	Minimum	0.0243 (± 0.0001)	0.0159 ⁵⁶	0.0084	146 (± 2.5)	1.62 × 10 ⁻¹⁵	2.19 × 10 ¹⁹	6.41 × 10 ¹⁴	34,100
	Q1	5.9024 (± 0.0518)	0.0159 ⁵⁶	5.8865	34.1 (± 1.4)	2.08 × 10 ⁻¹⁷	1.54 × 10 ²²	3.67 × 10 ¹⁷	41,900
	Median	6.5876 (± 0.2294)	0.0159 ⁵⁶	6.5717	27.4 (± 1.4)	1.08 × 10 ⁻¹⁷	1.72 × 10 ²²	8.42 × 10 ¹⁷	20,400
	Q3	5.9260 (± 0.1205)	0.0159 ⁵⁶	5.9101	20.3 (± 0.2)	4.39 × 10 ⁻¹⁸	1.55 × 10 ²²	2.30 × 10 ¹⁸	6,710
	Maximum	5.7587 (± 0.0832)	0.0159 ⁵⁶	5.7428	5.9 (± 0.4)	1.09 × 10 ⁻¹⁹	1.50 × 10 ²²	3.17 × 10 ²⁰	47
	Biorelevant	0.5507 (± 0.0074)	0.0159 ⁵⁶	0.5345	161 (± 3.3)	2.17 × 10 ⁻¹⁵	1.39 × 10 ²¹	1.28 × 10 ¹⁵	1,090,000
Indomethacin	Minimum	0.0186 (± 0.0001)	0.0088 ¹²⁵	0.0098	126 (± 2.5)	1.05 × 10 ⁻¹⁵	1.64 × 10 ¹⁹	9.31 × 10 ¹²	1,760,000
	Q1	1.2285 (± 0.0070)	0.0088 ¹²⁵	1.2197	19.1 (± 0.2)	3.64 × 10 ⁻¹⁸	2.05 × 10 ²¹	3.35 × 10 ¹⁷	6,120
	Median	2.4484 (± 0.0074)	0.0088 ¹²⁵	2.4396	29.2 (± 1.6)	1.30 × 10 ⁻¹⁷	4.11 × 10 ²¹	1.88 × 10 ¹⁷	21,900
	Q3	2.5207 (± 0.0005)	0.0088 ¹²⁵	2.5119	6.02 (± 0.1)	1.14 × 10 ⁻¹⁹	4.23 × 10 ²¹	2.20 × 10 ¹⁹	192
	Maximum	4.7625 (± 0.0472)	0.0088 ¹²⁵	4.7537	5.71 (± 0.7)	9.75 × 10 ⁻²⁰	8.00 × 10 ²¹	4.88 × 10 ¹⁹	164
	Biorelevant	0.1270 (± 0.0018)	0.0088 ¹²⁵	0.1182	131 (± 5.6)	1.18 × 10 ⁻¹⁵	1.99 × 10 ²⁰	1.00 × 10 ¹⁴	1,980,000
Phenytoin	Minimum	0.0152 (± 0.0004)	0.014 ¹²⁶	0.0012	117 (± 1.5)	8.40 × 10 ⁻¹⁶	2.89 × 10 ¹⁸	1.44 × 10 ¹²	2,000,000
	Q1	0.0139 (± 0.0001)	0.014 ¹²⁶	-	16.6 (± 0.4)	2.41 × 10 ⁻¹⁸	-1.18 × 10 ¹⁷	-2.05 × 10 ¹³	5,760
	Median	0.0318 (± 0.0002)	0.014 ¹²⁶	0.0178	23.5 (± 0.8)	6.80 × 10 ⁻¹⁸	4.24 × 10 ¹⁹	2.61 × 10 ¹⁵	16,200
	Q3	0.0283 (± 0.0004)	0.014 ¹²⁶	0.0143	6.53 (± 0.1)	1.46 × 10 ⁻¹⁹	3.41 × 10 ¹⁹	9.81 × 10 ¹⁶	348
	Maximum	0.0833 (± 0.0019)	0.014 ¹²⁶	0.0693	5.18 (± 0.2)	7.28 × 10 ⁻²⁰	1.65 × 10 ²⁰	9.52 × 10 ¹⁷	174
	Biorelevant	0.0211 (± 0.0006)	0.014 ¹²⁶	0.0071	123 (± 3.0)	9.72 × 10 ⁻¹⁶	1.70 × 10 ¹⁹	7.34 × 10 ¹²	2,320,000
Felodipine	Minimum	0.0221 (± 0.0001)	0.0197 ⁵⁶	0.0024	170 (± 5.4)	2.59 × 10 ⁻¹⁵	3.75 × 10 ¹⁸	9.24 × 10 ¹¹	4,060,000
	Q1	0.0281 (± 0.0001)	0.0197 ⁵⁶	0.0084	17.9 (± 0.6)	2.98 × 10 ⁻¹⁸	1.32 × 10 ¹⁹	2.83 × 10 ¹⁵	4,670
	Median	0.0510 (± 0.0006)	0.0197 ⁵⁶	0.0313	19.3 (± 1.2)	3.77 × 10 ⁻¹⁸	4.91 × 10 ¹⁹	8.31 × 10 ¹⁵	5,910
	Q3	0.0817 (± 0.0007)	0.0197 ⁵⁶	0.0619	6.13 (± 0.1)	1.21 × 10 ⁻¹⁹	9.72 × 10 ¹⁹	5.14 × 10 ¹⁷	189
	Maximum	0.3560 (± 0.0034)	0.0197 ⁵⁶	0.3363	5.12 (± 0.2)	7.03 × 10 ⁻²⁰	5.27 × 10 ²⁰	4.79 × 10 ¹⁸	110

Drug	Media	[Dt] concentration in simulated media (g/L)	[D] concentration in aqueous media (blank) (g/L)	n[D-M] ^a (g/L)	DLS size ^a (intensity dist. d, nm) (drug loaded micelle diameter)	Mass 1 sphere (g) (drug loaded micelle weight)	Number of micelle entrapped drug molecules in 1 L of drug-loaded FaSSIF	Number of micelles per 1 L of FaSSIF	Number of drug molecules per micelle
Felodipine	Biorelevant	0.0541 (± 0.0010)	0.0197 ⁵⁶	0.0344	85.6 (± 1.2)	3.29 × 10 ⁻¹⁶	5.39 × 10 ¹⁹	1.05 × 10 ¹⁴	515,000
Fenofibrate	Minimum	0.0078 (± 0.0001)	0.000291 ¹²⁷	0.0075	124 (± 3.9)	9.87 × 10 ⁻¹⁶	1.25 × 10 ¹⁹	7.57 × 10 ¹²	1,650,000
	Q1	0.0099 (± 0.0001)	0.000291 ¹²⁷	0.0096	16.9 (± 0.3)	2.56 × 10 ⁻¹⁸	1.61 × 10 ¹⁹	3.76 × 10 ¹⁵	4,270
	Median	0.0139 (± 0.0001)	0.000291 ¹²⁷	0.0137	20.6 (± 2.5)	4.59 × 10 ⁻¹⁸	2.29 × 10 ¹⁹	2.99 × 10 ¹⁵	7,660
	Q3	0.0148 (± 0.0001)	0.000291 ¹²⁷	0.0145	6.51 (± 0.2)	1.44 × 10 ⁻¹⁹	2.41 × 10 ¹⁹	1.00 × 10 ¹⁷	241
	Maximum	0.0615 (± 0.0005)	0.000291 ¹²⁷	0.0612	5.51 (± 0.1)	8.76 × 10 ⁻²⁰	1.02 × 10 ²⁰	6.99 × 10 ¹⁷	146
	Biorelevant	0.0176 (± 0.0003)	0.000291 ¹²⁷	0.0173	102 (± 1.9)	5.54 × 10 ⁻¹⁶	2.89 × 10 ¹⁹	3.13 × 10 ¹³	924,000
Griseofulvin	Minimum	0.0376 (± 0.0006)	0.00864 ⁵⁶	0.0289	129 (± 2.4)	1.12 × 10 ⁻¹⁵	4.94 × 10 ¹⁹	2.58 × 10 ¹³	1,910,000
	Q1	0.0582 (± 0.0016)	0.00864 ⁵⁶	0.0496	18.4 (± 0.2)	3.28 × 10 ⁻¹⁸	8.46 × 10 ¹⁹	1.51 × 10 ¹⁶	5,600
	Median	0.0578 (± 0.0008)	0.00864 ⁵⁶	0.0491	22.8 (± 1.3)	6.21 × 10 ⁻¹⁸	8.38 × 10 ¹⁹	7.90 × 10 ¹⁵	10,600
	Q3	0.0658 (± 0.0041)	0.00864 ⁵⁶	0.0572	6.75 (± 0.2)	1.61 × 10 ⁻¹⁹	9.76 × 10 ¹⁹	3.55 × 10 ¹⁷	275
	Maximum	0.1082 (± 0.0024)	0.00864 ⁵⁶	0.0996	5.09 (± 0.2)	6.90 × 10 ⁻²⁰	1.69 × 10 ²⁰	1.44 × 10 ¹⁸	118
	Biorelevant	0.0562 (± 0.0022)	0.00864 ⁵⁶	0.0476	17.9 (± 1.6)	3.04 × 10 ⁻¹⁸	8.12 × 10 ¹⁹	1.57 × 10 ¹⁶	5,190
Carvedilol	Minimum	0.5716 (± 0.0138)	0.0279 ⁶³	0.5437	163 (± 2.3)	2.25 × 10 ⁻¹⁵	8.05 × 10 ²⁰	2.41 × 10 ¹⁴	3,340,000
	Q1	0.0837 (± 0.0002)	0.0279 ⁶³	0.0558	122 (± 1.8)	9.46 × 10 ⁻¹⁶	8.27 × 10 ¹⁹	5.90 × 10 ¹³	1,400,000
	Median	0.1064 (± 0.0006)	0.0279 ⁶³	0.0785	199 (± 2.2)	4.15 × 10 ⁻¹⁵	1.16 × 10 ²⁰	1.89 × 10 ¹³	6,150,000
	Q3	0.1275 (± 0.0011)	0.0279 ⁶³	0.0996	179 (± 3.6)	3.00 × 10 ⁻¹⁵	1.48 × 10 ²⁰	3.32 × 10 ¹³	4,450,000
	Maximum	0.5022 (± 0.0110)	0.0279 ⁶³	0.4743	5.30 (± 0.2)	7.80 × 10 ⁻²⁰	7.03 × 10 ²⁰	6.08 × 10 ¹⁸	116
	Biorelevant	0.0952 (± 0.0016)	0.0279 ⁶³	0.0673	624 (± 12.9)	1.27 × 10 ⁻¹³	9.96 × 10 ¹⁹	5.29 × 10 ¹¹	188,000,000
Tadalafil	Minimum	0.0056 (± 0.0002)	0.00073 ¹²⁸	0.0049	132 (± 2.3)	1.21 × 10 ⁻¹⁵	7.54 × 10 ¹⁸	4.04 × 10 ¹²	1,870,000
	Q1	0.0056 (± 0.0001)	0.00073 ¹²⁸	0.0049	19.7 (± 0.7)	3.98 × 10 ⁻¹⁸	7.60 × 10 ¹⁸	1.24 × 10 ¹⁵	6,150
	Median	0.0093 (± 0.0002)	0.00073 ¹²⁸	0.0086	23.0 (± 0.1)	6.39 × 10 ⁻¹⁷	1.33 × 10 ¹⁹	1.35 × 10 ¹⁵	9,880
	Q3	0.0113 (± 0.0002)	0.00073 ¹²⁸	0.0105	6.4 (± 0.1)	1.40 × 10 ⁻¹⁹	1.63 × 10 ¹⁹	7.53 × 10 ¹⁶	216
	Maximum	0.0496 (± 0.0008)	0.00073 ¹²⁸	0.0488	5.3 (± 0.1)	7.97 × 10 ⁻²⁰	7.55 × 10 ¹⁹	6.13 × 10 ¹⁷	123
	Biorelevant	0.0098 (± 0.0001)	0.00073 ¹²⁸	0.0090	92.2 (± 1.8)	4.10 × 10 ⁻¹⁶	1.40 × 10 ¹⁹	2.22 × 10 ¹³	634,000

^a n·[D-M] is the concentration of drug that is micelle bound and is calculated as the difference between the total and free drug solubilities (i.e. difference between [D_t] and [D])

6.5.2. Solubility Enhancement

The calculated solubility enhancement values are presented in Table 6.6.

Table 6.6: Calculated solubility enhancement values (-fold)

Drug	Media					
	Minimum	Q1	Median	Q3	Maximum	Biorelevant
Naproxen	2	371	414	373	362	35
Indomethacin	2	140	278	286	541	14
Phenytoin	1	1	2	2	6	2
Felodipine	1	1	3	4	18	3
Fenofibrate	27	34	48	51	211	60
Griseofulvin	4	7	7	8	13	7
Carvedilol	20	3	4	5	18	3
Tadalafil	8	8	13	15	68	13

6.5.3. Theoretical Calculation of Drug Molecules per Mixed Micelle in SIF

As observed in Table 6.5, the concentration of the acidic drug phenytoin in the Q1 media was effectively the same as in the buffer solution. There was no impact of colloidal structures on solubility enhancement here, therefore the micelle associated drug fraction was zero.

It was found that the number of drug molecules per micelle is estimated to be the lowest in the maximum simulated intestinal fluid media for every drug. This is not surprising as the particle size, measured by dynamic light scattering is the smallest in the maximum media points. This is logical as the structures are smaller so there is less space for the drug molecules in the micelles. The smaller particle sizes result in a lower mass of drug loaded micelle weight per sphere (g). An example of this can be found with the neutral drug griseofulvin in the maximum media. One drug molecule is estimated per micelle where the size (diameter) of the colloidal structure is measured to be 5.09 ± 0.2 nm and the mass of one sphere/drug loaded micelle is 6.90×10^{-20} g.

The number of calculated drug molecules per micelle for each drug in each of the six simulated intestinal fluids is presented in Figure 6.1.

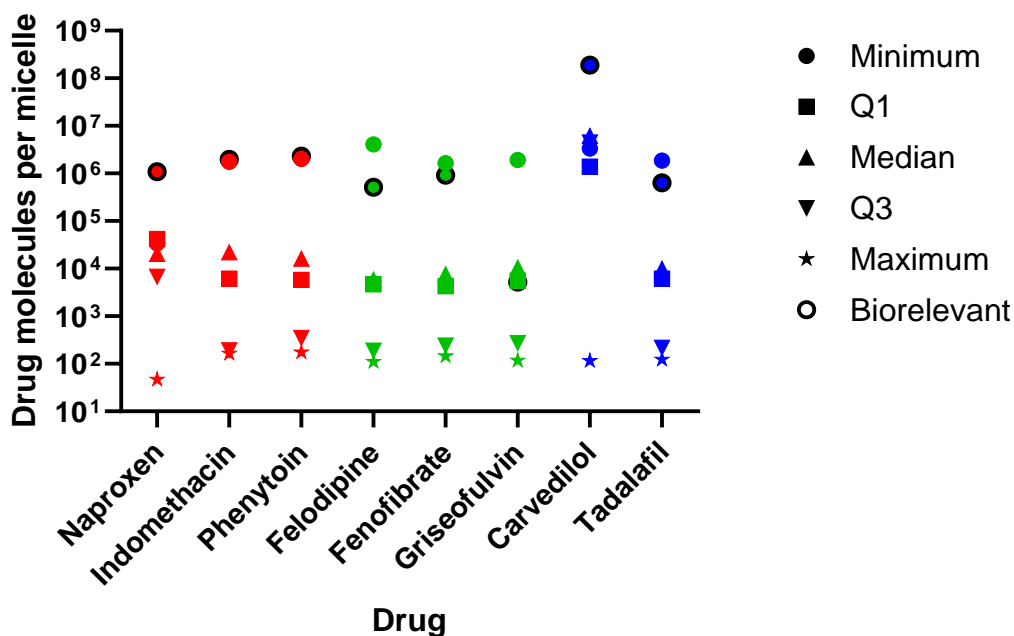


Figure 6.1: Number of calculated drug molecules per micelle for each drug in each of the six simulated intestinal fluid media. Red symbols indicate acidic drug data points, green are neutral drug data points and blue are basic drug data points

The drugs with the largest number of drug molecules estimated per micelle was found for carvedilol and felodipine, in the biorelevant and minimum media, where the drug molecules estimated were 188,000,000 and 4,060,000, respectively. This can be attributed to the larger sizes of the structures measured (624 ± 12.9 nm for carvedilol) and (170 ± 5.4 nm for felodipine) which gives the micelles the ability to accommodate a larger number of drug molecules per micelle.

The greatest number of micelles per 1 L of FaSSIF and also the greatest number of micelle entrapped drug molecules in 1 L of drug loaded FaSSIF for the majority of the drugs was recorded in the maximum media point, although this results in the lowest estimated number of drug molecules per micelle as the other drug containing SIF samples have a bigger difference between these two numbers. This can be observed in the neutral drug felodipine. The calculated number of micelles per 1 L of FaSSIF, in the maximum media, was found to be 4.79×10^{18} , while the number of micelle entrapped drug molecules in 1 L of drug loaded FaSSIF was calculated to be 5.27×10^{20} , giving an estimated 110 drug molecules per micelle. In comparison, the calculated number of micelles per 1 L of FaSSIF, in the median media, was found to be 8.31×10^{15} , while the number of micelle entrapped drug molecules in 1 L of drug loaded FaSSIF was calculated to be 4.91×10^{19} , giving an estimated 5,910 drug molecules per micelle. The particle size of the colloidal structures formed between felodipine in the fluid is measured to be

larger in the median media than in the maximum media, at 19.3 ± 1.2 nm and 5.12 ± 0.2 nm, respectively.

The number of drug molecules estimated per micelle increases considerably for every drug (except naproxen), when ($\text{pH} \times [\text{TAC}]$) is increased from the Q1 to the median SIF point. This can be explained for naproxen as the particle size measured decreases from the Q1 media to the median media, from 34.1 ± 1.4 nm to 27.4 ± 1.4 nm, therefore reducing the number of drug molecules per micelles from 41,900 to 20,400. An increase in particle size is recorded for all other drugs resulting in the increase in estimated drug molecules per micelle.

The number of drug molecules per micelle is calculated to be greatest in the minimum or in the biorelevant media. For the neutral drugs, the number of drug molecules calculated was greatest in the minimum SIF media, while for the acidic and basic drugs (with the exception of tadalafil) the estimated number of drug molecules per micelle was found to be the highest in the biorelevant SIF. Again, in the exception case of tadalafil, this can be linked to the particle size of the colloidal structures measured. The structures of tadalafil in the biorelevant SIF fluid are measured to be 92.2 ± 1.8 nm which give an estimated 634,000 drug molecules per micelle, while the structures of tadalafil in the minimum SIF media are measured to be 132 ± 2.3 nm, resulting in an estimated 1,870,000 drug molecules per micelle.

While it seems that the estimated number of drug molecules per micelle is directly linked to the particle size of the colloidal structures measured. This is also related to the solubility of the drug in the SIF. It was previously found and discussed in Chapter 3 that the particle size is linked to the drug solubility and concentration of the amphiphiles in each of the simulated media.

As the concentration of amphiphiles increases with increasing media point, the solubility of the drug also increases and with this there is a decrease in particle size of the colloidal structures formed, measured by dynamic light scattering. This theory can be observed in the acidic drug indomethacin where the [TAC] is 1.88 mM in the minimum media, the drug solubility is 51.9 ± 0.1 μM and the particle size of the structures are 126.2 ± 2.5 nm which result in an estimated 1,760,000 drug molecules per micelle. In the median media, the [TAC] is 3.74 mM, the drug solubility is 6842.8 ± 20.7 μM and the particle size of the structures are 29.2 ± 1.6 nm, which results in an estimated 21,900 drug molecules per micelle. In the maximum media, where [TAC] is 10.01 mM, the solubility of indomethacin is 13310.6 ± 131.9 μM and the particle size of the structures are 5.71 ± 0.7 nm, which results in an

estimated 164 drug molecules per micelle. The solubility and particle size relationship was thought to be due to the lipophilic drug being solubilised into the hydrophobic core of the micelle structure and increased interactions between the drug and the micelle.

Griseofulvin is the only drug in common that is used in both the study carried out by Polli *et al.* and also the work carried out in this thesis. Polli *et al.* estimated a total number of griseofulvin drug molecules to be 48.3 per micelle of FaSSIF V2, while this was estimated to be between 118 drug molecules and 1,910,000 drug molecules per micelle in our suite of simulated intestinal fluid. The values used in the calculations can be found in Table 6.7, for ease of comparison.

Table 6.7: Parameters used in the calculation of number of griseofulvin molecules per micelle of FaSSIF V1 and V2

Parameter	Polli FaSSIF V2	Minimum	Q1	Median	Q3	Maximum	Biorelevant
[D _i] concentration in simulated media (g/L)	0.0121 (± 0.0002)	0.0376 (± 0.0006)	0.0582 (± 0.0016)	0.0578 (± 0.0008)	0.0658 (± 0.0041)	0.1082 (± 0.0024)	0.0562 (± 0.0022)
[D] concentration in aqueous media (blank) (g/L)	0.0118	0.00864	0.00864	0.00864	0.00864	0.00864	0.00864
n[D-M] ^a (g/L)	0.000350	0.0289	0.0496	0.0491	0.0572	0.0996	0.0476
DLS size (drug loaded micelle diameter, nm)	63.8 (± 0.8)	129 (± 2.4)	18.4 (± 0.2)	22.8 (± 1.3)	6.75 (± 0.2)	5.09 (± 0.2)	17.9 (± 1.6)

Parameter	Polli FaSSIF V2	Minimum	Q1	Median	Q3	Maximum	Biorelevant
Mass 1 sphere (g) (drug loaded micelle weight)	Not reported	1.12 $\times 10^{-15}$	3.28 $\times 10^{-18}$	6.21 $\times 10^{-18}$	1.61 $\times 10^{-19}$	6.90 $\times 10^{-20}$	3.04×10^{-18}
Number of micelle entrapped drug molecules in 1 L of drug- loaded FaSSIF	5.97 $\times 10^{17}$	4.94 $\times 10^{19}$	8.46 $\times 10^{19}$	8.38 $\times 10^{19}$	9.76 $\times 10^{19}$	1.69×10^{20}	8.12×10^{19}
Number of micelles per 1 L of FaSSIF	1.23 $\times 10^{16}$	2.58 $\times 10^{13}$	1.51 $\times 10^{16}$	7.90 $\times 10^{15}$	3.55 $\times 10^{17}$	1.44×10^{18}	1.57×10^{16}
Number of drug molecules per micelle	48.3	1,910,000	5,600	10,600	275	118	5,190

^a $n \cdot [D-M]$ is the concentration of drug that is micelle bound and is calculated as the difference between the total and free drug solubilities (i.e. difference between $[D_t]$ and $[D]$).

The number of drug molecules of griseofulvin in the SIF is not directly comparable between studies as the study by Polli *et al.* has used FaSSIF V2 while this work focuses on FaSSIF V1. A key difference in the composition of the fluid is that version 2 contains more phospholipid (0.2 mM) but it also contains a lower concentration of sodium chloride salt and maleic acid buffer (68 mM and 19.12 mM, respectively) compared to FaSSIF V1 which has a concentration of 0.075 mM (phospholipid), 105 mM (salt – NaCl) and 28.65 mM (buffer – phosphate). The higher phospholipid concentration may contribute to the larger structures formed within the FaSSIF V2 fluid, while the smaller structures measured in the new suite of fluids are more effective at solubilising the hydrophobic griseofulvin. In all media but the minimum media (where the number of micelles per 1 L of FaSSIF is lower and the size of the micelles are greater), there are fewer, larger colloidal structures in the FaSSIF V2 fluid which

suggests that the critical micelle concentration is lower. As a result, there is a lower number of micelles that are available to solubilise the griseofulvin, giving a lower solubility, compared to that of griseofulvin in the new suite of fluids. Although the structures of the drug loaded new suite of fluids are measured to be smaller than in the version 2 fluid, an increased number of drug molecules per micelle is observed. This indicates that the drug loading capacity per micelle is better in the smaller structures. The smaller structures may have more hydrophobic core space available for encapsulating the lipophilic drug giving rise to a greater estimated number of drug molecules per mixed micelle.

6.5.4. Solubility Enhancement

The calculated solubility enhancement is presented in Table 6.6. It was found that the acidic drugs naproxen and indomethacin presented with the highest media solubility enhancement. The greatest increase was found to be a 414-fold increase in naproxen in the median media point and a 541-fold increase in indomethacin in the maximum media point. The lowest solubility enhancement values calculated were for the acidic drug phenytoin and for the neutral drug felodipine, where both of these drugs in the minimum and Q1 media were calculated to be one. This indicates that there is no solubility enhancement effect and no impact of colloidal structures on solubility.

The solubility enhancement tends to increase with increasing ($\text{pH} \times [\text{TAC}]$), which can be seen with the neutral drug fenofibrate where the solubility enhancement in the minimum media is 27-fold, increasing to 48-fold in the median media, which increases to 211-fold in the maximum media point. As the ($\text{pH} \times [\text{TAC}]$) increases, the drug solubility measured by HPLC also increases, as does the solubility enhancement. Interestingly, when comparing this solubility data to the estimated number of drug molecules of fenofibrate per micelle, there is not as clear of a relationship. Typically, as solubility and ($\text{pH} \times [\text{TAC}]$) or $[\text{TAC}]$ is increased, the estimated drug molecules per micelle decreases, which is expected. However, there is the increase from 4,270 drug molecules per micelle in the Q1 media to 7,660 drug molecules per micelle in the median media. This has previously been discussed and is thought to be due to the slight increase in particle size measured in the median fluid.

6.5.5. Relationship with Chemical Structure

The results from the particle size analysis and the estimation of drug molecules per micelle reveal a complex relationship between each drug's chemical properties. This includes molecular weight, lipophilicity, hydrophilicity, pK_a , and size and their behaviour in micellar systems. A deeper

understanding of how these factors influence the results can be achieved by considering the chemical properties of each drug.

The acidic drugs naproxen and indomethacin contain carboxyl groups, while phenytoin has an imide group which can deprotonate to their ionised form. The ionised drugs are more soluble in water (Table 2.8) and are less likely to partition into the hydrophobic core of the micelle structures. As such, the resulting colloidal structures that form from acidic drugs in the SIF may be larger as the ionised form of the drugs may keep the drug towards the outer hydrophilic/aqueous phase of the colloid. This theory does not seem to be in agreement with the data recorded by DLS, as the sizes measured of the acidic drugs in the SIF does not seem to be considerably greater than the structures formed by the neutral or basic drugs in any of the SIF media. It could be said, collectively, as a group, the structures formed by the acidic drugs in the biorelevant media are larger than those formed by the neutral or basic drugs (with the exception of carvedilol) but this may not be due to a direct relationship between the structure of the drug and the particle size of the colloidal structure formed. Looking at the size (diameter) of the colloidal structures formed of indomethacin and phenytoin in this media (131.0 ± 5.8 nm and 122.9 ± 3.0 nm, respectively) and comparing this to the estimated number of drug molecules per colloid at 1,980,000 and 2,320,000, there does not appear to be a direct link between the colloidal structure size and predicted number of drug molecules per micelle. The molecular weight of indomethacin and phenytoin are 357.79 g/mol and 252.3 g/mol, respectively. Incorporating this information, there does not appear to be a link between the molecular weight of the drug, the size of the drug loaded colloidal structure measured and the estimated number of drug molecules per colloid of these two drugs.

In Table 6.3, the estimated number of drug molecules per micelle provides further information as to how ionisation and molecular structure affect micelle packing. Phenytoin and indomethacin have relatively high estimated numbers of drug molecules per micelle in the biorelevant media (2,320,000 and 1,980,000, respectively). The difference in molecular weights may contribute to the difference between the number of drug molecules per micelle predicted. Phenytoin is a smaller molecule with a molecular weight of 252.3 g/mol while indomethacin is larger at 357.79 g/mol. One hypothesis is that the smaller naproxen structure will allow for more molecules to be packed into a micelle, while the bulkier indomethacin structure, will occupy more space per molecule, therefore decreasing the overall number of drug molecules in comparison. However, this is not true for naproxen which has a molecular weight of 230.26 g/mol and an estimated number of 1,090,000 drug molecules per micelle in the biorelevant media. The molecular weight of naproxen is similar to that of phenytoin, however

the estimated number of drug molecules per micelle is considerably different, therefore disproving this hypothesis.

The basic drugs, carvedilol and tadalafil both contain functional groups that can accept protons. Carvedilol contains a secondary amine group, while tadalafil contains a piperazine ring (six membered ring containing two opposing nitrogen atoms), where the lone pairs on the nitrogen atoms can accept protons, therefore creating the positively charged protonated/ionised form. The ionised forms of these drugs can electrostatically interact with the negatively charged bile salt, which may further aid their incorporation into the colloidal structures. This type of interaction may lead to smaller colloidal particles. This, however, is not observed experimentally by DLS. The size of the carvedilol loaded colloids are considerably greater in all media except the maximum media (where the size of the structures is similar to the other drugs), while the colloidal structures containing tadalafil are around the same size as those measured by acidic and neutral drugs in the SIF media. In the Q1 media, where the degree of drug ionisation for carvedilol and tadalafil is 78.8 % and 99.9 %, the diameter of the colloidal structures formed is measured to be 121.8 ± 1.8 nm and 19.7 ± 0.7 nm. The difference in particle size may be, in part, linked to the molecular structure. Carvedilol has a bulkier structure at 406.47 g/mol, compared to tadalafil with a slighter smaller molecular weight of 389.40 g/mol. The smaller tadalafil structure may enable more efficient packing of drug molecules within the micelle. When comparing the diameter of the structures measured to the estimated number of drug molecules per colloid, this is calculated to be 1,400,000 and 6,150, for carvedilol and tadalafil, respectively in the Q1 media. As for the acidic drugs, there does not seem to be a direct relationship between the structure of the molecule, the particle size of the drug loaded colloidal structure measured by DLS and the estimated number of drug molecules per micelle.

6.5.6. Use of Biorelevant FaSSIF for Solubility Prediction

From Table 6.6, it can be seen that the calculated solubility enhancement for the biorelevant fluid is comparable to that observed for most drugs in both the median and Q3 media. This indicates that the biorelevant media is adequate for making some solubility predictions. The calculated solubility enhancement for the acidic drugs, naproxen and indomethacin, is considerably greater in the median and Q3 media than in the biorelevant media. Naproxen has a calculated solubility enhancement value of 414-fold and 373-fold in the median and Q3 media, while this decreases greatly in the biorelevant fluid to 35-fold. Indomethacin has a calculated solubility enhancement value of 278-fold and 286-fold in the median and Q3 fluid, which decreases to 14-fold in the biorelevant fluid, which highlights the difference between the enhancement abilities of the fluids.

The other acidic, neutral and basic drugs in the SIF have similar calculated solubility enhancement values to those in the biorelevant fluid. For example, the neutral drug fenofibrate, has a calculated solubility enhancement value of 48-fold and 51-fold in the median and Q3 media which increases to 60-fold in the biorelevant media. The basic drug tadalafil, has a calculated value of 13- and 15-fold in the median and Q3 media which remains at 13-fold in the biorelevant media. Compared to the lower and higher (pH × [TAC]), the calculated solubility enhancement for drugs in the biorelevant fluid does not correlate well. This clearly shows where the biorelevant FaSSIF can be used as a predictive tool, as it represents the mean samples of the new suite of SIF fairly well and emphasised the need for other fluids that are representative of *in vivo* gastrointestinal variability.

6.6. Conclusion

Polli *et al.* developed and used a predictive model in order to predict the dissolution and solubility enhancement of model BCS class II drugs in simulated intestinal fluid. This model was used to estimate the number of drug molecules per colloid or mixed micelle structure in a series of simulated intestinal fluids.

Using the model, this was applied to experimental data measured in previous chapters of this thesis (solubility – Chapter 2, particle size – Chapter 3) and the number of drug molecules per micelle was estimated, as well as the -fold solubility enhancement in the FaSSIF media. It was found that the number of drug molecules per micelle was estimated to be the lowest in the maximum simulated media for every drug, where the colloidal particle size measured by dynamic light scattering was the smallest. Analysis of the data and results indicates that there is a direct relationship between particle size of the colloidal structures and the number of estimated drug molecules per structure. As expected, as the particle size decreases, as does the estimated number of drug molecules per micelle. The larger structures can accommodate a greater number of drug molecules per micelle. Solubility enhancement was also calculated, with the acidic drugs, naproxen and indomethacin proving to be most solubility enhanced in the suite of simulated intestinal fluid. The lowest solubility enhancement was observed for the acidic drug phenytoin and the neutral drug felodipine which both presented with a 1-fold enhancement. In other words, there was no solubility enhancement effect present and no impact of colloidal structures on solubility.

6.7. Further Work

6.7.1. Molecular Dynamics

Molecular dynamics (MD) simulations were first performed in the late 1950's and have increasingly grown in popularity over the last decade, where they have been used to both interpret and guide experimental work¹²⁹. They are a useful investigative technique that can be used to study the behaviour of systems at a level of detail that experimental methods cannot yet achieve¹³⁰. They are also used as an alternative to experimental evaluation of molecular interactions⁴⁹. Using a known or predicted structure as a starting point, with the known positions of all the atoms in the system, it is possible to calculate the force applied to each atom by other atoms in the system. By applying Newton's laws of motion, it is possible to determine the position of each atom over time. The simulation proceeds by repeatedly calculating the forces applied to each atom which is then used to update their positions and velocities. The resulting output is a simulation that presents the atomic-level arrangement of the system at each time point during the simulated time period¹²⁹.

Coarse-grained modelled MD (CGMD) is frequently used to simulate larger systems on great time and size scales¹²⁹. CGMD is a somewhat simplified and lower-resolution type of MD where a number of atoms are grouped together to create "beads" that present as particles for the model system, in contrast to the standard/tradition "all atom" MD simulations where each atom is presented as a particle^{49, 131}. Figure 6.2 is an example of a coarse-gained representation of a molecular structure, created based on molecules and figures from Parrow *et al.*⁴⁹

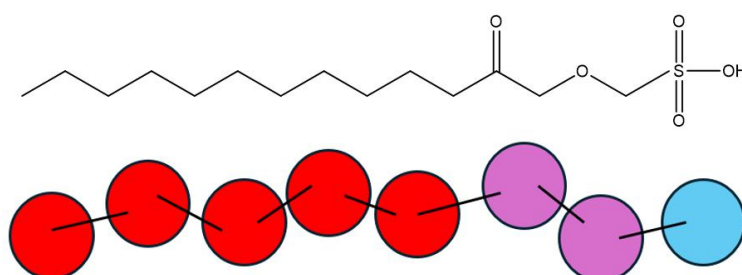


Figure 6.2: Example of a coarse-grained representation of a molecular structure. Based on figures and molecules from Parrow *et al.*⁴⁹

CGMD has been used in an interesting study by Parrow *et al.* to investigate fasted state human duodenal fluid with the aim of identifying the impact of interindividual variability of the various components present within human intestinal fluid (HIF) and the affect this will have on drug solubilisation. Using experimental data from the 2016 study by Riethorst *et al.* the composition and concentration data was obtained from aspirated HIF then simulations were performed modelling the self-assembly of mixed micelles. A few of the structures were then further studied with model, neutral drugs. The findings from this study show that the colloidal structures were ellipsoidal micelles with a determined size between 2 and 7 nm. The micelles were found to enhance the solubility of the poorly water soluble drugs, with the drug affinity correlating with the hydrophobicity. The simulations indicated that the composition of micelles and drug lipophilicity affect the solubilisation mechanism of the model drugs analysed which will result in affected drug absorption in different individuals^{26, 49}. The work carried out in this chapter calculates the solubility enhancement in SIF for different drugs. This relates to this study as our aim is to predict the number of drug molecules per micelle and the solubility enhancement provided to each drug in the SIF which in turn yields information regarding the drug solubilisation and absorption in the various media.

There are limitations associated with all types of mathematical modelling such as: the simplifying assumptions that are made (depending on the model) e.g. spherical particle size and uniform density of colloidal structures.

The work carried out here may improve the systems by providing a better understanding of both solubility and solubility variability according to the composition of the SIF at the site of absorption. Future work of the results presented here include integration of relevant data into PBPK modelling such as using GastroPlus, or molecular dynamics simulations to better understand the colloidal-drug associations that may influence solubility enhancement. It would be interesting to observe the simulations and behaviour of the drugs of interest in the six fasted state fluids, using coarse-grained molecular dynamics and compare this with the data collected in this thesis. Additionally, collecting dissolution data would enable calculation of the dissolution enhancement provided by each of the SIF which would provide further understanding of the complex mechanisms of drug solubilisation.

Chapter 7

Conclusions and Future Outlook

7. Conclusions and Future Outlook

7.1. General Conclusions

This thesis has provided a deeper understanding of the relationship between drug solubility, amphiphile concentration and the size of colloidal structures formed in fasted state simulated intestinal fluid that is reflective of *in vivo* gastrointestinal variability. Knowledge of this is essential for optimising drug delivery and absorption, particularly for orally administered drugs.

The main conclusions, aligned to each research chapter, can be summarised as follows:

1. Solubility analysis of fasted state simulated intestinal fluid

A new suite of simulated intestinal fluid, reflective of *in vivo* gastrointestinal variability was created. The composition encompassed that which was revealed from a range of human intestinal fluid samples from a clinical study. The solubility of eight poorly soluble BCS class II drugs were measured and the data showed that the solubility was typically greater in the acidic drugs than in the neutrals or bases. The drug solubility tended to increase with increasing media point i.e. ($\text{pH} \times [\text{TAC}]$).

2. Dynamic light scattering of fasted state simulated intestinal fluid

Particle size data was collected using dynamic light scattering which highlighted the polydispersity present within the samples. Trends relating to solubility and particle size were identified and it was found that in nearly all of the drugs analysed, the general trend indicates that while solubility is to some extent affected by pH and [TAC] or ($\text{pH} \times [\text{TAC}]$), the relationship between solubility and particle size is linked with the total concentration of amphiphiles, [TAC].

3. Nanoparticle tracking analysis of fasted state intestinal fluid

Particle size data was collected using nanoparticle tracking analysis which confirmed the polydispersity present within the samples. Trends relating to size with regards to increasing ($\text{pH} \times [\text{TAC}]$) (media point) and/or drug type were identified and it was found that typically, the drug solubilised in the maximum media point (the greatest ($\text{pH} \times [\text{TAC}]$) value) resulted in the greatest modal size measured. A comparison with DLS data showed a distinct pattern was present in the size comparison of the acidic drugs between the two measurement techniques. As the total amphiphile concentration is increased, the acidic drugs are better solubilised which may be linked to a decrease in particle size, measured by dynamic light scattering. The particle size of the acidic drug samples measured by NTA did not vary

considerably, which may be a result of dilution. The neutral drugs presented a similar pattern to the acidic drugs. The basic drug loaded samples of carvedilol exhibited a greater particle size measurement by DLS than for NTA (with the exception of the maximum SIF sample). This was thought to be a result of the high concentration of drug solubilised into the media point.

4. Small angle X-ray scattering (SAXS) analysis of fasted state intestinal fluid

Data was collected of drug and drug free SIF samples using the labSAXS instrument at the Diamond Light Source facility. However, once processed it was found that the samples are too weakly scattering to be detected by a labSAXS instrument.

5. Simulated intestinal fluid mixed micelle size and solubility relationship

The experimental data collected from previous chapters was used in a simple mathematical model in order to estimate the number of drug molecules per colloid or mixed micelle structure in the series of SIF. It was found that the number of drug molecules per micelle was estimated to be the lowest in the maximum simulated media for every drug, where the colloidal particle size measured by dynamic light scattering was the smallest. Analysis of the data and results indicates that there is a direct relationship between particle size of the colloidal structures and the number of estimated drug molecules per structure. As expected, as the particle size decreases, as does the estimated number of drug molecules per micelle. The larger structures can accommodate a greater number of drug molecules per micelle.

This study provides important insights into the complex and interdependent relationship between drug solubility, the concentration of amphiphilic components, and the size and distribution of colloidal structures formed in fasted state simulated intestinal fluid. Through a combination of experimental techniques this work demonstrates how variations in physiological conditions, such as pH and total amphiphile concentration ([TAC]), directly influence the formation and behaviour of micellar structures, which in turn affect the solubilisation capacity for poorly soluble drugs. These findings are essential for informing the strategic development of oral drug formulations, offering a deeper understanding of how colloidal dynamics impact drug bioavailability in the gastrointestinal tract.

7.2. Further Work

While this research has provided valuable insights and advanced the understanding of solubility, amphiphile concentration and structure size, it also highlights several opportunities for further investigation to fully elucidate the role of particle size, geometry and even inter/intra-molecular

interactions in determining the structure and behaviour of drug and drug free colloidal structures formed in simulated intestinal fluid.

The findings in this thesis could be further explored by integrating advanced analytical techniques such as molecular dynamics simulations, cryo-electron microscopy (cryo-EM), and synchrotron-based small angle X-ray scattering (SAXS) to gain deeper insights into the structural organisation, dynamic behaviour, and intermolecular interactions of drug loaded colloidal particles in SIF. These approaches would allow for high-resolution characterisation of micelle structure and drug encapsulation mechanisms, enabling the development of predictive models for drug solubilisation and absorption in the gastrointestinal environment.

Future studies should focus on molecular dynamics simulations, cryo-electron microscopy (cryo-EM) and SAXS to allow a detailed explanation of the structural behaviour, interaction mechanisms and dynamic properties of the colloidal particles in SIF, giving a deeper understanding into how these factors influence solubility, absorption and stability in the complex environment of the GI tract.

Future work should also expand the range and number of drugs studied to better capture the diversity of physicochemical properties relevant to oral drug delivery. Including compounds with varying solubility profiles, molecular weights, and ionisation states would enable a broader assessment of how micellar systems behave across different drug classes. This expanded dataset would be particularly valuable for refining and validating the predictive modelling approaches developed in this Chapter 6 of this work. By incorporating a wider variety of drug structures into future molecular dynamics simulations and structural modelling efforts, more generalisable trends could be identified. This would ultimately support the development of robust, transferable models capable of predicting drug-micelle interactions, encapsulation efficiency, and solubility enhancement for new drug candidates under GI conditions.

Atomistic and coarse-grained models of molecular dynamics (MD) simulations may provide detailed insights into the atomic level interactions within smaller particles. The work carried out in Chapter 6 estimates the number of drug molecules per micelle and the solubility enhancement provided to each drug in the SIF which then provides information regarding the drug solubilisation and absorption in the various media. Using MD simulations in combination with this work may provide molecular-level insights into drug encapsulation and micelle stability which would aid in providing a predictive

framework for designing micelle-based drug delivery systems with optimised loading capabilities and enhanced solubility that is tailored to the intestinal environment.

Cryo-EM work may reveal structural changes across particle sizes and geometries as this technique can provide near-atomic levels of structural detail such as surface morphology and self-assembly/organisation, which is essential for understanding how particle size and shape impact drug absorption and the overall functionality within the intestines. When combined with SAXS and other particle size techniques previously used in this thesis, i.e. DLS and NTA, cryo-EM could offer a high-resolution analysis of size, shape and structural organisation. Together, these methods enable a robust characterisation of particle morphology and structural dynamics, which will lead to a fuller understanding of the relationship between particle architecture and behaviour in the complex GI environment.

Transmission Electron Microscopy (TEM) serves as a complementary technique to SAXS in characterising colloidal structures. While SAXS offers insights into size distributions and shape on the nanometre scale across bulk populations, TEM provides direct imaging of individual particles with spatial resolution. This makes TEM particularly useful for validating the morphological assumptions made during SAXS data modelling, such as shape anisotropy, core-shell structures, or micelle aggregation states. When used in conjunction with SAXS, TEM can help connect high-throughput structural averages with particle specific details. For example, SAXS may indicate the presence of elongated or worm-like micelles, which could then be directly visualised and confirmed through TEM. This dual approach enhances confidence in structural interpretations and allows for more accurate modelling of micellar and colloidal assemblies under physiologically relevant conditions.

Finally, it would be beneficial to this work to further explore SAXS, using a synchrotron beamline such as I22 or B21 at the Diamond Light Source where the stronger X-ray source and longer detector distances would allow for scattering data to be measured for the samples created in this work. The scattering data can then be modelled to determine the radius of gyration and particle size distributions which would enable characterisation of particle size and shape.

Appendices

Appendix 1 – Diamond Light Source Application for Beamtime

Appendix 1: Diamond Light Source Application for Beamtime



Summary of Proposal 38942

Requested Access Route:	Rapid		
Submission(s):	1st Report Pending		
Principal Investigator:	Dr Martin Ward, University of Strathclyde		
Alternate Contact(s):	Miss Zoe McKinnon, University of Strathclyde		
Co-Investigator(s):	Miss Rachel Feeney, University of Strathclyde		
Title:	Exploring the Role of Colloidal Structures in Drug Solubility and Absorption in Simulated Intestinal Fluids (SIF)		
Requested Instrument(s):	labSAXS (9 shifts)		
Total Shifts Requested:	9	RCaH requested:	No
Industry Involved:	No	Industry Group Links:	Yes
Science Area(s):	Medicine, Chemistry, Biology and Bio-materials		
Abstract:	<p>Drug solubility within intestinal fluid is a critical factor influencing oral drug absorption. However, predicting solubility in such a complex medium is challenging due to the variability in intestinal fluid composition.</p>		

The objectives of this work include using small-angle X-ray scattering (SAXS) data to:

1. Measure the colloidal shape present to aid in identifying the specific structures in these SIF samples.
 2. Explore the particle structure (e.g., core-shell) and how this changes according to the drug within the system.
- These assessments will provide insights into the mechanisms by which drugs interact with colloidal particles within SIF. This information will inform future molecular dynamic simulations of these interactions, aiming to build predictive models for drug solubility within intestinal media.

labSAXS Instrument Questions

Question	Answer
Please select energy	Ga MetalJet (9.25 keV)
Sample's Vacuum Stability	Stable under vacuum
Please select from the sample environments below	Capillary Rack
Please indicate the reciprocal space Qmin (1/nm) value	0.02
Please indicate the reciprocal space Qmax (1/nm) value	1.5

Samples:

Name	CAS No	Type	
Drug-free simulated intestinal fluid samples (x6)	345909-26-4	ChemicalSubstance:	liquid/solution
Potassium hydroxide	1310-58-3	ChemicalSubstance:	liquid/solution
Hydrochloric acid	7647-01-0	ChemicalSubstance:	liquid/solution
Naproxen (drug) samples in simulated intestinal fluid (x6)	22204-53-1	ChemicalSubstance:	solid
Tadalafil (drug) samples in simulated intestinal fluid (x6)	171596-29-5	ChemicalSubstance:	powder

Equipment:

Name	Type
balance	
pH meter	

Equipment:

Name	Type
------	------

pH meter (for sample prep)	
----------------------------	--

rotary mixer	
--------------	--

rotary mixer (for sample prep)	
--------------------------------	--

stirrer hotplate	
------------------	--

stirrer hotplate (for sample prep)	
------------------------------------	--

Experimental Method:	Method
-----------------------------	--------

Sample Preparation:	Samples to be prepared at Strathclyde and mailed into Diamond for analysis
----------------------------	--

Instrument Experiment and Environment:	Samples to be prepared at Strathclyde and mailed into Diamond for analysis
---	--

Experimental Method:	Method
-----------------------------	--------

Sample Preparation:	Simulated intestinal fluid (SIF) samples (containing sodium taurocholate, sodium oleate, cholesterol and soybean lecithin) will be prepared at strathclyde then reconstituted at Diamond using deionised water. 267 uL of SIF will be added to a tube containing naproxen/tadalafil, along with 267 uL sodium chloride (salt), 267 uL sodium phosphate monobasic monohydrate (buffer) and 3199 uL deionised water. The pH will then be adjusted to target using dilute 0.1-0.5 M hydrochloric acid (HCl) and/or 0.1-1 M potassium hydroxide (KOH). This samples will then need to shaken prior to analysis by labSAXS.
----------------------------	--

PPE required: lab coat, goggles, nitrile gloves

Instrument Experiment and Environment:	Simulated intestinal fluid (SIF) samples (containing sodium taurocholate, sodium oleate, cholesterol and soybean lecithin) will be prepared at strathclyde then reconstituted at Diamond using deionised water. 267 uL of SIF will be added to a tube containing naproxen/tadalafil, along with 267 uL sodium chloride (salt), 267 uL sodium phosphate monobasic monohydrate (buffer) and 3199 uL deionised water. The pH will then be adjusted to target using dilute 0.1-0.5 M hydrochloric acid (HCl) and/or 0.1-1 M potassium hydroxide (KOH). This samples will then need to shaken prior to analysis by labSAXS
---	---

PPE required: lab coat, goggles, nitrile gloves

User Office	 diamond	Doc No: SCI-USO-DOC-0073.doc Issue: 1 Page: 1 of 2
-------------	--	--

DL-SAXS Rapid Access Proposal

Completed application should be uploaded to the proposal in UAS

Experiment Title	Exploring the Role of Colloidal Structures in Drug Solubility and Absorption in Simulated Intestinal Fluids	
Beamline Requested	DL-SAXS	
Proposal No	User Office to assign	
Principal Investigator Name	Hannah Batchelor	
Principal Investigator Establishment	University of Strathclyde	
Principal Investigator Email	hannah.batchelor@strath.ac.uk	
Date Proposal Submitted	13/06/2024	
Sample Environment (one only)	Tick One	
1. Solid Sample Rack		
2. Capillary Rack	✓	
List of Samples 18 total 6 drug free different simulated intestinal fluid (SIF) samples, 6 samples with naproxen and 6 with tadalafil		
Brief Science Case (including key objectives 500 words max and a figure if appropriate)		
<p>Drug solubility within intestinal fluid is a critical factor influencing oral drug absorption. However, predicting solubility in such a complex medium is challenging due to the variability in intestinal fluid composition. This variability arises from inter-individual differences, sampling location within the gastrointestinal (GI) tract, and timing relative to food intake. To address this, a suite of simulated intestinal fluid (SIF) media has been developed to better represent the diversity observed in human intestinal fluid (HIF).</p> <p>Research at Strathclyde has shown that drug solubility in these simulated fluids depends significantly on their composition. Additionally, the size and number of colloidal structures formed within these fluids are also composition-dependent. These colloidal structures, which include lipid droplets, (multi)-lamellar vesicles, and micelles, play a crucial role in enhancing the solubilizing capacity for certain drugs. However, for lipophilic compounds, strong entrapment within specific structures can lead to decreased absorptive flux, highlighting the importance of endogenous colloidal structures in the solubility-permeability interplay that underpins the bioavailability of lipophilic drugs.</p> <p>Cryogenic transmission electron microscopy (cryo-TEM), negative stain-TEM, and cryo-scanning electron microscopy have visualized these structures in HIF. Small spherical or ellipsoidal micelles with low aggregation numbers form from bile salts alone. In contrast, larger structures like rods, discs, vesicles, and worms emerge when bile salts</p>		

are mixed with phospholipids, cholesterol, and triglyceride digestion products. The absolute concentration of bile salts and the relative concentrations of other lipid components are key determinants of these structures.

The nanostructures formed in simulated intestinal fluids significantly influence the solubility of hydrophobic drugs and nutrients. The extent of this influence depends on the lipid composition and the resulting colloidal structures. Therefore, any differences between the structures present in the solubilizing nanoaggregates within SIFs must be well-defined to enable meaningful comparisons.

We have generated dynamic light scattering (DLS) data on a series of SIF media containing a range of drugs. The data (see Fig. 1) highlights the very different structures formed when naproxen or tadalafil are added to the series of media.

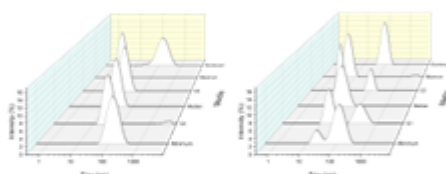


Fig. 1. DLS size and intensity distribution for naproxen (left) and tadalafil (right) in the SIF media.

The objectives of this work include using small-angle X-ray scattering (SAXS) data to:

1. Measure the colloidal shape present to aid in identifying the specific structures in these SIF samples.
2. Explore the particle structure (e.g., core-shell) and how this changes according to the drug within the system.

These assessments will provide insights into the mechanisms by which drugs interact with colloidal particles within SIF. This information will inform future molecular dynamic simulations of these interactions, aiming to build predictive models for drug solubility within intestinal media.

By advancing our understanding of how drugs interact with the colloidal structures in intestinal fluids, we can better predict drug solubility and enhance the effectiveness of oral drug delivery systems. This research represents a significant step toward optimizing drug formulations for improved bioavailability and therapeutic efficacy.

Appendix 2 – Script Written for SAXS Measurement

Appendix 2: Script Written for SAXS Measurements

The following information is the script written for SAXS measurements recorded on the morning of the 15th of August 2024.

```
scanTimeInSeconds = 3600  
numberOfExposures = 1
```

```
## reset detector to expect Ga x-rays  
so;ct;sc  
## reset detector to turn off virtual det  
virDET_enable 1
```

```
## Set distance for measurements  
umv x -1.42  
umv z -3.154  
#set_distance 4600  
## Record AgBeh  
umv z 21.0964  
umv x -4.2266  
#multiexp numberOfExposures 900 901
```

```
virDET_enable 0  
umv z -3.154  
## position empty cap  
umv x 44.0814  
#multiexp numberOfExposures scanTimeInSeconds scanTimeInSeconds+1
```

```
## position water background  
umv x 37.0814  
multiexp numberOfExposures scanTimeInSeconds scanTimeInSeconds+1
```

```
## position biorelevant buffer background  
umv x 30.0814  
multiexp numberOfExposures scanTimeInSeconds scanTimeInSeconds+1
```

```
## position biorelevant fassif  
umv x 23.0814  
multiexp numberOfExposures scanTimeInSeconds scanTimeInSeconds+1
```

```
## position SIF background  
umv x 16.0814  
multiexp numberOfExposures scanTimeInSeconds scanTimeInSeconds+1
```

```
## position Min blank sample  
umv x 9.0814  
multiexp numberOfExposures scanTimeInSeconds scanTimeInSeconds+1
```

```
## position Q1 blank sample  
umv x 2.0814  
multiexp numberOfExposures scanTimeInSeconds scanTimeInSeconds+1
```

```

## position Median blank sample
umv x -4.92
multiexp numberOfExposures scanTimeInSeconds scanTimeInSeconds+1

umv x -1.42
umv z -3.154
set_distance 1000

## Record AgBeh
umv z 21.0964
umv x -4.2266
multiexp numberOfExposures 900 901

umv z -3.154
## position empty cap
umv x 44.0814
multiexp numberOfExposures scanTimeInSeconds scanTimeInSeconds+1

## position water background
umv x 37.0814
multiexp numberOfExposures scanTimeInSeconds scanTimeInSeconds+1

## position biorelevant buffer background
umv x 30.0814
multiexp numberOfExposures scanTimeInSeconds scanTimeInSeconds+1

## position biorelevant fassif
umv x 23.0814
multiexp numberOfExposures scanTimeInSeconds scanTimeInSeconds+1

## position SIF background
umv x 16.0814
multiexp numberOfExposures scanTimeInSeconds scanTimeInSeconds+1

## position Min blank sample
umv x 9.0814
multiexp numberOfExposures scanTimeInSeconds scanTimeInSeconds+1

## position Q1 blank sample
umv x 2.0814
multiexp numberOfExposures scanTimeInSeconds scanTimeInSeconds+1

## position Median blank sample
umv x -4.92
multiexp numberOfExposures scanTimeInSeconds scanTimeInSeconds+1

```

The following information is the script written for SAXS measurements recorded between the evening of 15th of August and the 16th of August 2024.

```

scanTimeInSeconds = 3600
numberOfExposures = 1

```

```

## reset detector to expect Ga x-rays
so;ct;sc
## reset detector to turn off virtual det
virDET_enable 1

## Set distance for measurements
umv x -1.42
umv z -3.154
set_distance 4600
## Record AgBeh
umv z 21.5086
umv x -4.2232
multiexp numberOfExposures 900 901

virDET_enable 0
umv z -3.5662
## position empty capThursay
umv x 44.0848
multiexp numberOfExposures scanTimeInSeconds scanTimeInSeconds+1

## position SIF background
umv x 16.0848
multiexp numberOfExposures scanTimeInSeconds scanTimeInSeconds+1

## position Min blank sample
umv x 9.0848
multiexp numberOfExposures scanTimeInSeconds scanTimeInSeconds+1

## position Q1 blank sample
umv x 2.0848
multiexp numberOfExposures scanTimeInSeconds scanTimeInSeconds+1

## position Median blank sample
umv x -4.92
multiexp numberOfExposures scanTimeInSeconds scanTimeInSeconds+1

## position Min and naproxen
umv x -8.42
multiexp numberOfExposures scanTimeInSeconds scanTimeInSeconds+1

## position Min and tadalafil
umv x -11.92
multiexp numberOfExposures scanTimeInSeconds scanTimeInSeconds+1

## position Q1 and naproxen
umv x -15.42
multiexp numberOfExposures scanTimeInSeconds scanTimeInSeconds+1

## position Q1 and tadalafil
umv x -18.92
##multiexp numberOfExposures scanTimeInSeconds scanTimeInSeconds+1

## position Median and naproxen
umv x -22.42

```

```

multiexp numberOfExposures scanTimeInSeconds scanTimeInSeconds+1

## position Median and tadalafil
umv x -25.92
multiexp numberOfExposures scanTimeInSeconds scanTimeInSeconds+1

## position biorelevant and naproxen
umv x -29.42
multiexp numberOfExposures scanTimeInSeconds scanTimeInSeconds+1

## position Q3 sample
umv x -36.42
##multiexp numberOfExposures scanTimeInSeconds scanTimeInSeconds+1

## position Maximum sample
umv x -39.92
multiexp numberOfExposures scanTimeInSeconds scanTimeInSeconds+1

umv x -1.42
umv z -3.154
set_distance 1000

## Record AgBeh
umv z 21.5086
umv x -4.2232
multiexp numberOfExposures 900 901

umv z -3.5662
## position empty cap
umv x 44.0848
multiexp numberOfExposures scanTimeInSeconds scanTimeInSeconds+1

## position water background
umv x 37.0848
multiexp numberOfExposures scanTimeInSeconds scanTimeInSeconds+1

## position biorelevant buffer background
umv x 30.0848
multiexp numberOfExposures scanTimeInSeconds scanTimeInSeconds+1

## position biorelevant fassif
umv x 23.0848
multiexp numberOfExposures scanTimeInSeconds scanTimeInSeconds+1

## position SIF background
umv x 16.0848
multiexp numberOfExposures scanTimeInSeconds scanTimeInSeconds+1

## position Min blank sample
umv x 9.0848
multiexp numberOfExposures scanTimeInSeconds scanTimeInSeconds+1

## position Q1 blank sample
umv x 2.0848

```

multiexp numberOfExposures scanTimeInSeconds scanTimeInSeconds+1

position Median blank sample

umv x -4.92

multiexp numberOfExposures scanTimeInSeconds scanTimeInSeconds+1

position Min and naproxen

umv x -8.42

multiexp numberOfExposures scanTimeInSeconds scanTimeInSeconds+1

position Min and tadalafil

umv x -11.92

multiexp numberOfExposures scanTimeInSeconds scanTimeInSeconds+1

position Q1 and naproxen

umv x -15.42

multiexp numberOfExposures scanTimeInSeconds scanTimeInSeconds+1

position Q1 and tadalafil

umv x -18.92

##multiexp numberOfExposures scanTimeInSeconds scanTimeInSeconds+1

position Median and naproxen

umv x -22.42

multiexp numberOfExposures scanTimeInSeconds scanTimeInSeconds+1

position Median and tadalafil

umv x -25.92

multiexp numberOfExposures scanTimeInSeconds scanTimeInSeconds+1

position biorelevant and naproxen

umv x -29.42

multiexp numberOfExposures scanTimeInSeconds scanTimeInSeconds+1

position Q3 sample

umv x -36.42

##multiexp numberOfExposures scanTimeInSeconds scanTimeInSeconds+1

position Maximum sample

umv x -39.92

multiexp numberOfExposures scanTimeInSeconds scanTimeInSeconds+1

References

1. Batchelor, H., *Biopharmaceutics From fundamentals to industrial practice*. John Wiley & Sons: Chichester, West Sussex, England, 2022.
2. Krishna, R.; Yu, L., *Biopharmaceutics applications in drug development*. Springer: New York, 2007.
3. Stielow, M.; Witczyńska, A.; Kubryń, N.; Fijałkowski, Ł.; Nowaczyk, J.; Nowaczyk, A., The Bioavailability of Drugs—The Current State of Knowledge. *Molecules* **2023**, *28* (24).
4. Atkinson, A. J.; Huang, S.-M.; Lertora, J. J. L.; Markey, S. P., Chapter 4 - Drug Absorption and Bioavailability. In *Principles of Clinical Pharmacology (Third Edition)*, Academic Press: 2012; pp 41-53.
5. Benet, L. Z.; Hosey, C. M.; Ursu, O.; Oprea, T. I., BDDCS, the Rule of 5 and drugability. *Advanced Drug Delivery Reviews* **2016**, *101*, 89-98.
6. Charalabidis, A.; Sfouni, M.; Bergström, C.; Macheras, P., The Biopharmaceutics Classification System (BCS) and the Biopharmaceutics Drug Disposition Classification System (BDDCS): Beyond guidelines. *International Journal of Pharmaceutics* **2019**, *566*, 264-281.
7. Papich, M. G.; Martinez, M. N., Applying Biopharmaceutical Classification System (BCS) Criteria to Predict Oral Absorption of Drugs in Dogs: Challenges and Pitfalls. *The AAPS Journal* **2015**, *17* (4), 948-964.
8. Dahan, A.; Miller, J. M.; Hilfinger, J. M.; Yamashita, S.; Yu, L. X.; Lennernäs, H.; Amidon, G. L., High-Permeability Criterion for BCS Classification: Segmental/pH Dependent Permeability Considerations. *Molecular Pharmaceutics* **2010**, *7* (5), 1827-1834.
9. Solubility. In *IUPAC Compendium of Chemical Terminology*, 3rd ed.; International Union of Pure and Applied Chemistry: 2006.
10. Llompart, P.; Minoletti, C.; Baybekov, S.; Horvath, D.; Marcou, G.; Varnek, A., Will we ever be able to accurately predict solubility? *Scientific Data* **2024**, *11* (1), 303.
11. Savjani, K. T.; Gajjar, A. K.; Savjani, J. K., Drug Solubility: Importance and Enhancement Techniques. *ISRN Pharmaceutics* **2012**, *2012*, 195727.
12. Mahaffy, P. G.; Treichel, P., *Chemistry : human activity, chemical reactivity*. Toronto, Ontario : Nelson Education: Toronto, Ontario, 2014.
13. Zhuang, B.; Ramanauskaite, G.; Koa, Z. Y.; Wang, Z.-G., Like dissolves like: A first-principles theory for predicting liquid miscibility and mixture dielectric constant. *Science Advances* *7* (7), eabe7275.
14. Katzung, B. G., *Basic & Clinical Pharmacology*. Fourteenth ed.; McGraw-Hill Education: United States of America, 2018.
15. Serajuddin, A. T. M., Salt formation to improve drug solubility. *Advanced Drug Delivery Reviews* **2007**, *59* (7), 603-616.
16. Fallingborg, J., Intraluminal pH of the human gastrointestinal tract. *Danish medical bulletin* **1999**, *46* (3), 14.
17. Dowd, F. J.; Johnson, B. S.; Mariotti, A. J., 2 - Pharmacokinetics: The Absorption, Distribution, and Fate of Drugs. In *Pharmacology and Therapeutics for Dentistry (Seventh Edition)*, Mosby: 2017; pp 15-43.
18. Dey, S.; Halder, D.; Chatterjee, T.; Guria, T.; Jha, S. K.; Nayak, A. K.; Sen, K. K., Chapter 3 - Solubility of drugs. In *Physico-Chemical Aspects of Dosage Forms and Biopharmaceutics*, Academic Press: 2024; pp 43-59.
19. Chaudhry, S. R.; Linman, M. N. P.; Omole, A. E.; Peterson, D. C., *Anatomy, Abdomen and Pelvis: Stomach*. Treasure Island (FL): StatsPearls Publishing: 2024.
20. Collins, J. T.; Nguyen, A.; Badireddy, M., *Anatomy, Abdomen and Pelvis, Small Intestine*. Treasure Island (FL): StatsPearls Publishing: 2024.
21. Azzouz, L. L.; Sharma, S., *Physiology, Large Intestine*. Treasure Island (FL): StatsPearls Publishing: 2019.

22. Riethorst, D.; Baatsen, P.; Remijn, C.; Mitra, A.; Tack, J.; Brouwers, J.; Augustijns, P., An In-Depth View into Human Intestinal Fluid Colloids: Intersubject Variability in Relation to Composition. *Molecular Pharmaceutics* **2016**, *13* (10), 3484-3493.
23. Parrow, A.; Larsson, P.; Augustijns, P.; Bergström, C. A. S., Molecular Dynamics Simulations of Self-Assembling Colloids in Fed-State Human Intestinal Fluids and Their Solubilization of Lipophilic Drugs. *Molecular Pharmaceutics* **2023**, *20* (1), 451-460.
24. Pyper, K.; Brouwers, J.; Augustijns, P.; Khadra, I.; Dunn, C.; Wilson, C. G.; Halbert, G. W., Multidimensional analysis of human intestinal fluid composition. *European Journal of Pharmaceutics and Biopharmaceutics* **2020**, *153*, 226-240.
25. Shalon, D.; Culver, R. N.; Grembi, J. A.; Folz, J.; Treit, P. V.; Shi, H.; Rosenberger, F. A.; Dethlefsen, L.; Meng, X.; Yaffe, E.; Aranda-Díaz, A.; Geyer, P. E.; Mueller-Reif, J. B.; Spencer, S.; Patterson, A. D.; Triadafilopoulos, G.; Holmes, S. P.; Mann, M.; Fiehn, O.; Relman, D. A.; Huang, K. C., Profiling the human intestinal environment under physiological conditions. *Nature* **2023**, *617* (7961), 581-591.
26. Riethorst, D.; Mols, R.; Duchateau, G.; Tack, J.; Brouwers, J.; Augustijns, P., Characterization of Human Duodenal Fluids in Fasted and Fed State Conditions. *Journal of Pharmaceutical Sciences* **2016**, *105* (2), 673-681.
27. Nassar, S.; Menias, C. O.; Palmquist, S.; Nada, A.; Pickhardt, P. J.; Shaaban, A. M.; Gaballah, A. H.; Elsayes, K. M., Ligament of Treitz: Anatomy, Relevance of Radiologic Findings, and Radiologic-Pathologic Correlation. *American Journal of Roentgenology* **2021**, *216* (4), 927-934.
28. Abuhassan, Q.; Khadra, I.; Pyper, K.; Halbert, G. W., Small scale in vitro method to determine a bioequivalent equilibrium solubility range for fasted human intestinal fluid. *European Journal of Pharmaceutics and Biopharmaceutics* **2021**, *168*, 90-96.
29. Dunn, C.; Perrier, J.; Khadra, I.; Wilson, C. G.; Halbert, G. W., Topography of Simulated Intestinal Equilibrium Solubility. *Molecular Pharmaceutics* **2019**, *16* (5), 1890-1905.
30. Khadra, I.; Zhou, Z.; Dunn, C.; Wilson, C. G.; Halbert, G., Statistical investigation of simulated intestinal fluid composition on the equilibrium solubility of biopharmaceutics classification system class II drugs. *European Journal of Pharmaceutical Sciences* **2015**, *67*, 65-75.
31. Dressman, J. B.; Amidon, G. L.; Reppas, C.; Shah, V. P., Dissolution Testing as a Prognostic Tool for Oral Drug Absorption: Immediate Release Dosage Forms. *Pharmaceutical Research* **1998**, *15* (1), 11-22.
32. Galia, E.; Nicolaidis, E.; Hörter, D.; Löbenberg, R.; Reppas, C.; Dressman, J. B., Evaluation of Various Dissolution Media for Predicting In Vivo Performance of Class I and II Drugs. *Pharmaceutical Research* **1998**, *15* (5), 698-705.
33. Klein, S., The Use of Biorelevant Dissolution Media to Forecast the In Vivo Performance of a Drug. *The AAPS Journal* **2010**, *12* (3), 397-406.
34. Fuchs, A.; Leigh, M.; Kloefer, B.; Dressman, J. B., Advances in the design of fasted state simulating intestinal fluids: FaSSIF-V3. *European Journal of Pharmaceutics and Biopharmaceutics* **2015**, *94*, 229-240.
35. Abuhassan, Q.; Khadra, I.; Pyper, K.; Augustijns, P.; Brouwers, J.; Halbert, G. W., Fasted intestinal solubility limits and distributions applied to the biopharmaceutics and developability classification systems. *European Journal of Pharmaceutics and Biopharmaceutics* **2022**, *170*, 160-169.
36. Inês Silva, M.; Khadra, I.; Pyper, K.; Halbert, G. W., Small scale in vitro method to determine a potential bioequivalent equilibrium solubility range for fed human intestinal fluid. *European Journal of Pharmaceutics and Biopharmaceutics* **2022**, *177*, 126-134.
37. Jantratid, E.; Janssen, N.; Reppas, C.; Dressman, J. B., Dissolution Media Simulating Conditions in the Proximal Human Gastrointestinal Tract: An Update. *Pharmaceutical Research* **2008**, *25* (7), 1663-1676.
38. Psachoulas, D.; Vertzoni, M.; Butler, J.; Busby, D.; Symillides, M.; Dressman, J.; Reppas, C., An In Vitro Methodology for Forecasting Luminal Concentrations and Precipitation of Highly

- Permeable Lipophilic Weak Bases in the Fasted Upper Small Intestine. *Pharmaceutical Research* **2012**, *29* (12), 3486-3498.
39. Kiela, P. R.; Ghishan, F. K., Physiology of Intestinal Absorption and Secretion. *Best Practice & Research Clinical Gastroenterology* **2016**, *30* (2), 145-159.
40. Parekh, P. Y.; Patel, V. I.; Khimani, M. R.; Bahadur, P., Self-assembly of bile salts and their mixed aggregates as building blocks for smart aggregates. *Advances in Colloid and Interface Science* **2023**, *312*, 102846.
41. Clulow, A. J.; Parrow, A.; Hawley, A.; Khan, J.; Pham, A. C.; Larsson, P.; Bergström, C. A. S.; Boyd, B. J., Characterization of Solubilizing Nanoaggregates Present in Different Versions of Simulated Intestinal Fluid. *The Journal of Physical Chemistry B* **2017**, *121* (48), 10869-10881.
42. Long, M. A.; Kaler, E. W.; Lee, S. P.; Wignall, G. D., Characterization of Lecithin-Taurodeoxycholate Mixed Micelles Using Small-Angle Neutron Scattering and Static and Dynamic Light Scattering. *The Journal of Physical Chemistry* **1994**, *98* (16), 4402-4410.
43. Leigh, M.; Klofer, B.; Schaich, M., Comparison of the Solubility and Dissolution of Drugs in Fasted State Biorelevant Media (FaSSIF and FaSSIF-V2). *Dissolution technologies* **2013**, *20* (3), 44-50.
44. Jamil, R.; Polli, J. E., Prediction of In Vitro Drug Dissolution into Fed-state Biorelevant Media: Contributions of Solubility Enhancement and Relatively Low Colloid Diffusivity. *European Journal of Pharmaceutical Sciences* **2022**, *173*, 106179.
45. Gallo, A.; Pellegrino, S.; Pero, E.; Agnitelli, M. C.; Parlangei, C.; Landi, F.; Montalto, M., Main Disorders of Gastrointestinal Tract in Older People: An Overview. *Gastrointestinal Disorders* **2024**, *6* (1), 313-336.
46. Esmaeili, H.; Mousavi, S. M.; Hashemi, S. A.; Lai, C. W.; Chiang, W.-H.; Bahrani, S.; Inamuddin; Adetunji, C. O., Chapter 7 - Application of biosurfactants in the removal of oil from emulsion. In *Green Sustainable Process for Chemical and Environmental Engineering and Science*, Elsevier: 2021; pp 107-127.
47. Lu, Y.; Yue, Z.; Xie, J.; Wang, W.; Zhu, H.; Zhang, E.; Cao, Z., Micelles with ultralow critical micelle concentration as carriers for drug delivery. *Nature Biomedical Engineering* **2018**, *2* (5), 318-325.
48. Basak, R.; Bandyopadhyay, R., Encapsulation of Hydrophobic Drugs in Pluronic F127 Micelles: Effects of Drug Hydrophobicity, Solution Temperature, and pH. *Langmuir* **2013**, *29* (13), 4350-4356.
49. Parrow, A.; Larsson, P.; Augustijns, P.; Bergström, C. A. S., Molecular Dynamics Simulations on Interindividual Variability of Intestinal Fluids: Impact on Drug Solubilization. *Molecular Pharmaceutics* **2020**, *17* (10), 3837-3844.
50. Klumpp, L.; Nagasekar, K.; McCullough, O.; Seybert, A.; Ashtikar, M.; Dressman, J., Stability of Biorelevant Media Under Various Storage Conditions. *Dissolution Technologies* **2019**, *26*, 6+.
51. Doak, A. K.; Wille, H.; Prusiner, S. B.; Shoichet, B. K., Colloid Formation by Drugs in Simulated Intestinal Fluid. *Journal of Medicinal Chemistry* **2010**, *53* (10), 4259-4265.
52. Perrier, J.; Zhou, Z.; Dunn, C.; Khadra, I.; Wilson, C. G.; Halbert, G., Statistical investigation of the full concentration range of fasted and fed simulated intestinal fluid on the equilibrium solubility of oral drugs. *European Journal of Pharmaceutical Sciences* **2018**, *111*, 247-256.
53. Abuhassan, Q.; Khadra, I.; Pyper, K.; Augustijns, P.; Brouwers, J.; Halbert, G. W., Structured solubility behaviour in bioequivalent fasted simulated intestinal fluids. *European Journal of Pharmaceutics and Biopharmaceutics* **2022**, *176*, 108-121.
54. Kazakevich, Y.; Lobrutto, R., *HPLC for Pharmaceutical Scientists*. First ed.; John Wiley & Sons, Inc.: Hoboken, New Jersey, 2007.
55. Shimadzu What is HPLC (High Performance Liquid Chromatography)? https://www.shimadzu.com/an/service-support/technical-support/analysis-basics/basic/what_is_hplc.html (accessed 10 June 2024).
56. Wishart, D. S.; Knox, C.; Guo, A. C.; Shrivastava, S.; Hassanali, M.; Stothard, P.; Chang, Z.; Woolsey, J., DrugBank: a comprehensive resource for in silico drug discovery and exploration. *Nucleic Acids Research* **2006**, *34*.

57. Zhou, Z.; Dunn, C.; Khadra, I.; Wilson, C. G.; Halbert, G. W., Statistical investigation of simulated fed intestinal media composition on the equilibrium solubility of oral drugs. *European Journal of Pharmaceutical Sciences* **2017**, *99*, 95-104.
58. Rimmer, C. A.; Simmons, C. R.; Dorsey, J. G., The measurement and meaning of void volumes in reversed-phase liquid chromatography. *Journal of Chromatography A* **2002**, *965* (1), 219-232.
59. HPLC UV detection. <https://www.crawfordscientific.com/chromatography-blog/post/hplc-uv-detection> (accessed 05 July 2024).
60. Augustijns, P.; Wuyts, B.; Hens, B.; Annaert, P.; Butler, J.; Brouwers, J., A review of drug solubility in human intestinal fluids: Implications for the prediction of oral absorption. *European Journal of Pharmaceutical Sciences* **2014**, *57*, 322-332.
61. Teleki, A.; Nylander, O.; Bergström, C. A. S., Intrinsic Dissolution Rate Profiling of Poorly Water-Soluble Compounds in Biorelevant Dissolution Media. *Pharmaceutics* **2020**, *12* (493), 18.
62. Horvath, T. D.; Haidacher, S. J.; Hoch, K. M.; Auchtung, J. M.; Haag, A. M., A high-throughput LC-MS/MS method for the measurement of the bile acid/salt content in microbiome-derived sample sets. *MethodsX* **2020**, *7*, 100951.
63. Hamed, R.; Awadallah, A.; Sunoqrot, S.; Tarawneh, O.; Nazzal, S.; AlBaraghthi, T.; Al Sayyad, J.; Abbas, A., pH-Dependent Solubility and Dissolution Behavior of Carvedilol—Case Example of a Weakly Basic BCS Class II Drug. *AAPS PharmSciTech* **2016**, *17* (2), 418-426.
64. Berkhout, J.; N, A.; Rathnanand, M., pKa Determination of Carvedilol by Spectrophotometry. *Research Journal of Pharmacy and Technology* **2021**, 2714-2716.
65. Bhat, P. A.; Dar, A. A.; Rather, G. M., Solubilization Capabilities of Some Cationic, Anionic, and Nonionic Surfactants toward the Poorly Water-Soluble Antibiotic Drug Erythromycin. *Journal of Chemical & Engineering Data* **2008**, *53* (6), 1271-1277.
66. Boyd, B. J.; Bergström, C. A. S.; Vinarov, Z.; Kuentz, M.; Brouwers, J.; Augustijns, P.; Brandl, M.; Bernkop-Schnürch, A.; Shrestha, N.; Prémat, V.; Müllertz, A.; Bauer-Brandl, A.; Jannin, V., Successful oral delivery of poorly water-soluble drugs both depends on the intraluminal behavior of drugs and of appropriate advanced drug delivery systems. *European Journal of Pharmaceutical Sciences* **2019**, *137*, 104967.
67. de Smidt, J. H.; Offringa, J. C. A.; Crommelin, D. J. A., Dissolution Rate of Griseofulvin in Bile Salt Solutions. *Journal of Pharmaceutical Sciences* **1991**, *80* (4), 399-401.
68. McGown, L. B.; Nithipatikom, K., Sodium Taurocholate Micelles in Fluorometric Analysis. *Journal of Research of the National Bureau of Standards* **1988**, *93* (3), 443-434.
69. Silva, M. I.; Khadra, I.; Pyper, K.; Halbert, G. W., Structured solubility behaviour in fed simulated intestinal fluids. *European Journal of Pharmaceutics and Biopharmaceutics* **2023**, *193*, 58-73.
70. Stetefeld, J.; McKenna, S. A.; Patel, T. R., Dynamic light scattering: a practical guide and applications in biomedical sciences. *Biophysical Reviews* **2016**, *8* (4), 409-427.
71. Babick, F.; Hodoroaba, V.-D.; Unger, W. E. S.; Shard, A. G., Chapter 3.2.1 - Dynamic light scattering (DLS). In *Characterization of Nanoparticles*, Elsevier: 2020; pp 137-172.
72. Falke, S.; Betzel, C., Dynamic Light Scattering (DLS). In *Radiation in Bioanalysis: Spectroscopic Techniques and Theoretical Methods*, Springer International Publishing: Cham, 2019; pp 173-193.
73. ISO 22412:2017 Particle size analysis, Dynamic light scattering (DLS). British Standards Institute: 2017.
74. Panalytical, M. Dynamic Light Scattering: An Introduction in 30 Minutes. <https://www.malvernpanalytical.com/en/learn/knowledge-center/technical-notes/tn101104dynamiclightscatteringintroduction> (accessed 14 June 2024).
75. Lockwood, D. J., Rayleigh and Mie Scattering. In *Encyclopedia of Color Science and Technology*, Luo, M. R., Ed. Springer New York: New York, NY, 2016; pp 1097-1107.
76. Panalytical, M. What is Multiple Scattering? <https://www.materials-talks.com/wp-content/uploads/2018/03/FAQ-What-is-multiple-scattering.pdf> (accessed 12 July 2024).

77. Paar, A. The principles of dynamic light scattering. <https://wiki.anton-paar.com/uk-en/the-principles-of-dynamic-light-scattering/> (accessed 14 June 2024).
78. Dynamic Light Scattering - Common Terms Defined.
79. Khoshakhlagh, P.; Johnson, R.; Langguth, P.; Nawroth, T.; Schmueser, L.; Hellmann, N.; Decker, H.; Szekely, N. K., Fasted-State Simulated Intestinal Fluid "FaSSIF-C", a Cholesterol Containing Intestinal Model Medium For In Vitro Drug Delivery Development. *Pharmaceutics, Drug Delivery and Pharmaceutical Technology* **2015**, *104*, 12.
80. Nobbmann, U., HeNe Laser and APD in the Zetasizer. Malvern Panalytical: 2015.
81. Kloefer, B.; Hoogevest, P.; Moloney, R.; Kuentz, M.; Leigh, M.; Dressma, J., Study of a Standardized Taurocholate-Lecithin Powder for Preparing the Biorelevant Media FaSSIF and FaSSIF. *Dissolution Technologies* **2010**, *8*, 6-13.
82. Bose, A.; Roy Burman, D.; Sikdar, B.; Patra, P., Nanomicelles: Types, properties and applications in drug delivery. *IET Nanobiotechnology* **2021**, *15* (1), 19-27.
83. Mazer, N. A.; Benedek, G. B.; Carey, M. C., Quasielastic light-scattering studies of aqueous biliary lipid systems. Mixed micelle formation in bile salt-lecithin solutions. *Biochemistry* **1980**, *19* (4), 601-615.
84. Xie, X.; Cardot, J.-M.; Garrat, G.; Thery, V.; El-Hajji, M.; Beyssac, E., Micelle dynamic simulation and physicochemical characterization of biorelevant media to reflect gastrointestinal environment in fasted and fed states. *European Journal of Pharmaceutics and Biopharmaceutics* **2014**, *88* (2), 565-573.
85. Filipe, V.; Hawe, A.; Jiskoot, W., Critical Evaluation of Nanoparticle Tracking Analysis (NTA) by NanoSight for the Measurement of Nanoparticles and Protein Aggregates. *Pharmaceutical Research* **2010**, *27* (5), 796-810.
86. Gallego-Urrea, J. A.; Tuoriniemi, J.; Hassellöv, M., Applications of particle-tracking analysis to the determination of size distributions and concentrations of nanoparticles in environmental, biological and food samples. *TrAC Trends in Analytical Chemistry* **2011**, *30* (3), 473-483.
87. Nanosight NS300 User Manual. Malvern Panalytical: 2019.
88. Nanosight Pro System Basic Guide. Malvern Panalytical: 2023.
89. Comfort, N.; Cai, K.; Bloomquist, T. R.; Strait, M. D.; Ferrante Jr, A. W.; Baccarelli, A. A., Nanoparticle Tracking Analysis for the Quantification and Size Determination of Extracellular Vesicles. *J. Vis. Exp.* **2021**, (169), 33.
90. Kim, A.; Ng, W. B.; Bernt, W.; Cho, N.-J., Validation of Size Estimation of Nanoparticle Tracking Analysis on Polydisperse Macromolecule Assembly. *Scientific Reports* **2019**, *9* (1), 2639.
91. Malvern, Nanosight Pro User Guide. 2024.
92. Particle size analysis — Particle tracking analysis (PTA) method. International Organisation for Standardisation: 2016.
93. Panalytical, M. Nanoparticle Tracking Analysis (NTA). <https://www.malvernpanalytical.com/en/products/technology/light-scattering/nanoparticle-tracking-analysis> (accessed 14 June 2024).
94. ISO19430 - Particle Tracking Analysis Method. <https://www.malvernpanalytical.com/en/learn/knowledge-center/technical-notes/tn190429ntaiso19430> (accessed 06 August 2024).
95. Kestens, V.; Bozatzidis, V.; De Temmerman, P.-J.; Ramaye, Y.; Roebben, G., Validation of a particle tracking analysis method for the size determination of nano- and microparticles. *Journal of Nanoparticle Research* **2017**, *19* (8), 271.
96. Panalytical, M. NanoSight Pro - Size, Polydispersity, and Span. <https://www.malvernpanalytical.com/en/learn/knowledge-center/technical-notes/tn240304-size-polydispersity-and-span> (accessed 25 August 2024).
97. Gross, J.; Sayle, S.; Karow, A. R.; Bakowsky, U.; Garidel, P., Nanoparticle tracking analysis of particle size and concentration detection in suspensions of polymer and protein samples: Influence

- of experimental and data evaluation parameters. *European Journal of Pharmaceutics and Biopharmaceutics* **2016**, *104*, 30-41.
98. Navarro Sanchez, M. E.; Soulet, D.; Bonnet, E.; Guinchard, F.; Marco, S.; Vetter, E.; Nougarede, N., Rabies Vaccine Characterization by Nanoparticle Tracking Analysis. *Scientific Reports* **2020**, *10* (1), 8149.
 99. Polat, H.; Kutluay, G.; Polat, M., Analysis of dilution induced disintegration of micellar drug carriers in the presence of inter and intra micellar species. *Colloids and Surfaces A: Physicochemical and Engineering Aspects* **2020**, *601*, 124989.
 100. Micelle Characterization by DLS: Bringing Viscosity into the Equation. Anton Paar: 2016; p 5.
 101. Pedersen, J. S., Analysis of small-angle scattering data from colloids and polymer solutions: modeling and least-squares fitting. *Advances in Colloid and Interface Science* **1997**, *70*, 171-210.
 102. British Standards Institution, i. b., *Particle size analysis. Small angle X-ray scattering (SAXS) [internet resource]*. London : BSI: London, 2020.
 103. Glatter, O.; Kratky, O., *Small angle x-ray scattering*. London Academic Press: London, 1982.
 104. Jeffries, C. M.; Ilavsky, J.; Martel, A.; Hinrichs, S.; Meyer, A.; Pedersen, J. S.; Sokolova, A. V.; Svergun, D. I., Small-angle X-ray and neutron scattering. *Nature Reviews Methods Primers* **2021**, *1* (1), 70.
 105. Al-Tikriti, Y.; Hansson, P., A small-angle X-ray scattering study of amphiphilic drug self-assemblies in polyacrylate microgels. *Colloids and Surfaces A: Physicochemical and Engineering Aspects* **2024**, *686*, 133403.
 106. Burke, J. E.; Butcher, S. E., Nucleic Acid Structure Characterization by Small Angle X-Ray Scattering (SAXS). *Current Protocols in Nucleic Acid Chemistry* **2012**, *51* (1), 7.18.1-7.18.18.
 107. Smith, A. J.; Alcock, S. G.; Davidson, L. S.; Emmins, J. H.; Hiller Bardsley, J. C.; Holloway, P.; Malfois, M.; Marshall, A. R.; Pizzey, C. L.; Rogers, S. E.; Shebanova, O.; Snow, T.; Sutter, J. P.; Williams, E. P.; Terrill, N. J., I22: SAXS/WAXS beamline at Diamond Light Source – an overview of 10 years operation. *J Synchrotron Radiat* **2021**, *28* (3), 939-947.
 108. Yamashita, N.; Ikura, R.; Yamaoka, K.; Kato, N.; Kamei, M.; Ogura, K.; Igarashi, M.; Nakagawa, H.; Takashima, Y., Mechanical properties and molecular adhesion exhibited by inorganic-organic composite elastomers. *Polymer Chemistry* **2024**, *15* (41), 4196-4203.
 109. Wu, H.; Li, Z., A new dual-thickness semi-transparent beamstop for small-angle X-ray scattering. *J Synchrotron Radiat* **2024**, *31* (5), 1197-1208.
 110. Beamline Layout & Technical Specifications. <https://www.diamond.ac.uk/Instruments/Soft-Condensed-Matter/small-angle/Offline-SAXS/Beamline-Layout---Technical-Specification.html> (accessed 22 October).
 111. The metal-jet technology. <https://www.excillum.com/products/metaljet/> (accessed 21 October).
 112. González, A.; Egelman, E. H., 1.5 X-Ray Crystallography: Data Collection Strategies and Resources. In *Comprehensive Biophysics*, Elsevier: Amsterdam, 2012; pp 64-91.
 113. Offline SAXS. <https://www.diamond.ac.uk/Instruments/Soft-Condensed-Matter/small-angle/Offline-SAXS.html> (accessed 22 October).
 114. DECTRIS, User Manual Eiger R/X Detector Systems. 2018.
 115. DECTRIS, Technical Specifications Eiger R 1M Detector Systems. 2019.
 116. Apply for Beamtime. <https://www.diamond.ac.uk/Users/Apply-for-Beamtime.html> (accessed 23 October).
 117. Pickering, K. S.; Huband, S.; Shafran, K. L.; Walton, R. I., In situ X-ray Scattering of the Crystallisation of Basic Magnesium Chlorides using a Laboratory Instrument. *Chemistry–Methods* **2022**, *2* (9), e202200033.
 118. Caselli, L.; Conti, L.; De Santis, I.; Berti, D., Small-angle X-ray and neutron scattering applied to lipid-based nanoparticles: Recent advancements across different length scales. *Advances in Colloid and Interface Science* **2024**, *327*, 103156.

119. Huang, T. C.; Toraya, H.; Blanton, T. N.; Wu, Y., X-ray powder diffraction analysis of silver behenate, a possible low-angle diffraction standard. *J. Appl. Cryst* **1993**, *26* (2), 180-184.
120. DAWN User Manual. Diamond Light Source: Didcot, UK, 2016.
121. Khanday, M. A.; Rafiq, A.; Nazir, K., Mathematical models for drug diffusion through the compartments of blood and tissue medium. *Alexandria Journal of Medicine* **2017**, *53* (3), 245-249.
122. Jamil, R.; Polli, J. E., Prediction of in vitro drug dissolution into fasted-state biorelevant media: Contributions of solubility enhancement and relatively low colloid diffusivity. *European Journal of Pharmaceutical Sciences* **2022**, *174*, 106210.
123. Siepmann, J.; Siepmann, F., Mathematical modeling of drug delivery. *International Journal of Pharmaceutics* **2008**, *364* (2), 328-343.
124. Balakrishnan, A.; Rege, B. D.; Amidon, G. L.; Polli, J. E., Surfactant-mediated dissolution: Contributions of solubility enhancement and relatively low micelle diffusivity. *Journal of Pharmaceutical Sciences* **2004**, *93* (8), 2064-2075.
125. Comer, J.; Judge, S.; Matthews, D.; Towers, L.; Falcone, B.; Goodman, J.; Dearden, J., The intrinsic aqueous solubility of indomethacin. *ADMET and DMPK* **2014**, *2* (1), 18-32.
126. Schwartz, P. A.; Rhodes, C. T.; Cooper Jr, J. W., Solubility and ionization characteristics of phenytoin. *Journal of Pharmaceutical Sciences* **1977**, *66* (7), 994-997.
127. Granero, G. E.; Ramachandran, C.; Amidon, G. L., Dissolution and Solubility Behavior of Fenofibrate in Sodium Lauryl Sulfate Solutions. *Drug Development and Industrial Pharmacy* **2005**, *31* (9), 917-922.
128. Choi, J.-S.; Park, J.-S., Design of PVP/VA S-630 based tadalafil solid dispersion to enhance the dissolution rate. *European Journal of Pharmaceutical Sciences* **2017**, *97*, 269-276.
129. Hollingsworth, S. A.; Dror, R. O., Molecular Dynamics Simulation for All. *Neuron* **2018**, *99*, 29.
130. Liwo, A.; Czaplewski, C.; Sieradzan, A. K.; Lipska, A.; Samsonov, S. A.; Murarka, R. K., Theory and Practice of Coarse-Grained Molecular Dynamics of Biologically Important Systems. *Biomolecules* **2021**, *11* (1347), 31.
131. Salo-Ahen, O. M. H.; Alanko, I.; Bhadane, R.; Bonvin, A. M. J. J.; Honorato, R. V.; Hossain, S.; Juffer, A. H.; Kabedev, A.; Lahtela-Kakkonen, M.; Larsen, A. S.; Lescrinier, E.; Marimuthu, P.; Mirza, M. U.; Mustafa, G.; Nunes-Alves, A.; Pantsar, T.; Saadabadi, A.; Singaravelu, K.; Vanmeert, M., Molecular Dynamics Simulations in Drug Discovery and Pharmaceutical Development. *Processes* **2021**, *9* (1).